The Interplay Between the Neuronal Plasma Membrane and Cell Signaling in Alzheimer's Disease

by

Morgan Robinson

A thesis

presented to the University of Waterloo

in fulfillment of the

thesis requirement for the degree of

Doctor of Philosophy

in

Pharmacy

Waterloo, Ontario, Canada, 2023

Examining Committee Membership

The following served on the Examining Committee for this thesis. The decision of the Examining Committee is by majority vote.

External Examiner:	DR. MICHAEL JACKSON Professor Department of Medicine University of Manitoba
Supervisors:	DR. MICHAEL BEAZELY Associate Professor School of Pharmacy University of Waterloo
	DR. ZOYA LEONENKO Professor Department of Physics and Astronomy, Biology University of Waterloo
Internal Member:	DR. SHAWN WETTIG Professor School of Pharmacy University of Waterloo
Internal-External Member:	DR. JOHN MIELKE Associate Professor Department of Public Health and Health Systems University of Waterloo
Other Member:	DR. ROBIN DUNCAN Associate Professor Department of Kinesiology University of Waterloo

Author's Declaration

This thesis consists of material all of which I authored or co-authored: see Statement of Contributions included in the thesis. This is a true copy of the thesis, including any required final revisions, as accepted by my examiners.

I understand that my thesis may be made electronically available to the public.

Statement of Contributions

This work was completed by me, however certain portions include contributions from other students and scientists. A portion of the work presented here has been accepted for publication in a peer-reviewed journal for which I am co-first author. All work is my own unless otherwise reported in this statement of contribution.

Below are specific contributions from persons other than me:

Chapter 3: Data collection for Chapter3 was completed with the assistance of Erik Herz. I developed and trained Erik on all protocols and supervised the collection of these data. I supervised the development of a simple script written by Minh Phung used to extract bilayer thickness, breakthrough force and indentation depth values from the raw data. All other analyses and all writing were completed by me in its entirety.

Chapter 5: Melatonin cell viability and rescue data was collected by Kartar Singh whom I supervised for these experiments. I designed the experimental protocols and trained Kartar on all methods related to cell culturing and cell viability studies. I analyzed the data and wrote the discussion in its entirety.

Chapter 6: Data collection was completed with the assistance of Kartar Singh, who I supervised. I developed and trained Kartar on all protocols used in the collection of these datasets. Kartar performed a subset of sample preparation and phase contrast optical microscopy. Data analysis and all writing were completed by me in its entirety.

Chapter 7: Data collection was completed with the assistance of Kartar Singh and Sean Newbury, whom I supervised. I developed and trained them both on all protocols used. Kartar prepared samples and Sean Newbury performed Western Blots for a subset of the datasets used in this chapter. Data analysis and all writing were completed by me in their entirety.

Abstract

The lack of understanding in the molecular and cellular mechanisms of Alzheimer's disease (AD) has hindered efforts towards finding treatments that effectively modify disease trajectory. Therapeutic development for AD has focused on targeting amyloid-β (Aβ) pathology, long thought to be the cause of AD pathogenesis, but these have failed in clinical trials. Aβ is a sticky aggregation-prone protein that disrupts membrane structure and interferes with specific receptors in the brain, impairing synaptic plasticity, an important process for learning and memory, and eventually causes cell death. The interplay between disruption of the neuronal membrane and neuronal receptors in AD overlaps with inflammation and oxidative stress in a feedback loop that makes it difficult to ascertain the causes and effects of AD. More recent genetic and epidemiology data indicates that lipid metabolism is critical in AD pathogenesis, underscoring the need to understand how brain lipid composition (especially cholesterol) in brain affects amyloid toxicity. In the first part of this work the relevant background literature of lipid mediated mechanisms of AD is discussed and an overview of methods used herein are provided.

In the second part, the results of biomedical nanotechnology experiments where atomic force microscopy (AFM) was used to study interactions of supported lipid bilayers (SLBs) with melatonin and Aβ at the molecular level. Chapter 3 shows the characterization of biophysical changes that melatonin induces in SLBs of DOPC/DPPC/Cholesterol by AFM and atomic force spectroscopy (AFS). Overall, AFM imaging revealed that melatonin increases disordered domain coverage, reduces bilayer thickness and indentation depth, increases membrane fluidity, and decreases membrane adhesion, though large variability was observed. In Chapter 4, for the first-time contact mode high-speed AFM (HS-AFM) was shown to be able to image lipid membranes of different compositions. HS-AFM was used to capture large areas of membranes comparing the effects of Aβ monomers and oligomers to different phase separated lipid bilayers composed of low and high cholesterol showing different interaction mechanisms.

In the third part of this thesis the influence of membrane composition and amyloid toxicity on HT22 neuronal cell viability, cholesterol metabolism, morphology, and receptor tyrosine kinase (RTK) signaling pathways was elucidated. Beginning in Chapter 4, cholesterol oxidase assays and AFM verify cell cholesterol content reduction and Aβ structure, respectively. There was no effect of Aβ on cholesterol recovery and cell viability studies show that cholesterol

depletion was modestly protective against both Aβ monomers and oligomers. In Chapter 5, the cholesterol-dependent effects of Aβ monomers and oligomers on HT22 cell morphology by phase contrast optical microscopy and atomic force microscopy (AFM) reveal apoptotic and necrotic populations of HT22 cells exposed to Aβ and that that membrane cholesterol depletion prevents these changes in morphology. In Chapter 7, the effects of cholesterol and Aβ on baseline Tyrosine Receptor Kinase B (TrkB) receptors and PDGF receptor-α (PDGFRα) signaling, reveal that RTK signaling is cholesterol-dependent and that high concentration Aβ oligomers increase the likelihood of RTK impairment, but there was no statistically significant effect of Aβ on PDGFRα signaling.

This work provides experimental evidence that membrane cholesterol is not strongly involved in the mechanisms of Aβ toxicity in HT22 cells, but its reductions may be mildly protective. RTK signaling in HT22 cells is impaired by Aβ but is not involved in the protective mechanisms of cholesterol depletion. Aβ disrupts membrane biophysical structure and receptor signaling pathways triggering metabolic dysfunction and both apoptotic and necrotic cell death mechanisms.

Acknowledgements

This doctoral dissertation could not have been accomplished without the support of many people whom I would like to acknowledge. First, I would like to thank my supervisors Drs. Michael Beazely and Zoya Leonenko who provided me with critical support, guidance and mentorship over the past six years; their wisdom and counsel has been invaluable to me. They each provided unique perspectives, both in their approaches to problem solving, in their scientific theories and praxes, but also in their leadership styles. I have learned a great from both of them, not only about science, but also about life; I will carry these lessons with me everywhere I go. Second, I must acknowledge the rest of my thesis advisory committee, Drs. Shawn Wettig, John Mielke, and Robin Duncan, who all engaged with me in stimulating scientific discussions and provided me with encouragement at each stage of my work, especially through the most trying of times.

Next, I would like to acknowledge Prof. Mervyn Miles from the University of Bristol who supervised the HS-AFM work in Chapter 4. He was not only a vast source of knowledge and refined my understanding of the principles of AFM and engineering physics, but also offered much encouragement and was good friend to me while I was away from Canada. I would like to thank University of Bristol scientists Drs. Loren Picco and Oliver Payton for assistance with instrumentation, and Prof. Annela Seddon for use of her wet lab space.

I must also acknowledge my fellow lab members that I worked with over the years, our conversations were deep, interesting, and of the utmost quality. I would be remiss to not mention Drs. Francis Hane, Liz Drolle and Brenda Lee who trained me on the use of AFM and in lipid preparation protocols in Dr. Leonenko's lab; also, Drs. Nyasha Gondora, and Nawaz Ahmed who trained me in aseptic technique, and mammalian cell culture in Dr. Michael Beazely's lab. As well, I must thank the many trainees, post-doctoral fellows, fellow graduate students and undergraduates who worked on the front lines with me, moving the endeavor of science forward through their hard work and dedication to truth, thank you for all our many conversations and helping to shape my views of the natural world: Dr. Robbie Henderson, Jennifer Lou, James Livingstone, Kartar Singh, Sean Newbury, Marzi Khavandi, Carina Felice, Nanqin Mei, Yue Xu, Stephen Turnbull, Erik Herz, Minh Phung, Dr. Danielle McRae, and Irina Bukhteeva.

Finally, to Costa Rica – a beautiful refuge in my darkest of times – *pura vida*.

Table of Contents

List of Figures

Chapter 1

Chapter 2

Chapter 3

Chapter 4

Chapter 5

Chapter 6

Chapter 7

Chapter 8

List of Tables

Chapter 3

Chapter 4

List of Abbreviations

Alzheimer's disease (AD)

Amyloid-β (Aβ)

Amyloid precursor protein (APP)

Atomic force microscopy (AFM)

Atomic force spectroscopy (AFS)

Apolipoprotein-E (ApoE)

Arbitrary units (a.u.)

ATP-binding cassette subfamily A member 1 (ABCA1)

Blood-brain barrier (BBB)

Brain-derived neurotrophic factor (BDNF)

Central nervous system (CNS)

Diacylglycerol (DAG)

Dioleoyl phosphocholine (DOPC)

Dipalmitoyl phosphocholine (DPPC)

Diseased membrane (DM)

Docosahexaenoic acid (DHA)

Eicosapentaenoic acid (EPA)

Extracellular receptor kinases (ERK)

Familial AD (FAD)

Food and Drug Administration (FDA)

Gas chromatography coupled mass spectroscopy (GC/MS)

Genome wide association studies (GWAS)

G-protein coupled receptors (GPCRs)

Interleukin (IL)

Healthy membrane model (HM)

4-hydroxy-noneal (HNE)

β-Hydroxy β-methylglutaryl-CoA (HMG-CoA)

Ligand-gated ion channels (LGIC)

Long-term potentiation (LTP)

Low-density lipoprotein (LDL)

Lipopolysaccharide (LPS)

Liquid chromatography coupled mass spectroscopy (LC/MS)

Macrophage-colony stimulating factor (M-CSF)

Membrane lipid rafts (MLR)

Metabotropic glutamate receptor-5 (mGluR5)

Methyl-β cyclodextrin (MβCD)

Molecular dynamics (MD)

Multilamellar vesicles (MLVs)

3-(4,5-dimethylthiazol-2-yl)-2,5-diphenyltetrazolium bromide (MTT)

Neural growth factor (NGF)

Neurofibrillary tangles (NFT)

Neurotrophic Growth Factor (NGF)

Nicotinic acetylcholine receptors (nAChR)

N-methyl D-aspartate (NMDA)

Nuclear Factor-κB (NFκB)

Nuclear magnetic Resonance (NMR)

P75 neurotropic growth factor receptor (P75NTR)

Phospholipase C-γ (PLCγ)

Platelet-derived growth factor (PDGF)

1-palmitoyl-2-oleoyl-sn-glycero-3-phosphocholine, powder (POPC)

Polyunsaturated fatty acids (PUFAs)

Reactive oxygen species (ROS)

Receptor tyrosine kinases (RTKs)

Serotonin (5-HT)

Supported Lipid Bilayer (SLB)

Toll-like receptors (TLR)

Traumatic brain injury (TBI)

Tropomyosin-related kinase B (TrkB)

Unilamellar vesicles (ULV)

"Now we scientists are used to this, and we take it for granted that it is perfectly consistent to be unsure – that it is possible to live and *not* know. But I don't know whether everyone realizes that this is true. Our freedom to doubt was born of a struggle against authority in the early days of science. It was a very deep and strong struggle. Permit us to question — to doubt, that's all — not to be sure. And I think it is important that we do not forget the importance of this struggle and thus perhaps lose what we have gained. Here lies a responsibility to society."

– Richard Feynman in *The Value of Science*, November 1955[1].

Chapter 1: The Role of Lipids in the Pathogenesis of Alzheimer's Disease

1.1 Introduction

Alzheimer's disease (AD) is one of the most pressing age-related diseases facing Canadian society today and despite over 100 years of research no treatments are available that slow AD progression[2–4]. AD is characterized clinically by symptoms of progressive cognitive impairment and dementia, including impaired learning, memory, mood disruption and language impairment[5–7]. These behavioral symptoms occur alongside neuropathological atrophy in areas of the brain involved in learning and memory, primarily in the hippocampus and the cortex, (Figure 1.1) [8–10]. These regions of atrophy represent significant loss of neurons and synapses and contain significant deposition of extracellular amyloid-β (Aβ) plaques and intracellular neurofibrillary tangles (NFTs) and adipose inclusions, shown on histological brain slice image in Figure 1.1[9,10]. The majority of AD cases are age-related (or sporadic AD), while a subset of cases are genetically-linked to amyloid production.

The defining molecular hallmark of AD is the accumulation of extracellular amyloid-β (Aβ) plaques (Figure 1.1), however this occurs alongside a variety of other features such as: intracellular neurofibrillary tangles (NFT), metabolic dysfunction, neuroinflammation, oxidative stress, disruption of neuronal signaling, and blood-brain barrier (BBB) disruption[9–12]. The precise cascade of events in AD pathogenesis is not known though much progress has been made in the last 30 years mapping out a general disease trajectory[13–15]. Currently, the big questions in AD regard the earliest stages of disease, prior to the onset of symptoms, where it is now expected that a prolonged preclinical phase (prodromal AD), of the disease where neuropathological changes occur before symptoms manifest[9–11,14,15]. Aside from the major hallmarks mentioned, several lines of evidence point to mechanisms involving lipid membrane disruptions as precipitating factors in rendering cells susceptible to amyloid toxicity that may resolve many long-standing questions[16–18]. At the molecule level amyloid induced permeability is membrane lipid composition dependent[19,20], while at the cellular level lipid composition affects amyloid-related pathological changes[21,22]. These molecular and cellular changes could relate to broader tissue level disruptions in impaired lipid homeostasis and innate immune system dysfunction both in the central nervous system (CNS) and co-incidentally within the periphery [18,23–27]. This literature review will start with a short summary of the current state of the Amyloid Cascade

Hypothesis, then provide a background on lipid membrane structure and the influence of lipid structure and composition on receptor signaling before looking more deeply into the contributions of the neuronal lipid membrane and membrane receptors in Aβ toxicity, and then finally, connect these ideas to the many epidemiological and genetic evidence that point to how changes in lipid homeostasis may be the key initiating factor in AD pathogenesis.

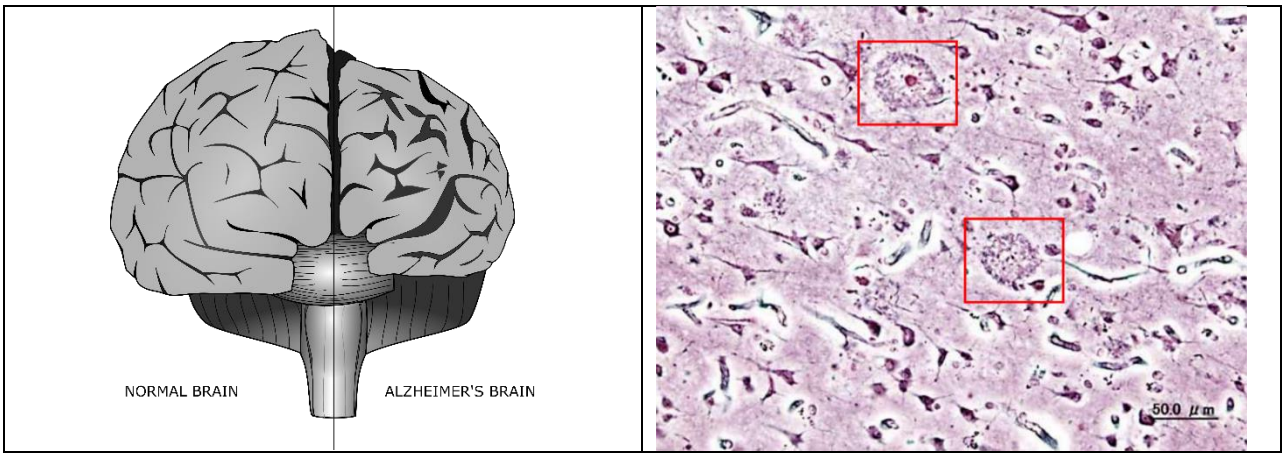

Figure 1.1. Alzheimer's disease pathology *involves gross structural changes in cortical and hippocampal regions, increases in interstitial spaces and overall loss of brain tissue (left). Histopathological image of brain slice from AD patient, extracellular Aβ plaques are highlighted with red boxes, image courtesy of the NIH (right).*

1.1.1 The Current State of the Amyloid Cascade Hypothesis

The precise cause of AD is not known in the majority of sporadic AD, however the accumulation the primary molecular hallmark, Amyloid-β, is known to occur very early in the disease trajectory[14,28]. Historically, a major milestone occurred in understanding the molecular mechanisms of AD neuropathology with the isolation and sequencing of the primary 4.2 KDa Aβ fragment in 1984 by Glenner and Wong[29]. Shortly thereafter, the gene encoding that Aβ fragment was located and cloned within what was later called the amyloid precursor protein (APP)[30]. This led to the formulation of the amyloid cascade hypothesis in the early 1990s, which suggested that AD was caused by the accumulation of amyloid due to an imbalance of production and clearance of Aβ monomers and their subsequent aggregation into toxic amyloid plaques (can be seen in histopathological slice from an AD brain, Figure 1.1 in red boxes)[31]. In the last few decades since, the amyloid cascade has been criticized due to the failures of Aβ-targeted treatments in clinical trials and the low correlation between Aβ load and development of symptoms. Regardless of whether Aβ is a useful target for treatment or prevention of AD alone, or must be targeted along with parallel molecular pathways, it plays an undeniable role in the

disease pathogenesis. Resolving these long-standing controversies depends on developing a more nuanced and complete description of the factors that contribute to Aβ neurotoxicity and not simply Aβ as the solo neurotoxic insult.

1.1.2 Amyloid-β Production, Aggregation, and Toxicity

The amyloid cascade has been the leading hypothesis for AD pathogenesis and although it provides a general description, it is not a complete picture of the disease. The amyloid cascade is shown in Figure 1.2. The Aβ cascade begins with cleavage of the amyloid precursor protein (APP), a transmembrane protein, to produce the toxic Aβ fragment. APP protein trafficking within cells follows the constitutive secretory pathway, once it reaches the cell membrane it is rapidly internalized, then it is recycled back through endocytic pathways to intracellular compartments, degradation in the lysosome or back to the cell membrane[32]. APP spends most of its time within the intracellular organelle membrane network, the Golgi-endoplasmic reticulum network[32]. Thus, the production of the Aβ occurs within neuronal compartments due to the catalytic cleavage of APP by β- and γ- secretases, both of which are primarily located within cells. Aβ accumulation within neurons has been shown to occur earlier in disease pathogenesis and to induce apoptosis preferentially over extracellular Aβ, though some Aβ is likely transported extracellularly [33–35]. APP has an alternative enzymatic processing pathway into non-amyloidogenic fragments by α-secretase, due to this cleavage site being within the Aβ region. This non-amyloidogenic processing occurs preferentially at the cell membrane where α-secretase is located[32]. Therefore it is not surprising (based on APP trafficking and different cleavage pathways in various cell compartments), that endosomal sorting has been implicated in disease pathogenesis[36]. This would suggest that endosomal/plasma membrane lipid composition could be an important factor and will be discussed more later in this chapter.

Molecular and cellular studies of Aβ toxicity have been quite informative in generating a general description of AD mechanisms. Though many specific molecular targets have been identified there are also a large set of non-specific cell processes that are also involved, such as membrane damage and oxidative stress [37–39]. Structure-toxicity relationships with Aβ have identified oligomers as the most toxic species and the emphasis has shifted from plaques towards the soluble Aβ oligomer as the culprit for causing AD[40,41], along with the expectation that late stages of the disease will be harder to treat. The Aβ monomer is a charged (6 negative and 3

positive residues), 38-43 amino acid peptide which includes the membrane spanning region of APP, and thus has several hydrophobic residues and an intrinsic membrane binding affinity[17,42]. After cleavage, Aβ monomers have a propensity to misfold and self-assemble[43–45]. First, and at low concentration, Aβ forms disordered low molecular weight oligomers which then further aggregate as the concentration of Aβ increases transitioning into more well-defined β-sheets and then these sheets align into protofibrils that grow into fibrils and eventually plaques[46–48]. Aggregation of Aβ in physiological conditions depends on a variety of factors; importantly, the lipid membrane (both intracellular and extracellular), provides an important interface for interaction (Figure 1.2). As Aβ accumulates at the neuronal surface it disrupts specific receptor signaling pathways and it causes major topographical defects in the membrane which both contribute to neuronal dysfunction (these pathways will be discussed in more details in following sections). This damage to the plasma membrane occurs alongside oxidative stress and metabolic dysfunction within neurons and other brain cells, in what appears to be positive feedback, eventually triggering apoptotic and necrotic cell death (these pathways will be discussed in more detail in the last section of this thesis). The toxicity of Aβ has made it a rational target for therapeutic intervention, though this has not yielded any major clinical success.

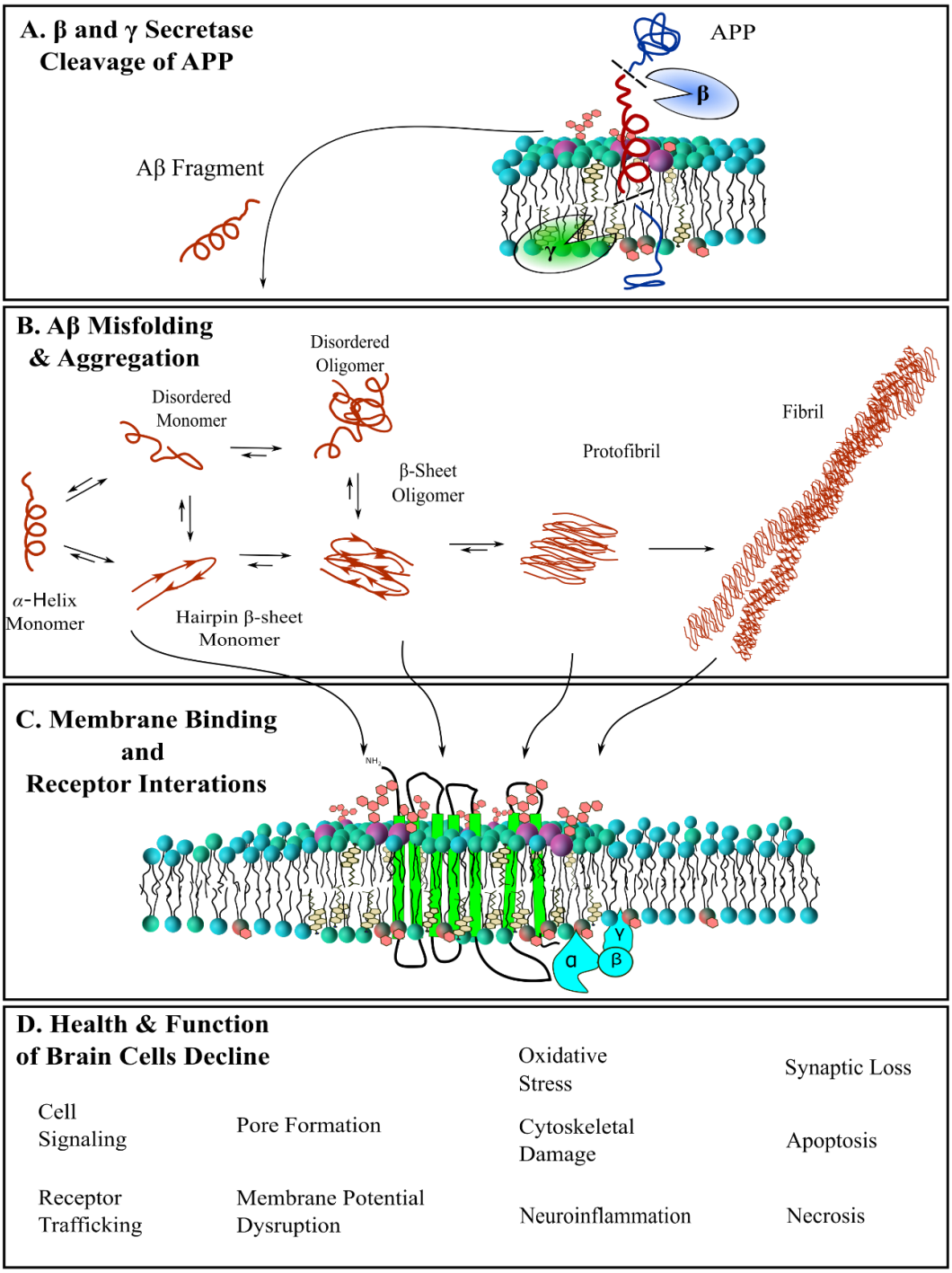

Figure 1.2. Amyloid-β production, aggregation and toxicity cascade. *Production of Aβ fragment from APP cleavage by β and γ secretases. Aβ aggregates into toxic oligomers and fibrils eventually forming plaques in the late stages of AD. Aβ has an intrinsic affinity for membranes due to its charge and hydrophobicity therefore it tends to accumulate on cell surfaces and interacts with membrane proteins. This has deleterious effects on membrane structure and cell signaling resulting in a chain reaction of oxidative stress, cytoskeletal damage, inflammation which triggers synapse loss and cellular toxicity.*

1.1.3 Amyloid-β Targeted Therapeutics

The amyloid cascade hypothesis has been criticized due to a lack of successful clinical trials targeting the amyloid cascade over the last 30 years, though more recent efforts suggest targeting amyloid during prodromal and early AD may be promising in a small subset of patients [49–51]. Very recently, and amid considerable controversy, aducanumab, a monoclonal antibody targeting Aβ has been given accelerated status by the US Food and Drug Administration (FDA) approval[52], despite the EMERGE and ENGAGE trials of aducanumab failing to demonstrate repeatable improvement in cognitive decline in patients[52]. Both the EMERGE and ENGAGE trials were cancelled for failing to meet primary endpoints, with one study exhibiting no improvement in primary outcomes (2% difference between placebo-controlled groups), and the other reaching a reduction in cognitive decline by 20%, both results from the high dose treatment group. Even, though both studies showed reduction in Aβ biomarker data[52], the safety profile of aducanumab in 40% of patients treated with high dose suffered from brain bleeding or swelling indicating a poor drug safety profile [53,54]. This is eerily similar to the results of other monoclonal antibodies and Aβ vaccines that have been shown to cause deposition of amyloid in cerebral vasculature triggering cerebral microhemorrhage – or brain bleeding in the microvasculature of the brain [55–57]. This type of reckless approval by the FDA is indicative of the continued failure and corruption of our scientific medical regulators to reign in the profit motive and other incentives of the pharmaceutical-medical industrial complex[58,59]. This controversial approval highlights the lack of effectiveness of Aβ-directed therapeutics, even in the early stages of AD. Regardless, it should be obvious by now that the complexity of AD would require more complex solutions than targeting a single molecular pathway and that the nuances of Aβ pathophysiology needs further elucidation.

1.2 The Structure and Function of the Plasma Membrane

The lipid membrane is a critical biological structure which defines the exterior surface of, and compartments within, biological cells and is a key interface for interaction between the cell and its environment, for cell-cell communication, and to compartmentalize intracellular processes within and between organelles. The plasma membrane is made from lipids that self-assemble into bilayer structures embedded with receptor proteins that when activated by specific molecules or induced by conformational changes in the membrane that inform adaptive cellular

behavior (illustrated in Figure 1.3 below)[60]. In general, the lipids that form bilayers are phospholipids and are highly amphiphilic molecules containing two hydrophobic acyl tails on one end connected to a hydrophilic headgroup on the other and which have geometries where the lowest energy configurations are bilayer structures, though more exotic structures are possible depending on lipid composition[60]. The physical properties of the lipids such as length of the fatty acid tail, degree of acyl tail saturation, the size and electrostatic properties of the head group and overall geometry are important factors in the organization of the membrane, including its local curvature and dynamic membrane processes[60–62]. Aside from a basic bilayer structure, lipid membranes can have more complex lateral heterogeneities that occur as a result of phase separation with the different regions being referred to as domains[60–63]. The denser domains typically associated with membrane proteins are referred to as membrane lipid rafts (MLRs), representation shown in Figure 1.3. Phase separation of synthetic and extracted lipid mixtures into domains is driven by thermodynamics of the membrane and occurs under certain lipid compositions and environmental factors such as temperature, with the different domains being classified according to their degree of order and disorder[61,63–66].

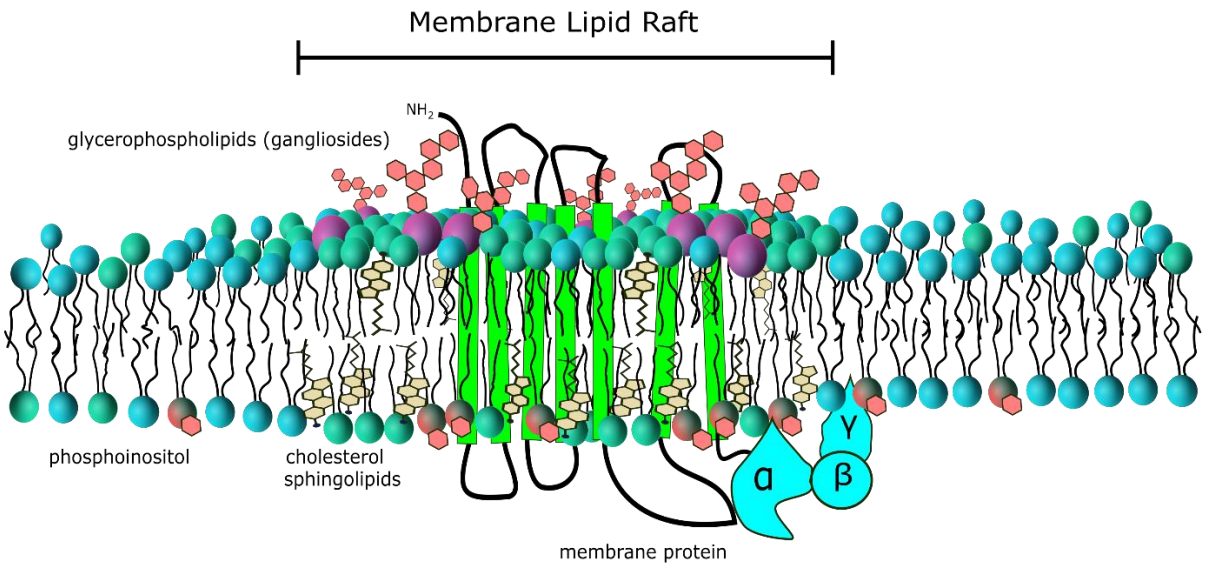

Figure 1.3. Organization of the lipid membrane*. A basic bilayer structure, with lateral heterogeneities that compartmentalize different cellular receptor signaling pathways. The MLR is a functional unit that includes protein embedded in a condensed, more ordered lipid domain. These MLRs "float" on a sea of disordered, more fluid lipid phases. The MLRs are enriched with cholesterol, sphingolipids and gangliosides, which exert a condensing effect through lipid-lipid interactions which include electrostatic, steric, and hydrophobic effects that increase tail packing density.*

The lipid membrane has long been overlooked as a passive structure in biology; however, it is now expected that the lipid membrane organization into micro- and nano-domains into

MLRs are crucial for regulation of cellular homeostasis [60,67,68]. MLRs are dynamic structures that have been proposed to compartmentalize and facilitate protein interactions, and dynamic membrane processes such as endocytosis and exocytosis[69]. These MLRs are enriched with cholesterol and sphingolipids and are studied by extraction of detergent-resistant membrane microdomains which contain MLR-associated proteins[68]. Cholesterol acts to increase tail-packing density of fatty acids in the membrane and can cause condensation of lipid domains by inducing liquid to gel phase transitions, and locally stiffening the membrane[65,70,71]. This effect is particularly strong for sphingolipids that interact preferentially with cholesterol due to electrostatic interactions of the amide bond connecting the sphingo-headgroup with the acyl tail[65,70,71]. Steric effects based on lipid geometry are also highly important for regulating membrane structure. The degree of order and disorder of the acyl tails correlates with the number of unsaturated bonds, with fully unsaturated lipids being able to pack more tightly and thus increase membrane order and extent of ordered domains [63,72,73]. The length of the acyl tail is very important with longer tails inducing more order in the membrane[74]. Not only do the tails of membrane lipids help to organize membrane structure but the headgroups also appear to be important as the headgroup of gangliosides, an important glycosphingolipid, couples with zwitterionic phosphocholine headgroups electrostatically[62]. In addition, lipid headgroup to tail ratio defines the geometry of different lipids, such that lipids with large headgroups, or lysophospholipids with only one tail, have a conical geometry while lipids with high degree of unsaturated lipid tails and small headgroups (such as phosphoethanolamines) have an inverted conical geometry[75]. Lipids with conical geometries have a tendency to promote positive membrane curvature, while inverted conical lipids promote negative curvature[75,76]. The geometries also affect lipid sorting with positive curvature lipids being preferred in the outer membrane leaflet and negative curvature lipids being preferred in the inner leaflet[75,76]. A variety of proteins (for instance: fusion proteins, caveolae, clathrin, synapsin and Aβ), are known to interact with membrane lipids to facilitate the formation of more complex membrane structures and modulate membrane function: such as in MLRs, endosomes, exosomes, and for cell adhesion[77–80]. Lipid membrane composition has been shown to affect membrane microdomain properties and have important implications in cellular behavior under normal physiological and pathophysiological states.

The polyunsaturated fatty acids (PUFAs) are a very important class of lipids not only for their role in membrane structure but also as precursors for important signaling cascades[81,82]. The lipids arachidonic acid, eicosapentaenoic acid (EPA) and docosahexaenoic acid (DHA) are important for fatty acids for membrane structure in particular for nervous system function[81,83]. Increased membrane DHA may lead to decreases in MLR cholesterol and sphingomyelin content as it induces disorder in the lipid membrane due to steric incompatibility with cholesterol, driving phospholipids to laterally rearrange, effectively increasing lipid raft size and fluidity, and modifying MLR distribution[83]. PUFAs have been found to localize within MLRs and non-MLR areas of the cellular membrane in a structurally dependent fashion [84]. EPA has a tendency towards distributing into non-raft domains and DHA appears to localize within raft domains nearly twice as much as EPA, while both DHA and EPA can induce membrane order and disorder depending on the region of the membrane upon which they partition[84]. This may be explained by considering that EPA partitioning into non-MLR regions increases MLR order by driving cholesterol to laterally organize within the raft, conversely DHA may have the opposite effect of displacing cholesterol from the MLR. The effects of PUFAs and cholesterol on membrane structural properties are very important in the brain, brain aging and AD, as brain lipid concentrations are enriched in these lipids and brain lipid composition and distribution changes with age and in AD[85,86].

Aging and peroxidative damage to membrane lipids change membrane composition and thus biophysical properties contributing to AD pathology[87,88]. PUFAs are highly susceptible to lipid peroxidation as they contain multiple double bonds which can be readily oxidized, producing biomarkers of oxidative stress, including: malondialdehyde and 4-hydroxy-noneal (HNE)[88,89]. Depletion of unsaturated fatty acids by lipid peroxidation may increase membrane rigidity and lipid membrane permeability[83,90–92]. Though it is a complicated effect as oxidation can shorten tails and increase the hydrophilicity of membrane lipid tails due to aldehyde and hydroxyl groups[93]. To a lesser extent, cholesterol can also be oxidized which reduces lipid membrane thickness, changing internal bilayer structure, inducing domain formation in model lipid membranes[94]. Oxidation of the membrane increases the number of MLRs through a combination of increased cholesterol[94] and decreased PUFAs, however it has been observed to have no effect on the lateral size of the domains, though these results are not likely to be

generalizable[83]. Lipids prone to oxidative damage will form reactive ketones and aldehydes that can damage membrane proteins, other lipids and which act as damage associated molecular patterns activating the toll-like receptors (TLR) of immune cells triggering inflammation[95]. Thus, oxidative damage can trigger an inflammatory-reactive oxygen feedback loop. Oxidative stress also upregulates sphingomyelinases that deplete membrane sphingolipids (including gangliosides), simultaneously increasing membrane ceramide levels[96]. This reduction in gangliosides may in turn modulate the size and distribution of MLRs within the membrane. Interestingly, in fibroblasts, despite increased membrane cholesterol during replicative cell aging there was an observed decrease in the proportion of membrane cholesterol found within MLRs, which suggests complex changes in lipid composition occur with age[97]. Since the cell membrane is generally an interface for interactions between the cell and its environment, it is not surprising that changes in plasma membrane lipid composition have been shown to affect processes at the membrane by changing membrane receptor distribution, trafficking, and function.

Other molecules also influence membrane lipid composition, structure, and function. Small endogenous signaling molecules like neurotransmitters and neurohormones have been shown to interact with lipids and have an influence on membrane properties. Dopamine is a tyrosine derived neurotransmitter that along with its precursor L-dopa may interact directly with lipid headgroups as suggested by all atom molecular dynamics (MD) simulations and measured by UV and NMR spectroscopy [98,99]. In a similar fashion serotonin has been predicted by MD simulations and experimental evidence indicates a likely interaction with lipid headgroups and influence membrane surface properties[100–103]. Melatonin is an indole related to serotonin which is more hydrophobic than both dopamine and serotonin that has been shown to be membrane active, in contrast to dopamine and serotonin, melatonin penetrates deeper into the hydrophobic core of the lipid membrane and increases membrane compressibility [100,104,105]. All three of these endogenous signaling molecules have been shown to have antioxidant properties and prevent lipid peroxidation [102,106–108]. Combined neurotransmitter interactions with lipid headgroups could facilitate these molecules finding and binding to their respective receptors and moreover serve a secondary role as a neuroprotective antioxidant, preventing lipid peroxidation within synapses.

1.3 Membrane Proteins, the Plasma Membrane and Neuronal Signaling

1.3.1 Membrane Receptor Types and Signaling Crosstalk

Membrane receptors are crucial for mediating interactions between cells and their environment, triggering signaling cascades that relay important information to the nucleus, informing cells on how to respond so that they can maintain cellular homeostasis and differentiate along their cell fate trajectories to serve organ-specific functions. There are several classes of membrane-receptor proteins that are important for neuronal function, neural signal propagation, synaptic transmission and plasticity; these classes are illustrated in Figure 1.4. G-protein coupled receptors (GPCRs) are observed ubiquitously as the largest class of receptors in physiology making them key targets for pharmacological intervention[109], they are involved in metabolic processes (lipid sensing and metabolism)[110], cellular differentiation (cell fate, maturation), and are perhaps most well known as targets for neurotransmitters, like epinephrine, dopamine and serotonin[111]. The receptor tyrosine kinases (RTKs) are another important family of receptor proteins which contain an intracellular catalytic region that phosphorylates downstream signaling participants, typically acting as receptors for larger growth factors and protein hormones such as insulin, platelet-derived growth factor (PDGF), neural growth factor (NGF), to promote neuronal growth during development and maintaining cellular homeostasis in adulthood[112]. RTKs typically require dimerization, which is facilitated by ligand binding to initiate the signaling cascade, and many have been shown to be membrane microdomain dependent. Finally, the ligand-gated ion channels (LGIC), also called ionotropic membrane receptors, are another class of receptor that are especially important for neuronal synaptic transmission so that neuron-neuron signal propagation can occur[113]. The LGICs in the post synapse of excitatory CNS neurons are the NMDA and AMPA receptors, both glutamatergic receptors, while inhibitory neurotransmission is mediated by GABA receptors. Activation of excitatory LGICs allow cations (Ca^{2+} and Na+) to enter the cell, evoking post-synaptic membrane potential spikes by depolarizing the membrane; in contrast, the inhibitory GABA receptors allow chloride anions to enter the cell lowering cell membrane potential further polarizing the neuron and preventing depolarization.

GPCRs are a class of structurally similar transmembrane proteins that contain 7 transmembrane helices[109,114]. Despite their similar structure GPCRs are the largest and most

diverse membrane receptors in eukaryotes[109]. GPCRs associate with heterotrimeric G-proteins, named because they partner with nucleotide guanosine phosphates (GDP/GTP)[114]. When a GPCR is activated, a conformational change causes the G_{α} to dissociate from the $G_{\beta\gamma}$ complex, a process involving conversion of the G_{α} associated GDP into GTP (Figure 1.4)[109]. These separated G-proteins can then inhibit or promote secondary intracellular signaling pathways depending on their identity, which has a variety of effects on cells activating transcription factors, such as Extracellular Receptor Kinases (ERK), Nuclear Factor-κB (NF-κB) controlling protein expression, metabolism, differentiation, and proliferation. These intracellular pathways do not occur in isolation but overlap with multiple redundant and/or overlapping signal cascades, resulting in complex signal crosstalk with other receptor signaling pathways.

In addition to direct activation of RTKs by their ligands, they can also be activated though intracellular pathways initiated by GPCR activation in an important type of receptor crosstalk phenomenon independent of the RTK ligand being present; this process is called transactivation[115]. In neurons, the tropomyosin-related kinase B (TrkB) is a MLR dependent RTK whose endogenous ligand is brain-derived neurotrophic factor (BDNF)[116]. BDNF is important for neuronal survival, neural plasticity and is neuroprotective against Aβ[117], while the TrkB receptor has been associated with AD [118]. The activation of TrkB receptor activates phospholipase C-γ (PLCγ) which converts phosphatidylinositol in the membrane into diacylglycerol (DAG) and inositol 1,4,5-trisphosphate, effectively depleting membrane phosphatidylinositol[119]. This inevitability will also affect membrane composition and structure, although this effect has not been characterized. TrkB activation is important for the regulation of glutamatergic ion channel receptors (such as NMDA receptors) in a PLCγ dependent fashion [120]. As well, the full-length isoform of TrkB can be transactivated by the serotonin ($5HT_7$) receptor[121], while 5-HT_7 can also transactivate platelet-derived growth factor (PDGF) receptor, another RTK, providing neuroprotection against N-Methyl D-Aspartate (NMDA) induced excitotoxicity[122]. This is one of many examples of complex signaling pathways which are occurring within neurons at any given moment in time.

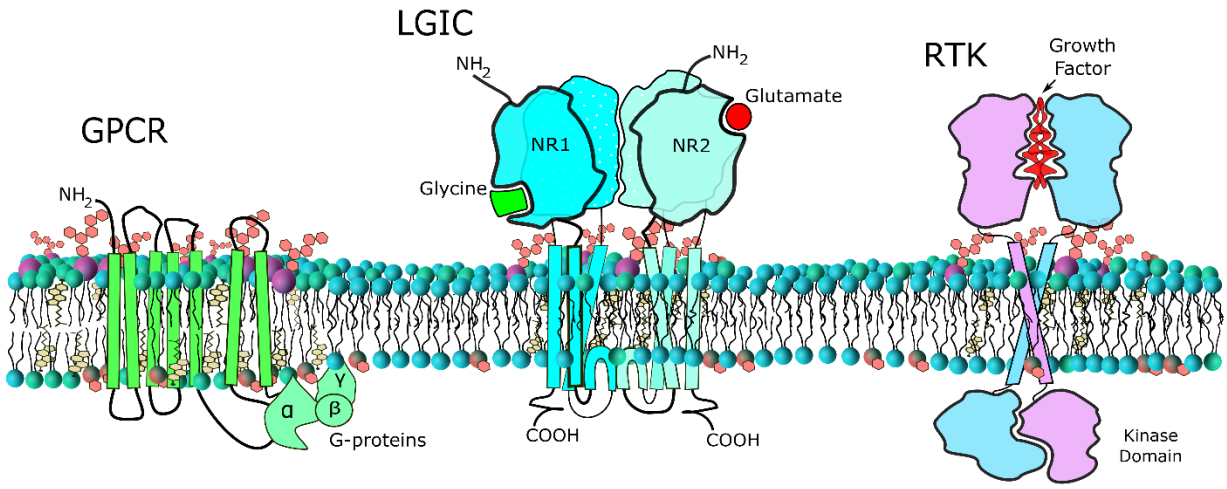

Figure 1.4. Key classes of membrane receptors embed in lipid bilayer. *GPCRs are the most abundant type of receptor in the human body, often referred to as metabotropic receptors. LGICs are the primary excitatory and inhibitor neurotransmitter receptors in the central nervous system. RTKs are growth factor receptors that mediate cell growth, proliferation and differentiation during development and aid in maintenance of cells during adulthood.*

1.3.2 The Membrane Dependence of Membrane Receptors and Proteins

The function of membrane receptors is modulated by the properties of the local lipid environment and thus the composition of the membrane and their localization in the membrane, for instance whether they are in MLRs or non-raft regions. This is important for immune and neuronal signaling and plays a crucial role in the production of Aβ. The mechanisms for this are complex as membrane cholesterol can affect ligand binding properties of membrane proteins by directly interacting with various residues of the protein (allosteric regulation) or indirectly by altering membrane properties that then affect conformation and stability of membrane proteins.

Cholesterol transporters can influence inflammatory signaling in microglia and macrophages by regulating membrane cholesterol content[123–125]. This was shown in ATP-binding cassette-A1 (ABCA1) knockout mice which have 27% more free cholesterol in the lipid rafts of the cell membranes of their macrophages and microglia, while phospholipid content remains unchanged; consequently, ABCA1 knockout mice macrophage are ultrasensitive to activation by lipopolysaccharide (LPS)[124]. Similarly membrane cholesterol increases were shown to increase neuroinflammation in spinal cord microglia in mice models with deleted cholesterol transporters, an effect linked to TLR4 activation, with normalization of membrane cholesterol alleviating inflammation associated neuropathic pain[126]. It was suggested that increased membrane cholesterol increases lateral TLR trafficking and MLR crosslinking both necessary for TLR activity[124]. The increase in cholesterol is counter-regulated by the formation of specific sterols

(oxysterols) which activate pathways for the removal of cholesterol from cells mediated by cholesterol efflux transporters (e.g. ABCA1) onto high-density lipoproteins, for example in the brain this is mediated by Apolipoprotein-E (ApoE) [125,127]. This suggests that innate immunity in both the periphery and in the brain is regulated by membrane cholesterol content as a means of modulating the inflammatory response[128]. This is likely important during acute infection to remove pathogenic material and damaged cell components, but in chronic inflammatory conditions (such as AD, type II diabetes, atherosclerosis), cholesterol aggravated inflammation may facilitate disease progression[129]. This principle of membrane lipid content modifying MLR distribution is an important concept in understanding signaling cascades in a variety of physiological and pathological states and certainly plays a role in neuronal signaling.

In the brain, GPCRs, RTKs and ion channels depend on the membrane for their function. The function of many serotonin receptors (including: 5-HT_{1A}, 5-HT_{2A} and $5HT_7$), have been shown to depend on membrane cholesterol[130–132]. Molecular dynamics simulations demonstrate that membrane cholesterol increases the stability of the serotonin-2A receptor (5-HT_{2A}) ultimately affecting the binding of various antipsychotic drugs[133]. Other studies indicate that membrane cholesterol can affect the interaction between GPCRs (like many of the 5-HT receptors) and their associated G-protein[132,134]. NMDA and TrkB receptors are found co-localized within membrane-microdomains, often used as models for MLRs[135–138]. The level of cholesterol can modify receptor activity as demonstrated by cyclodextrin-mediated cholesterol depletion from cultured neurons reducing glutamatergic excitotoxicity by decreasing expression of NMDA at the membrane[139]. TrkB activation has been shown to be membrane composition dependent, where cholesterol depletion reduced BDNF-induced translocation of TrkB to the membrane, impairing neurotransmitter release in cultured neurons and tissue slices[138]. As the majority of RTKs initiate dimerization upon ligand binding, it is likely this process requires the reorganization of the local lipid environment, this could in part explain the membrane lipid dependence on RTK activity.

The MLRs of cell membranes have been shown to be involved in AD pathology in relation to the toxic mechanisms of Aβ (to be discussed in the next section) and by affecting Aβ production [140,141]. Aβ is produced in cholesterol-sphingolipid enriched membrane microdomains during endocytic recycling[142], with reports indicating that cholesterol depletion reduces

amyloidogenic processing of APP by the secretases[143], although this contradicts an earlier report that indicated the opposite[144]. This is likely because decreased cholesterol reduces trafficking of β-site APP cleaving enzyme (or β-secretase), γ-secretase[145,146], and APP to membrane-microdomains[143]. This suggests that increased ceramide and cholesterol in the cell membrane due to oxidative stress and/or perturbed lipid metabolism may increase amyloidogenic processing of APP and Aβ production[96], possibly because oxidative stress depletes membrane phospholipids through lipid peroxidation[85,147]. Membrane composition has been implicated in the production of Aβ, conversely, Aβ has been shown to affect metabolism of MLR components, cholesterol, and sphingolipids, suggesting a potential physiological role for Aβ in lipid homeostasis through a counter-regulatory relationship[16,143–145,148,149].

1.4 The Toxic Mechanisms of Amyloid-B Depend on the Plasma Membrane

The toxic mechanisms of Aβ are complex and have been shown in separate studies to involve apoptotic and necrotic mechanisms that depend on membrane- and receptor-dependent processes[150,151]. The lipid membrane is an important site of Aβ binding and aggregation[42], and thus membrane composition and MLRs likely affect amyloid toxicity through mechanisms involving membrane disruption, calcium dysregulation and oxidative stress[140], ultimately inducing tau pathology. Non-specific interactions of Aβ with model lipid membranes demonstrate a composition-dependent effect on the biophysical properties of the membrane and structural defects in the membrane[19,20] and these interactions may result in the formation of reactive oxygen species (ROS) that damage membrane lipids[140]. Ultimately, disruption of the membrane perturbs signal propagation between neurons and along neural pathways, likely occurring well before neuronal cell death.

1.4.1 Cellular Studies Indicate Membrane Dependent Amyloid-β Toxicity

Conflicting reports have been published indicating that membrane cholesterol content can both enhance and reduce Aβ cytotoxicity, while decreased gangliosides appears to be neuroprotective against Aβ [21,22,152–156] . In PC12 and SH-SY5Y cells, Yip et al. reported that a 60% reduction in membrane cholesterol, achieved by methyl-β cyclodextrin (MβCD) treatment, increase in cell death of cells exposed to 22μM of preformed fibrillar Aβ[156]. In a report by Arispe et al., they demonstrated a similar effect in PC12 cells, where cholesterol depletion by

cyclodextrin or inhibition of *de novo* cholesterol metabolism made cells more vulnerable to Aβ, while increased cholesterol was neuroprotective[155]. Other reports however report the opposite, that reduction in cholesterol content protects cells against amyloid; for example, Wang et al. reported that in PC12 cells cholesterol and ganglioside sialic acid depletion reduced amyloid toxicity by limiting GTPase activity[154]. In mixed neuronal-astrocyte cultures, membrane-cholesterol positively correlated with both astrocytic and neuronal cell death induced by Aβ exposure[21]. Nicholson et al., in two separate studies, showed that increased membrane cholesterol content increased the susceptibility of mature hippocampal neurons to Aβ toxicity through mechanisms involving calpain-activated cleavage of tau protein and subsequent collapse of neuronal microtubules[152,153], and that this occurred alongside changes in the content and localization of NMDA receptors at the membrane[153]. Inhibition of glucosylceramide synthase, important for ganglioside biosynthesis, resulted in neuroprotection against Aβ oligomers *in vitro* and *in vivo*[157]. A reduction in ganglioside content of MLRs was shown to reduce Aβ oligomer recruitment to the MLRs in rat cortical neurons, subsequently preventing lipid peroxidation, membrane permeabilization and calcium dysregulation[140]. The conflicting reports of how membrane cholesterol mediates Aβ toxicity underscore a lack of understanding in the mechanisms of membrane dependent Aβ neurotoxicity.

1.4.2 Non-Specific Membrane Interactions in Aβ Toxicity

The molecular mechanism of Aβ-induced cytotoxicity depends on accumulation at the neuronal membranes through non-specific interactions[19,20,156,158–161]. Studies in model lipid systems indicate that Aβ induces defects in lipid membrane structure through a multistep process that involves Aβ binding to the membrane increasing membrane disorder and permeability, reorganization, conformational and changes of the dynamics of lipid molecules, then the formation of Aβ ion channels that perforate the membrane, ultimately disrupting membrane potential, ionic and osmotic homeostasis across the cell membrane[162–164]. These deleterious effects of Aβ depend on the identity Aβ peptides and the structure of higher order aggregates, as well as membrane composition, structure, and properties[19,20,165]. Interestingly there are differences in the aggregation rates and toxicity of different Aβ isoforms. The most toxic form of Aβ is the 42 or 43 amino acid peptides, while Aβ40 is less toxic and aggregates at slower rates. Aβ has been shown to directly induce lipid peroxidation in model lipid systems [166], suggesting

direct interactions of membrane lipids with Aβ play a role in oxidative stress observed *in vitro* and *in vivo*. These studies suggest that changes in lipid membrane composition occur in AD and may sensitize neuronal membranes to Aβ damage.

Biophysical studies demonstrate that cholesterol and gangliosides dramatically affect amyloid aggregation on model lipid membranes and that this induces severe topographical defects, increasing surface roughness, and increases permeability [19,20]. Atomic force microscopy (AFM) imaging has shown that nanoscale topographical and electrostatic features of cell membranes may cause preferential binding of charged Aβ residues and alignment of β-sheets for further growth into fibrils[20]. This was demonstrated when comparing Aβ aggregation on pure dioleoyl phosphocholine (DOPC) membranes containing cholesterol with pure DOPC membranes alone[20]. Membrane cholesterol also increases binding of Aβ to the membrane and appears to preferentially aggregate on gel-phase domains that are produced from the cholesterol-induced condensation of lipid molecules[161]. Other AFM studies indicate that Aβ forms multimeric channel-like structures when Aβ is reconstituted into a planar bilayer system, these channels were shown to be selective toward calcium ions but were blocked by zinc ions[164]. This information relates the calcium dysregulation observed *in vitro* and *in vivo* directly to the membrane perforating activity of Aβ.

The mono-sialic acid containing ganglioside GM1, has been shown to be important for oligomeric Aβ binding (but not fibril binding) to the cell membrane which then act as a seed for further amyloid binding [159,160,167]. The binding capacity of Aβ to model membranes was found to be increased with GM1 and cholesterol content, though the binding affinity was unaffected, and that binding initiated the transition from α-helix to β-sheet[159]. The presence of GM1 in the membrane increased Aβ binding to model membrane vesicles by a factor of 1.8, which corresponded to an increase in membrane permeability of the vesicles by a factor of 2 [160]. Another study by Drolle et al, using the black lipid membrane electrophysiology technique, demonstrated in complex neuronal model lipid membranes that mimic healthy and diseased neurons that losses in membrane GM1 and sphingolipids (which correlate with AD progression) increase susceptibility to Aβ ion currents, an indication of increased membrane permeability and damage[19]. Furthermore, Drolle et al. using AFM performed structural analysis of these healthy and diseased neuronal models identifying that those small decreases in GM1 and sphingomyelin had pronounced effects on membrane structure and influenced the interaction and penetration of

Aβ into the lipid bilayers[19]. Taken together this suggests that GM1 increases binding of Aβ to the membrane, but that insufficient GM1 sensitizes cells to the permeabilizing effect of Aβ possibly through loss of MLRs. AFM studies have also revealed a detergent-like effect of Aβ on model lipid membranes, where Aβ is suspected to solubilize and destabilize membrane interactions with the mica substrate, liberating them from the surface[168,169].

Not only is the outer plasma membrane a target for Aβ, but the mitochondrial membrane has been directly linked to oxidative stress and Aβ interactions[170–172], with changes in mitochondrial lipids in AD[173]. Lipid peroxidation may be directly induced by Aβ through interactions with copper ions, as copper-Aβ complexes can produce H_2O_2 in the presence of reducing agents and O_2 [166,174], all abundant in the mitochondria. These effects on the mitochondria may explain the impaired metabolism and oxidative stress observed in cell studies, animal models and AD patients.

1.4.3 Aβ – Membrane-Receptor Interactions in Alzheimer's Disease

Aβ-induced neuronal plasma membrane disruption will inevitably affect signaling pathways important for neuron-neuron communication across synapses, due to the high degree of membrane surface area across the hundreds of trillions of synaptic clefts in the neocortex and hippocampus of the human brain[175,176]. There are many receptor signaling systems associated with dysfunction in Alzheimer's disease and there is evidence for Aβ interactions with GPCRs, neurotrophic factor RTKs, and ion channels[118,177–180]. Traditionally, AD has been characterized by cholinergic dysfunction, with few minimally effective acetylcholinesterase inhibitor drugs approved for symptom management in AD [181,182]. Memantine is a potent NMDA receptor antagonist that is approved for treatment in moderate and advanced AD, which suggests there is evidence of excitotoxic NMDA mechanisms in AD[183–185]. Serotonin receptor activation has recently been shown to restore synaptic function in AD rat models and is associated with age-related changes in cognitive function[186]. A variety of important brain growth factor receptors have also been shown to be involved in Aβ toxicity such as P75 neurotropic growth factor receptor (P75NTR) [187,188] and TrkB receptors[117,118,177]. Finally, insulin receptor signaling, and insulin-degrading enzyme have been found to interact with Aβ and are dysregulated in AD[189–191].

Cholinergic dysfunction is associated with AD and though there are few drugs available on the market to improve cholinergic signaling for AD treatment, they are minimally effective

[181–183]. The cholinergic hypothesis of AD suggested that a loss of cholinergic neurons, especially the α7 nicotinic acetylcholine receptors (nAChR), and perturbed acetylcholine metabolism in the brain was the cause of learning and memory decline in AD patients[182,192,193]. Acetylcholinesterase inhibitors have been approved for use in mild to moderate AD for over 20 years; they act by increasing the amount of acetylcholine in the brain by preventing acetylcholine degradation[183]. These drugs provide a significant benefit in ameliorating the symptoms of cognitive decline for a short time (6 to 12 months) in early AD, although the benefit of long-term use is debatable[183]. The overuse of these drugs in treating AD may be problematic, as many patients are kept on acetylcholinesterase inhibitors much longer than is therapeutically beneficial, and long-term effects of these drugs are not well-studied[183].

There is good evidence to suggest that NMDA receptor activation is upregulated in AD to the point of generating excitotoxicity, which has been related to calcium signaling dysfunction and that this is related to the mechanisms of Aβ neurotoxicity[39,194]. Memantine is a potent NMDA receptor antagonist that has been shown to mitigate the symptoms of cognitive decline in AD[183,195]. A recent study has demonstrated that increased NMDA receptor levels in the membrane increases Aβ binding to the membrane, suggesting that membrane disruption of Aβ can be mediated by NMDA receptor levels in the membrane, which must act as binding sites for the toxic aggregates [196]. Further studies have shown that various subunits of the NMDA receptor can bind Aβ directly [197,198]. Aβ also promotes endocytosis of NMDA receptors and in line with that observation was shown to reduce NMDA-evoked currents using whole-cell recording[197].

Several GPCRs are known to interact directly with Aβ which modulates their activity. One example is the metabotropic glutamate receptor-5 (mGluR5) which has been shown to directly bind Aβ in co-immunoprecipitation and competitive binding assays[198]. Exposure of neurons to Aβ may cause mGluR5 to preferentially localize within dendritic spines by reducing lateral membrane diffusion of mGluR5 out of the synapse[198]. This indicates that Aβ accumulated at the synaptic membrane modulates receptor trafficking.

Serotonergic signaling, largely through 5-HT GPCRs, modulates a variety of neurotransmitter and neurotropic receptor pathways in neurons. Loss of serotonergic signaling has been associated with cognitive decline in aging and AD[199]. Serotonin signaling has been shown to induce changes in cholinergic and glutamatergic signaling[122,200–203], as mentioned

previously, both of which are implicated in AD. In addition to serotonin modulating neurotransmission serotonin receptor activation can also affect the activity of growth factor RTKs, including TrkB and PDGF receptors[204–206]. Activation of 5-HT receptors can have neuroprotective benefits against NMDA excitotoxicity in a PDGFβ receptor dependent fashion [122,200].

Several neurotrophic growth factor (NGF) receptors are affected by AD and Aβ pathology; the most well-known of which is the p75 neurotrophin receptor (p75NTR)[187,188,207,208], while the TrkB receptor is newly recognized for its potential importance in AD[118,178,209]. Treatment of SH-SY5Y human derived neuroblastoma cell line with Aβ was shown to increase membrane levels of the p75NTR receptor[208]. Aβ has been shown to directly interact with the extracellular domain of p75NTR and that neurons that express more p75NTR are more susceptible to Aβ toxicity through apoptotic mechanisms and are associated with neurite dysfunction[187,188]. Since P75NTR is a membrane bound protein whose extracellular domain binds Aβ, this may increase accumulation on the membrane contributing to the non-specific mechanisms of Aβ neurotoxicity, though this was not addressed in these studies. The p75NTR signaling overlaps with and modulates TrkB receptor activity[210]. BDNF which activates the TrkB receptor has been shown to protective against Aβ, *in vitro* and *in vivo*[117]. Conversely, Aβ has been shown to cause dysregulation of TrkB receptors by modifying TrkB isoform levels[177], reducing the ratio of full-length TrkB to truncated TrkB at the level of mRNA and in a calpain-dependent fashion[118,178].

Insulin signaling in the brain has been strongly linked to AD, with some researchers suggesting AD could be consider a type 3 diabetes[191,211]. Aβ competitively interferes with insulin and insulin-like growth factor (IGF) receptors and perturbs insulin signaling in that brain[211 129] and is a substrate and competes with insulin for insulin degrading enzyme[189,212]. The association of impaired insulin signaling in AD may not simply be due to direct Aβ interactions, but may also involve inflammation, and lipid dysregulation, which are both linked to brain insulin-resistance that can occur independent of-, or simultaneously with-, AD pathologies[213,214].

1.4.4 Signal Transduction Pathways Affected by Amyloid-β

The activation of membrane receptors triggers signal transduction pathways that relay information about the cellular environment to the nucleus of cells. Unsurprisingly several

proteins in these cell signaling pathways have been implicated in AD and/or associated with Aβ toxicity, these include, but are not limited to: ERK1/2, raf-kinase, and phosphatidylethanolamine binding protein (PEBP)[215,216]. These pathways are initiated at the cell membrane, with these proteins acting as downstream effectors of the receptor signaling pathways mentioned in the previous section. ERK1/2 signaling as been shown to be increased in response to toxic levels of Aβ[217,218]. PEBP has been shown to be decreased in AD mouse models[219] and decreased mRNA in CA1 region of the AD hippocampus[220]. PEBP is a cytosolic secondary messenger, and a phospholipid binding protein that plays a role in regulating signal transduction from the cell membrane acting to inhibit Raf kinase and also acting as a stimulatory protein for hippocampal cholinergic signaling[221], an important neurotransmitter system for learning and memory.

1.5 Inflammation and Lipid Metabolic Dysfunction in Alzheimer's Disease

The pathogenesis of AD at the earliest stages is not well understood, that is the specific cause and effect relationships, although progress has been made. The pathological mechanisms of the amyloid cascade, both the production of Aβ from APP and Aβ neurotoxicity, depend on membrane structure and composition[17,141,222]. Thus, a strong case can be made that lipid membrane composition and structure may play a role in AD pathogenesis. If this is the case on the molecular and cellular level, for it to be clinically relevant there should be evidence at the genetic and epidemiological levels. There is such evidence in lipidomic studies which indicate differences in brain lipid composition between AD patients and age-matched controls[223,224]. A good candidate for the mechanism of these changes in brain lipid composition is neuroinflammation, as this is ubiquitously observed in AD pathology, and inflammation is, in part, regulated by lipids and lipid metabolism[225,226]. Finally, genetic and epidemiological studies support the notion that neuroinflammation and perturbed lipid homeostasis are involved in AD pathogenesis [18,227].

1.5.1 Lipidomic Studies of Alzheimer's Disease

Changes in brain lipid composition has been observed in AD patients and animal models[85,223,224]. These changes in brain lipid levels do not speak to the changes at the level of specific brain cell types or subcellular structures though some anatomical information is available[223,224]. Overall, the following changes in brain lipid composition have been observed in AD patients and animal models, especially in AD sensitive brain regions, for instance: increased

ceramide and cholesterol ester levels[85,223,224], decreased white matter cholesterol[228], depletion of polyunsaturated fatty acids and increased saturated fatty acids[5,85,229], changes in membrane phospholipid content (i.e. phospho-inositol, -choline, -ethanolamine)[85,224,230], and in general decreases in sphingomyelin and ganglioside levels[224,231,232]. These changes in lipid composition need be considered carefully since brain lipids are found within cell membranes, as much of brain lipid content, especially cholesterol, is found within the myelin sheaths formed by oligodendrocytes that surround neuronal axons.

Analysis of brain lipid extracts from autopsy confirmed AD patients indicate increased ceramide levels, decreased sphingomyelin, increased cholesterol, and HNE (a marker of lipid peroxidation)[96]. These changes were found in brain areas associated with vulnerability to AD but were largely absent in non-vulnerable brain areas[96]. When looking only at non-AD aged mice (25 months) compared to young pups (3 and 6 months) there is an increase in ceramide and decrease in sphingomyelin, alongside increased HNE[96]. This is unsurprising as oxidative stress and inflammation are known to increase activity of sphingomyelinases which cleave the headgroup of the sphingolipid leaving ceramide in the membrane[233]. The fact that this was observed in non-AD aged mice indicates that these changes in lipid composition can precede and can occur independent of Aβ pathology[96]. Other studies indicate increased lipid peroxidation by-products and a reduction in unsaturated fatty acids in AD models and AD patients[229]. These changes can be associated with oxidative stress in the brain, and it appears that these changes can precede or occur independent of increased Aβ, although Aβ has been shown to cause oxidative stress induced lipid composition changes [140,170].

Several studies have indicated that brain cholesterol content in AD is decreased, likely due to loss of myelination[228] since cell membranes are expected to become enriched with cholesterol because of aging[97]. Brain white matter contains a large amount of myelin, which itself contains 70 to 80% of brain cholesterol[234]. This may suggest that cholesterol loss in AD preferentially occurs within myelin and not necessarily membrane cholesterol, although more work is needed in this area. Though lipidomics studies indicate major changes in brain lipids with aging and AD, the distribution of lipids amongst the various cell types in the brain, or the fraction of lipids within the membranes of each cell type is not well-established and data in this area may go a long way to understanding the aging brain. These studies indicate the importance

of lipids in AD, but it is hard to draw a causal link between changes in lipids and AD pathogenesis. Epidemiological and genetics studies may however provide evidence for the causative role for disturbed lipid homeostasis in the initiation of Aβ pathology and thus AD pathogenesis.

1.5.2 Genetic and Epidemiology of Alzheimer's Disease

There is a small subset of aggressive AD in the population, accounting for about 5% of cases; these are associated with mutations in APP or the presenilin subunits of the γ-secretase complex (PSEN1 and PSEN2), called familial AD (FAD) [18,235,236]. In FAD, the cause of neurodegeneration appears to be directly related to the overproduction of neurotoxic Aβ, either because the cleavage site of APP is more susceptible to enzymatic processing, or that the secretase activity is greatly enhanced[237]. Transgenic FAD mice are often used as models for AD in general [238–240], though there are many important distinctions between FAD and the more common late onset forms.

The more prevalent late-onset AD, accounting for 95% of AD cases, have a very similar phenotype to FAD with symptoms of impaired learning and progressive memory loss, the underlying molecular hallmarks of Aβ and NFTs, although occurring much later in life and progressing more slowly[18,237]. The greatest genetic risk factor for late onset AD is the APOE ε4 allele, with these individuals developing AD reliably sooner and progressing faster than others with other APOE alleles[18,241]. APOE is the quintessential cholesterol trafficking apolipoprotein in the brain[242,243]. In the last decade, genome wide association studies (GWAS) have identified more than 30 genes associated with increased risk for AD[24,25,27,244,245]. Many of these genetic loci are associated with endosomal sorting, cholesterol metabolism and trafficking, immune function, protein catabolism, and others that are more directly related to Aβ and tau pathways[18,24,25,27]. Genetic predisposition and/or epigenetic changes induced by lifestyle and environmental factors likely combine in some complex interaction to initiate AD cascade, with increasing evidence for lipid homeostasis and immune function as primary factors.

Epidemiological evidence indicates that traumatic brain injury (TBI), systemic infection, diet and mental health disorders are linked to risk of developing AD[18,129,227,239,246–249]. Diets high in saturated fat and sugar, sedentary lifestyle and psychosocial stress are common risk factors for a variety of metabolic diseases and mental health disorders that are also co-morbidities of

Alzheimer's disease, such as: obesity and type 2 diabetes[129,250], along with depression[247,248] and bipolar disorder[249]. High-fat diet and high fructose intake are known to cause inflammation-induced insulin resistance and have been associated with AD[239,251–253], while the anti-inflammatory Mediterranean diet has been shown to reduce risk of AD and thus may be neuroprotective[254–256]. The relationship between lifestyle-induced metabolic syndromes, mental health and AD remains unclear but is likely associated with inflammation, oxidative stress, perturbed insulin signaling and impaired brain lipid homeostasis.

1.5.3 Neuroinflammation, Cholesterol and Insulin in Alzheimer's Disease

There is an abundance of evidence that neuroinflammation plays a key role in AD, occurring alongside many of the co-morbidities discussed earlier. Microglia are resident immune effector cells of the brain. Activated microglia are found co-localized with Aβ plaques in both AD animal models and human patients[257], alongside elevated inflammatory biomarkers in the brain and periphery[225,226]. This is intuitive as Aβ balance in the brain is in large part regulated by degradation from microglia and macrophage phagocytosis[257–261]. Inflammation is also strongly related to insulin-resistance in type II diabetes, and this has been shown to disrupt brain cholesterol metabolism, linking the observations of impaired insulin signaling and lipid metabolism dysregulation to AD [129,262,263]. Neuroinflammation appears to act in positive feedback with Aβ, where systemic and neuroinflammation causes oxidative stress and perturbed lipid metabolism that increases production of Aβ, then the increase in Aβ levels contributes to further neuroinflammation and the cycle may run away. A model for this feedback mechanism is illustrated graphically in Figure 1.5.

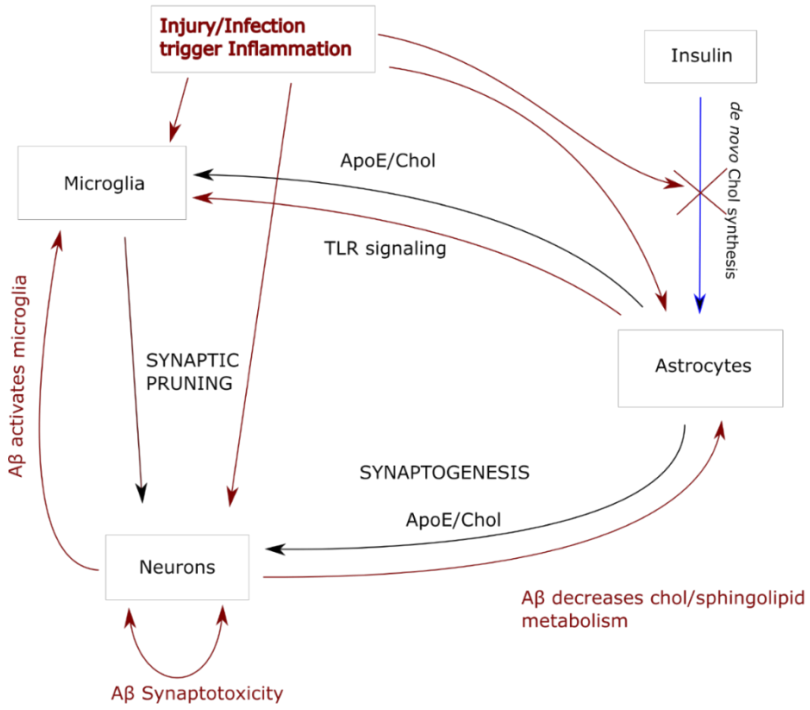

Figure 1.5. A feedback model of inflammation, Aβ, and cholesterol homeostasis in the pathogenesis of Alzheimer's disease. *Chronic injury and inflammation decrease de novo cholesterol synthesis in brain by acting on insulin. Inflammation upregulates ABCA1 cholesterol transporters in microglia, increasing trafficking of ApoE loaded cholesterol from astrocytes to microglia increasing TLR sensitivity towards damage associated molecular patterns and sustaining inflammation, in addition this reduces available cholesterol for neurons and oligodendrocytes which rely on cholesterol for synaptogenesis and myelin formation. Microglia play an important role in synaptic pruning, thus increased microglial activation may tip the balance of synaptogenesis and synaptic pruning towards a net loss in synapses. Injury to neurons from inflammation increases Aβ production which damages neurons especially through synaptotoxicity decreasing the number of synapses in brain, and which further activates microglia triggering positive feedback. Aβ has been shown to decrease cholesterol and sphingolipid production in brain, further limiting the cholesterol available for synaptogenesis and myelin, but also acting as a negative regulator of microglial activation. Aβ also interferes with insulin signaling in the brain by competing with insulin contributing to these overlapping feedback mechanisms. Thus, increases in inflammation causes increased Aβ production which over chronic periods of time is a major contributor to AD pathology through lipid mediated mechanisms.*

Proinflammatory cytokines act on brain targets through circumventricular organs by diffusion to produce changes in behavior associated with sickness, including weakness, lethargy, difficulty concentrating and social withdrawal[264]. In animals, peripheral injection of exogenous LPS, at levels below sepsis induction, induce expression of tumor necrosis factors (TNF) and Interleukin(IL)-1 in brain and results in flu-like symptoms and acute behavioral changes which cease after treatment[264]. Animal models of psychosocial stress have indicated that external stress induces oxidative stress and depression-like behavior while also increasing production of proinflammatory cytokines IL-1, IL-6 and TNF, this subsequently causes a detriment to learning and memory with eventual neurodegeneration being observed[265]. There is a well-known link between depression and AD which may occur through mechanisms involving chronic inflammation, as it has been observed that patients with severe depression have increased serum

proinflammatory biomarkers and the similarities between behavior associated with depression and sickness behaviour[264]. A recent and timely example of this can be seen in Covid-19 patients experiencing what has colloquially been labelled "long covid", which is typically associated prolonged respiratory symptoms alongside neurophysiological symptoms of brain fog, depression, fatigue, weakness, and impaired concentration which has similarities with AD pathology[266,267]. Or similarly the side effect profile of Covid-19 vaccines, especially the mRNA vaccines which induced fever in 13.9% of clinical trial participants[268], compared to only 4.8% in the Novavax clinical trials[269], which is more in line with typical side effects of traditional influenza vaccines[270]. A fever is indicative of a pronounced systemic and neurophysiological response from an immunological insult, as fever is triggered by a hypothalamic response. This combination of pandemic stress (exacerbated by prolonged lockdowns and economic hardship), direct illness from Covid-19, and widespread serious vaccine side effects could thus have far-reaching consequences on Alzheimer's disease risk in future.

Microglia have been increasingly recognized for the role they play in regulating normal synaptic function, but in inflammatory conditions may become overactive and detrimental to proper synaptic function. Microscopic studies demonstrate that microglia actively probe synapses and promote neuroplasticity during brain development[271]. Precisely what the microglia are doing as they probe synapses is not known but early evidence indicates they are able to modulate synaptic pruning and synaptogenesis using classical inflammatory signaling involving cytokine release and NADPH oxidase activation[271]. Studies indicate that Aβ can directly activate microglia to promote neuroinflammation, as Aβ can act as a ligand for the receptor for advanced glycation end-products (RAGE) and the macrophage-colony stimulating factor (M-CSF) cytokine receptor[272,273]. Activated microglia then produce cytokines (TNF-α, IL-1β, IL-6, IL-18) and chemokines (IL-8, macrophage inflammatory protein-1α and monocyte chemo-attractant protein-1) which further activate microglia and recruit white blood cells across the BBB into the brain[226]. Thus, activation of the neuroimmune system contributes to BBB disruption. Mechanisms of microglial sensitization have been proposed to explain how microglia become overly sensitized because of chronic neuroinflammation from early life stressors and that this increases risk for mental health and neurodegenerative disease later in life[274]. In this way the priming of microglia with repeated bouts of infection and TBI may increase the sensitivity to microglia activation and the subsequent response to Aβ and BBB disruption later in life[275,276].

Cholesterol metabolism in the brain is perturbed by inflammation through reduced insulin signaling and insulin-resistance[277]. Insulin acts on the hypothalamus to regulate lipid metabolism in the body and brain[277,278], as it activates sterol regulatory element binding proteins that trigger the biosynthesis of cholesterol and other lipids [279,280]. Cholesterol is synthesized almost entirely *de novo* within the adult brain by astrocytes and oligodendrocytes. Differentiated adult neurons lose their ability to produce cholesterol as they mature and rely on trafficking of cholesterol from glial cells by ApoE (recall that ApoE isoforms modify AD risk)[234,281]. Insulin-resistance or insulin-depletion in the brains of rodents reduces total synaptic membrane cholesterol which in turn limits synaptogenesis, this was demonstrated in both genetic and diet-induced diabetes rodent models[169]. Because immune cell signaling, especially the TLR-4 receptor activation is raft dependent[124], microglial sensitization can be similarly achieved through increased membrane cholesterol content[126], and neuronal plasticity requires cholesterol for synaptogenesis, during chronic neuroinflammation this may create a situation of insufficient cholesterol to maintain both neuronal and microglial processes putting undue stress on synaptic plasticity processes. In summary, during inflammation trafficking of cholesterol away from neurons towards microglia would limit synaptogenesis of neurons and increase synaptic pruning by microglia which may explain the increased sensitivity of neurons to Aβ, and loss of synapses associated with AD.

Due to the proposed role of cholesterol in AD, clinical studies of cholesterol modifying drugs could provide evidence to support or refute this model. Statins are lipid lowering drugs, reducing low-density lipoprotein (LDL) containing cholesterol[282], used in hypercholesterolemia (too much cholesterol in the blood), which is a risk factor for atherosclerotic cardiovascular disease (associated with arterial/veinous plaques)[283]. Statins act by reducing cholesterol metabolism by inhibiting β-Hydroxy β-methylglutaryl-CoA (HMG-CoA) reductase activity, this enzyme is the rate-limiting step in cholesterol metabolism[284]. Statin mechanism of actions also involve a reduction in vascular and myocardial inflammation, reductions in proinflammatory cytokines and C-reactive protein concentrations[284,285]. It appears that some statins may cause mild reversible cognitive impairment at high doses in a subset of patients[286,287]. Meta-analyses of RCTs on statins have also found no effect on cognitive function, though the doses in these RCTs was typically lower than what was identified in observational studies to trigger these cognitive deficits[288]. On the contrary some statins have also been associated with a reduction in the risk of dementia (as measured by reduction in prevalence)[289], for instance a meta-analysis of

observational studies suggests a mild protective effect of statins against AD risk[290], although some studies demonstrate no effect[291]. However, RCTs of statins in AD patients failed to demonstrate any benefit to cognition, although patients with elevated lipid levels were excluded from this study and presumptively these patients would have the greatest benefit[292]. This may indicate that reduction of AD risk would be effective if used earlier in life as a preventative measure, as compared to a treatment for positive diagnosis of AD later in life. In head-to-head comparisons, lipophilic and fungal-derived statins were associated with increased AD incidence compared to hydrophilic statins which did not modify disease risk[293]. In addition, significantly higher rate of cognitive performance deficits was reported by patients using more lipophilic statins compared to hydrophilic statins[294]. Lipophilic statins would have greater BBB permeation potential and thus would decrease brain levels of cholesterol more than hydrophilic statins, with the reduction in brain cholesterol from more lipophilic statins reducing myelination and cholesterol required for synaptic pruning. Thus, statin type, timing of statin use, hypercholesteremia and inflammatory status may explain the paradoxical effects of statins on the brain.

1.6 Conclusion

In AD, the lipid membrane is central to Aβ pathology, both production and toxicity. There are many genetic and epidemiological factors related to lipid and cholesterol metabolism that are mediators of AD risk including: ApoE isoforms and other genes identified in GWAS, lifestyle factors and disease co-morbidities that disrupt lipid metabolism and cause oxidative stress and lipid peroxidation. Inflammation is partially regulated by lipid mediators, and chronic inflammation is expected to be involved in AD pathogenesis and progression. Both lipid metabolism disruption and inflammation can contribute to increasing Aβ production and susceptibility to Aβ toxicity. Subsequently, Aβ causes inflammation and also perturbs lipid metabolism. This is a positive feedback system with the result being ever increasing inflammation, oxidative stress, metabolic dysfunction and Aβ accumulation. By the time symptoms have manifested in AD substantial loss of synapses has already occurred, and it is likely too late to reverse those losses, more so in the later stages of disease. If this hypothesis is correct, it may be necessary to target all three major systems in tandem with anti-inflammatory, antioxidant and Aβ targeted drugs, while removing dietary and lifestyle risk factors, prior to

onset of symptoms. This requires superior diagnostics to predict individuals at risk of AD prior to the onset of symptoms, possibly even decades before symptoms manifest and reversing the chronic inflammatory and metabolic dysfunction prior to the triggering of the Aβ accumulation feedback loop.

The molecular mechanisms of neuronal toxicity in AD involve contributions from each of these features (inflammation, lipid metabolic dysfunction, oxidative stress and Aβ), however the details are not clear. One of the main open questions is whether membrane structural damage or membrane receptor signaling is more consequential in the toxic mechanisms of Aβ, and moreover if lipid membrane composition modifies the primacy of these two interactions. Because the molecular mechanisms have not be fully elucidated, it is not yet clear which aspects are most important to target for disease prevention and treatment. The combinations of small molecules, growth factors, brain lipid composition and Aβ reduction that is necessary to prevent or cure the disease is not known. Lipid membrane function in physiology is often overlooked in favor of a focus on the central dogma of molecular biology: DNA, RNA and proteins as the primary mediators of biology function. Though the central dogma is of primary importance, it alone is insufficient to explain physiology, mechanisms of disease and life more generally, and thus the fundamental role of lipid membranes in compartmentalizing biological phenomena cannot be overlooked.

There are many outstanding big questions in AD research. The failure of Aβ directed therapeutics has made some question the central amyloid cascade hypothesis, however, Aβ accumulation during AD pathogenesis and the toxicity of soluble oligomers cannot be refuted. Therefore, the question that remains to be answered is whether or not Aβ is the primary cause or a secondary downstream insult. Moreover, questions remain as to what conditions make the brain sensitive to Aβ accumulation, some of these pertaining to the lipid membrane, oxidative stress and inflammation have been addressed in this introduction. That being said, the specific cellular and molecular mechanism of Aβ toxicity pertaining to specific interactions with membrane receptors or non-specific interactions with lipid bilayers remain to be fully elucidated. The questions that need to be answered include:

1. What factors make cells more susceptible to Aβ?
2. Are non-specific interactions of Aβ with the lipid bilayer or specific receptor interactions more important for toxicity?

3. Finally, is it possible to design experiments to distinguish between these two seemingly distinct pathways (specific *vs.* non-specific)?

In this thesis, the effects of melatonin, lipid membrane cholesterol composition and Aβ interactions with the lipid membrane will be elucidated at two levels: first, on the nanoscale, using AFM to study non-specific interacts on membrane biophysical structure and properties; and second, in HT22 cell culture to study the metabolic health, morphology and specific growth factor receptor signaling of neuronal cells. In the first part, new contributions to scientific knowledge presented here include: furthering the understanding of melatonin interactions with the lipid membrane using AFM; presenting the use of a new application of HS-AFM to the study of lipid membrane protein interactions. In the second part, a series of experiments on the cholesterol-dependent mechanisms of Aβ toxicity in HT22 cells is presented for the first time, including MTT cell viability assays, cell morphology, AFM of live HT22 cells for the first time; in addition, cell signaling data shows that RTK receptor signaling disruption is not the dominant mechanisms of cell toxicity, rather other receptors, or membrane damage is.

Chapter 2: Theory of Methods

2.1 Lipid Membrane Biophysics

2.1.1 Lipid Preparation for Solution and Topographical Experiments

The lipid membrane is a basic bilayer structure with hydrophilic headgroups on either side of a hydrophobic core of acyl tails. Because of this structure hydrophilic headgroups interact to form multilamellar structures at high concentration of lipids, (Figure 2.1). Unilamellar vesicles (also called liposomes) are prepared in a simple process of hydrating dried lipids in water or buffer and adding energy to break the resulting large multilamellar vesicles into smaller unilamellar vesicles, these can then be used for solution-based studies such as scattering experiments or fused to a support surface for topographical studies such as AFM (Figure 2.1). Broadly, the most popular methods for producing unilamellar vesicles from a polydisperse solution of multilamellar vesicles (MLVs) are sonication and extrusion[295]. Sonication is a method by which ultrasonic sound waves are passed through a sample in a water bath, these ultrasonic sound waves can deposit enormous local energy at the nanoscopic level within water as constructive interference of these waves vibrating through the medium occurs. This breaks large vesicles into smaller vesicles. Due to the intensity of the ultrasonic waves, rest cycles between bouts of sonication are required, a typical scheme is to sonicate 10 minutes, then let rest with gentle stirring for 10 minutes, repeating this cycle until the solution transitions from a cloudy/opaque solution to a clear/translucent solution. The time for sonication can vary from 1 to 8 hours depending on the lipids, buffer, and strength of the sonicator. Typically, sonication produces very small unilamellar vesicles between 30 and 50 nm in diameter[295,296], though reports of vesicles around 150nm have been reported[297]. Likely this variation is due to the length of sonication, where increased sonication times results in smaller vesicles, and lower polydispersity[298]. Extrusion is another method for producing unilamellar vesicle solution. Here the multilamellar solution is passed repeated through a filter under pressure, the more times the lipid are passed through the filter the greater the monodispersity of liposomes and the less contamination with MLVs. These filters typically have pore sizes between 50 and 100nm and produce vesicles approximately the size of the pore filter used. For studies with supported lipid bilayers, the vesicle solution is added to freshly cleaved mica or other hydrophilic substrate,

where vesicle fusion occurs. The vesicles collide with the surface, adsorb, rupture, and spread on the surface. These processes are lipid composition, temperature, pH, and concentration depend.

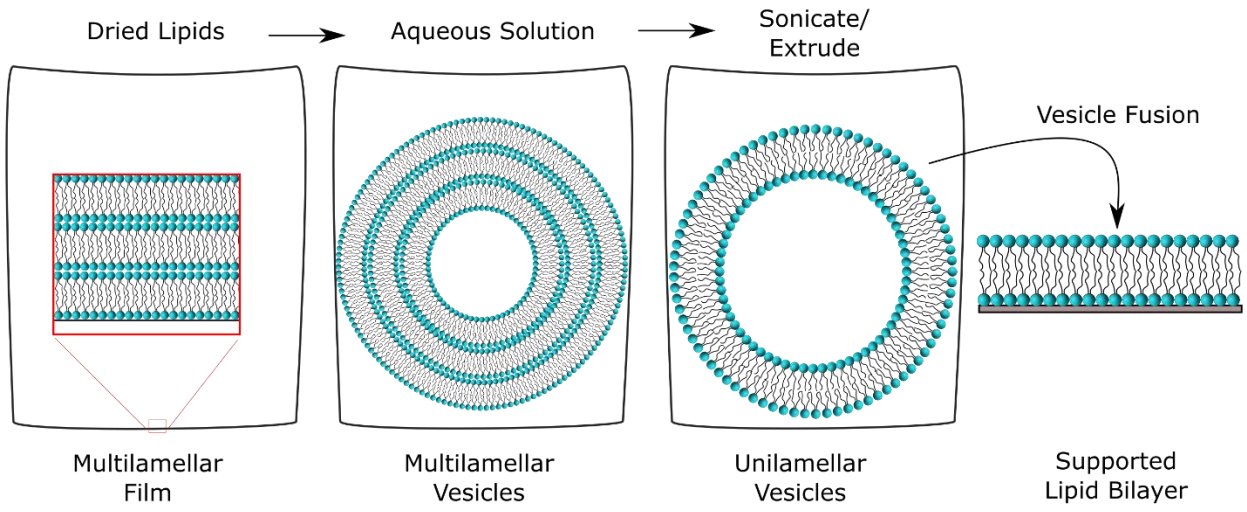

Figure 2.1. Vesicle fusion for producing supported lipid bilayers for surface analysis. *Lipids are mixed in solvent; solvent is removed by evaporation forming dried multilamellar lipid cakes on the sample container; multilamellar vesicles are produced by hydrating the lipid film; then multilamellar solution is sonicated or extruded multiple times to produce a unilamellar vesicle solution which can be used for solution-based studies or applied to a solid substrate to form a supported lipid bilayer for topographical analysis.*

2.1.2 Atomic Force Microscopy

The AFM is a powerful tool for characterizing the nanoscale structure of molecules, molecular systems and living cells, as well as measuring the mechanical properties biological systems from lipid bilayers, to living cells and as a means to measure molecule-molecule interactions, all under physiological conditions[299–301,66,302]. AFM is a mechanical microscope that operates by scanning an atomically sharp probe tip in physical contact with a sample across its surface, line-by-line in a raster pattern[299], generating a topographical image by means of mechanical interaction with the surface (Figure 2.2)[303]. The probe tip is mounted onto a mechanical lever that bends under the contact forces from the surface according to Hooke's law. If the force is kept constant by the AFM feedback system, in the case of contact mode or the RMS amplitude of cantilever oscillation during tapping mode imaging, then the height profile of each line will be extracted as the AFM feedback must move up and down to compensate for forces on the probe that correspond to vertical features of the sample surface. The voltage applied to the piezo-electric actuator necessary to move the AFM probe up and down can be calibrated and converted into a distance measurement to extract the height. This intrinsic interaction between the probe and the sample surface can be destructive, therefore optimization

of experimental conditions to minimize interaction forces is required, for instance cantilever spring constant, probe material, sample preparation, contact force and feedback settings.

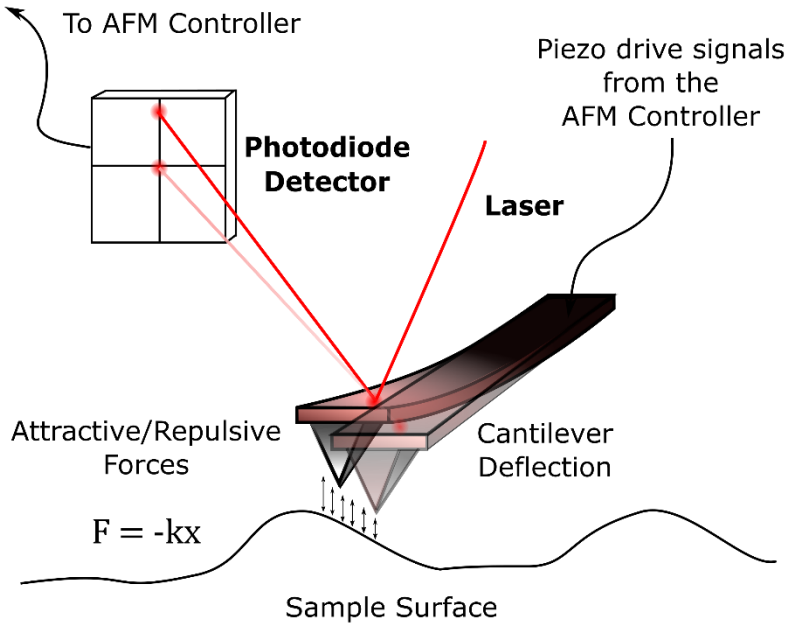

Figure 2.2. Atomic force microscopy *is a mechanical microscope with an atomically sharp probe tip attached to a flexible cantilever that bends according to Hooke's law. Interaction forces of the probe tip with the sample surface are detected by a photodiode detector that measures cantilever bending. A feedback system controls the height of the probe above the surface with a mechanoelectrical piezo actuator by maintaining a set cantilever bending corresponding to the force setpoint.*

2.1.3 Atomic Force Spectroscopy and Lipid Membrane Breakthrough Forces

Atomic force spectroscopy (AFS) is an operational mode of the atomic force microscope that operates strictly in the z-direction to directly measure interaction forces between the probe tip and the sample surface, rather than being scanned laterally to generate an image. Atomic force spectroscopy nanoindentation experiments can be used to study a diverse range of materials and biological systems. Nanoindentation experiments measure elastic modulus of materials during indentation and adhesive forces between the probe tip and sample surface during retraction.

When applied to lipid bilayers in solution force spectroscopy can be used to break through the membrane, the amount of force required is called the breakthrough force. This technique allows one to determine the local properties of membrane regions that can be correlated with the topography if an image is acquired of the area that is being probed. The breakthrough force of the membrane correlates with the integrity and permeability of the membrane. A typical breakthrough force curve is represented schematically in Figure 2.3. The

breakthrough force is defined as the peak force prior to the breakthrough event (B). The bilayer thickness is defined as the difference between the Tip-Sample separation at the membrane contact point (A) and the surface of the mica substrate (C). The contact region of the force curve is defined by the point where the force first begins to increase upon contact with the top of the bilayer and the point at which the probe ruptures the membrane, this contact region can be fit to a model to calculate the elastic modulus of the membrane, a measure of membrane fluidity/stiffness. The Tip-Sample separation length of the contact region is the indentation depth. On the retraction portion of the curve adhesion between the probe and the membrane can be extracted, membrane adhesion is an important feature for binding of molecules to the lipid bilayer.

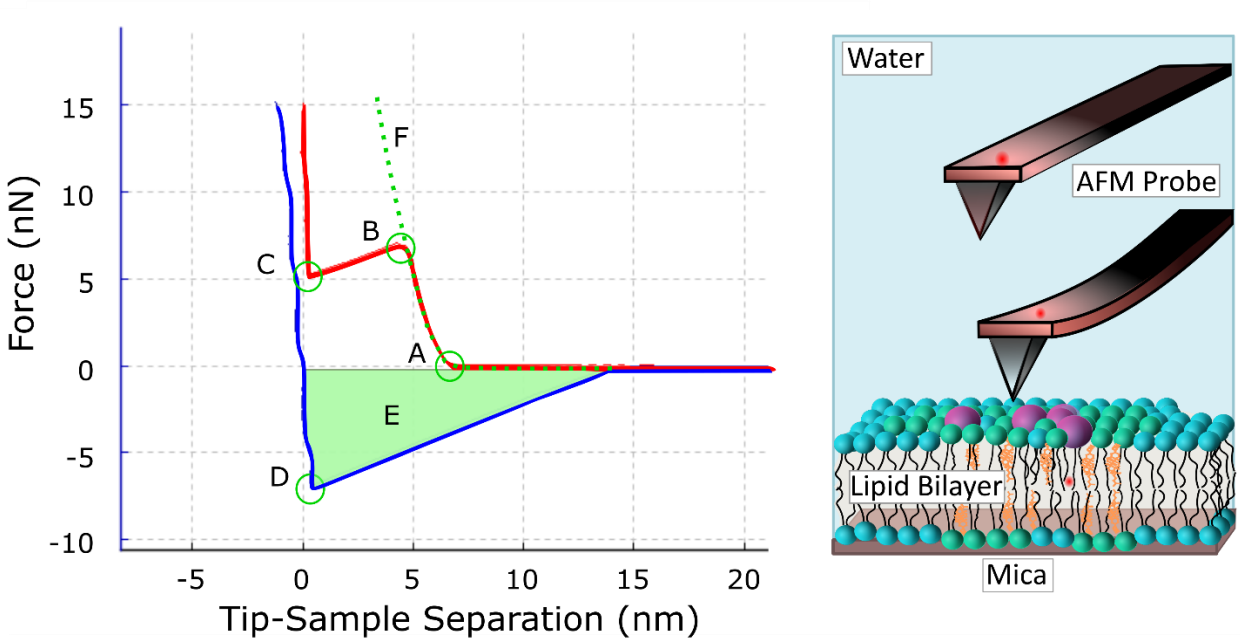

Figure 2.3. Atomic force spectroscopy for lipid bilayer breakthrough forces*. Left: Force Plot A: Contact Point; B: Breakthrough Event; C: Mica contact point; D: Peak Adhesion Force; E: Area under the retract curve is the work of adhesion; F: Hertz/Sneddon indentation model fit. Right: Lipid bilayer breakthrough force representation.*

2.2 Molecular and Cellular Biology

2.2.1 Cell Lines vs Primary Cultures

Cell culture provides a high throughput and efficient means of studying molecular and cellular processes in physiology, pathophysiology, and pharmacology. These cell culture models represent a reductionist model for studies of cell signaling, toxicity, metabolism, growth, proliferation, and differentiation. Cell culture can model the vast diversity of cell types and states, including different subtypes and disease states and even to study cell type interactions in

co-cultures. Most mammalian cells are adherent, meaning they require a solid support upon which to adhere and grow, though there are exceptions, such as blood cells and cells with certain cancerous phenotypes. These solid supports must be treated in such a way as to permit cell adhesion, which requires a charged or hydrophilic surface upon which to adhere. More sensitive cells may require more advanced biochemical modification with molecular supports such as, poly-lysine, collagen, or fibronectin. The solid support upon which cells are plated affect their growth and cell properties such as cell stiffness, strength of cellular adhesion and many others.

In general, there are two classes of cell culture: primary cells that are isolated and plated directly from animal tissues; and cell lines that are derived from tissues and immortalized to be passaged and replated dozens of times. Primary cultures are harvested directly from living organisms, dissociated from their native organs, separated from cell types that are not of interest, and then plated into suitable media on appropriately prepared tissue culture plates. These cells exhibit phenotype closer to their parental cells *in vivo* than cell lines, however they are difficult to isolate, requiring specialized skills and training to work with and highly susceptible to damage during routine culturing. In contrast cell lines are immortalized, being able to replicate indefinitely, so are more robust but often lose important characteristics of the native unmodified cells due to genetic mutations that are incurred during immortalization and gain properties that are not representative of the cell type, most obviously, the ability to replicate indefinitely. The difference between primary cells and cell lines can be highlighted by looking at neuronal cells. Primary neuronal cultures exhibit complex neuronal electrophysiological properties including supporting action potentials and even more complex phenomena such as long-term potentiation (LTP), a critical correlative feature of learning and memory. In contrast, neuronal-derived cell lines including HT22, PC12, SH-SY5Y cells are scantly used in electrophysiology studies because of their lack of electrical activity. The advantages of cell lines are that they can be passaged dozens of times, and for all intents and purposes, passaged indefinitely. This makes them a more cost-effective alternative to primary tissues and prevents the sacrifice of animals which is an important ethical consideration for biological research. In addition, cell lines grow much faster improving the efficiency of experimentation by making them higher throughput.

2.2.2 HT22 Hippocampal Cells

The HT22 neural cell line was sub-cloned from a previous cell line, the HT-4 cells which were derived from primary hippocampal cells of mouse origin[304]. The original HT-4 cell line was

immortalized using a temperature sensitive SV40 T-antigen viral vector which when grown at nonpermissive temperatures exhibits neural cell markers such as expression and secretion of NGF, exhibit cholinergic properties, and express functional NMDA receptors, while not expressing glial differentiation markers[305–307]. HT-22 cells have enhanced sensitivity to glutamate, which makes it useful for studies of ischemic stroke, and have been verified to express functional NMDA receptors[304,308]. HT-22 cells also maintain the cholinergic properties of their HT-4 parent cell line, expressing acetylcholine receptor, transporters, and choline acetyltransferase[309]. In addition, HT-22 cells are sensitive to glutamate and Aβ making them suitable to studying AD mechanisms[310,311].

2.2.3 MTT Cell Viability Assay

MTT-assays are a powerful method for studying the metabolic capacity of cells *in vitro*, this correlates with the number of cells and the efficiency of their mitochondria within a population of cells. Cells are fed 3-(4,5-di**M**ethyl**T**hiazol-2-yl)-2,5-diphenyl**T**etrazolium bromide (MTT), a molecule that is metabolized by mitochondrial reductase into the product (formazan) to be detected by absorbance using a standard plate reader, this reaction and experimental outline is shown below (Figure 2.4). This general strategy can be used to study different metabolic pathways in cells by changing the metabolic substrate fed to cells, although depending on the metabolic pathway in question other secondary detection reagents may be necessary.

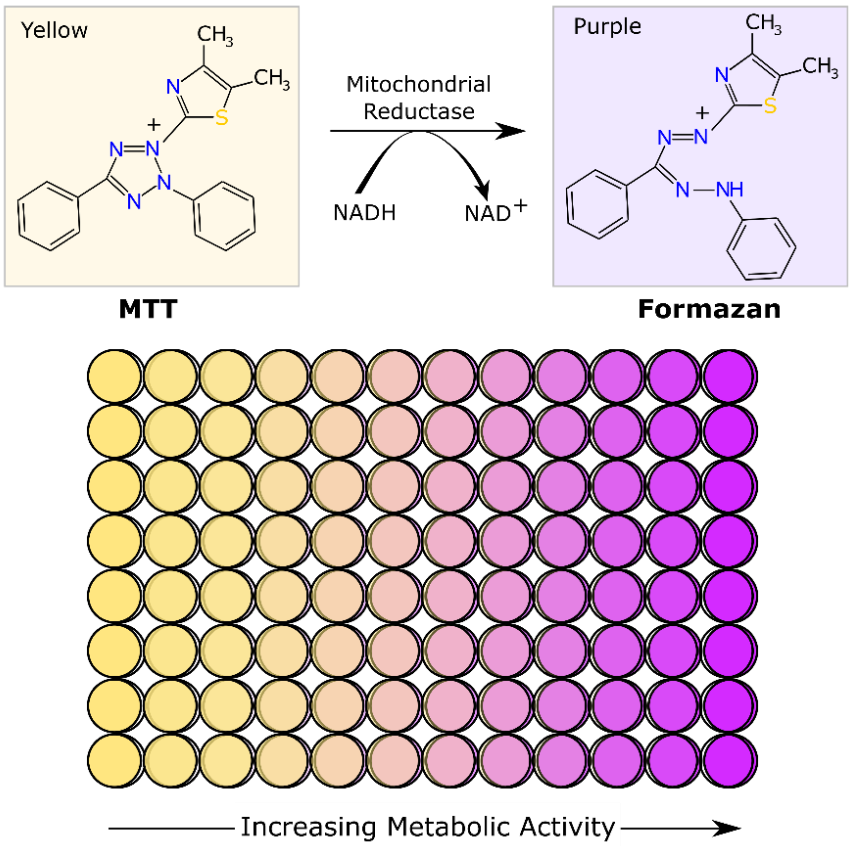

Figure 2.4. MTT cell viability assay. *Cells are fed yellow MTT reagent which is converted to purple Formazan product by mitochondrial metabolism. Greater metabolic activity correlates with Formazan production, this can be due to an increase in cell count, or a relative increase in metabolic activity relating to mitochondrial health.*

2.2.4 Phase Contrast Optical Microscopy

Phase contrast optical microscopy principles were developed by Frits Zernike who won the Nobel prize in physics for his work. Prior to the invention of phase contrast optical microscopy, thin transparent specimens could not be imaged with good image contrast because the human eye and camera films are only sensitive to changes in light intensity and to a lesser extent frequency neither of which are strongly affected by transparent samples. However, thin transparent samples decrease the phase of diffracted light compared to the direct undeviated incident light, slowing it down depending on the thickness and refractive index of the transparent object, approximately by a factor of ¼. This phase shift can be used to generate contrast by using optical devices that create constructive interference between the thin samples and the undeviated light, then removing most of the background with a grey light filter, so that amplitude absorbing objects appear dark over the background[312]. The ~1/4 phase shift is not sufficient to cause a

substantial change in light amplitude through interference over the direct light background, however if the phase difference was ½ there would be greater interference of the diffracted light yielding improvements in contrast. By using a phase plate that increases the phase difference of the direct undeviated light by ¼, phase differences between the incident light and the sample near ½, effectively allowing destructive interference of light amplitude absorbing objectives, which appear dark over the background[312]. This increase in light amplitude (intensity), due to phase interference also results in constructive interference creating halo artifacts in the image at the boundaries between the sample and the direct undeviated background light.

New quantitative phase imaging approaches have been developed that utilize well-defined monochromatic lasers and digital cameras to accurately measure the phase shifts in the light at each pixel, and through holographic principles algorithms reconstruct the path lengths allowing for true quantitative 3D images, that can provide cell volume and mass data[313]. Cell volume and mass data is important for measuring growth rates and changes in cell morphology, which, at its most fundamental level, is the change in mass from one region of the cell (protein, lipid, and nutrients) to another region of the cell. This can provide biophysical quantification of cell metabolism that is more accurate than simply measuring surface area in the plane of the tissue culture plate[314,315].

2.2.5 Fluorescence Microscopy

In fluorescence microscopy, illumination light absorbed by fluorophores within the sample excites them causing the emission of light shifted to a longer wavelength. This emitted light from the fluorophore can be isolated with optical filters allowing the fluorophore to be imaged separately from the rest of the incident light on the sample. In widefield epifluorescence, the most basic form of fluorescence microscopy, the excitation wavelength at the sample is achieved with high-powered Zenon Arc lamps, or newer high-powered LEDs. The incident light passes through an excitation filter which selects a single wavelength of light upon which to illuminate the sample. This filter wavelength is chosen to excite the fluorophore. A dichromatic beam splitter after the excitation filter sends the excitation wavelength light through the objective to the sample and which is reflected back toward the incident light source instead of traveling to the detector while the emitted light is permitted by the beam splitter. Thus, the dichroic beam splitter permits only the emitted light from the fluorophore to travel to the detector or camera. With this approach one fluorophore is imaged at a time, meaning filter cubes need to be switched

each time, however by using multiple fluorophores colocalization experiments can be performed to identify interactions between proteins within the cells.

Fluorophores for all kinds of different applications have been developed with different delivery strategies to identify molecules and their location within cells and tissues. Small molecule fluorescent dyes that bind specific molecules are a popular means of visualizing structures within cells, however they tend to be cytotoxic thus are not useful for live cell imaging, such as DAPI (for nucleic acids), phalloidin (for Actin). Another common method for fluorescence microscopy is immunocytochemistry which makes use of fluorescently labelled antibodies raised against the target of interest, this allows for the quantification and localization of the target protein. In immunocytochemistry, cells are permeabilized with detergent, treated with antibody and fixed, which does not allow for *in situ* live cell imaging, and this biochemical processing could affect the proteins of interest. One of the most popular approaches makes use of molecular genetic engineering to label proteins with green fluorescent protein (GFP) by splicing the gene for GFP to one end of the protein of interest. However, with this approach GFP conjugation can interfere with the functionality of these proteins, although this can be used with live cells given that GFP is non-toxic. Membrane permeable small molecule fluorophores are also widely used for a variety of applications *in situ* including ion sensitive dyes and voltage sensitive dyes for studying electronic properties of cells. Hydrophobic fluorophores have also proven useful for studying phase separation in giant unilamellar vesicles, or labelling membrane microdomains within living cells, with the caveat that small concentrations of these molecules can have an impact on lipid phase diagrams.

2.2.6 Gel Electrophoresis and Western Blotting

Identification and quantification of specific proteins and their activation state within a sample is necessary to understand biological processes. For this purpose, polyacrylamide gel electrophoresis (PAGE) is used to separate proteins by their molecular weight which can then be identified by Western blot with chemiluminescent or fluorescent label-conjugated antibodies (Figure 2.5). PAGE works by running proteins through pores in a gel made of an acrylamide polymer network in the presence of sodium dodecyl sulfate (SDS), in all buffers and the gel. The samples containing proteins of interest are pipetted into the loading/stacking gel. The proteins become charged as the SDS, an anionic surfactant that aids in denaturation of proteins, binds to hydrophobic regions, this adds negative charge to the protein. An electric field is applied to the

gel which causes the negatively charged proteins to move under an electromotive force. The gel acts as a resistor to the flow of proteins. The rate of protein movement through the gel depends on the pore size of the acrylamide network. The relative rate at which different proteins move through the gel depends primarily on the size of the protein, as SDS concentrations are extremely high dominating over the intrinsic charge of the proteins, due to most proteins having a near net neutral charge. In effect, low molecular weight proteins will travel faster, and move further down the gel compared to the higher molecular weight proteins, separating the proteins in the sample by their size. A ladder, or size marker, is typically used to help in the identification of proteins (first lane on Figure 2.5).

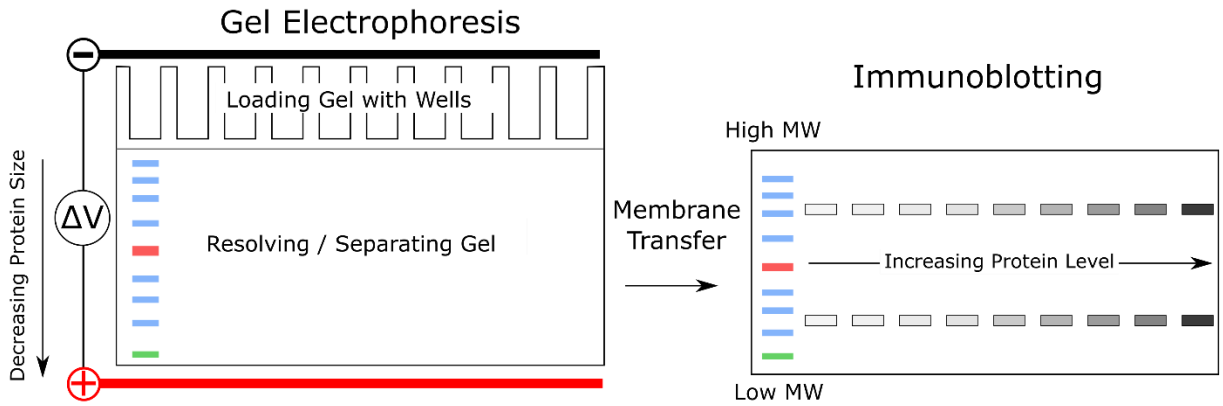

Figure 2.5. Western blot *has two primary stages first proteins in a sample are separated by weight using SDS-PAGE then second the proteins are transferred to a polymer membrane (nitrocellulose or PVDF) where specific proteins are identified using chemiluminescent or fluorescent labelled antibody in the immunoblotting (Western Blot) stage, with brighter signal indicating higher levels of signal. A protein ladder containing stained proteins of known molecular weight is typically included in gel electrophoresis to aid in identification of different proteins.*

2.2.7 Lipid Extraction and Lipidomics

The Folch method for lipid extraction is a solvent/solvent separation method where hydrophobic lipids are separated from the hydrophilic components of the sample through the two phases: water and solvent. In the Folch method, cell or tissue homogenate is mixed at a 1:20 (by volume) ratio in 2:1 chloroform/methanol solution (v/v). This is then washed with 0.2 equivalents of 0.9% NaCl solution. This results in a two-phase system with the top phase is mostly water and methanol which contains polar compounds, and bottom phase is mostly chloroform with non-polar lipid compounds. Phospholipids, sterols, and glycerides would end up in the bottom solvent phase, while there would be a mixture of highly polar lipids, like gangliosides, in each phase.

Lipidomic profiling of the gross extracts from cells and tissues informs the effects of lipid metabolism during physiological and disease processes. There are different methods to identify and quantify lipid composition using a variety of methods including biochemical assays, liquid chromatography, and NMR. Biochemical assays can be used to detect specific lipids in a sample and are particularly useful for measuring broad classes of lipids, such as sphingolipids or cholesterol. The cholesterol oxidase assay is a popular assay for quantifying total cholesterol and cholesterol esters. Lipid extracts are treated with cholesterol oxidase and/or cholesterol esterase which produces H_2O_2 in stoichiometric quantities that can be detected with the use of commercial detection reagents such as AMPLEX Red plus horse radish peroxidase. NMR is also a useful strategy for quantifying characteristics of lipid profiles such as the degree of saturated/unsaturated fatty acids within a sample. The most recent advances in lipidomics rely on spectroscopy combined with chromatography, such as liquid chromatography coupled mass spectroscopy (LC/MS), gas chromatography MS (GC/MS), and LC tandem MS (LC/MS/MS). This allows more detailed lipidomic data to be extracted from a sample even down to the fatty acid and even its position on the glycerol backbone.

Chapter 3: The Effects of Melatonin on the Structure and Breakthrough Forces of Phase Separated Supported Lipid Bilayers by Atomic Force Microscopy

3.1 Introduction

Melatonin is an important hormone that is best known its role in regulating circadian rhythms in mammals[316,317]. Melatonin levels decrease with age and even more profoundly with the progression of Alzheimer's disease (AD) compared to age-matched controls, noting that melatonin level decline precedes symptomatic disease and that AD is associated with sleep disturbances[318,319]. Currently, there is no cure for AD and novel therapeutics to slow disease progression have been controversial, highlighting the need for deeper understanding of basic AD mechanisms and therapeutics[52,320]. AD is characterized by the aggregation of extracellular amyloid-β (Aβ) plaques and intracellular neurofibrillary tangles of aggregated tau protein[321]. Amyloid aggregation has long been known to disrupt lipid bilayer function by inducing membrane defects, increasing membrane permeability, and disrupting membrane-receptor signaling and membrane potentials[19,20,164,167,322]. This disruption of the lipid structures by amyloid then results in disrupted cellular metabolism, oxidative stress, and lipid peroxidation[87]. Here lipid membrane composition and small molecules that can protect the membrane could be important for their effects on membrane structure, properties and protection from Aβ damage. For example, in complex model membrane systems that mimic healthy, and disease neuronal membranes developed in Drolle et al. 2017, lipid composition associated with advancing AD increased susceptibility of the membranes to Aβ damage[19]. There it was shown that membrane damage resulting from decreases in sphingolipids in model membranes were associated with nanodomain structure and interactions with Aβ at the structural level[19]. For this reason, the restoring or preventing deleterious membrane nanodomain structure could be important in the mechanisms of Aβ.

Melatonin is useful for reducing the AD-related sleep disturbances, but is not effective in slowing or improving learning and memory in symptomatic AD, though its role as a preventative therapy before symptoms is yet to be tested thoroughly[318]. Melatonin has been shown to improve learning and memory in rodent models of AD and has been shown to protect cultured neurons

and cell lines from Aβ toxicity[240,323–326]. The protective effect of melatonin was shown to be independent of melatonin receptor activation[325], as melatonin ligands with no antioxidant activity were unable to protect cells from Aβ. This suggests that non-specific properties of melatonin are responsible for its protective effects, such as its antioxidant, anti-Aβ aggregation, or perhaps its effect on membrane structure and properties[240,323,324,327–329]. The effect of melatonin on the nanoscale domains may explain its protective effect.

Melatonin is amphipathic (logP ~ 1.6, with a maximum aqueous solubility of 400μM), as such it can partition into hydrophobic compartments within cells such as lipid droplets and bilayers; this has been confirmed by several studies that indicate melatonin can incorporate into phospholipid systems including micelles, bilayers and multilamellar lipid layers [330–335]. The ability of melatonin to partition into lipid bilayers has been shown to influence the properties of lipid bilayers, decreasing membrane thicknesses, increasing membrane compressibility and fluidity[100,104,333,336]. Molecular Dynamics (MD) simulations of melatonin with lipid bilayers suggest that melatonin partitions preferentially into the region of the lipid bilayer between the headgroup and fatty acid tails, while NMR and IR spectroscopy has shown preference for lipid headgroups in inverted micelle systems[330,333]. Melatonin has also been shown to counteract the stiffness that cholesterol induces in lipid membranes[336]. More recently, the effects of melatonin on complex lipid models composed of three or more lipid types have been studied that reveal melatonin influences phase separation and membrane microdomain structures, these studies were done with neutron scattering and NMR methods which do not reveal the structure of the nanodomains directly[331,335]. In summary, most of these studies involve studying only a single lipid model and have not explored the effects of melatonin on the nanoscale domains. In this chapter, the effects of melatonin on the structure of nanodomains using AFM for the first time will be presented, then the structure of the lipid membrane will be correlated with the nanomechanical properties such as breakthrough forces and bilayer thickness. Although more complex 5 component models have been developed earlier in Leonenko's lab (Drolle et al, 2017)[19], the domain structure in these membranes is very complex and the domain size is very small. Thus, in order to address the role of domains in melatonin action, in this work we selected a simpler 3 component lipid model which shows characteristic nanodomains and suitable to follow their changes upon melatonin insertion.

3.2 Materials and Methods

3.2.1 Materials

Cholesterol, powder. Sigma Grade ≥99%. 1,2-dioleoyl-sn-glycero-3-phosphocholine (DOPC, powder. >99% (TLC)). 1,2-dipalmitoyl-sn-glycero-3-phosphocholine (DPPC, powder. >99% (TLC)). Chloroform for HPLC, ≥99.8%, amylene stabilized MilliQ ultrapure water (deionized to a resistivity of 18.2 MΩ·cm). Milli-Q water (resistivity > 18.4 MΩ.cm). N-acetyl-5-methoxytryptamine (Melatonin, powder, ≥98% TLC).

3.2.2 Vesicle Fusion

Sonication was used to create a homogenous vesicle solution suitable for deposition. Briefly, DOPC/DPPC/Chol were solubilized in chloroform then mixed to make a weight ratio of 2:2:1. Chloroform was evaporated under a dry nitrogen stream to produce a thin film of multilamellar lipid bilayers. The lipid films were then hydrated with MilliQ water to a 1.0 mg/ml solution. The hydrated lipid solution was processed through multiple rounds of sonication and magnetic stirring at 10-minute intervals, for 2 cycles past the point where small uniform vesicles (SUVs) are formed as indicated by solution clarity, about 9 to 12 cycles or 3 to 4 hours. This SUV solution was then added to freshly cleaved mica in a JPK liquid cell and left to incubate at room temperature for 1 - 2 hours to produce a SLB. The SLB was then rinsed gently with 3 ml of MilliQ water, maintaining hydration throughout. After imaging and force spectroscopy measurements on control DPPC/DOPC/cholesterol bilayers 400µM solution was then added to the liquid cell for two hours of incubation followed by imaging and AFS procedures were repeated to compare with controls.

3.2.3 Atomic Force Microscopy

Atomic force microscopy images were collected using intermittent contact mode in liquid (JPK Nanowizard II). AFM tip was loaded on an electrostatic discharge (ESD) mat. Triangular AFM probes with a high resonant frequency and low cantilever stiffness (nominal frequency: 50 kHz, and spring constant: 0.3 N/m) were used, qp-BioT/AC AFM tips from Nanosensors (radius < 10nm). The optical microscope was used to locate a marked position on mica substrate (on the bottom side of the mica) — this allows the same local region to be imaged/probed before and after melatonin incubation to prevent variability associated with large scale sample variation ~

than 100µm × 100µm. The sample is then left to reach thermal equilibrium on the AFM stage, 5-15 minutes. The AFM probe was engaged to approach the surface, and feedback controls were optimized with integral and proportional gains, resonant frequency, and photodiode signal. For statistics, scans of three different regions (4x4 µm each) per sample to ensure sufficient variance in membrane topology/morphology and verify the reproducibility of the membrane features before breakthrough forces using AFS were done. To analyze images minimal processing was done in JPK Data Processing software such as interpolating line defects, polynomial plane/line-fitting, and/or low pass filtering (no greater than 10 nm smoothing in slow and fast scan directions). Image statistics were computed using JPK Data Processing software such as surface roughness, 1D raw data histograms, and arbitrary line cross sections.

3.2.4 Force Spectroscopy

We used the standard calibration of the spring constant with the thermal noise method, and the contact region of the extend curve to calibrate the sensitivity[337]. These values are verified at the end of the experiment day on a clean piece of mica, with variation of approximately 1%. After calibration, AFS measurements were performed. During these measurements, the probe is lowered to the surface, upon contact with the surface tip-sample interaction is recorded to create a graph of the vertical deflection of the cantilever bending on one axis (this corresponds to the force on the probe via the sensitivity measurement), while vertical position above the sample is recorded on the other (see Figure 2.3 for representative plot). In each of the imaged regions, extension and retraction force curves were collected — 500-900 points. A retract and extend speed of 1 µm/s is used throughout.

The resulting extension force curves were first parsed with JPK data processing software, discarding non-standard curves. A linear fit is subtracted from the baseline offset of the vertical deflection, next a linear fit along the straight regime of the section from contact to breakthrough point, this accounts for contact-point offset of the vertical tip-position. Lastly, height correction due to cantilever bending is done by cantilever deflection subtraction from the piezo height. JPK software was used to compute the elastic modulus of the contact region of the force curve. Sneddon/Hertz model for a parabolic indenter was used and is appropriate based on qp-BioT tip geometry and indentation depths that are comparable to our tip radius. This reasoning stands because in softer materials the initial parabolic shape has a small contribution to total contact

area and thus the tip can be approximated to be conical in shape. Adhesive forces and work of adhesion were extracted from the retract curves using JPK/SPM data processing software. In-house breakthrough force script was used to extract breakthrough force, indentation depth, and bilayer thickness, points A, B and C on Figure 2.3.

Breakthrough force, indentation depth, bilayer thickness and elastic modulus statistics such as means, standard deviations were calculated and tested by 1-Way ANOVA to assess statistical significance. The resulting histograms of the nanomechanical parameters were also plotted and fit to bimodal gaussian distributions, these distributions were compared using most probable values (location of the histogram fit peak), and the proportion of the area under the distribution fit using Origin Pro 2021 multipeak fit analysis.

3.3 Results and Discussion

3.3.1 Atomic Force Microscopy

When a multicomponent lipid bilayer is phase separated, wherein one component is in the gel phase and the other in a fluid phase, the gel or liquid ordered(L_O) phase lipids protrude above the liquid disordered (L_D) more fluid domains, resulting in variable bilayer thickness on the scale of approximately 0.5-2 nm depending on the lipid model (Figure 3.1)[74,331,338]. This distinction appears because of differing lipid melting temperatures and a hydrophobic mismatch of phases which has an unfavorable energy state, causing domain formation—thereby reducing hydrocarbon surface area exposure to hydration layers of water[74]. Cholesterol content is enriched in the L_O domains and is proportional to lateral ordered domain size[63,339]. DOPC has a transition temperature at -16.5℃, leaving it in a L_D phase at room temperature, while DPPC has a transition temperature at 41.3℃ giving it a L_O state at room temperature[63]. For all experiments in this study DPPC/DOPC/Cholesterol at a weight ratio of 40:40:20 (~1:1:1 molar ratio) was used. This model was chosen because of the well-established phase separation and known miscibility transition temperature of 29°C from Veatch et al., (2003)[63]. In Figure 3.1, incomplete bilayer coverage on mica is shown with cross section of the lipid bilayer revealing a bilayer height of between 5.5 to 6.4 nm and domain heights between 0.6 to 0.9 nm.

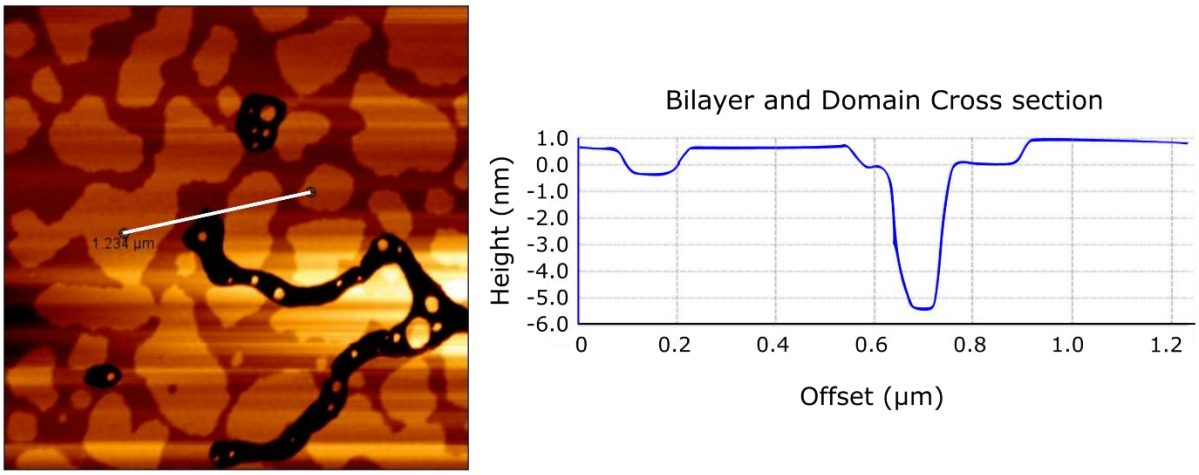

Figure 3.1. Incomplete coverage for DOPC/DPPC/Chol Bilayer, with bilayer and domain cross section. *Bilayer thickness is 5.5 to 6.4nm, with difference between ordered and disordered domains of ~0.6 to 0.9 nm, 4×4 µm image.*

After exposure to melatonin the model membrane undergoes striking visual changes illustrated in Figure 3.2 in ~ 45% of independent lipid experiments (4 out of 9 experiments). In the other 5 out of 9 experiments, little (2) to no changes (3) in membrane surface structure were observed. Therefore, only images with dramatic changes and excellent image quality were analyzed rigorously. The control shows a phase separated lipid bilayer structure with nano and microscale lateral heterogeneity, taller L_O domains in gold and lower L_D domains in dark brown (Figure 3.2). 1D data histograms from the raw image data were produced for each image to extract height differences between domains and domain surface area extent shown in Figure 3.3. The first peak is the most probable plane leveled height corresponding to the disordered membrane regions, while the second peak is the most probable plane leveled height corresponding to the ordered membrane regions. Domain height differences were extracted by taking the difference between the most probable heights between gaussian peak fits on the 1D histogram plots. Domain extent was measured by the area under each gaussian peak fit and represented as a ratio of disorder to order area (A_D/A_O). The mean height difference between the ordered and disordered domains for Control DPPC/DOPC/Cholesterol membrane was 0.63 ± 0.09 nm, which was not statistically different from DPPC/DOPC/Cholesterol with melatonin which had a height difference of 0.62 ± 0.07 nm (n = 4, N = 12). The lack of effect on the height difference between the two domains could indicate either equivalent incorporation of melatonin into each phase, or if accumulation of melatonin is preferential in one domain region, then there must be rearrangement of lipids between the different phases to offset any effect on the height

differences.

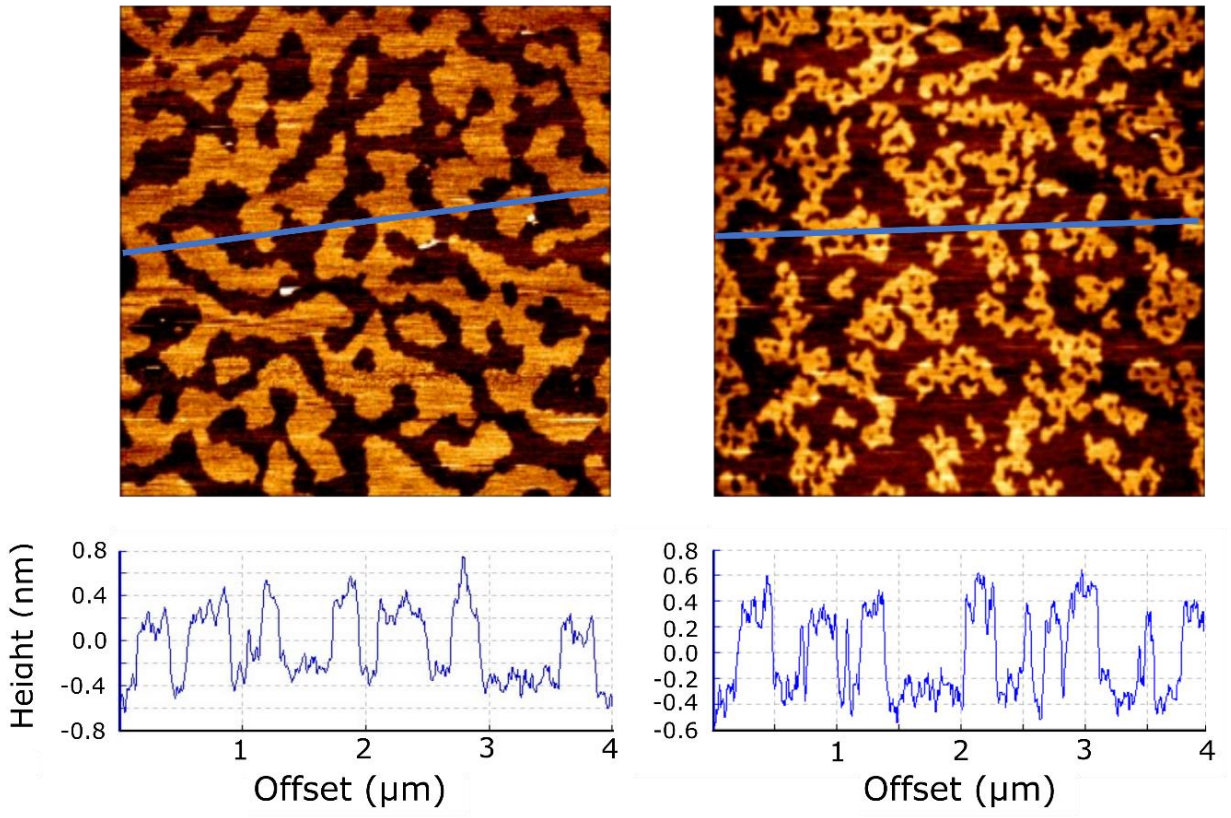

Figure 3.2. Atomic force microscopy images of melatonin effect on DOPC/DPPC/Cholesterol membrane *(40:40:20): Left – control; Right – after 2-hour 400μM melatonin incubation, image scale 4 μm x 4μm, cross sections shown in blue on image.*

The most striking effect on the membrane after melatonin incorporation was the significant loss of surface area in L_O domains to surrounding L_D domains (Figure 3.2 above). The area ratio (A_D/A_O) before melatonin incubation was 0.74 ± 0.15 (or 42.2 ± 4.8 % disorder region per image) and after melatonin was 1.26 ± 0.27 (or 55.2 ± 5.2 % disorder per image) $p < 0.001$. This agrees with several studies that suggest melatonin increases membrane disorder, fluidity and decrease in bilayer thickness by melatonin, in contrast to cholesterol which tends towards the opposite effects, thus resulting in higher percentage of L_D domain coverage[104,333,335,336,340]. Whether there is more incorporation of melatonin into the disordered domains of the bilayer or ordered domains is less clear from these images. There appears to be additional increase of L_D regions within the centers of L_O domains which indicates that melatonin can localize within the zones of highest cholesterol concentration, this likely involves competitive process that have previously been suggested from NMR studies, Langmuir compression isotherms and molecular

dynamics simulations where melatonin has been shown to oppose the effect of cholesterol on the compressibility and phase transitions of cholesterol containing membranes [335,336,340]. The possibility of melatonin incorporation and competition with cholesterol domains can occur because of hydrophobic effects driving melatonin into the bilayer, there is an overlap in lipid affinity, where melatonin interactions predominant with the lipid headgroups competing for hydrogen bonding with cholesterol[340]. Melatonin has also been shown to stabilize nano and micro scale domains and induce phase transitions by increasing relative disorder of domains enriched in unsaturated lipid tails[331] – this was suggested to be due to preferential interactions with the unsaturated lipid POPC in a similar POPC/DPPC/Cholesterol system by NMR[335]. This may in part explain the resulting increase in L_D bilayer regions observed here, though it cannot be ruled out that equal amounts of melatonin are in each phase based on this work.

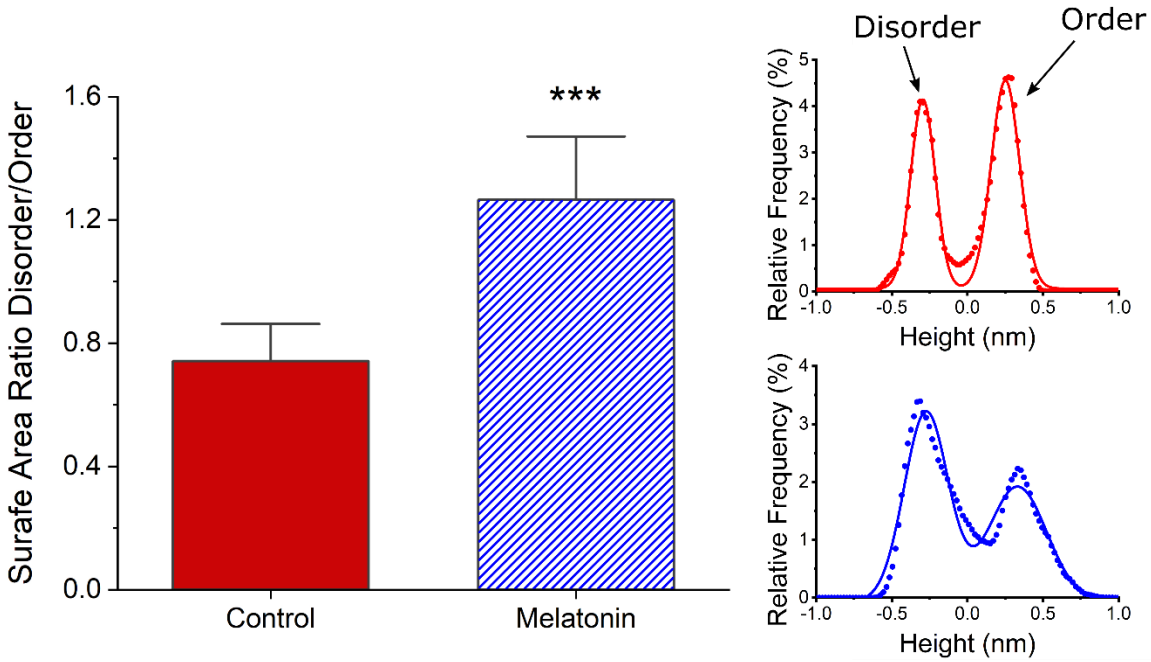

Figure 3.3. Representative 1D histogram of height data in DPPC/DOPC/Cholesterol membrane control and after melatonin *incubation for 2h at 400μM with Gaussian Bimodal Distribution Fit. The estimation of extent of each domain is represented by the area under each corresponding peak fit, first peak for disordered (L_D) and second peak for ordered (L_O). The results of the surface area ratio and height difference n = 4; (N=12); Melatonin increases surface area of the L_D phase over the control by 30.6 % ***p < 0.001, T-test.*

3.3.2 Atomic Force Spectroscopy – Breakthrough Forces

Atomic force spectroscopy (AFS) is a unique nanotechnology tool for molecular and cellular biology as well as material sciences, that can allow for nanomechanical mapping of a

sample. In biological applications AFS is used to measure single molecule protein-protein interactions[311,341], cell-cell interactions[342], and the mechanical properties of biofilms and living cells[343]. The mechanical properties of lipid bilayers can also be studied with nanoscale precision allowing the measurement of the breakthrough force, bilayer thicknesses, elastic modulus and adhesion forces[344,345]. When AFS measurements are made after imaging a region of interest mechanical information can then be correlated with the topographical map. These membrane mechanical properties depend, not only on the material properties of the membrane, but also on the cantilever and probe properties in particular the cantilever spring constant, and probe geometry[345]. The breakthrough force data of SLB provides several important parameters of the nanomechanical properties of lipid bilayers that relate to- or correlate with- important biological phenomena such as membrane stability/integrity, permeability, fluidity, and adhesive properties. For example, a reduction in membrane thickness with increasing cholesterol content in DOPC bilayers correlates with decrease in membrane permeability[346]. Also, the elastic modulus of lipid bilayers is often used as a measure of membrane fluidity. Figure 3.4 shows a representative lipid bilayer breakthrough force curve and illustration of the AFM bilayer system.

It is frequently observed that even small variations in temperature, lipid ratio, and tip radius can present challenges in terms of increasing sample to sample variability of the final supported membranes [66,344,347,348]. The importance of a measuring out precise and consistent lipid ratio during preparation is paramount as morphology of phases is heavily dependent on cholesterol content and small variations in cholesterol can lead to large changes in nanoscale topography[339]. To ensure proper sample preparation and vesicle fusion into a complete symmetric bilayer with large-scale homogeneity, considerations about the structure of lipids at time of deposition, pH and ionic strength of solution, electrostatic interactions, and surface properties of the support are important[347,348].

The choice of AFM tip and cantilever and the variation in tip geometry will influence the quality and consistency of the data. For imaging applications in liquid, the cantilever needs to have a sufficiently high resonant frequency but with low Q characteristics, which affects the force resolution and is related to the optimal force constant. The force constant is also important to achieve reasonable deflection when indenting samples for force spectroscopy. The larger the tip radius, the smaller the maximum stresses on the material in the area, therefore reducing probability of inducing plastic deformation of the membrane structure[345]. It is important to pay

attention to the sample deformation in soft samples, since tip-sample contact geometry can change with increasing penetration, though for SLBs the indentation region is between 1.5 – 2.5 nm so that for very sharp probes little changes would be expected. In addition, a probe with a larger radius will be less discriminant at the tip-sample interface between L_O and L_D domains, which may be a consideration for very small domains, or for very large probe tips. Additionally, limitations in obtaining a precise value for the elastic modulus lie in accurately determining each domain's Poisson ratio, which was assumed to be 0.5 for both phases in this study as is common for bilayer measurements), though it may be expected that there are small differences of less than 5% here between ordered and disordered domains. Changes in tip geometry during AFS measurements due to high contact forces causing blunting or the adsorption of organic molecules onto the tip may change tip geometry and interaction with the bilayer, as time progresses during an experiment there is an increased likelihood of damage or contamination to the probe. Because of the experimental design here, the influence of melatonin was measured on the same sample and similar region as controls, thus it is expected that there is increased risk of changes to the tip for melatonin vs control. Generally increasing the tip/sample contact area would be expected to cause an apparent increase in the breakthrough forces and would overestimate the elastic modulus, while bilayer thickness would not be expected to change with tip damage/contamination and indentation depth would be also less sensitive to changes. Moreover, AFS measurements at the boundary between the ordered and disordered phases may generate additional sources of error as the tip sample contact area in these locations would be asymmetric and may not fit the assumption of the Sneddon parabolic indenter model.

Breakthrough force analysis of the samples wherein visual changes from melatonin were evident are summarized in Table 3.1 where the means of the breakthrough force, bilayer thickness, indentation depth, elastic modulus, adhesion force and work of adhesion for n = 3 independent atomic force spectroscopy sample preparations with N=2100 total force curves per sample condition (each for control and melatonin). One of the independent experiments was excluded due to non-physical mechanical parameters, which could have been due to probe damage or AFM calibration error. Statistical significance was assessed between the membranes before and after melatonin incorporation for the global means. Then statistical significance was applied separately to the best bimodal gaussian fits for the nanomechanical parameter distributions and the most probable nanomechanical parameters for the disordered and ordered

domains where extracted. This captures both the effects of melatonin on the general bilayer properties and each set of domains separately. Because of the small size of the domains following melatonin treatment, the force volume analysis did not allow us to distinguish between L_O and L_D domains therefore force curves were averaged between domains, representing a technical limitation of analyzing nanodomains.

Table 3.1. **The nanomechanical effects of melatonin on phase separated DPPC/DOPC/Chol membrane**, *mean ± SD, *p<0.05.*

	Extend Curve				**Retract Curve**	
	Breakthrough Force (nN)	Bilayer Thickness (nm)	Indentation Depth (nm)	Elastic Modulus (MPa)	Adhesive Force (nN)	Work of Adhesion (10^{-17} J)
Control	4.4 ± 2.7	6.2 ± 0.1	2.07 ± 0.20	249 ± 132	3.7 ± 2.6	2.8 ± 2.4
Melatonin	4.1 ± 2.2	5.9 ± 0.1	1.77 ± 0.19	228 ± 112	3.2 ± 2.2	1.9 ± 1.6
% Difference	3.8 ± 9.8%	***2.7 ± 0.5%**	***14.5 ± 5.7%**	5.4 ± 6%	16 ± 12%	***31 ± 13%**

The average breakthrough force value trended towards a reduction however the result was not statistically significant across the three independent samples, in 2/3 independent experiments breakthrough force was reduced by ~ 10% whereas in 1/3 experiments breakthrough force was increased by ~10%. When looking more closely at the distribution of breakthrough forces (Figure 3.4), melatonin causes an increase in the difference between the ordered and disorder phases, implying melatonin is reducing the overlap in the force required to rupture each of the membrane phases; this can be seen that the control distribution fits a single gaussian curve whereas with melatonin present a bimodal gaussian distribution is apparent. In a sense melatonin increases the contrast between domains in terms of the breakthrough forces, this is analogous to what was previously observed in NMR experiments of POPC/DPPC/Cholesterol containing membranes[335].

The average overall bilayer thickness was significantly reduced by 2.7 ± 0.5%, although the reduction was not statistically significant for each domain separately. From previous neutron scattering work, it was shown that melatonin decreases the thicknesses and increases chain disorder in DPPC and DOPC membranes, in contrast to cholesterol which has the effect of

increasing chain order and thickening the membrane [333]. In this previous work, DOPC membranes with 9% and 28% melatonin the bilayer thicknesses were reduced from 5.13 nm to 5.01 and 4.91 nm respectively (2.3% and 4.3% difference), while for DPPC bilayer thicknesses were decreased from 5.63 nm to 5.5 and 4.9 nm (2.3% and 13%)[333], this suggests a greater effect of melatonin on the DPPC lipid bilayer, likely due to DOPC bilayer having greater chain disorder and more room laterally for melatonin to occupy without influencing bilayer properties. This correlates with the trends that were observed in this AFM/AFS study, where bilayer thickness of the disordered phase (enriched with DOPC), decreased by only 1% compared to 3.8% for the ordered domains (enriched with DPPC). So, it seems the ordered domains are more influenced by melatonin, but the amounts of melatonin in each phase remain unclear.

A similar trend between indentation depth and bilayer thickness was observed, where melatonin reduced the indentation depth of the probe tip in the membrane across the entirety of the membrane 14.5 ± 5.7% ($p<0.05$). The bimodal distribution fits however were not significantly different in their most probable peak fits (in part due to inter-sample variability), but also implying equivalent decrease in indentation depth across each domain, 9.1 ± 9.1% for the disordered domain, and 17.7 ± 13.8% for the ordered domains. Thus, melatonin thins and decreases penetration depth into the lipid bilayer.

Finally, with the elastic modulus there was not a statistically significant effect of melatonin exposure for the global mean, however a statistically significant decrease of 14.6 ± 2.8% in the most probable elastic modulus of the disordered membrane region was measured. This suggests that melatonin is softening the disordered membrane domains to a greater extent than the ordered domains, this may also be attributed to the increase in the proportion of disordered membrane domain coverage. As has been shown in previous work Melatonin has an inverse relationship to cholesterol in terms of its effects on area per lipid molecule and compressibility of lipid membranes — melatonin increases the area per lipid and elastic compressibility and cholesterol decreases these parameters[333,336]. Based on these new data this is confirmed that melatonin has an effect to increase membrane fluidity, with contributing factors from the increase in proportion of disordered membrane phases and the increase in the elastic modulus of the disordered membrane phase.

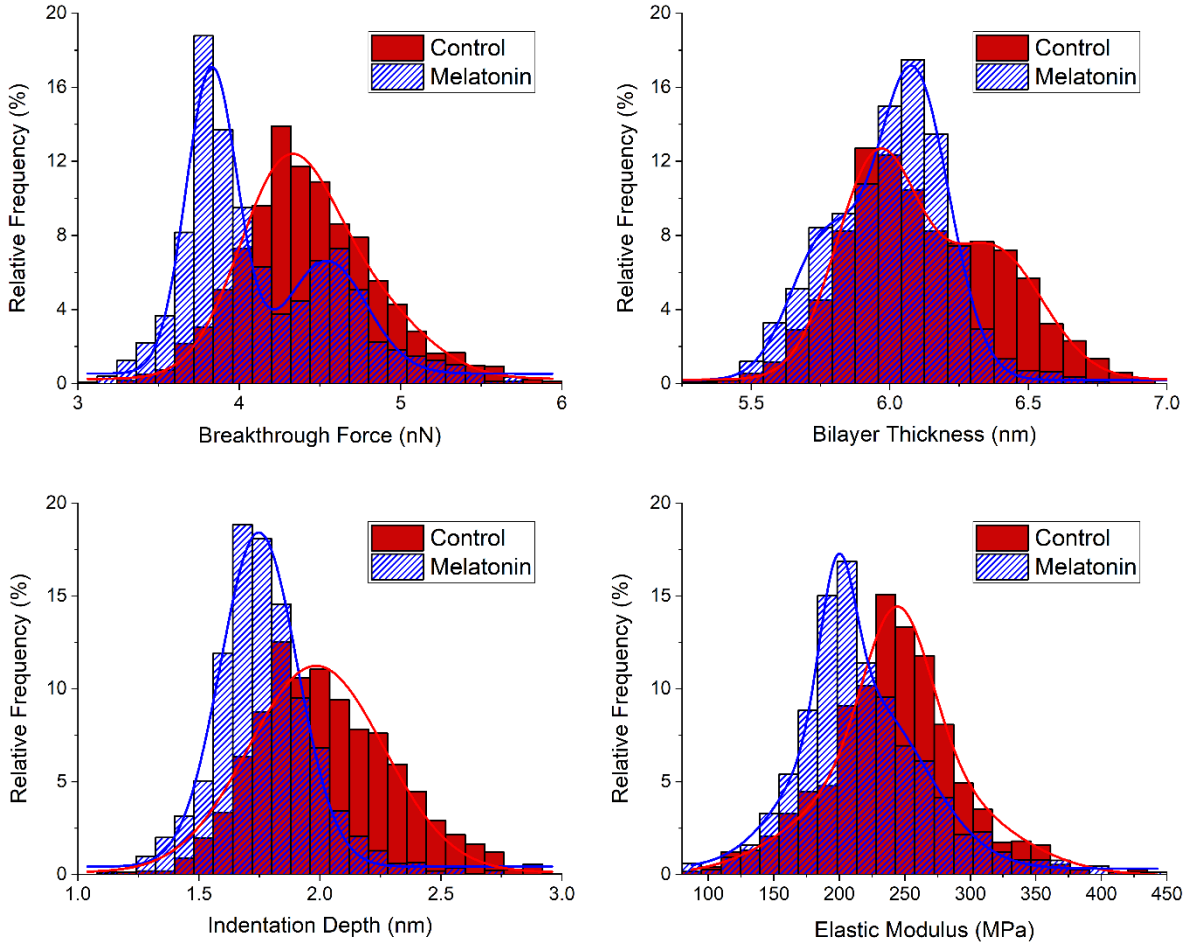

Figure 3.4. Histogram of nanomechanical properties of bilayer from breakthrough force plots: bilayer thicknesses, breakthrough forces, indentation depth and elastic modulus. *Histograms were the mean shifted average of n=3 independent samples, total of N=2100 force curves. In general, melatonin decreased bilayer thickness, breakthrough forces, indentation depths and the elastic modulus of the disordered phases.*

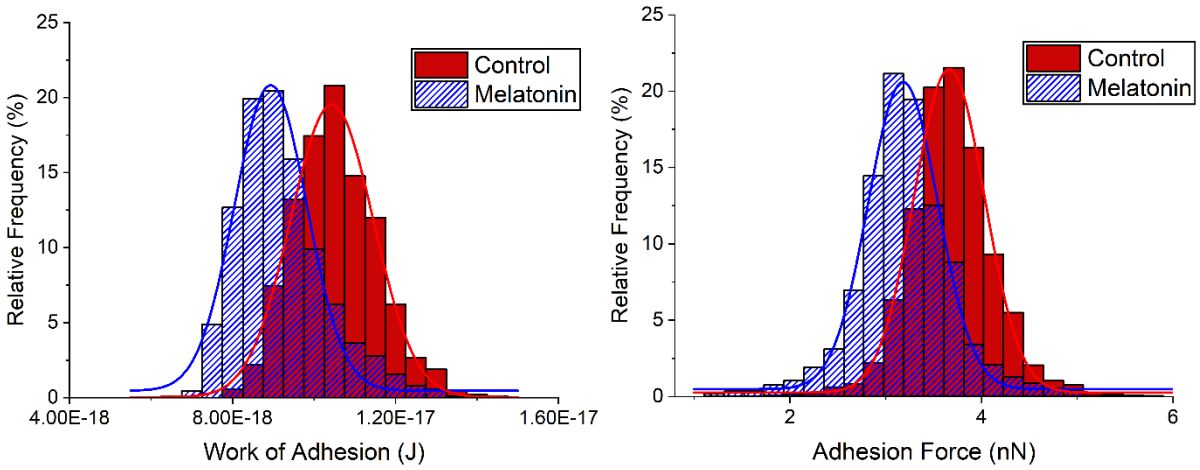

Figure 3.5. Histogram of adhesion force and work of adhesion. *Both distributions are significantly shifted to the left indicating that melatonin reduces adhesive forces between the lipid membrane and the AFM probe.*

Adhesion is a very important property for membrane function especially in the context of AD, where Aβ is known to bind to and disrupt membrane structure. It has been observed that Aβ can bind preferentially to L_O or L_D phase domains depending on the lipid model and perhaps aggregation state of Aβ[161], and that lipid rafts and membrane microdomains (which are often modeled biophysically as ordered gel phase domains), play a critical role in the mechanisms of Aβ production, aggregation and toxicity[17,141]. From the adhesion data, histograms shown in Figure 3.5 above, these data indicate that melatonin reduces the work of adhesion by 31.1 ± 13.4% ($p<0.05$), and trends towards reducing the adhesive forces (16.2 ± 12.5%, though not significant) between the probe tip and the lipid bilayer. This may imply that a membrane saturated with melatonin would be less susceptible to Aβ binding and thus less susceptibility to Aβ toxicity. At melatonin concentrations between 0.1 to 1.0 millimolar, melatonin molecules have been shown to incorporate into the lipid membrane and increases membrane fluidity; with molecular dynamics simulations suggesting that the melatonin orients parallel to lipid tails in the headgroup region[100,333,336]. In previous NMR experiments using a three-component POPC/DPPC/Cholesterol system, it was found that perdeuterated POPC tails were more susceptible to transitioning into a phase coexistence with the addition of melatonin than the same model comprised of fully deuterated DPPC, suggesting a greater interaction between the more disordered asymmetrically unsaturated lipid and melatonin. Taken together with the results here, specifically that L_D membrane regions have significantly lower elastic modulus after melatonin exposure, it adds more evidence to the idea that these disordered regions are indeed more susceptible to influence from melatonin, which appears to occur with other small amphiphilic

molecules, both endogenous signaling molecules (like neurotransmitters), pharmaceutical compounds and drugs[347,349,350].

The effect of melatonin to increase the extent of the L_D domains of lipid bilayers by AFM is similar to an effect observed for serotonin in a report by Dey et al. (2021)[350]. In that report, serotonin was observed to cause disordering of ordered domains in a lipid bilayer composed of DOPC, sphingomyelin and cholesterol at a 2:2:1 ratio. Visually similar to what is reported here for 45% of samples prepared from powder. Notably they also reported a decrease in the bilayer indentation force, which was not significant in our study, though the trend was in the same direction. DOPC has two unsaturated fatty acid tails and thus is highly susceptible to oxidation, which can trigger a chain reaction of lipid peroxidation that can travel within the plane of the membrane. The variability in the effects of melatonin may be influenced by temperature (which was not carefully controlled), and/or changes in lipid composition as a result of oxidation.

3.4 Conclusion

In this work the effects of melatonin on the domain structure of complex phase separated lipid bilayers was studied by AFM and AFS breakthrough forces for the first time. The composition of our lipid model is simple compared to biological neuronal membranes (which are composed of many hundreds of different lipids), but more complex than models frequently seen in literature which are commonly composed of one or two lipid types. The DOPC/DPPC/Chol model has the added complexity of phase segregation into L_O and L_D phases in ambient conditions. Cholesterol affects fluidity and mechanical stiffness of membranes as well as the lateral domain structure. These are important factors in cholesterol dependent cellular processes and have been implicated in AD pathology and Aβ toxicity. The interaction of melatonin and other small molecules with cholesterol containing membranes is thus important for furthering our understanding of cell processes.

Based on these preliminary data, the inconsistency in the effect of melatonin on the SLBs may point to issues in sample preparation from dry powder or controlling for environmental factors like temperature. Sometimes we observed these changes, in 4 out of 9 experiments, while only minor changes were detected in 2 out of 9, and the remaining 3 no discernable changes were found. This effect could be due to lipids prepared from dry powder which may be more susceptible to oxidative damage, as they require an additional processing step (weighing) and are

directly exposed to air, unlike for instance lipids that come dissolved in chloroform from the manufacturer. Phase separation behavior is highly sensitive to changes in lipid composition and when near to a lipid melting temperature, are sensitive to temperature. It is known that these models have miscibility transition temperatures near 29 C, and similar to ice melting in water, the closer to this transition temperature the more sensitive the structure of lipids are to small changes in temperature. Moreover, lipids, especially unsaturated fatty acids like DOPC and cholesterol to a lesser extent, are susceptible to peroxidation and oxidation respectively. Once peroxidation of the fatty acid tail is initiated a chain reaction of peroxyl radicals can propagate laterally through the membrane and cause membrane damage. This effectively changes the composition of the lipid bilayer and thus the mechanisms of interaction with melatonin. Analytic biochemistry using GC/MS or LC/MS/MS could be used to identify if this is occurring, however this expertise was not possible during these experiments. This work needs confirmation by repeating these experiments.

In this chapter, stark changes in model phospholipid membranes following exposure to high concentrations melatonin for short exposure duration are reported. Typical peak melatonin concentrations in serum are approximately 100pg/ml, or ~ 0.43nM[351] , though local concentrations in the pineal gland and surrounding brain regions near the pineal recess would be expected to be much higher and the fraction dissolved in the lipid compartments such as the cell membrane higher than hydrophilic cerebral spinal fluid and blood. The data presented in this chapter contributes to a greater understanding of the influence of melatonin on phospholipid bilayers, specifically regarding its interaction with phospholipid bilayers and the effects thereof. For the first time it has been shown that the addition of melatonin from the aqueous phase visibly changed the topographical structure of a phase separated lipid bilayer, decreasing surface area of L_O domains due to melatonin incorporation into both phases along with an apparent displacement of cholesterol from the L_O phase. In terms of the biophysical properties of the lipid bilayer, the topographical changes correlate with a decrease in membrane thickness, increase in the number of breakthrough forces in the disordered force regime. Melatonin also reduced the work and force of adhesion of the probe to the membrane. This decrease in cholesterol associated effects may be involved in the protective effects of melatonin against Aβ toxicity by reducing the extent of membrane microdomains which have been reported to act as seeds for amyloid oligomer binding and aggregation in addition to the reduction of adhesion to the lipid bilayer.

Chapter 4: Contact Mode High-Speed AFM of Phase Separated Lipid Bilayers to Study Melatonin and Amyloid-β Interactions

4.1 Introduction

The cell membrane is a critical interface in biology which serves not only to define the extent of the cell, but also serves to compartmentalize communication and interaction both within the cell and between the cell and the environment. The lipid membrane provides a structure for supporting membrane bound receptor proteins and thus facilitating specific receptor-ligand interactions as well as receptor trafficking which is important for receptor signaling pathways and disease processes[352,353]. In addition, the lipid bilayer is directly involved in less specific interactions that are important for physiological processes including: changes in lipid membrane composition (enrichment with cholesterol, phospholipids and polyunsaturated fatty acids), interactions of small molecules and the non-specific binding of peptides and proteins[354–356]. Peptide and protein binding to lipid membranes occur for a variety of purposes, one example is pore forming anti-microbial proteins (AMP) which bind to the membrane, oligomerize and produce topographical defects and/or pores which damage the membrane, depolarize the cell and disrupt osmotic pressure within the cell resulting in cellular toxicity[357–361]. In Alzheimer's disease, amyloid-β (Aβ) binds to the neuronal cell membranes causing cellular toxicity by damaging the cell membrane and interfering with neuron signalling[362–365]. Interestingly, new research indicates Aβ may serve as an anti-microbial peptide as an important physiological function showing protection against microbial infections in animal models and being upregulated during cutaneous wound repair [366–368].

Atomic force microscopy (AFM) is the essential tool in nanoscience especially for analysis of biological samples that requires nanoscale spatial precision however traditionally it is limited by low imaging rates – on the order of minutes – therefore dynamic process cannot be imaged[303,369]. AFM generates topographical images by means of mechanical interaction with the surface. Forces between an atomically sharpened probe and the sample surface cause a proportional bending of a micrometer sized cantilever upon which the tip is attached. In contact mode, maintenance of constant tip sample forces by adjusting the height of the tip relative to the

sample as the probe scans over the surface provides a topographical map of the sample. An in-house contact mode HS-AFM system that can produce images at video rates has been developed previously. This system not only allows for capturing millisecond dynamic changes in topography but also to generate large scale topographical images with extremely high spatial resolution within much shorter time periods than standard AFM[370,371]. It has been previously demonstrated that this HS-AFM technology can be used for imaging biological samples and capturing processes despite high contact forces with the surface, for instance collagen[372], DNA in ambient and liquid conditions[373] as well as the dissolution of tooth enamel from citric acid[374]. The tip is in contact at a sustained non-zero force as the tip travels at high velocities over the surface thus there is a possibility of the HS-AFM causing damage to the sample or in some way interfering with the interaction of interest. For the first time in this chapter, it has been reported that lipid membranes and peptide lipid membrane interactions important for the mechanisms and treatment of diseases can be captured despite the extremely soft nature of lipid membranes and reveal differing interaction mechanisms between Aβ monomers and oligomers with model lipid bilayers of varying cholesterol composition.

4.2 Methods and Materials

4.2.1 Complex Lipid Bilayer/Amyloid-β Preparation

DPPC, 1-palmitoyl-2-oleoyl-sn-glycero-3-phosphocholine (POPC) purchased from Sigma Aldrich, Cholesterol and dioleoyl-sn-glycero-3-phosphocholine (DOPC) purchased from Avanti Polar Lipids, and Sphingomyelin and GM1 Ganglioside sodium salt from bovine brain purchased from Santa Cruz Biotechnology. Each lipid was dissolved in chloroform at a concentration of 1mg/ml mixed at various ratios then evaporated under dry N_2 gas. Lipid mixtures in chloroform were left overnight to evaporate producing a multilamellar thin film of mixed lipid layers. The thin films were then suspended in ultrapure water to 0.5mg/ml and a SUV solution for vesicle fusion was produced using the sonication method. Vesicle solutions were made one day prior to use, stored in the fridge overnight and then run through two cycles of 15 min sonication followed by 15 min of stirring immediately prior to vesicle fusion onto freshly cleaved mica substrate. Aβ(1-42) ultrapure, HFIP treated, (rPeptide) was prepared in monomeric and oligomeric form following protocols previously described[375]. Monomeric Aβ was prepared immediately prior to injection at 100μM in ultrapure water, 20uL of this solution is added to the

200uL liquid droplet for a final concentration of approximately 10 µM. Aβ oligomers were incubated overnight at 4°C at least 18 hours at 100 µM in ultrapure water, then injected into the liquid cell to a final concentration of 10 µM.

4.2.2 HS-AFM

A modified version of a previously described HS-AFM system[373,374] was constructed in-house and mounted onto a Dimension 3100 AFM which allows for standard and HS-AFM operation, see Figure 4.1. The HS-AFM is a stage scanner with dual sets of flexure bars driven by piezoelectric actuators in both the fast and slow scan directions to generate motion in the x-y plane with the applied voltages defining the scan window size, and the frequency parameters set according to the desired frame rate. The window scan size was calibrated by moving the Dimension piezo tube a known distance in the x and y directions while tracking a prominent feature on the AFM movie. The cantilever was mounted onto the Dimension scan tube set to move in a 1 × 1 nm at 1 Hz line rate effectively providing negligible motion in the x-y plane while still allowing the scan tube to provide control over the z movement using the Dimension feedback and controller system. A constant cantilever deflection was maintained by the Dimension feedback. The HS-AFM controller (written in-house using LabView) applies a sinusoidal voltage to drive the scan stage, both fast and slow scan axes with the frequency parameters set according to the desired frame rate. In-house written data collection software takes the magnitude of the cantilever bending from the Dimension photodiode as the stationary probe sits in contact with the surface via the standard optical lever method – data is then linearized to account for the sinusoidal motion of the scan stage. MLCT cantilevers with nominal spring constants of 0.01 N/m purchased from Bruker were used in all cases for both standard and HS-AFM contact mode imaging.

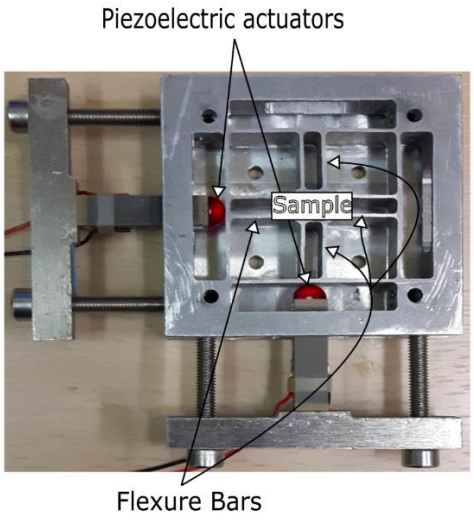

Figure 4.1. HS-AFM dual axis flexure scan stage. *Sinusoidal AC voltage drive signals applied are to the piezo from the AFM controller. The amplitude of the sin waves determines the frame/image size, while the frequency governs the frame rate.*

4.3 Results and Discussion

4.3.1 Comparison of Standard AFM and HS-AFM on Lipid Membranes

Complex lipid mixtures are often used to study the organization and biophysical properties of lipid membranes that possess micro- and nano-domains, typically model membranes composed of 3 or more lipids are considered complex. Here, complex mixtures composed of 5 different lipid species: mainly, equimolar DPPC and POPC (69 - 73 % by mole), with cholesterol (18% by mole), sphingomyelin (6 – 10% by mole) and gangliosides (>3% by mole). These complex model lipid systems were used previously as biomimetic Alzheimer's disease membranes showing how changes in lipid membrane composition (gangliosides and sphingomyelins), render lipid bilayers susceptible to Aβ toxicity[19]. Standard AFM image of one of these model membranes is shown below along with a HS-AFM image of the same membrane, same region in Figure 4.2. Calibration of HS-AFM XY scale can be done one of two ways; the first is to directly compare identical features under standard and high-speed operation provided a standard image is taken before. Alternatively, under high-speed operation the scan tube can be translated by a set distance across the surface, the resulting translation can be seen and measured by tracking features on the HS-AFM. The scale bar on the HS-AFM image was generated using the second technique. There are small discrepancies between measuring distances in this way as compared to the x-y scale generated from the Dimension under standard operation. Calibration of the z scale using this modified dimension HS-AFM system is less trivial, since the HS-AFM

image is generated by taking the deflection signals and plotting them, there is no feedback system with which to calibrate the scale. One way is to compare two identical features captured under standard and high-speed operation and calibrate them this way, otherwise force curves on the samples can be taken and the feedback/deflection signals can be extracted to calibrate the cantilever sensitivity. This method of calibrating sample sensitivity may be affected by sample deformation, though for lipid bilayers the bilayer thickness is quite small, so that after the probe breaks through the bilayer to the mica subsurface, this part of the contact curve should be suitably hard to get a good approximation of the cantilever sensitivity.

To compare the images taken under high speed and standard operation Figure 4.2 below shows a side-by-side comparison of the same region of a complex lipid membrane. It appears there is non-linear distortion of the HS-AFM image when comparing to the standard speed; it appears as though there is compression along the fast scan axis in addition to a clockwise skewing of the image. Although the tip trajectory over the scan stage is much more complex than these two simple transformations and additional motion of the cantilever tip in the z direction need to be accounted for to perfectly map standard AFM images to the HS-AFM frames. Regardless of this distortion HS-AFM imaging resolution is still excellent compared to standard AFM. Though there appears to be greater overall image noise this is highly variable and depends more on tip and sample quality. One advantage is that there is less line-to-line mismatches aberrations and AFM artefacts, which keeps image processing time down.

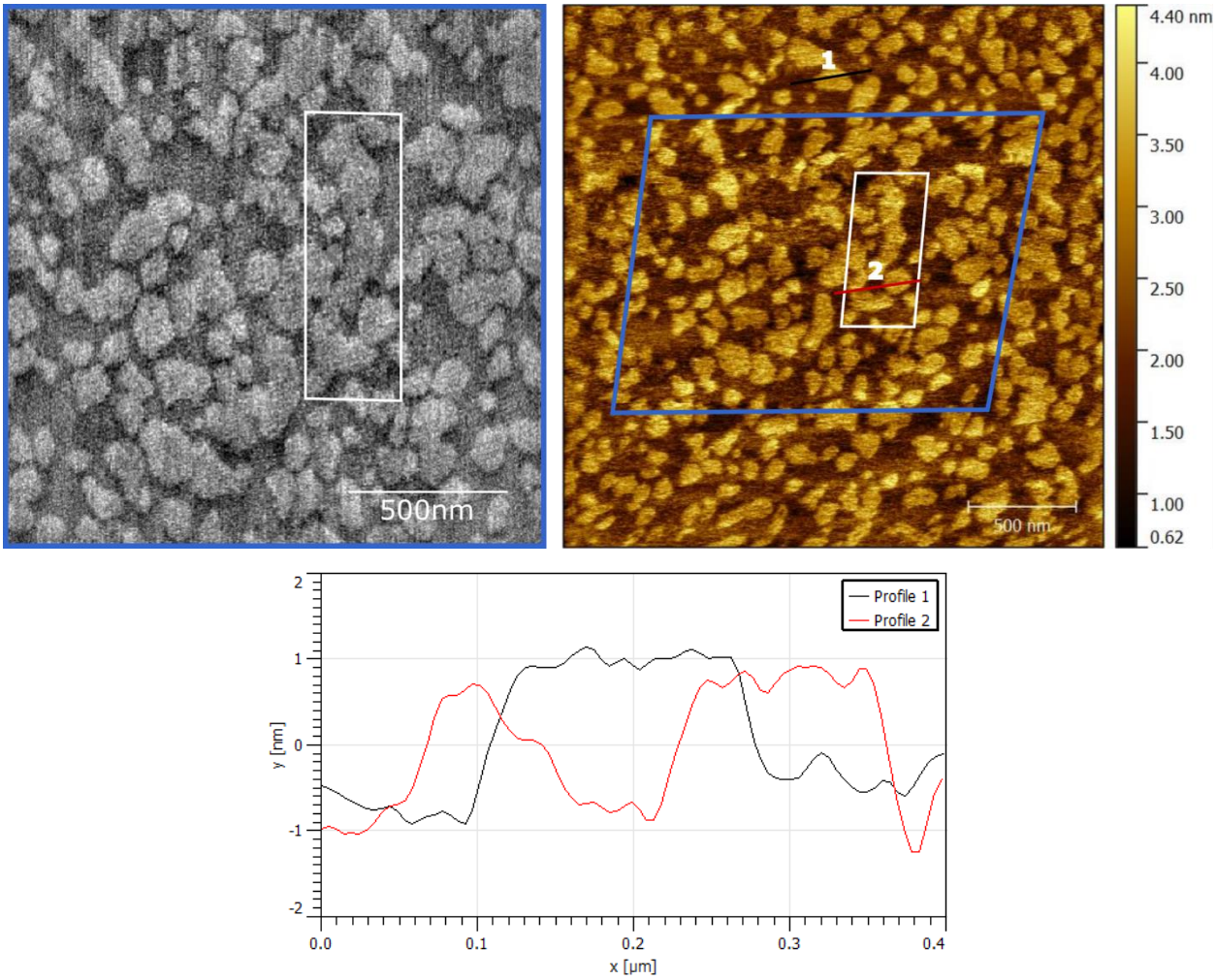

Figure 4.2. Side-by-side comparison of lipid bilayers under HS-AFM (left pane) and standard AFM (right pane). *HS-AFM scale calibrated from the standard AFM image. Profile indicated on the Standard AFM image higher ordered domains (correspond to cholesterol, sphingomyelin and ganglioside enrichment), are 1.2 – 1.6 nm above the disordered domains.*

4.3.2 Stability of Lipid Membranes During HS-AFM

To test the stability of the membrane under prolonged HS-AFM imaging several areas of a complex membrane at a continuous 2 fps were imaged (Figure 4.3 & 4.4). The stability of the complex membranes during HS-AFM imaging was highly variable but in general the length of incubation time greatly increased the stability of the supported lipid bilayer on the surface. Figure 4.3 shows HS-AFM imaging immediately after preparing the complex lipid membrane at a constant 2 fps for ~2 minutes (120 AFM frames), after which time significant damage to the membrane was observed as the higher ordered domain lipids appear to be swept away. Damage to the membrane was more apparent at the edges of the scan region, where the velocity of the probe is lowest, and the acceleration is at a maximum. As the probe scans across the surface at

high-speed hydrodynamic lift off of the probe tip above the hyper-confined ice-like ultrastructure of the 1nm water layer above the surface is the best explanation for how high contact forces and speeds of the AFM probe tip during high-speed scanning prevents damage to the surface – albeit not completely – as is the case here. At slower speeds, near the edges of the scan window, the effect of hydrodynamic lift off would be minimized and the probe may come into momentary contact with the lipids, below the confined water layer. Then when the probe picks up speed, heading back toward the middle of the frame, the probe would lift higher above the surface as hydrodynamic lift off increases.

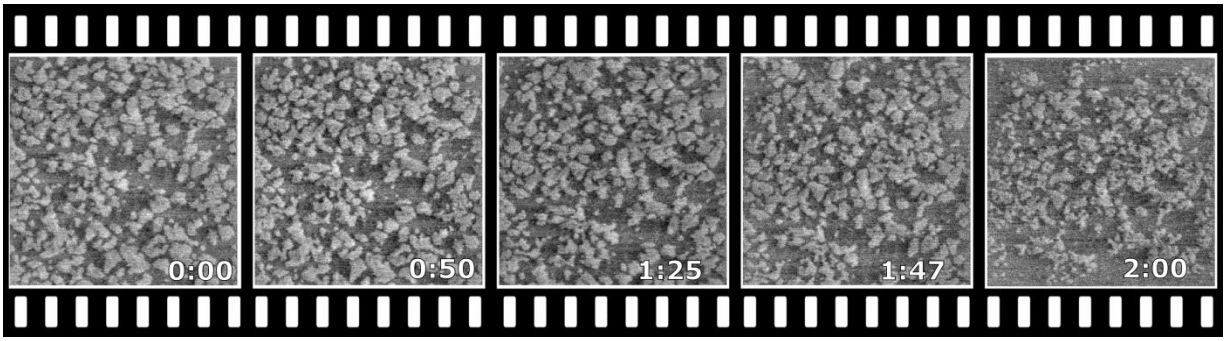

Figure 4.3. Instability of complex neuronal model membrane imaged with HS-AFM *continuously for 2 minutes continuously at 2 fps. It appears the higher domains are being swept away over the course of the 2-minute scan time with the most pronounced effects disruption at the edges of both the slow and fast scan directions where the lateral AFM probe tip velocity goes to a minimum and the acceleration is at a maximum.*

Figure 4.4 shows ten frames over a period of 52 minutes on a different area of the same membrane as Figure 4.3, but 2 hours later. There is some drift due to the height adjustment of Dimension scan tube under feedback however it can clearly be seen that high resolution HS-AFM movies of the membrane are very stable over very long scan times. There are no noticeable changes in the lateral domain arrangement or topographical height. The improvement in stability was greatly improved even after 30 to 60 minutes of additional adsorption time (membrane stable over 30 minutes), then increased gradually with longer adsorption times to stability upwards of 1 hour, although it cannot be ruled out that changes in temperature and variation in mica substrate properties that can affect membrane absorption on the surface. Reducing tip sample contact time and thus total energy applied to the surface by taking snapshots of the surface or moving the AFM scan window, should greatly reduce any damage of the surface induced by HS-AFM imaging at the expense of lower time scale resolution.

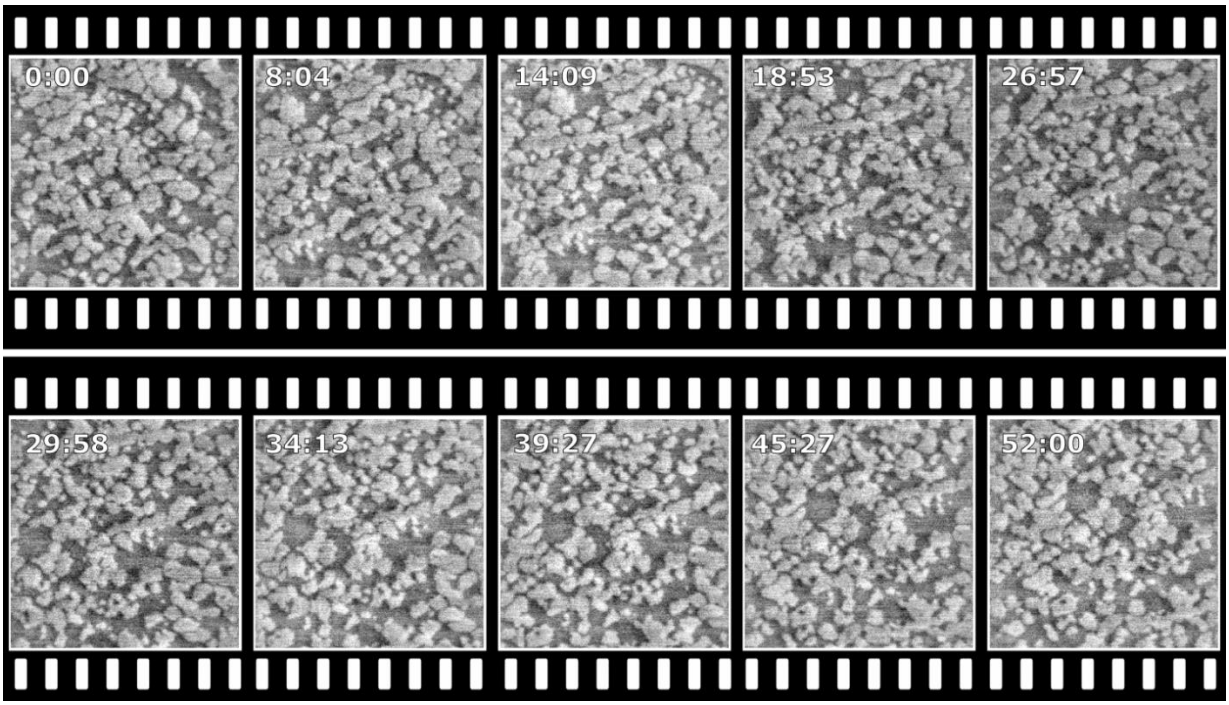

Figure 4.4. Stability of the complex lipid bilayer after additional 4 hours. *Membrane stable over very long scan times upwards of 52 minutes are possible at 2 fps, a total of 6240 frames. Some drift of the image frame occurs due to small changes in force feedback adjustments by the AFM but no changes in lateral domain structure or height changes are caused by the high-speed AFM, scan size ~2 µm × 2 µm.*

4.3.3 The Effect of Melatonin on Complex Neuronal Membranes

During scanning melatonin was added to the liquid droplet to a final concentration of 400µM – the maximum predicted solubility for melatonin in water (Figure 4.5). At time 0 minutes melatonin was added to the fluid droplet and multiple imaging regions were scanned over this time. Melatonin appears to open regions of disorder within these higher more ordered domain regions, breaking up the membrane, red box in Figure 4.5. These higher domains correspond to more densely packed cholesterol enriched regions and would also contain sphingomyelin and gangliosides for which cholesterol is known to interact with to induce the formation of ordered domain and membrane lipid rafts[376,377]. This disruptive effect of melatonin is likely a combination of melatonin binding to the membrane microdomain, intercalation into the membrane and then lateral domain rearrangement of the lipid bilayer membrane microdomains. The increase in membrane disordered regions is consistent with the fluidizing effects of melatonin[100,104,335]. The effects of HS-AFM imaging on the lipid bilayer cannot be excluded and is likely responsible for accelerating the lateral rearrangement. This is supported by the observation that the large intact ordered membrane domain at frame 30:00 (Figure 4.5, red

box), has been exposed to melatonin for that duration of time, and although the structure prior to HS-AFM imaging cannot be determined, after this large domain enters the HS-AFM scan window the large domain appears to begin breaking up within a few hundred HS-AFM frames, increasing proportion of disordered regions over the 18 minutes shown. This effect of melatonin is similar to the effects reported in Chapter 3, where the disordered/fluid phase is expanded and effects reported in the literature for serotonin – a related indole neurotransmitter[350]. It cannot be ruled out that the energy being input into the lipid bilayer by the HS-AFM imaging could be accelerating the process of ordered domain separation.

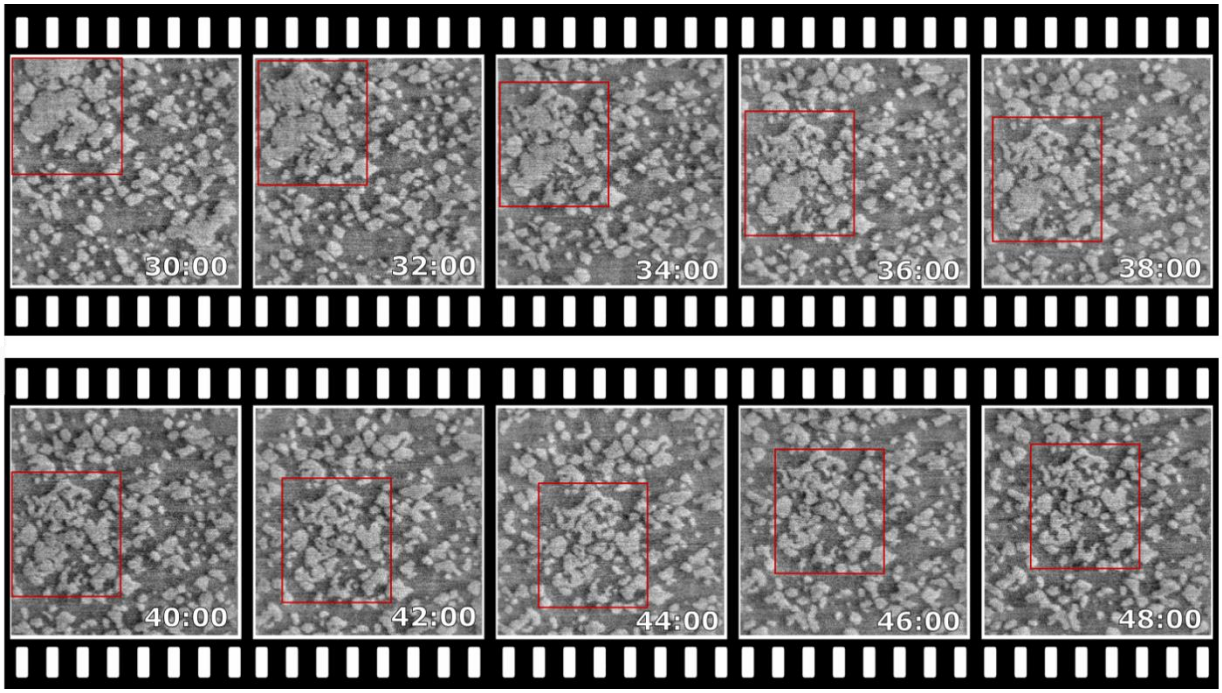

Figure 4.5: Effect of melatonin on lateral rearrangement of the ordered lipid membrane domains *over minute-long time scales due to melatonin and HS-AFM imaging.*

4.3.4 The Effect of Amyloid-β Injection on HS-AFM Imaging During Scanning

The addition of Aβ to the lipid membrane during imaging is shown in Figure 4.6. The membrane was very stable under HS-AFM imaging over 2400 AFM frames prior to the addition of amyloid. The addition of amyloid to the flow cell often caused a temporary loss of stability and significant drift due to the manual injection procedure which is very difficult to perform without disturbing the HS-AFM, therefore, imaging the same region before, during and after injection is not always practically possible. It was frequently observed that Aβ injection during scanning resulted in disruption of the HS-AFM video capture, which could result in image

distortion, imaging failure and damage to the membrane within the scan window, upon the amyloid reaching the scan area. In the experiment shown in Figure 4.6, Aβ appears to destabilize the membrane, or the tip-membrane interaction, and it appears that the higher more densely packed lipid domains seem to be most affected – see Figure 4.6. Similar disruptions in HS-AFM imaging occurred during other trials where Aβ was added during scanning. After about 4 minutes of HS-AFM scanning the image contrast between ordered and disordered domains was dramatically reduced compared to before Aβ injection. HS-AFM image roughness dramatically increased within 5 to 10 frames after Aβ solution diffused across the scan window. Very shortly (~2-3 seconds), after the 4-minute time point imaging failed completely. This clearly highlights the importance of tip-sample interactions as it scans across the surface of lipid bilayer and cannot be neglected, regardless this damaging effect is only observed when Aβ is added to the liquid cell; control injections of water do not result in any long-term disruption of the membrane during high-speed scanning (not shown).

There are various potential explanations for the behavior: Aβ could be disrupting the surface and the HS-AFM sweeps the lipids within the vicinity away, Aβ could also be binding and aggregating on the tip causing it to become more adhesive disrupting not only the membrane but also the forces between the tip and the surface. This could be due to a combination of amyloid binding directly to the membrane and/or amyloid aggregating on the tip of the probe and affecting tip-sample forces. If amyloid is aggregating on the tip, it could be expected to cause some adhesion between the probe and the membrane as the HS-AFM scans across the surface. If so, then the dimension feedback system would have to compensate for these additional forces to satisfy the force setpoint which could cause the AFM to lift off the surface or to be driven deeper into the surface. On the other hand, if the feedback system over or under compensates than this too could disrupt HS-AFM imaging, image quality and/or complete imaging failure. Overall, this increase in tip lipid bilayer interactions induced by sticky aggregation prone Aβ appears to disrupt HS-AFM imaging and may increase chances of damage to the lipid bilayer.

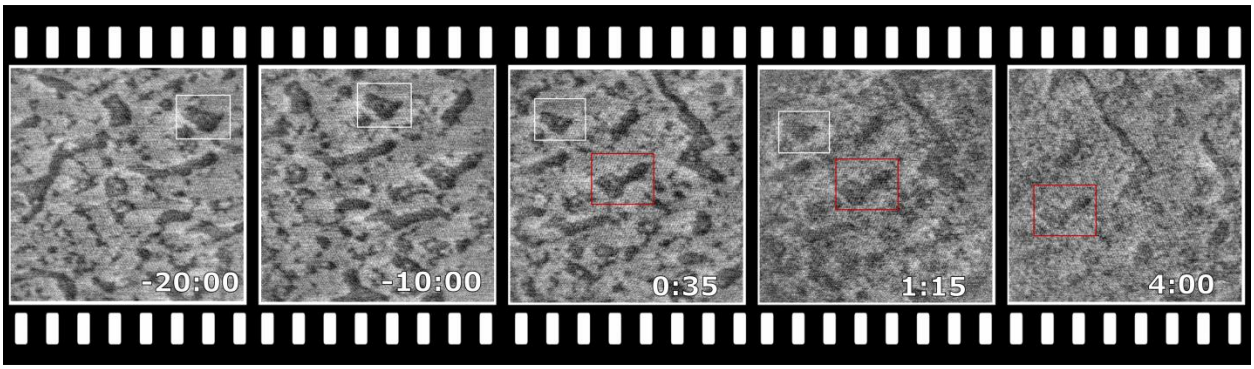

Figure 4.6: Destabilization of HS-AFM imaging upon addition of Aβ. *Membrane region was scanned continuously at 2 frames per second for 20 minutes, Aβ was added during scanning at t = 0. Beginning around 35 seconds, a dramatic increase in membrane roughness is observed, domain structures appear to be disrupted uniformly. With time this disruption is more pronounced as at 4 minutes, shortly after imaging fails completely.*

4.3.5 The Effect of Amyloid-β on DOPC/DPPC/Chol Lipid Bilayers

In this study two different phase separated lipid bilayer models were used to study the effects of different aggregation states of Aβ (monomer and oligomer), on interactions with lipid bilayers. Here membrane vesicles were formed and then allowed to self-assemble into supported lipid bilayers where control images were taken with HS-AFM system and then these lipid bilayers were treated with 10μM Aβ (either monomer or oligomer), for 1 hour before being rinsed and then imaged again. Sample homogeneity across very large ~ 2 - 4 mm areas was determined by manual moving the scan stage with the course adjust. For data collection, the HS-AFM scan window size was tuned to be about 3.5 x 3.5 μm then the scan window was set to raster across 10 steps in each x and y direction (for 100 frames), in 2 μm step sizes over 3 different regions on each membrane. One powerful advantage of HS-AFM imaging is that within one or two frames of imaging it can be determined whether a good lipid bilayer is formed, and an assessment of large-scale sample homogeneity can be determined within only a matter of 1 or 2 minutes, thus making troubleshooting poor sample preparation very effective.

Figure 4.7 shows several frames stitched together of DOPC/DPPC/Cholesterol containing lipid bilayers at 1:1:1 and 2:2:1 molar ratio, with cross sections showing differences in domain heights between 0.7 and 1.0 nm for both membranes. These height differences correspond to the two distinct phases of these membranes, the disordered phase enriched in unsaturated phospholipids, and the ordered phase – enriched in cholesterol and unsaturated lipids. Membranes with lower cholesterol concentration (2:2:1), tended to have more narrow domains that were interconnected across large scan areas, whereas high cholesterol membranes tended to

have more isolated domains, although this effect was variable, and likely depends on fluctuations in ambient temperature and small variations in lipid ratios from sample to sample.

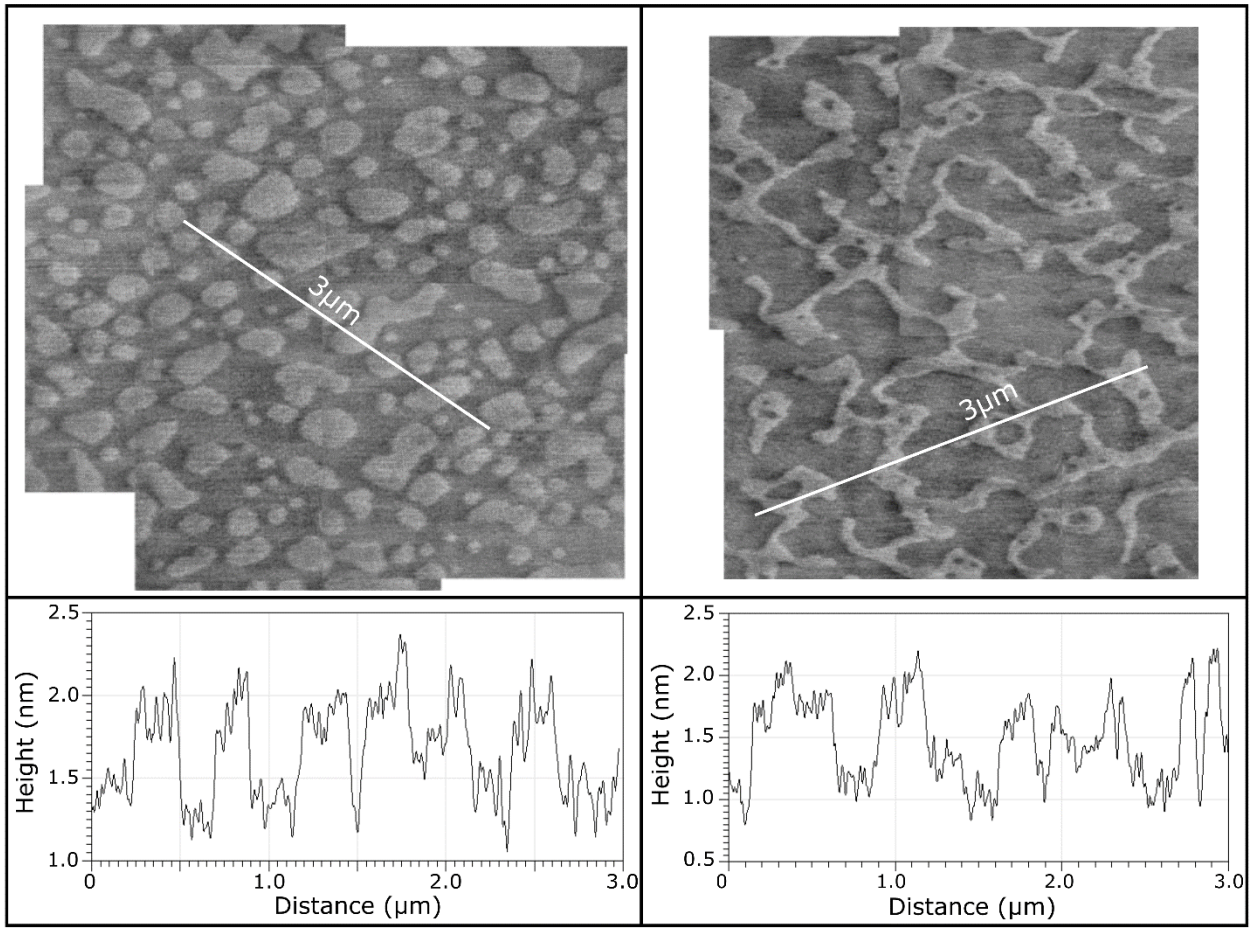

Figure 4.7. The structure of DOPC/DPPC/Cholesterol lipid bilayers at different molar ratios *of 1:1:1 (left) and 2:2:1 (right) with cross sections displayed, domain heights for both 0.7 to 1.0 nm.*

After acquiring control images of these two membrane models, Aβ as unaggregated monomers or pre-aggregated oligomers were added and imaged. It is observed that as the HS-AFM scan window moves to a new scan region containing Aβ aggregates on the surface, some of these taller aggregates are swept off or possibly pressed into the lipid bilayer by the AFM probe. This could be due to differences in binding affinity of the taller aggregates on the surface or due to greater shear forces at larger heights from the AFM probe as it scans at high speed over taller image features on the surface. This leaves behind stable aggregates that are more strongly bound to the ordered domain lipid bilayer surface which are stable under high-speed scanning for at least 100s of HS-AFM frames.

Figure 4.8 shows low concentration cholesterol membranes treated with Aβ prepared in monomeric form. Variability in lipid membrane domain structure prior to Aβ exposure was frequently observed for reasons mentioned previously: i.e., temperature, and small differences in stoichiometry of lipids. It was observed that Aβ monomers bind preferentially to the ordered membrane microdomains, taller domains, producing structures that protruded above the lower disordered membrane phase by 1.8 ± 0.3 nm after 2 hours and 2.2 ± 0.2 nm after 8 hours. Aβ incubation for 2 hours on lipid bilayers produced less tightly bound Aβ aggregates on the surface. After 8 hours, Aβ monomer and lipids appear to organize into very stable multi-layered domains, of 0.9 and 2.2 nm above the disordered lipid phase. At the 2-hour timepoint the RMS roughness of the Aβ region on the membrane was increased by 43 ± 18%, then after 8 hours this increased to 70 ± 16%. The increase in surface roughness with time is likely due to the increased height of Aβ aggregates on the ordered domains in the 8-hour timepoint.

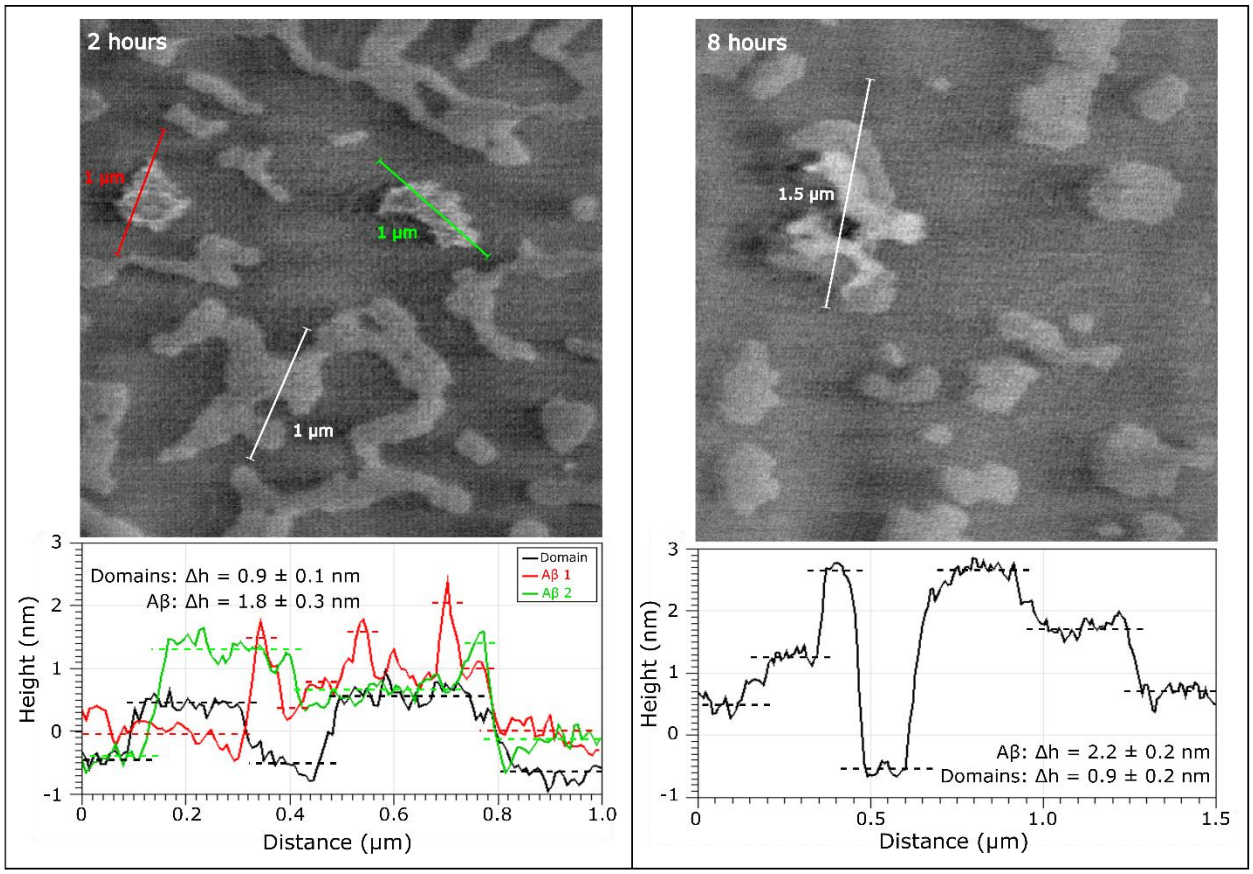

Figure 4.8. Low cholesterol lipid bilayers treated with monomeric prepared Aβ for 2 hours and 8 hours*. Aggregates preferentially bind to ordered membrane microdomains and are initially unstable, able to be swept off the surface of the lipid bilayer by HS-AFM imaging (2019-05-16), after 8 hours aggregates form stable multilayers on ordered domains.*

We observe several different morphologies of Aβ monomers on high cholesterol containing membranes, it is observed that Aβ monomers bind to ordered membrane domains, which are most apparent at the boundaries of the domains (Figure 4.9). This leaves what appears to be a pore-like structure which depends on the size of the ordered domain. More detailed frame by frame analysis of the pore-like structure reveals 4 to 5 globular aggregates arranged in a ring. This similar morphology of ion channels was detected previously, though in a different lipid model system and different Aβ preparation using proteoliposome deposition, where Aβ was mixed with the lipids in organic solvent, left to evaporate and produce a thin film and then resuspended into a supported lipid bilayer[378]. This proteoliposome system is much less physiologically relevant than the protocol used here, as Aβ is expected to deposit onto cell membranes from the extracellular space. Ordered domain heights are approximately 0.9 ± 0.1 nm above the disordered phase with Aβ monomers protruding to 1.8 ± 0.3 nm above the disordered phase, for this Aβ-lipid membrane complex. Aβ aggregates on the lipid membrane surface increased membrane surface RMS roughness by 63 ± 15% and 64 ± 12% for the ordered domain aggregates and the small pore structures, respectively.

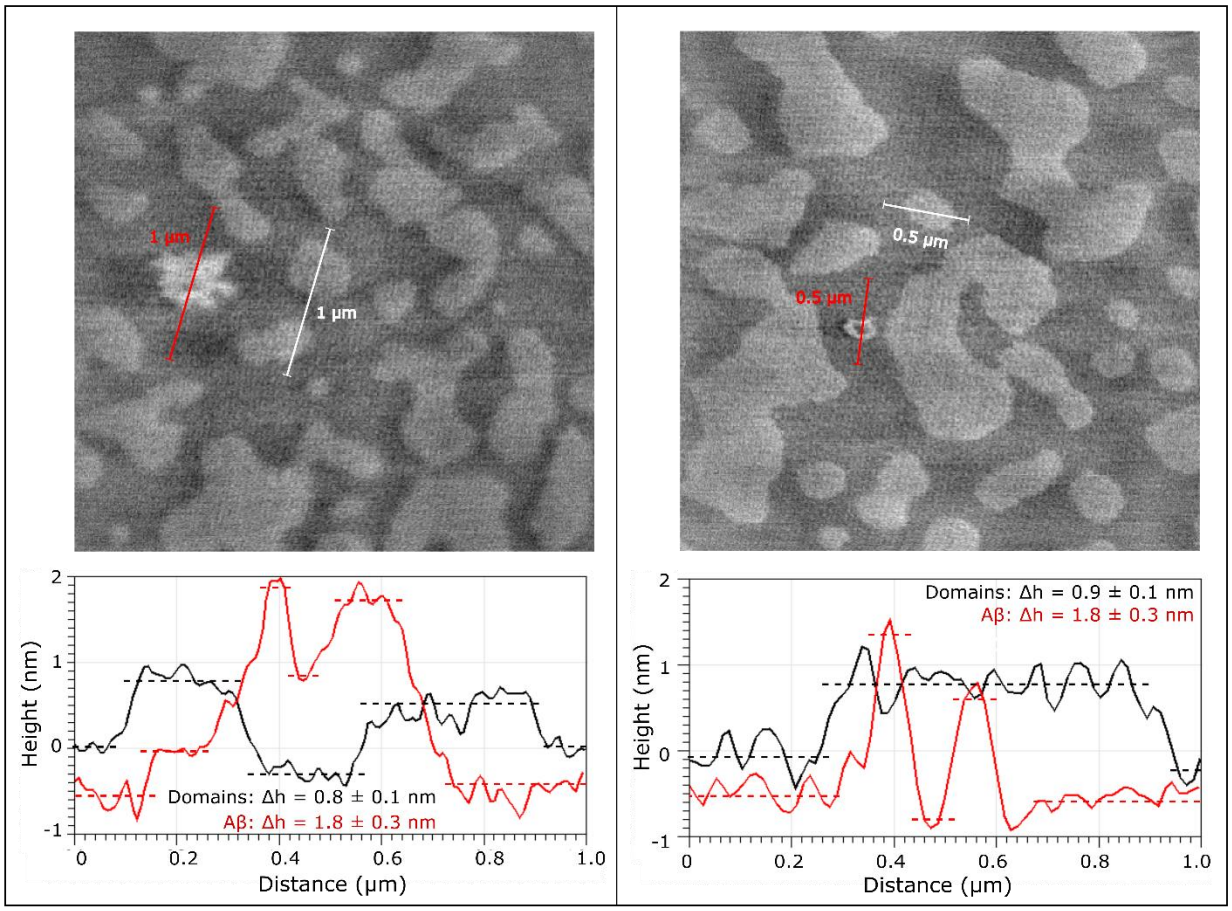

Figure 4.9. High cholesterol lipid bilayers treated with unaggregated Aβ monomers. *Aβ preferentially binds to ordered domains(left), in some instances forming what appear to be small pore-like structures (right).*

Low cholesterol lipid bilayers treated with preformed oligomeric Aβ exhibited unique membrane interactions (Figure 4.10), first the oligomers did not appear to exhibit preferential binding to the ordered membrane phases, Aβ oligomers bound to the disordered and ordered domains indiscriminately resulting in disruption to both phases of the lipid bilayer, inducing holes alongside the protruding Aβ oligomers in clusters. The height of the tallest oligomers above the disordered phase was 1.5nm with minimum heights below the plane levelled mean, indicative of holes in the membrane. These aggregates had increased surface roughness, by 16 ± 9 %, which was the lowest roughness among all the groups. This is likely due to the aggregates penetrating deeper into the disordered phases of the lipid bilayer, rather than sitting atop the ordered phases.

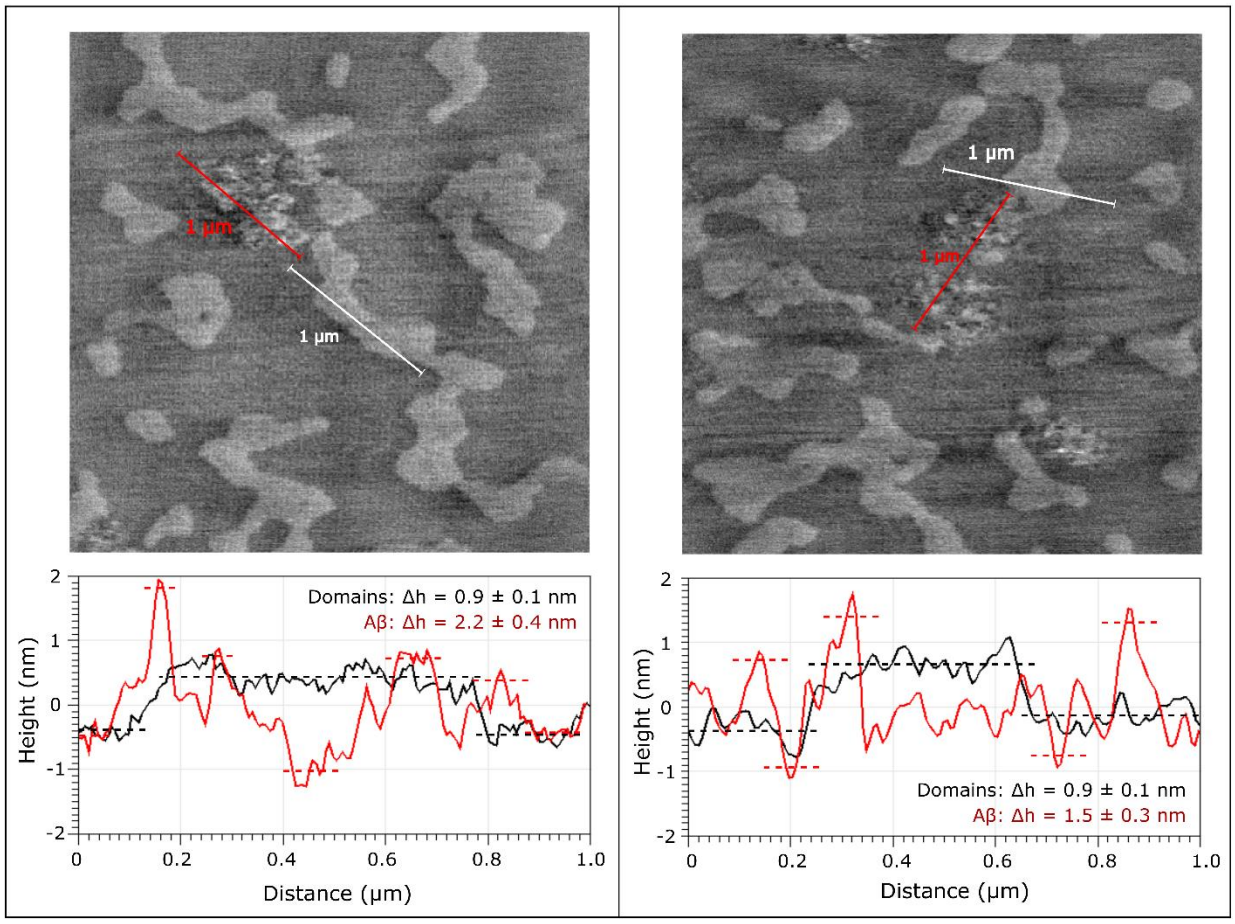

Figure 4.10. Low cholesterol lipid bilayer treated with preformed Aβ oligomers. *Aβ oligomers bind indiscriminately to membrane, with no apparent preference for ordered or disordered domains. Aβ oligomers appear to penetrate the membrane creating patches with multiple perforations. Increase in membrane surface roughness is observed in regions where Aβ oligomers have bound to and disrupted membrane topography.*

High cholesterol lipid bilayers exposed to Aβ oligomers also exhibited more obvious damage to the lipid bilayers in the form of holes more than monomeric Aβ, as in the case of low cholesterol membranes (Figure 4.11). There are two different types of interaction mechanisms observed for Aβ oligomers with high cholesterol membranes. First, binding and aggregation onto the ordered domains like in the case of monomers sitting about 1.8 nm above the membrane surface. Second, there was also a distinct formation of large and deep holes in the membrane, penetrating as much as 2.1 nm below the ordered phase. This type of extraction of the lipids from the membrane surface by amyloid is likely due to some solubilization like effects that have been reported previously[168]. It may be difficult to say for certain whether the measurement of these holes is accurate due to the speed of the HS-AFM probe over the surface and the hydrodynamic lift-off effect, and the lifetime of the confinement-induced structured water may allow the probe

to not penetrate the full depth of the bilayer thickness. Typically, bilayer thickness is reported to be at minimum 5 nm, therefore the 2.1 nm depth of the hole could be indicating removal of only the top leaflet. Regardless, the damage to the membrane is apparent, and distinct compared to all other conditions tested here. Surface roughness analysis does not reveal a difference between the two conditions compare 41 ± 17 % and 40 ± 27 increase in RMS surface roughness of the Aβ aggregates, complete roughness analysis for all conditions is listed in section 4.5: Supplementary Material.

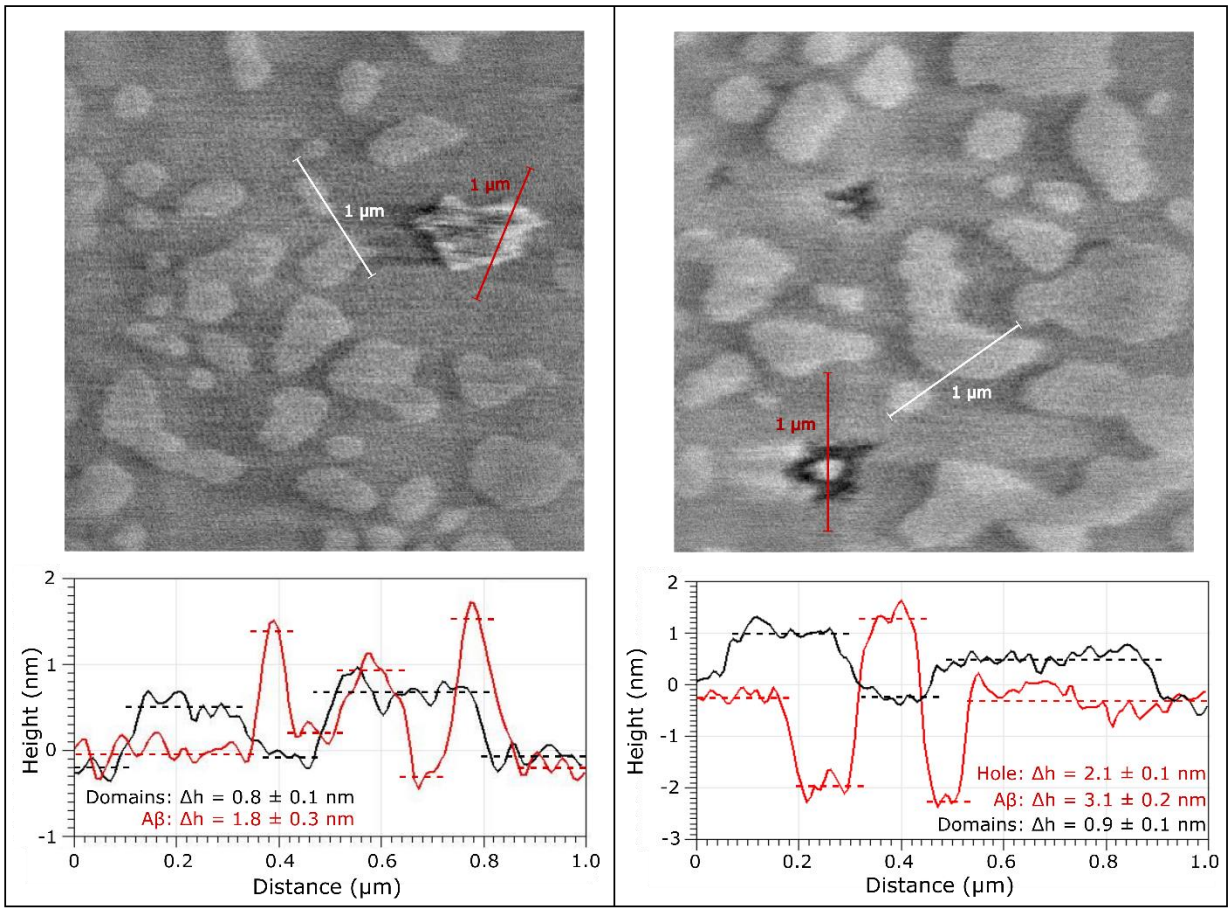

Figure 4.11. High cholesterol membranes treated with preformed Aβ oligomers*. Two primary interaction mechanisms occurred, one where amyloid bound to the top of the membrane, preferentially on ordered domains forming semi stable structures, and one in which amyloid bound to the membrane and generated holes in the surface, with a central structure at similar height as the ordered membrane domain.*

Low and high cholesterol lipid bilayers treated with Aβ monomers and oligomers exhibit different membrane interactions with some common trends across treatment conditions. In all cases Aβ increased surface roughness, (both mean and RMS), as well as increases in height on all the AFM images. Preferential binding of Aβ monomers and oligomers to high cholesterol

ordered lipid domains was observed most cases, except for low cholesterol membranes treated with oligomers. In both low and high cholesterol membranes Aβ monomers bound to ordered domains and formed aggregates on top of the membrane, in comparison Aβ oligomers were observed to penetrate the membrane and form holes in the lipid bilayer. Aβ oligomers are known to be more toxic than monomers, this difference in toxicity could be due to the differences observed in this HS-AFM study, that oligomers are more likely to penetrate and form holes in the membrane, whereas monomers simply bind to the membrane surface and not able to penetrate the membrane. The surface roughness did not correlate with penetration into the membrane, but with the greater height difference (Δh) and therefore may not be a good measure of membrane damage.

4.4 Conclusion

In this chapter, the use of contact mode HS-AFM for studying lipid bilayers and protein membrane interactions is presented for the first time. Typical AFM experiments are long and arduous to collect data, when a single high-resolution image often takes upwards of 20 minute to gather, then process and analyze. The ability to gather images of comparable quality on the orders of seconds means that projects have the potential to be sped up by several orders of magnitude. Overall, the results here show that it is possible to constantly image an extremely soft sample under constant high-speed scanning to study peptide-lipid and lipid-small molecule interactions.

Constant contact HS-AFM imaging of soft biological samples membranes exhibits destructiveness to poorly fused lipid bilayers. The constant contact high speed scanning was also observed to induce mixing of the lipid bilayer components reducing ordered domain visibility. However, nondestructive high-quality imaging of the lipid bilayer was also shown to be highly reproducible, provided sufficient bilayer fusion has occurred. Non-destructive HS-AFM imaging relies on interesting probe-sample dynamics during high-speed scanning: hydrodynamic lift-off of the probe tip and super-lubricity of the ultra-confined water structure trapped between the tip and the sample have been proposed explanations. HS-AFM is a relatively non-destructive method for imaging soft bilayers comparable image quality to standard contact AFM mode in liquid. It is possible to limit the effects of the tip over longer-term imaging by taking snapshots and not undergoing constant imaging or scanning over multiple areas spending a short period of

time at each location – although these strategies would lower the time resolution of HS-AFM imaging. Newer HS-AFM systems that use laser doppler and do not have active feedback systems may also be superior for imaging peptide lipid interactions, as the probe height can be kept constant and the force on the surface controlled by height, rather than in feedback system which is sensitive to fluctuations in forces during scanning. The ability to image dynamic membrane processes on second level timescales, as well as collecting several orders of magnitude more data has exciting applications.

This work contributes to the understanding of different interaction mechanisms that can occur between Aβ and lipid membranes. Aβ monomers tended toward binding on top of ordered lipid membrane domains in both low and high cholesterol cases. Whereas Aβ oligomers bound to both domains and often resulted in perforations in the lipid bilayer. In the low cholesterol case, the perforations were smaller and surrounded by Aβ aggregates while in the high cholesterol case the holes generated were much larger indicative of a detergent-like effect solubilizing the membrane. There were large differences in the interaction mechanisms, as indicated by the differences in surface topographies, between the different cholesterol levels and the aggregation state of Aβ, and within repeated experiments. These differences exhibit time-dependencies and thus rates of molecular diffusion and proteo-lipid organization are likely important in Aβ toxicity. Oligomers are far more likely to penetrate the membrane and form holes in the bilayer than monomers, possibly explaining the enhanced toxicity of oligomers compared to monomers.

4.5 Supplementary Material

Table 4.1. Roughness analysis for low cholesterol membranes treated with Aβ monomers for 2-hour and 8-hour incubation times.

Frame Surface	2-hour	2-hour	8-hour	8-hour
	Full Frame	Aβ	Full Frame	Aβ
Mean Roughness	385 ± 42	551 ± 79	359 ± 42	646 ± 73
RMS Roughness	483 ± 51	688 ± 91	467 ± 51	794 ± 81
% Difference Ra	-	43 ± 18 %	-	80 ± 16 %
% Diff. RMS	-	42 ± 17 %	-	70 ± 15 %
Line Profile				
	Ordered Domain	Aβ	Ordered Domain	Aβ
Mean Roughness	380 ± 66	583 ± 125	386 ± 95	736 ± 223
RMS Roughness	416 ± 68	685 ± 140	436 ± 102	857 ± 235
% Difference Ra	-	53 ± 27 %	-	91 ± 40 %
% Diff RMS	-	64 ± 26 %	-	96 ± 36 %
Background (Ra)	140 ± 79	-	114 ± 27	-
Background (RMS)	169 ± 91	-	141 ± 30	-

Table 4.2. Roughness analysis for high cholesterol membranes treated with Aβ monomers that aggregate on ordered domains and form pores.

Frame Surface	On Domains	On Domains	Pores	Pores
	Full Frame	A-β	Full Frame	A-β
Mean Roughness	388 ± 25	635 ± 87	359 ± 42	646 ± 73
RMS Roughness	483 ± 32	755 ± 93	467 ± 51	794 ± 81
% Difference Ra	-	56 ± 14	-	49 ± 14
% Diff. RMS	-	63 ± 15	-	64 ± 12
Line Profile				
	Ordered Domain	Aβ	Ordered Domain	Aβ
Mean Roughness	363 ± 61	675 ± 98	386 ± 45	569 ± 41
RMS Roughness	405 ± 64	758 ± 103	426 ± 43	664 ± 43
% Difference Ra	-	**86 ± 22**	-	**48 ± 13**
% Diff. RMS	-	**87 ± 21**	-	**48 ± 14**
Background (Ra)	167 ± 36	-	126 ± 21	-
Background (RMS)	208 ± 44	-	155 ± 20	-

Table 4.3. Low cholesterol membranes treated with Aβ Oligomers on disordered domains.

Frame Surface		
	Full Frame	Aβ
Mean Roughness	451 ± 31	522 ± 32
RMS Roughness	354 ± 24	406 ± 26
% Difference Ra	-	16 ± 9
% Diff. RMS	-	15 ± 9
Line Profile		
	Ordered Domain	Aβ
Mean Roughness	334 ± 64	414 ± 63
RMS Roughness	380 ± 62	513 ± 77
% Difference Ra	-	**24 ± 24**
% Diff. RMS	-	**35 ± 16**
Background (Ra)	143 ± 43	-
Background (RMS)	177 ± 52	-

Table 4.4. High cholesterol membranes treated with Aβ oligomers morphology includes aggregates on ordered domains and hole formation.

Frame Surface	On Domains	On Domains	Holes	Holes
	Full Frame	Aβ	Full Frame	Aβ
Mean Roughness	403 ± 40	569 ± 79	349 ± 41	489 ± 119
RMS Roughness	508 ± 49	727 ± 98	440 ± 52	631 ± 169
% Difference Ra	-	43 ± 17	-	43 ± 29
% Difference RMS	-	41 ± 17	-	40 ± 27
Line Profile				
	Domain	Aβ	Domain	Aβ
Mean Roughness	359 ± 52	518 ± 116	350 ± 67	582 ± 189
RMS Roughness	375 ± 49	631 ± 131	385 ± 64	701 ± 219
% Difference Ra	-	**61 ± 28**	-	**66 ± 38**
% Diff. RMS	-	**68 ± 24**	-	**82 ± 35**
Background (Ra)	141 ± 34	-	121 ± 27	-
Background (RMS)	174 ± 43	-	144 ± 29	-

Chapter 5: The Effects of Cholesterol and Melatonin on Amyloid-β Toxicity in HT22 Cells

5.1 Introduction

The lipid membrane is an often-overlooked aspect of normal cell physiology and disease pathology; one area where it has been shown to be of particular importance is in brain function and Alzheimer's disease (AD)[360]. In the pathogenesis of AD, Amyloid-β (Aβ) progressively accumulates in brain regions necessary for learning and memory resulting in progressive brain atrophy[379]. The production of Aβ from the amyloid precursor protein (APP) is initiated by membrane-associated enzymes, β- and γ-secretases, the presenilin subunits which are known to have genetic link to early onset familiar AD[18,237]. The production of Aβ is cholesterol dependent with a positive correlation between cholesterol levels and recruitment of presenilin 1 and 2 (PSEN1 and PSEN2) to the lipid bilayer where APP is cleaved[143,146]. Aβ also appears to exhibit toxic effects that are cholesterol dependent, where increased cholesterol content appears to increase susceptibility of cells to Aβ toxicity, however there have been conflicting reports in this area[21,152,153].

Cholesterol strongly affects cell membrane properties from a biophysical point of view, including membrane fluidity, permeability, and membrane nanoscale structure (as demonstrated in previous chapter)[65,357,380]. These membrane properties affect receptor signaling pathways through mechanisms involving membrane protein conformational dynamics, protein recycling, trafficking, and distribution[124,381]. In model systems, cholesterol interacts with other membrane phospholipids and sphingolipids condensing them into phase-separated membrane microdomains, with cholesterol and sphingomyelins enriched in these ordered membrane phases (shown in Chapter 3 and 4)[63,73]. These different membrane phases have been proposed to form membrane lipid rafts (MLRs) which compartmentalize different membrane receptor signaling structures that act as an anchor for the cytoskeleton to the lipid membrane and facilitate dynamic membrane processes such as endosome/vesicle formation and fusion [382,383]. This may be particularly important in brain, the most cholesterol abundant organ in the body[234].

As mentioned in Chapter 3, melatonin has been shown to be protective against Aβ toxicity in several cell and animal models of AD[240,323–325,327], although the mechanisms do not

appear to be mediated by melatonin receptors[325]. Therefore, non-specific mechanisms such as their influence on lipid membrane properties and structure, or through antioxidant mechanisms have been suggested[108].

The structure and function of the lipid bilayer is essential for normal physiology. Aβ damage to the membrane is a part of disease pathogenesis involving mechanisms such as oxidative stress and increased membrane permeability[362,365]. The initial events that lead to amyloid overproduction and accumulation are not precisely clear, but much evidence points to changes in brain lipid composition such as in the association with metabolic diseases or due to aging[129]. Aβ in different aggregation states binds to the lipid membrane producing topographical defects which result in structural changes to the lipid membrane that can increase membrane permeability, cause depolarization of the membrane and eventually oxidative stress – overall resulting cellular toxicity[158,357–361]. The binding of Aβ to neuronal cell membranes interferes with neuron signaling, whether through direct binding of Aβ to membrane receptors, or again indirectly through non-specific binding and disruption to the lipid membrane itself[39,196,384]. In this chapter, cell viability data of HT22 cells that have been depleted of cholesterol by treatment with methyl-β-cyclodextrin (MβCD), or treated with melatonin, and exposed to monomeric and oligomeric Aβ is presented.

5.2 Methods and Materials

5.2.1 Cell Culture

HT22 cells were cultured in DMEM/F12 media (Hyclone) supplemented with FBS (Hyclone), pen/strep (Gibco) at 37°C at 5% CO_2 in a humidified environment. Cells were plated into 96- or 6-well BioLite cell culture treated plates (Fisher Scientific) at a cell density of 100,000 cells/ml, incubated for 20 to 24 hours to become 50-60% confluent. Once this confluency was achieved, cell culture media was exchanged to differentiation media composed of Neurobasal media (phenol-red free, Gibco), supplemented with N-2 (containing human transferrin, insulin, progesterone, putrescine, and selenite, Gibco), and L-glutamine (2mM). Cells were left to differentiate for 24 hours. Then, cells were treated with 0.5% methyl-β cyclodextrin (BioReagent for cell culture, Sigma Aldrich) for 1 h to remove cholesterol. Cell culture media was then replaced with fresh differentiation media and treated with Aβ in different aggregation

states across a range of concentrations from 0.5 to 10 μM for 24 hours before cholesterol or cell viability analysis.

5.2.2 Amyloid-β Preparation and AFM Aβ Structural Analysis.

Recombinant Amyloid-β 1-42 (HFIP, rPeptide) was prepared in monomeric or oligomeric forms according to a modified version of protocols by Stine et al., [385] similar to previous studies [38,311]. Briefly, 1 mg lyophilized Aβ was dissolved in 1 ml HFIP, and 100 μg was aliquoted into microcentrifuge tubes where HFIP was left to evaporated under anhydrous vacuum for 24 hours, before being moved to -20 °C freezer until needed on the day of treatment. To produce monomeric Aβ, on treatment day, 100 μg Aβ was dissolved in 4.17 μl DMSO (5 mM solution), sonicated for 10 min, then diluted to 100 μM in supplemented neurobasal media. For Oligomeric Aβ, monomeric solution is prepared as above and then incubated overnight in the fridge at 4°C for 24 hours.

To characterize the structure of Aβ monomers and oligomers, solutions were diluted in MilliQ water (18.2 MΩ) to 10 μM. Solutions were pipetted onto freshly cleaved mica substrate and left to incubate for 10 to 15 minutes. Aβ solution on mica was then rinsed with equivalent volume of MilliQ water 2 or 3 times, then samples were dried and placed into clean petri dishes for later imaging. Imaging was performed using JPK Nanowizard II, in tapping mode using VESP probes (Bruker).

5.2.3 Cholesterol Oxidase Assay

Fluorometric Amplex Red Cholesterol Assay Kit (ThermoFisher) was used to measure cholesterol content of HT22 cells, with modifications for cell culture applications (Figure 5.1). Cells were plated into 6-well plates. After treatment, cells were washed with 1ml ice-cold PBS. 500 μL of reaction buffer (according to manufacturer's instructions), was added to each well, a cell scrapper was used to remove cells, homogenized through high gauge (0.22) needle, then transferred to microcentrifuge tube by pipet. Samples were boiled for 10 minutes to inactivate cellular cholesterol esterase and other enzymes that might interfere with Amplex detection reagent. Reaction reagents were prepared according to manufacturer's instructions (Amplex Red, HRP, cholesterol oxidase) and loaded into 96-well plates. Homogenates were transferred into reaction reagent solution in 96 well plate, placed in incubator for 30 minutes at 37°C, then read

in plate reader at 530 to 560 nm excitation and 587nm emission. BSA protein assay was used to control for difference.

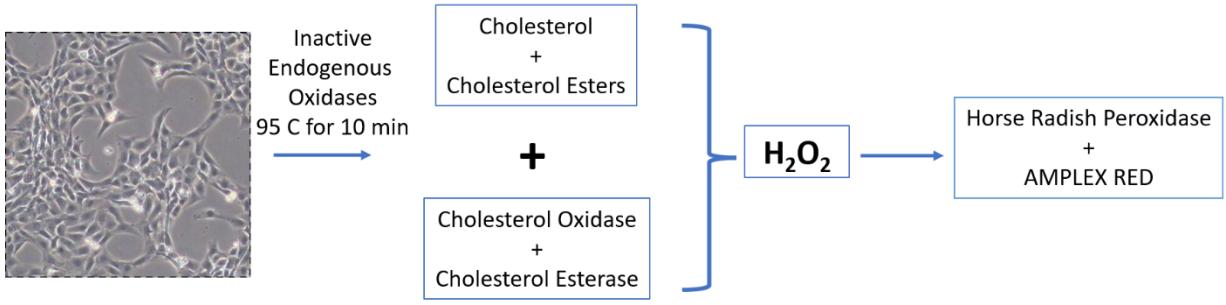

Figure 5.1. Cholesterol oxidase assay for validating cholesterol depletion. *Cells endogenous oxidase activity is inactivated by heating at 95 C for 10 minutes. Cholesterol Oxidase and Esterase is added to the sample producing hydrogen peroxide as a byproduct of cholesterol metabolism. This is then detected by the use of AMPLEX Red detection reagent.*

5.2.4 MTT Assay

MTT assay was used to measure Aβ toxicity after cholesterol removal or melatonin treatment. After Aβ treatment, cell culture media was exchanged for supplemented neurobasal media containing 0.5 mg/ml MTT solution, then cell culture plates were returned to 37°C at 5% CO_2 in a humidified environment for 3 to 4 hours. After incubation, cells were lysed and formazan product within cells was solubilized using a solution of acidified 90% isopropanol, 10% Triton X-100. Absorbance measurements were then made at 570 and 690 nm, with the 690 nm background signal subtracted from the 570 nm signal for data analysis.

5.3 Results and Discussion

5.3.1 Amyloid Monomer and Oligomer Structure by AFM

The atomic force microscope (AFM) is a powerful tool for characterizing the nanoscale structure of molecules, molecular systems and living cells, as well as measuring the mechanical properties of biological systems from lipid bilayers, to living cells and as a means to measure molecule-molecule interactions, all under physiological conditions[299–301,66,302]. AFM was used to characterize the aggregation state of Aβ which has confirmed that preparations contained no fibrils in any of our images. Typical AFM imaging studies of amyloid aggregation use buffers or MilliQ water for dispensing the amyloid onto mica substrates. However, in this cell culture study amyloid was prepared in media which contains high concentrations of small molecules, such as sugars, amino acids, vitamins, minerals, and larger biological molecules, 0.127mM Transferrin

and 0.086mM insulin full chain present in the N-2 supplement. These media components may interact with and become included into the amyloid aggregates, which could affect aggregation rates and structures, in addition to media components absorbing onto the mica surface. Indeed, it was observed that there was higher-than-normal background on the mica surface in the AFM images compared to what is typical for amyloid structural studies using AFM. This higher-than-normal background may obscure amyloid monomers absorbed on the mica surface, increasing the lower limit of the Aβ size distribution, and increasing the effective Aβ particle size. Regardless of these difficulties, monomeric Aβ had typical particle sizes of 0.5 – 4 nm, whereas Aβ oligomers had larger particle sizes and higher variability ranging from 2 to 15 nm, with some protofibrils detected, representative images shown in Figure 5.2. A total of n = 6 independent Aβ oligomer preparations with N=24 images and a total of n = 4 monomeric preparations with N=11 images were collected.

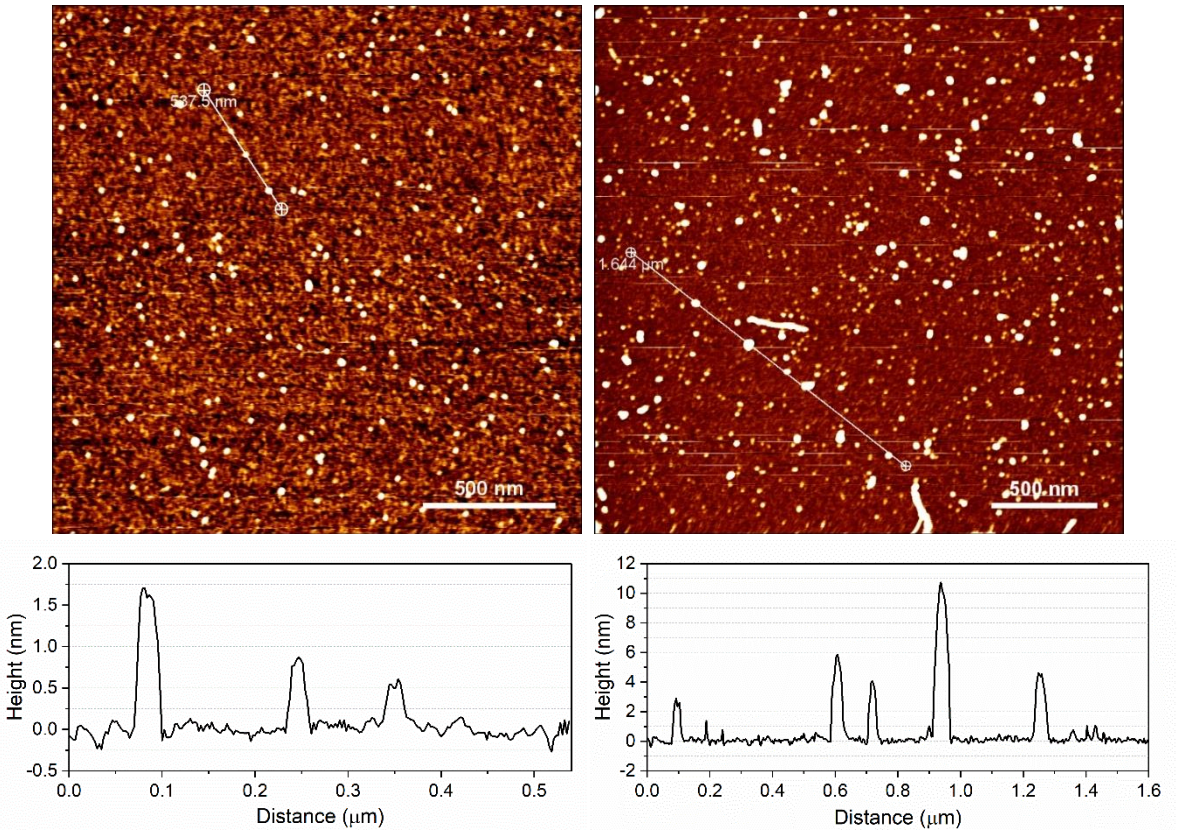

Figure 5.2. AFM images of monomeric and oligomeric amyloid-β on mica. *(left) Monomeric Aβ had typical particle size of 0.5 – 1.5 nm, (right) whereas Aβ oligomers were much larger with particle sizes ranging from 2 to 12 nm.*

5.3.2 Effect of Aβ42 on Cholesterol Metabolism

MβCD is very commonly used to sequester cholesterol from lipid bilayers in molecular and cellular studies. The methylated pore of the cyclodextrin has sufficient size and hydrophobicity to capture cholesterol molecules. MβCD is often used to model the effects of membrane lipid raft disruption and the cholesterol dependence of membrane-receptor signaling, for instance being shown to lower the levels, and modify the trafficking, of NMDA receptors in neurons preventing ischemic injury[139]. This is important as NMDA receptors appear to act as a binding site for Aβ at neuronal membranes, and because cholesterol reduction is implicated in Aβ toxicity as mentioned in the introduction[363], as well NMDA receptors may act as binding sites for initiating Aβ aggregation on lipid membranes[196].

In this report, 0.5% MBCD treatment for 1 hour was sufficient to cause a reduction in cholesterol levels immediately following cholesterol sequestration to 52 ± 9 % of control levels. Cholesterol content of neurons increased slightly to 57 ± 4 % at 8 hours and had mostly returned to normal control levels (90 ± 20 %) after 24 hours, though large variance was observed at this longer time point (Figure 5.3). There was no statistically significant difference in the levels of cholesterol or the rate of cholesterol recovery when HT22 cells were treated with Aβ (Figure 5.3) by two-way ANOVA with Tukey's multiple comparison to control cholesterol levels (α=0.05). The level of cholesterol reduction achieved by MBCD immediately following treatment is similar to what has been reported in other studies[139,386]. Another method that has been used to study the effects of cellular cholesterol in cell culture and animal models is with statins. Statins are a class of pharmaceutical that inhibit HMG-CoA reductase activity, this is the rate limiting enzyme in cholesterol biosynthesis. However reduction of HMG-CoA to mevalonic acid also impairs the production of isoprenoids which are a diverse and complex class of molecules that are involved in a large set of physiological processes and are implicated in a wide variety of disorders, including AD[282,387,388]. Therefore, the use of statins to maintain lower levels of cholesterol throughout the duration of these 24-hour experiments would create confounding effects that would make it difficult to ascertain the role of membrane cholesterol specifically. With that said, there are still likely confounding effects of such a pronounced cholesterol recovery in the HT22 cells because cell viability experiments were performed at the 24-hour timepoint.

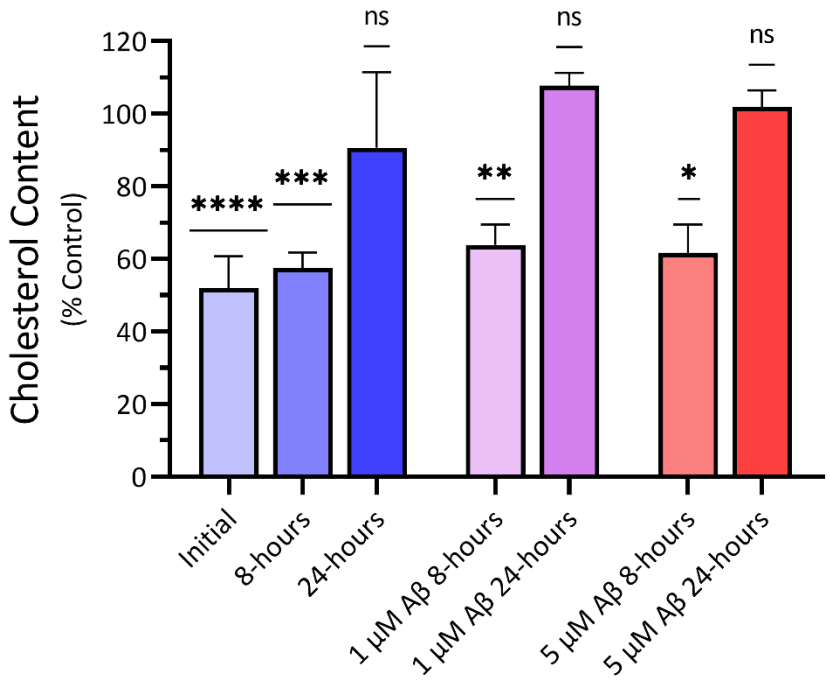

Figure 5.3: Cholesterol content of HT22 cells after treatment with MβCD and Aβ oligomers after 8 and 24 hours. *MβCD reduced cholesterol content of cells by 50% immediately following treatment. Two-way ANOVA with Tukey's multiple comparisons reveals a time dependent recovery of cholesterol in all cases, p<0.05*,0.01**,0.005***,0.001****, n = 5. Mean ± SEM shown.*

Aβ, APP and the secretases that process APP have been shown to affect cholesterol and sphingomyelin metabolism as demonstrated in a presenilin knockout embryonic mouse model wherein Aβ40 was shown to reduce HMG-CoA reductase activity in, while Aβ42 did not affect cholesterol biosynthesis[148]. The authors of that paper suggest one of the roles of APP and its processing into Aβ is to act in a regulatory feedback loop on lipid metabolism, further linking the importance of lipids, lipid metabolism to the Aβ cascade in Alzheimer's disease pathogenesis. However, that report used embryonic mouse cells, whereas HT22 cells used in these experiments is an immortalized cell line with cancerous phenotype that would not be present in the embryonic mouse model.

5.3.3 The Effect of Cholesterol Reduction on Amyloid-β Toxicity.

The protocols to produce different aggregation states of Aβ in this work were adapted from Stine et al. 2011, in that paper Aβ toxicity was screened in N2A cells with preformed oligomers exhibiting a reduction in cell viability to 50% of control at a concentration of 0.1 µM, whereas unaggregated Aβ only reduced cell viability to around 90% at 0.1 µM over 24 hour

treatment[385]. The lower toxicity of monomer Aβ, compared to oligomer Aβ, has also been reported in other studies, however the difference in toxicity between the two species depends on the cell type[41,389,390]. The lower toxicity of monomers was not observed for the preparations used here on HT22 cells, where unaggregated monomeric and oligomeric Aβ exhibited nearly identical dose response curves with an IC50 of 2.5 μM and 2.3 μM for monomers and oligomers, respectively shown in Figure 5.4 (monomers: $n = 4 – p < 0.005$; oligomers: $n=7 – p < 0.05$). This is most likely due to substantial aggregation over the 24-hour 37 °C treatment period and the high sensitivity of HT22 cells to Aβ toxicity. This study indicates that for incubation times greater than 24 hours in HT22 cells are probably too long to properly assess differences in monomer vs oligomer Aβ toxicity by MTT assay.

Cholesterol depletion was protective against both forms of Aβ. A two-way ANOVA (n=4 for monomers and n=7 for oligomers) with cholesterol content and amyloid treatment are the two factors was performed. There was no interaction between cholesterol content and amyloid toxicity. The main effect of cholesterol reduction was a statistically significant reduction in toxicity against both monomeric and oligomeric Aβ by approximately 10 ± 2 % in each case, this effect was most notable at 2.5 μM for monomeric Aβ and 1.0μM for oligomeric Aβ, by Tukey's multiple comparisons ($p<0.05$* for both Aβ species). This is at a low end compared to previous neuroprotective studies in HT22 cells. Other Aβ toxicity studies that utilized HT22 cells found reductions in cell viability caused by 5.0 μM Aβ to be between 50 to 60 % of control [310,311]. This is in line with our study here, where both monomeric and oligomeric Aβ (at 5.0 μM) caused reductions in cell viability of 56 ± 3 % and 52 ± 11 %, respectively. In Wu et al. they show that treatment with 100 and 500 μM nicotine caused recovery from 5.0 μM Aβ toxicity by 10 to 20 %, in a dose-dependent response in HT22 cells. As well, it was shown previously that SG pseudopeptide aggregation inhibitors prevented toxicity from 5.0 μM Aβ oligomers by 15 to 18% at 1:1 and 1:2 ratio of Aβ to inhibitor, also in HT22 cells[311].

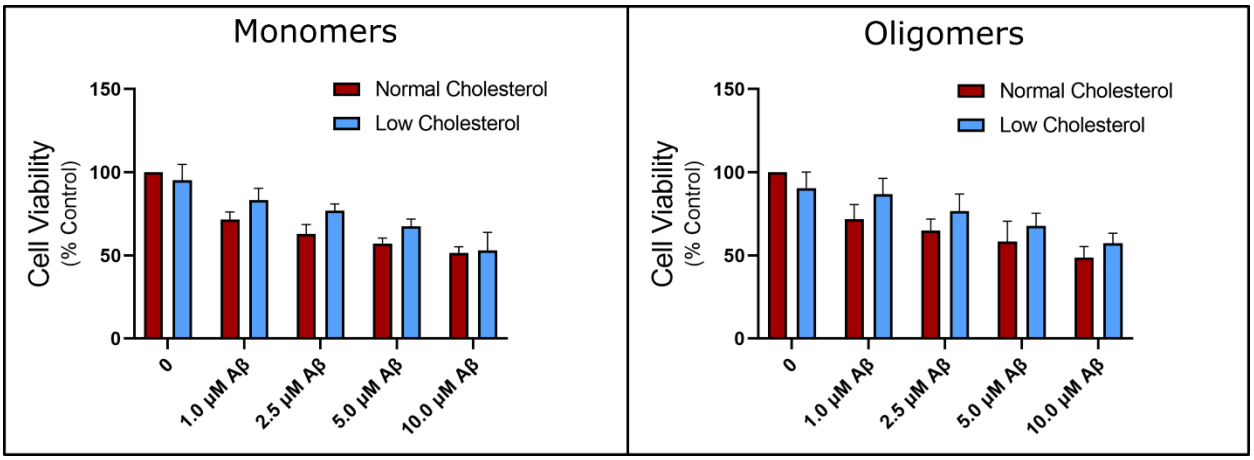

Figure 5.4. Cell viability following application of increasing Aβ monomers and oligomers *to HT22 cells with normal and depleted cholesterol levels. Two-way ANOVA found no interaction between cholesterol depletion and amyloid. A Statistically significant effect was found in the main effects showing cholesterol depletion has a mild protective effect compared to normal cholesterol for both oligomers and monomers (n=4 for monomers, n=7 for oligomers). Plotted as mean + SEM.*

Previous reports have identified important aspects of the impact that cholesterol has on the cellular pathology of Aβ-induced neuronal dysfunction[21,22,152–154,391]. Abramov et al. 2011 showed that amyloid toxicity was enhanced in astrocyte/neuronal co-cultures that were enriched in cholesterol[21]. They observed that cholesterol content was higher in astrocytes than neurons, and that astrocytes were more susceptible to increased calcium flux in astrocytes. They also showed that the presence of cholesterol increased amyloid-induced calcium permeability in unilamellar liposomes, thus demonstrating on the molecular and cellular level that cholesterol was facilitating amyloid-induced membrane calcium permeability. This study also evaluated the proportion of dead cells finding that despite astrocytes having greater calcium permeability and membrane cholesterol, neurons had far higher cell death, and that cell death of each cell type increased after cholesterol enrichment.

5.3.4 The Effect of Melatonin on Amyloid-β Oligomer Toxicity

Melatonin is a small molecule that has been shown to protect against *in vitro* Aβ toxicity in SH-SY5Y cells (human neuroblastoma), primary mouse hippocampal neurons, and rat astroglioma c6 cells[324,325,392]. Since this protection is not necessarily dependent on melatonin receptors, there is a possibility of membrane-dependent effects of melatonin neuroprotection against Aβ. In this study of HT22 cells, control HT22 cells treated with 2.5 μM and 5.0 μM Aβ had reductions in cell viability to 69.1 % and 57.9 % of control (Figure 5.5). Overall, melatonin was found to be protective against Aβ toxicity (two-way ANOVA). No interaction between

melatonin treatment and Aβ was found. Melatonin at 10 µM was observed to increase cell viability to 87.4 % and 79.1 % following 2.5 µM and 5.0 µM Aβ treatment ($p<0.05$* for both concentrations by two-way ANOVA with Tukey's multiple comparisons – Figure 5.5). That is an approximate 18 and 22 % increase in cell viability after treatment with Melatonin. However, at 8.0 µM Aβ there was no statistically significant difference between control and melatonin treated cells, implying a limitation in the potential benefit (two-way ANOVA with Tukey's multiple comparisons, n=5, $p < 0.001$). Compared to previous reports, this protective effect is high, comparable to 500 µM nicotine, and 10 µM SG inhibitor in HT22 cells, and significantly higher than cholesterol reduction observed in this chapter [310,311].

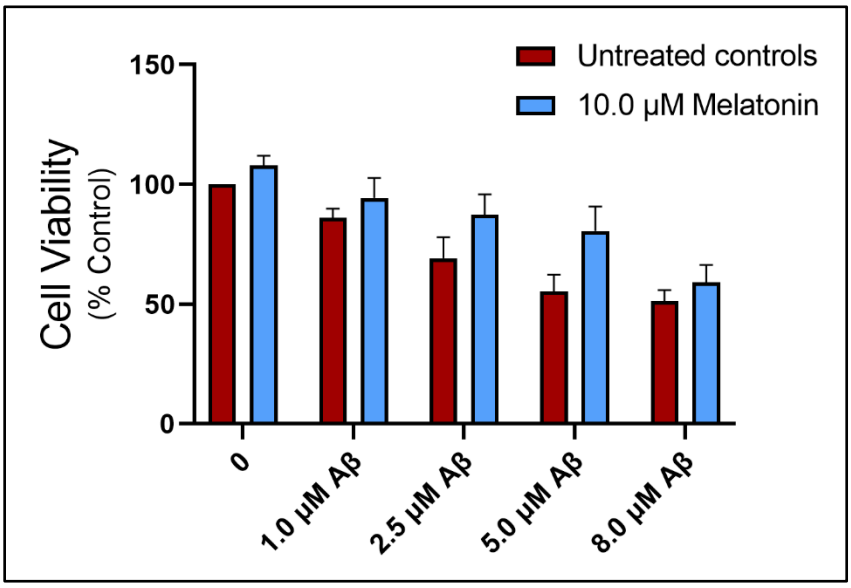

Figure 5.5. Cell viability of cells treated with 10 µM melatonin and Aβ oligomers. *Two-way ANOVA with Tukey's multiple comparison did not find an interaction but did detect a significant protective effect of melatonin in the main effect (n=5). Plotted as mean + SEM.*

There are several proposed protective mechanisms of melatonin against Aβ. Melatonin has two endogenous receptors that are expressed in neurons, however a previous report has shown that the neuroprotection by melatonin is independent of receptor activation[325]. As mentioned previously, Aβ triggers oxidative stress in cells as part of its toxic mechanisms, and since melatonin is a potent antioxidant, it may protect mitochondria from oxidative stress impaired MTT metabolism. These protective effects of melatonin on the lipid bilayer may be of particular importance it has been shown to prevent initiation of lipid peroxidation by localizing near the headgroup region of lipid bilayers[105,332,356,393] and scavenge free radicals from the cytosol and extracellular fluid, thereby preventing or slowing oxidative stress. In addition,

melatonin may affect structural properties of lipid bilayers that prevent amyloid from binding, inserting, or causing defects in the membrane, however concentrations of melatonin required to achieve significant changes in lipid biophysical properties may be larger than what was evaluated here, for instance small increases in fluidity – as measured by monolayer compressibility, were observed in monolayer studies of DPPC at 100 μM, ten times larger than the concentration tested here. The influence of cholesterol on the nanostructure of lipid bilayers (observed in chapter 4), is far greater than that of melatonin (Chapter 3), yet the effect of melatonin to reduce Aβ toxicity is much greater, this would suggest that the membrane structure dependent effects of cholesterol and melatonin on Aβ toxicity is low. Thus, antioxidant properties of melatonin are a more likely source of its protective effect against Aβ. Nonetheless, it is also important to note that these combined effects of melatonin as a membrane-protective antioxidant and regulator of membrane properties and structure could be complimentary.

5.4 Conclusion

AFM analysis was used to assess the structure of Aβ aggregates to correlate with toxicity to cholesterol depleted and melatonin treated HT22 cells finding that unaggregated Aβ monomers were slightly smaller than preformed oligomers. Aβ oligomers did not affect cholesterol levels or cholesterol recovery from MBCD sequestration from HT22 cells. Unaggregated Aβ, assumed to be predominantly monomeric when cells were first treated, was not significantly less toxic than preformed Aβ oligomers in terms of the IC50, despite having smaller size distribution. This is likely due to substantial aggregation over the 24-hour treatment period. Cholesterol reduction and melatonin were both protective against amyloid toxicity as assessed by the IC50, with cholesterol reducing Aβ toxicity by a factor of 2, and melatonin by a factor of 3. Compared to other studies of Aβ toxicity in HT22 cells cholesterol depletion had a low protective effect, while melatonin had a much stronger protective effect.

Chapter 6: The Effects of Cholesterol and Amyloid-β Toxicity on HT22 Cell Morphology by Phase Contrast and AFM

6.1 Introduction

Alzheimer's disease (AD) is characterized clinically by progressive impairment in learning and memory which correlates with neurodegeneration in the central nervous system (CNS). The hippocampus and entorhinal cortex are affected in earlier disease stages as these are the most susceptible brain regions to AD pathology[379]. Later in disease progression more degeneration of the cerebral cortex is observed which correlates with further long-term memory loss, impairments in normal activities of daily life, sleep disturbances and inability to process and utilize language[13,28]. The extensive loss of grey matter is preceded by morphological changes at the cellular level where synaptic density of dendritic spines is reduced, effectively decreasing the number of connections between neurons[394–396]. In AD, the synapses connecting axonal terminals and dendritic spines are lost through a variety of processes involving the accumulation of amyloid-β (Aβ) and damage to the neuronal membrane[394], oxidative stress, hyperphosphorylation of tau protein and collapse of the cytoskeleton, alongside inflammation, and metabolic dysfunction. Many of these molecular and cellular mechanisms involve the cell membrane, for instance cytoskeletal protein anchoring to the cell membrane, oxidative stress causing lipid peroxidation. Thus, the effects of membrane cholesterol and Aβ on the lipid membrane could affect neuronal cell morphology (through cell adhesion and cytoskeleton), which could be important for understanding the cholesterol dependence of Aβ toxicity.

Cell volume and mass data are important for measuring growth rates and changes in cell morphology due to disease states. Volumetric morphology changes occur when mass within one region of the cell (protein, lipid, and nutrients) move to another, this can provide biophysical quantification of cell metabolism and cell migration that is more accurate then measuring surface area in the plane of the tissue culture plate[314,315]. Phase contrast optical microscopy is a widely available method for doing basic morphological characterization of 2D cell culture systems. The phase shift introduced by thin transparent samples is used to generate constructive interference between the thin samples and the incident light, then background light is removed, so that amplitude absorbing objects appear dark over the background [312]. This increase in light amplitude (intensity) due to constructive interference creates optical effects that are not

representative of the true sample thickness, producing halo artifacts at interfacial boundaries within the sample, thus true 3D quantitative imaging using basic phase contrast is not possible. New quantitative phase imaging approaches have been developed that utilize a laser wavefront to accurately measure the phase shifts caused by the sample at each pixel, and through holographic principles reconstruct the path lengths allowing for true quantitative 3D images that can provide cell volume and mass data[313]. These types of quantitative 3D phase imaging are powerful but require specialized optical systems that are not widely available, therefore methods to extract 2D quantitative information regarding cell culture are especially useful for smaller and less well-equipped labs.

One means of overcoming this inability to gather 3D live cell morphology from optical methods is with the atomic force microscope [397]. AFM can be combined with basic optical microscopy and AFM has far greater resolution than quantitative phase imaging allowing for visualization of surface topology rather than simply cell volume and density, in addition AFM can be used to probe cellular mechanics such as Young's modulus, though it suffers from being lower throughput [299–301,66,302]. AFM has been used to characterize the nanoscale structure and properties of living neuronal growth cones, yielding height profiles and elastic modulus of different regions of the neuron growth cone[398]. The effects of fresh and globular Aβ oligomers on cultured endothelial cells has also been explored by AFM where morphology changes within as early as 30 minutes following treatment, where cells appear to contract their cytoskeleton under AFM imaging effects which the authors attribute to Aβ ion channels[399]. A force spectroscopy study with AFM showed that 5 μM Aβ42 greatly increased the stiffness of both N2A and HT22 cells after only 30 minutes of treatment, this effect was attributed to increases in osmotic pressure and incorporation of Aβ peptides into the cell membrane causing membrane stiffness to increase[400]. A similar AFM and force spectroscopy study in aging primary culture models yielded opposite effect, with Aβ decreasing cell membrane stiffness in aged cells with depleted cholesterol over similarly short time scales [400,401]. The difference in these two studies could be related to the choice of cell line vs primary cell culture, the choice of probe, and/or force spectroscopy force regime used. The effects of Aβ in chronic cell culture models, rather than acute models, has not been explored by AFM imaging in live cell culture.

In this study, phase contrast optical microscopy and simple image processing techniques were used in combination with atomic force microscopy to characterize 2D and 3D

morphological effects of cholesterol and Aβ on HT22 cells. This chapter shows that it is useful to combine 2D analysis of phase contrast imaging with complimentary nanoscale imaging technique to generate descriptive 3D information of HT22 cells and reveal the effects of Aβ toxicity on live cells. Phase contrast microscope images of HT22 cell populations, with normal and reduced cholesterol, treated with 1 µM and 5 µM Aβ were analyzed using ImageJ software to extract relative quantitative changes in cell contact area, perimeter, and circularity in the plane of the cell culture dish. Next, AFM was used to characterize HT22 cell morphology on the single cell level providing a descriptive characterization of how phase contrast microscopy images relate to the 3D volume of cells and how Aβ induces different changes in HT22 cell morphology with nanoscale resolution.

6.2 Methods and Materials

6.2.1 Cell Culture

HT22 cells were cultured in the same fashion as to Chapter 4, plated in 6-well BioLite cell culture treated plates (Fisher Scientific) at a cell density of 100,000 cells/ml, incubated for 20 to 24 hours to become 50-60% confluent in full growth media. Once this confluency was achieved, cell culture media was exchanged to supplemented Neurobasal differentiation media for 24 hours. Cells were then treated with 0.5% methyl-β cyclodextrin (BioReagent for cell culture, Sigma Aldrich) for 1 h to remove cholesterol, then fresh differentiation media was exchanged containing media, or Aβ in different aggregation states at 1 and 5 µM for 24 hours before microscopy. After microscopy, cells were harvested for protein signaling analysis in Chapter 6.

6.2.2 Amyloid-β Preparation and AFM Aβ Structural Analysis

Recombinant Amyloid-β 1-42 (HFIP, rPeptide) was prepared in monomeric or oligomeric forms according to the modified version of protocols by Stine et al., [385] as in Chapter 4, details for preparation and structural characterization of Aβ monomers and oligomers are described there.

6.2.3 Phase Contrast Optical Microscopy

After treatment, cells were imaged using Olympus IX51 compound inverted optical microscope at 4x and 10x magnification using identical lighting, contrast, and camera settings.

For both monomers and oligomers, n = 6 independent plates across multiple passage numbers were imaged, with N=2 wells per passage for a total of N = 12 images analyzed.

For image quantification, raw data was imported into ImageJ, converted into 8-bit grey scale, contrast enhancement of 5% (including histogram normalization) for each image was applied. Threshold was set manually for each image to minimize background image artifacts (caused by shadows from condensation in the plate lids, differences in cell culture plate plastic, particulate within media), typical thresholds spanned 63 to 70 arbitrary units, varying no more than 10%. Noise was then reduced using the "Despeckle" feature. The ImageJ "Analyze Particle" feature was used with Shape Descriptors, Area, and Perimeter selected to identify cells and extract cell features. A size threshold in the "Analyze Particle" menu was set to 125 μm^2 and 175 μm^2.

6.2.4 Combined Phase Contrast Optical/Atomic Force Microscopy

After treatment HT22 cells were maintained at 37 °C until ready for imaging. JPK Nanowizard II AFM (JPK life sciences), mounted on Olympus IX71 equipped with 40x LCAch N objective was used for phase contrast microscopy. MLCT AFM probes were used for contact mode imaging cantilever nominal spring constant k = 0.01 N/m, nominal tip radius 20nm. QPBio-AC probes (Nanosensors) cantilever nominal spring constant of k = 0.1 N/m, resonant frequency of 50 kHz was used for tapping mode imaging.

6.3 Results and Discussion

6.3.1 Phase Contrast Optical Microscopy

As mentioned in the introduction of this chapter, traditional phase contrast optical microscopy does not allow for true quantitative 3D imaging of cells, that the value of each pixel in a sample does not correspond to the path length the light traversed through the sample. However, quantification in the 2D sample plane, or the footprint, of certain features in the sample is possible within the limitations imposed by physical sample, microscope resolution, the pixel density of the camera, and the specific parameters of the image processing and analysis algorithm[314]. These approaches have been shown to work adequately for subconfluent cultures where overlapping cells do not interfere with the boundary region between cells that can obscure contrast. If cells are overconfluent under or over counting of cells and obscuring of their morphology in the plane of the dish can be obscured.

In this study, phase contrast images were processed to produce a shadow or footprint of the cell on the tissue culture dish, to do this contrast was maximized, and threshold was set to extreme values making only the strongest light absorbing regions within the field of view visible (Figure 6.1 middle frame), this removes the background, and light halos around cells. The resulting image is biased towards the cell body, which contains the densest most light absorbing part of the cell, dominated by the nuclear region. Cell morphology of HT22 cells depends on cell density and position of the cell relative to other cells within the monolayer. A cell surrounded by other cells tends to have smaller and more circular morphology (Figure 6.1 top panel blue arrows), in contrast cells on the periphery of a cluster tend to have lower circularity and are elongated (Figure 6.1 top panel green arrows). This suggests that there is a cell density dependent effect on cell morphology. This is likely due to growth of overlapping HT22 cells and contact inhibition induced by the surrounding cells, i.e. inhibition of cell growth and migration of cells within a cluster and of continued cell migration of cells on the periphery of a cell cluster. A lack of contrast between cells within a dense cell cluster, especially for cells undergoing cell division is also apparent.

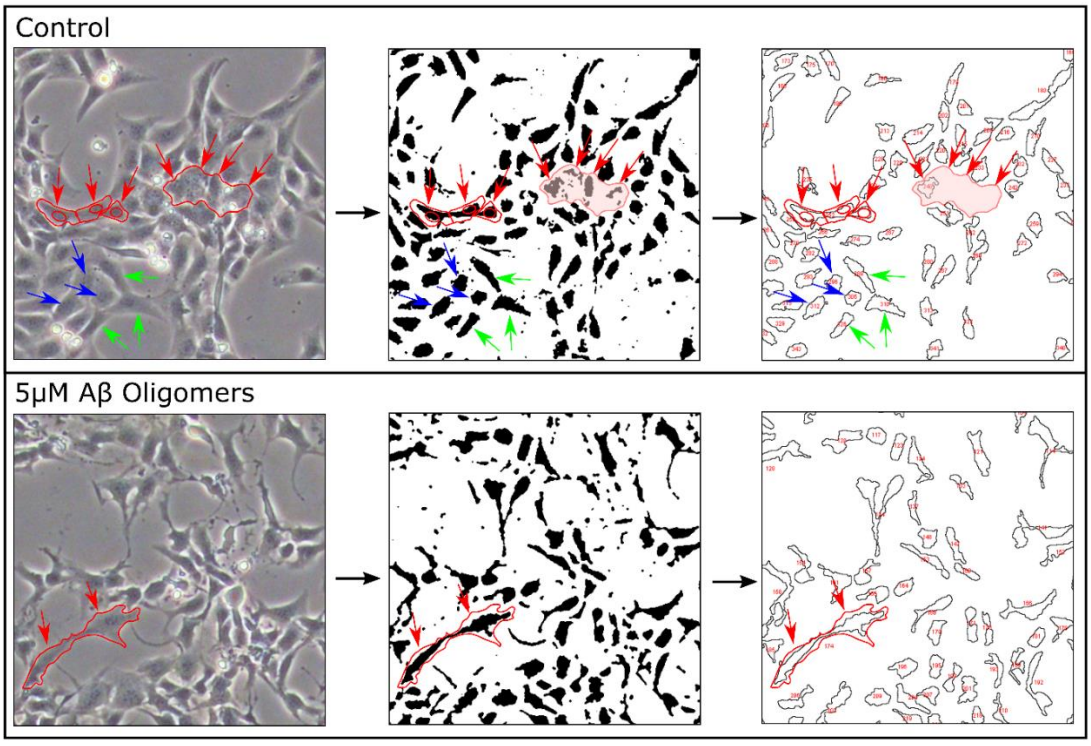

Figure 6.1. Method for performing image processing and quantification. *Phase contrast image was converted to 8-bit greyscale, contrast was enhanced, then ImageJ particle analyzer was used to count cells and compute cell measurements including cell area, perimeter, and circularity.*

The method of image processing used in this study of removing background and enhancing contrast, and threshold detection using built in ImageJ tools is not perfect at identifying cells. In Figure 6.1, the three red arrows on the left in the "Control" images and two arrows on the "5 µM Aβ Oligomers" image indicate a region of the sample containing two or three cells that were misidentified as a single cell. This is an example of how over confluent cultures can be difficult to assess using automated cell counting in phase contrast optical microscope images. Another flaw in the cell detection algorithm occurs where identifying a cell is not possible, this can be seen in the control image of Figure 6.1 indicated by the four red arrows on the right of the images. Based on the size of the footprint of this region it would be expected to count at least three or four different cells, however the contrast of the boundaries between the cells is not sufficiently high to detect a difference over background, and only one of the four is observed. The boundary between these cells is not clear in the raw unprocessed image, the nuclear material within this mass of cells is distributed uniformly and no well-defined nuclear envelope can be seen suggesting these cells may be undergoing cell division. By lowering the threshold for the particle size, it is possible to identify an additional cell in this region, but the boundary between cells within this cluster still remain obscured, Figure 6.2 below shows a comparison between a 125 µm^2 and 175 µm^2 particle size threshold. Despite these limitations in automating quantification of cell morphology, interesting effects on morphology were able to be quantified.

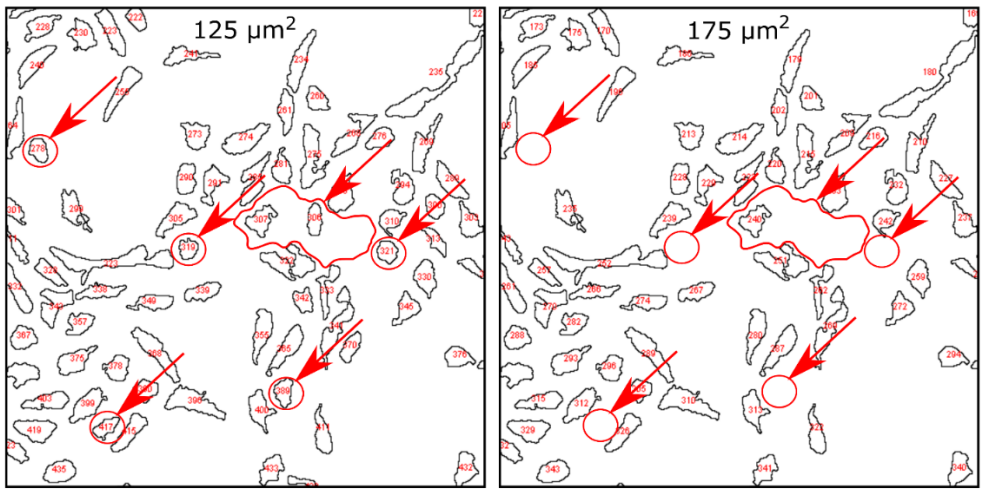

Figure 6.2. Particle size detection threshold is important for identifying cells. *Control cells shown from Figure 6.1 above, left pane particle size threshold 125 µm^2, right pane particle size threshold of 175 µm^2.*

Striking effects of 5 μM Aβ on HT22 cell morphology compared to control cells (Figure 6.3 A vs. C) were found that are reflected in the image processing and analysis that was performed. Control HT22 cells in general have a pyramidal morphology, with smooth boundaries and few projections. Following treatment with 5 μM Aβ HT22 cells appear to become dilapidated, shriveled, they have more rough boundaries, and long protrusions from the cell body appear in cells indicated by red arrows on Figure 6.3, below. The amount of these long protrusions is dramatically increased for cells treated with 5 μM Aβ. This is reflected in the image quantification where a statistically significant increase in cell area and perimeter (Figure 6.4), and a decrease in cell circularity were observed only for cells treated with 5.0 μM Aβ (Figure 6.5), $p<0.05$* by two-way ANOVA with Tukey's multiple comparison to control ($\alpha<0.05$, $n=6$). The qualitative changes in cell morphology, dilapidated with long thin projections from the cell body, correlates with the significant decreases in cell circularity. More detailed analysis of individual cell morphology is not possible at 10x magnification but will be discussed in the next section related to AFM imaging. In contrast, low concentration (1 μM) Aβ treatment caused no obvious effects on HT22 cell morphology visually with a slight increase in cell perimeter and area and decrease in circularity, though these differences were not statistically significant compared to control (Figure 6.4 and 6.5).

Cholesterol depleted cells exhibited a slight increase in cell perimeter and area and decrease in circularity though not statistically significant two-way ANOVA from normal cholesterol groups on the whole. Cholesterol depletion partially restored cell circularity, perimeter and area in cells treated with 5μM Aβ, as it was not statistically different from the control cells. This indicates that cholesterol depleted cells exhibited less Aβ-induced changes in cell morphology and cell damage. This suggests that metabolic improvements, as measured by MTT cell viability assay in chapter 5, correlate with cell morphology data.

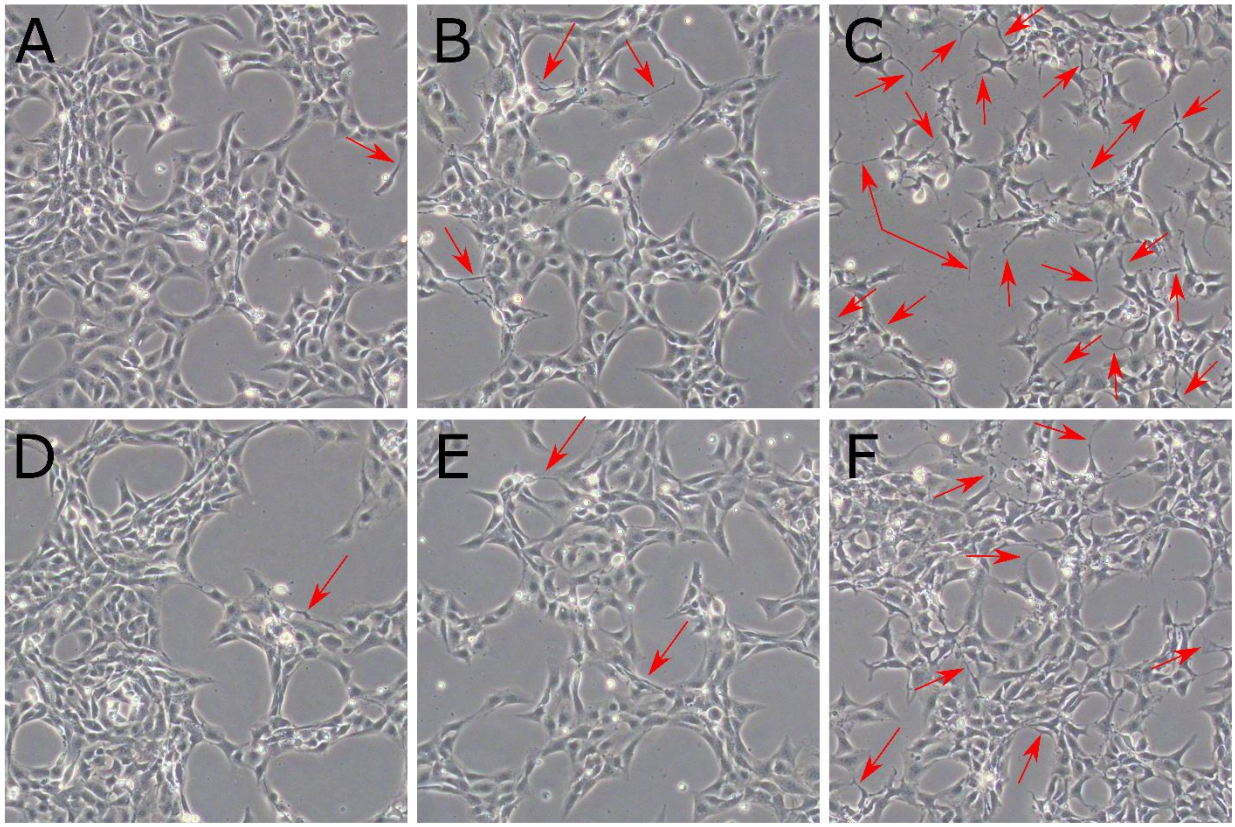

Figure 6.3. Phase contrast optical microscopy of HT22 cells cholesterol depleted and treated with Aβ*. A. control, B. 1µM Aβ, C. 5µM Aβ, D. Cholesterol-depleted, E. Cholesterol Depleted + 1 µM Aβ, F. Cholesterol Depleted + 5 µM Aβ. Red arrows point to neurons containing long cell protrusions.*

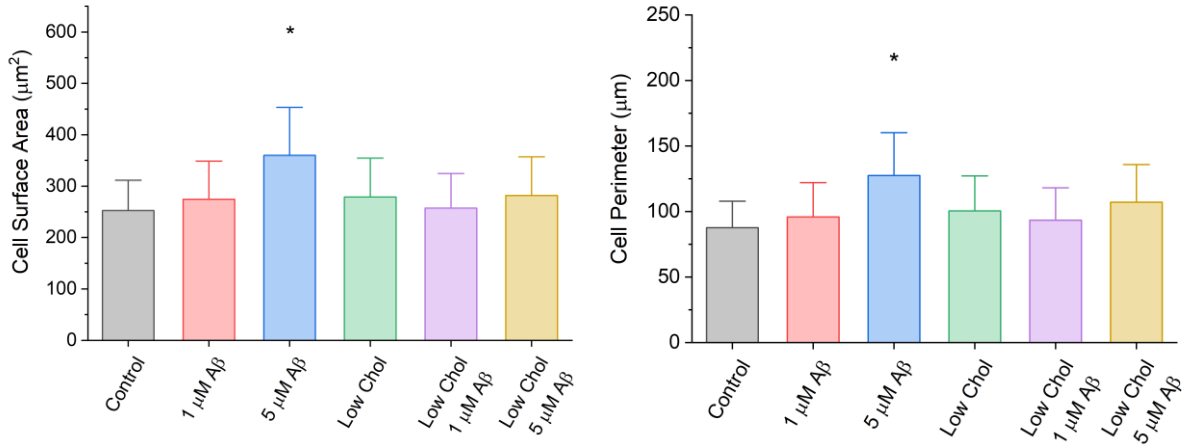

Figure 6.4. Average cell area and perimeter for cholesterol depleted and Aβ treated HT22 cells *comparing low and high concentration Aβ and with low cholesterol. Significant changes in cell surface area (left) and cell perimeter (right) were observed for HT22 cells treated with 5 µM Aβ (Two-way ANOVA, with Tukey's multiple comparison to control, $p < 0.05$*, n=6). Mean ± SD plotted.*

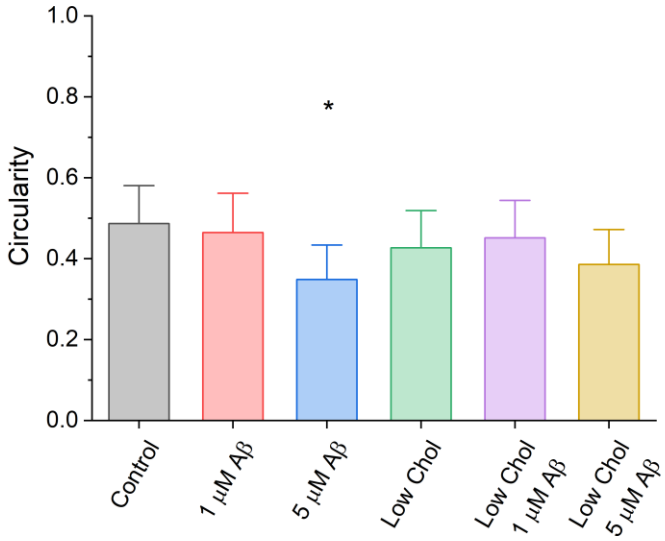

Figure 6.5. Cell circularity for cholesterol depleted and Aβ treated HT22 cells*. There was no difference detected between control and low cholesterol cells overall however, HT22 cells treated with 5 μM Aβ oligomers had significantly lower cell circularity compared to control cells (Two-way ANOVA, p < 0.05* with Tukey's multiple comparison to control, n=6). Mean ± SD.*

These results could be improved by using superior quality imaging multi-well plates, higher resolution camera, and higher-powered objectives, and by imaging at lower cell confluency. However, in the experiment design used in this series of studies, cells were imaged prior to being harvested for cell signaling analysis in Chapter 7. This improves the total amount of data generated from a single cell culture experiment, making a more efficient process. In principle, each image could be used to directly correlate changes in cellular morphology or cell density with cell signaling data in Chapter 7.

6.3.2 AFM Imaging of HT22 Cells and Aβ-Induced Morphological Changes.

Live AFM imaging of HT22 cells reveals valuable information about cell morphology. Figures 6.6, 6.7 and 6.8 show representative undifferentiated, differentiated, and Aβ-treated differentiated HT22 cells, respectively. The important parameters that can extracted from AFM height images are cell volume and height profile of different regions of cells. There are two size regimes of cell topography, the overall size of the cell, on the order of 1.5 – 4 μm, and the local nanoscale topography of the cell surface which includes lipid membrane and cytoskeletal features. Imaging both simultaneously is not possible with standard contact mode AFM due to the extremely large differences in the scale of the overall cell and these nanoscale features, which vary by orders of magnitude. More specifically, optimization of the nanoscale structure of the

cell would result in feedback parameters that are too sensitive to account for huge changes in vertical height, this results in oscillations of the AFM cantilever and probe that can damage cells. Therefore, feedback parameters were set to lower gain values and image the largescale structure of the cell, at the expense of the AFM height following the nanoscale topography. Adaptive feedback AFM imaging technology has been invented which is not available on the JPK Nanowizard II, which could allow for overcoming this issue. Even though the height images are not able to capture the nanoscale topography of some cells, bending of the cantilever under contact force allows for visualization of the actin-myosin cytoskeleton in the deflection images. The 3D shading effect occurs as the probe climbs up the cell exerting a greater force (higher intensity showing as bright on the image), than when the probe descends the other side of the cell (lower intensity showing up darker on the image). Because the membrane is susceptible to deformation and penetration, forces must be kept under 1nN. Deformation of the cell under contact forces is still inevitable, so the AFM images provide an estimation of cell height under force, and a representation of a cell under vertical compression and shear stress.

Living cells will respond to mechanical stimuli depending on the magnitude, direction, and duration of the force and on the type and state of the cell. The cellular response includes acute changes, initially the activation of actin-myosin cytoskeleton to resist mechanical compression, then changes in cell adhesion and other proteins involved in cell migration to move away from mechanical stimuli or shift cellular organelles to reinforce regions of the cell under pressure, and activation of volume/pressure regulating ion channels. Chronic changes in gene expression of these same systems can occur under sustained forces such as pressure and volume regulating ion channel expression (to increase osmotic pressure and resist compression) and increased expression of cytoskeletal proteins and mechanical sensing proteins. Cell mechanics involve several important subsystems including membrane integrity, osmotic pressure regulation (ion channels), and cytoskeleton regulation. Under AFM imaging mechanic stimuli occurs for 15 to 20 minutes, long enough for some of these changes to occur.

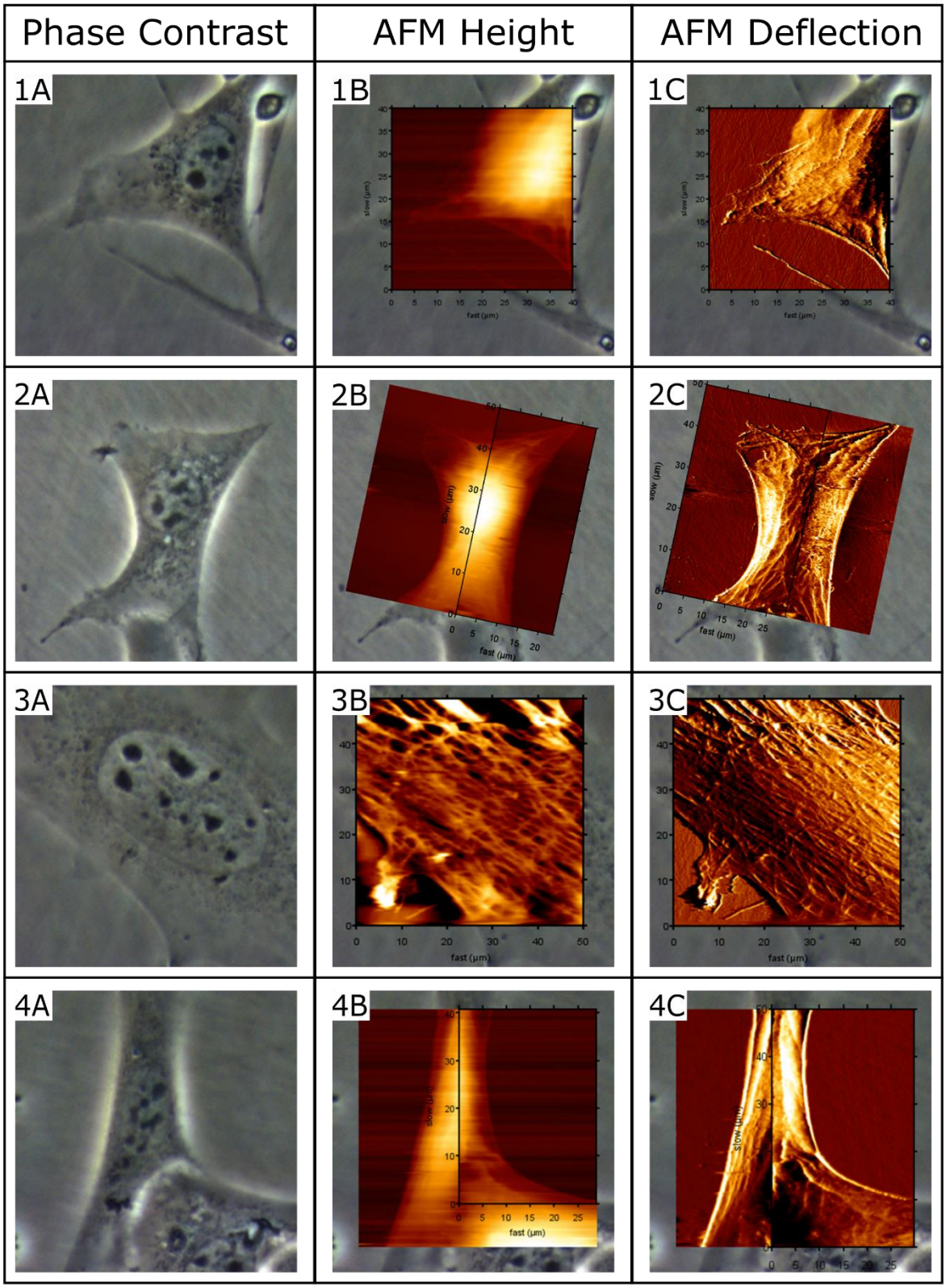

Figure 6.6: AFM/phase contrast optical microscopy overlay images of undifferentiated HT22 cells*. A. Optical; B. Height; C. Vertical deflection of undifferentiated HT22 cells show different cell morphology types: pyramidal (1 and 4), rectangular (2) and during cell division (3).*

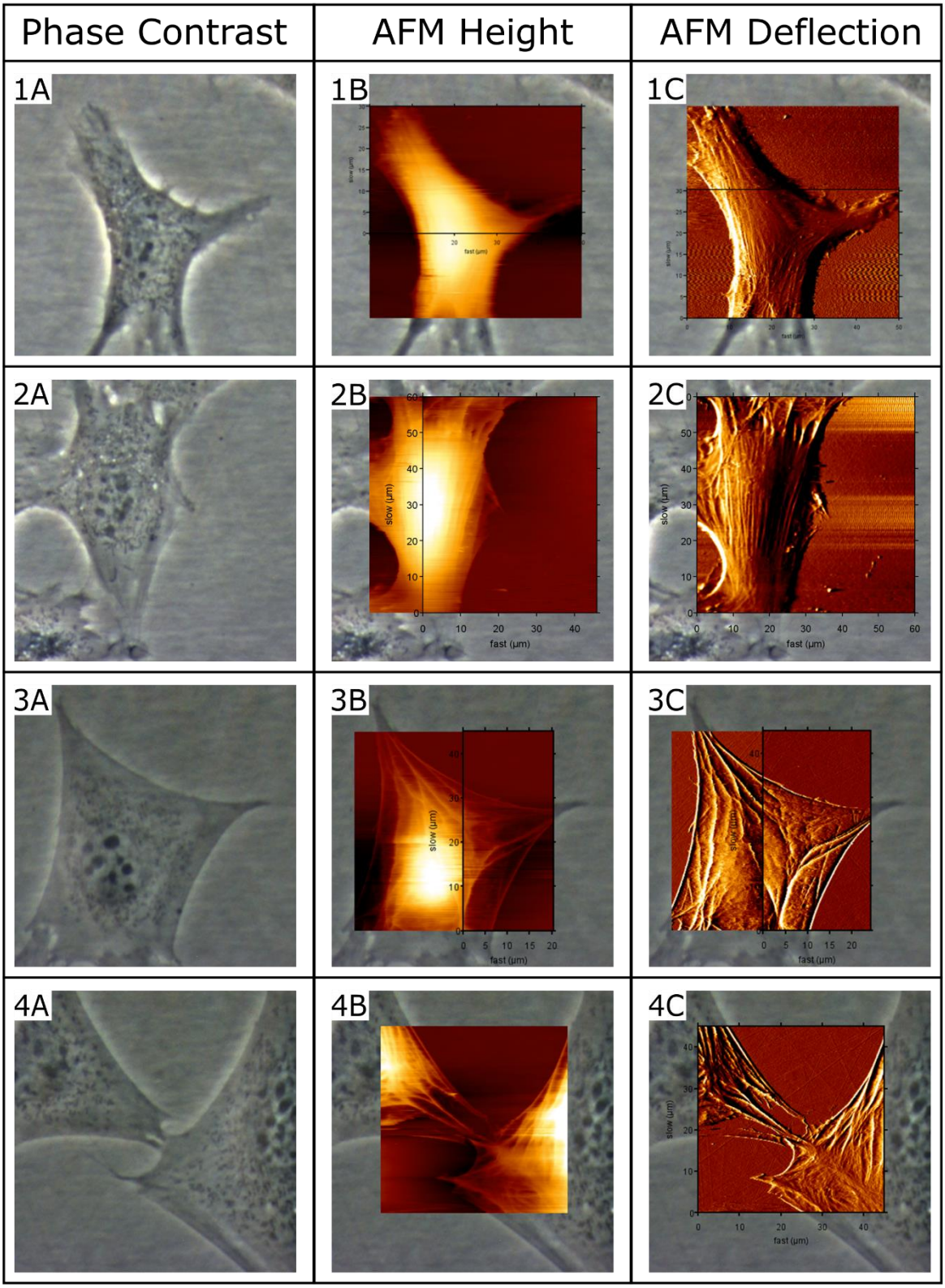

Figure 6.7. AFM/phase contrast optical microscopy overlay images of differentiated HT22 cells. *Several different morphologies are shown. Differentiated HT22 cells were more likely to exhibit a flattened morphology, spreading along the plane of the plate. Cytoskeletal structure of the differentiated neurons had higher contrast on height and vertical deflection images. This may be indicative of a reduced rate of cell proliferation.*

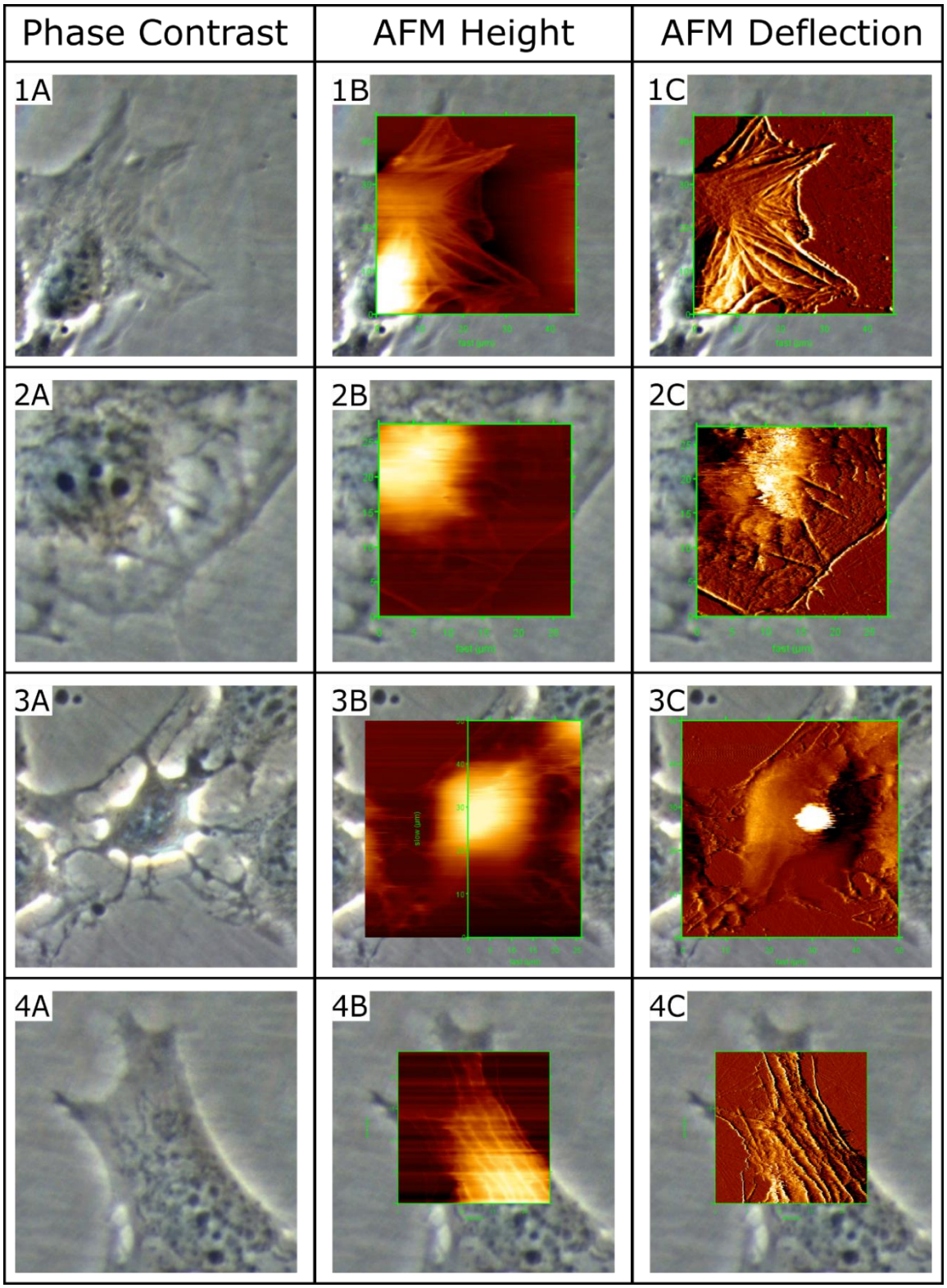

Figure 6.8. AFM/phase contrast optical microscopy overlay images of differentiated HT22 cells treated with Aβ*. Cell 1 exhibits no obvious damage. Cell 2 exhibits cytoskeletal and holes in the membrane. Cell 3 exhibits dilapidated morphology, cytoskeleton is clearly visible, cell is detaching from the surface and AFM probe deflection shows very high adhesive forces at the peak of the soma. Cell 4 is contracting along the actin filaments likely stimulated by contact between probe and cell.*

AFM height images of HT22 cells can be analyzed to estimate cell volume and the heights of various parts of cells, for instance the cell body, or soma, which contains the nucleus, as well as the peripheral regions of the cell. Below in Figure 6.9, shows the height distributions at the tallest point of the cell body, containing the nucleus for undifferentiated, differentiated and Aβ treated cells. Undifferentiated cells were significantly taller than differentiated cells with a much broader distribution of heights, 2.8 ± 0.2 μm compared to 2.1 ± 0.1 μm by standard T-test, $p<0.05$*. This may be due to undifferentiated cells being in different stages of the cell cycle. For example, cell 3 in Figure 6.6 shows a very large cell that is undergoing cell division, this cell has a height of 4.1 ± 0.1 μm, the next tallest cell in the undifferentiated cell population also had a much larger cell footprint and exhibited similar morphology. There were no cells detected in the differentiated population that had this large, inflated morphology. The differentiated control cells exhibited no significant difference in cell height compared to Aβ-treated differentiated cells 2.1 ± 0.1 compared to 2.1 ± 0.3, standard T-test. The peripheral region of the cells, outside the nuclear region, had large variations in the height of the actin-myosin cytoskeletal stress fibers of over the regions in between them. In general, the heights of these stress fibers are between 90 and 220 nm above the surrounding cell surface regardless of the differentiation or Aβ treatment. The general cross section of cells is parabolic, where more than 90% of the cell volume is in the central region of the cell, a representative cross section and image is shown in Figure 6.9, below. The fact that the cytoskeleton is shown with such good contrast on the vertical deflection image and that the height change of the stress fibers is quite high implies that the AFM probe is compressing the cell, in regions between the actin-myosin cytoskeleton.

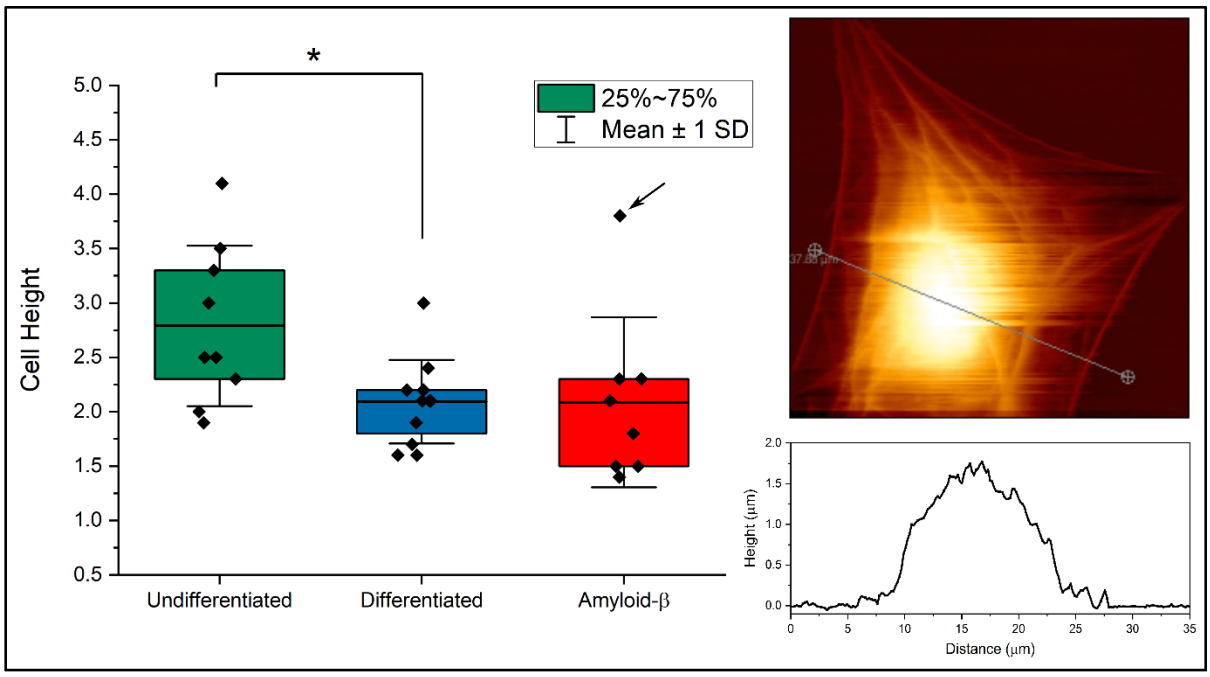

Figure 6.9. Height profile distributions of HT22 cell somas. *Undifferentiated cells had significantly taller cell bodies than differentiated cells. No effect of Aβ on the height distribution was detected, though one large outlier in the Aβ treated cells was 2.5 SD away from the mean (pointed to with an arrow). This cell is amongst the population of dilapidated cells that were difficult to image due to impaired cell adhesion (cell shown in Figure 6.11). AFM image with cross section shows a representative differentiated HT22 cell with the height profile. T-test comparing Undifferentiated vs Differentiated and Differentiated vs. Differentiated + Aβ, $p<0.05$, n=9 undifferentiated, n=10 differentiated, n=7 differentiated + Aβ.*

Previous AFM studies of the effects of Aβ involved acute treatments of less than 3 hours, and/or focused on the effects of Aβ on compressive cellular mechanics[399,400]. They found morphological changes induced by amyloid, especially in the retraction of the cell along the actin-myosin cytoskeleton. This may be due to amyloid directly, or a combination of amyloid and mechanical stimulation by the probe tip, though control images ascertain that amyloid is required for this effect, implying that at a minimum Aβ sensitizes cells to mechanical stimulation. In this study, cells were treated with Aβ for 24 hours prior to imaging so that the effects of Aβ after longer timescales could be studied. Furthermore, the combination of phase contrast optical microscopy and AFM reveal more detailed insight into the effects of Aβ on cell morphology that can be correlated with the effects on cell viability (from Chapter 5), and receptor tyrosine kinase signaling (in Chapter 7).

AFM images of HT22 cells treated with Aβ cause several effects on cell morphology. First there is a population of cells that have a similar morphology as untreated differentiated cells, where it is most likely that Aβ accumulation on these cells was not enough to have any detectable effect on cell morphology (Figure 6.8, Cell 1).

A second population of cells exposed to Aβ exhibited features of necrotic cell death. The phase contrast microscopy and AFM images of Cell 2 is shown zoomed in on figure 6.10. This cell has a peak height of 2.3 ± 0.1 nm, well within the range of untreated differentiated cells. The peripheral region of the cell has a relatively flat cross section. The outer peripheral region of the cell has a height of 55 ± 3 nm above the mica, with the outer cytoskeleton ridge being 118 ± 5 nm high. Regions of constructive interference (increased light intensity) on the phase contrast image (left panel, red arrows) correspond to holes in the cell surface topology on the AFM image (right panel, red arrows). These holes are 49 ± 5 nm deep and appear to penetrate to the mica surface below. The cytoskeleton of the peripheral cell region, outside the nuclear envelope, appears on the phase contrast image as lines of destructive interference, darker, lower signal than background, indicating the cytoskeleton is a light absorbing object compared to the cytoplasmic regions of the cells. The cytoskeleton is between 110 and 170 nm high above the non-cytoskeletal regions. If the cell surface is expected to be mostly planar, then these large changes in height (from 40 to 50 nm) over the actin-myosin cytoskeleton (100 to 200 nm), imply compression of regions between these stress fibers. The compression length between the actin-myosin stress fibers and the rest of the cell appears to be approximately 55 to 70%. Green arrows show where the cytoskeleton ends abruptly and may be an indication of cytoskeletal collapse induced by Aβ that could be related to microtubule associated protein tau pathology. Signs of cytoskeletal collapse are more obvious on the deflection image Figure 6.10 right panel. This cell could be in the earlier stages of transiting to a third morphological phenotype described next.

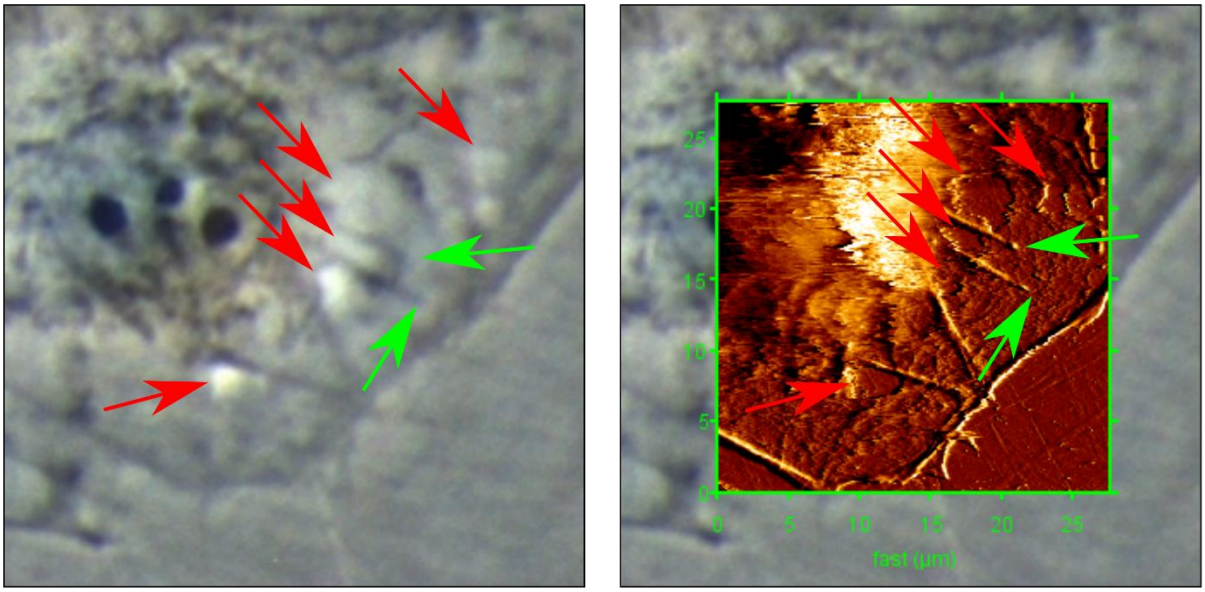

Figure 6.10. An HT22 cell treated with Aβ exhibiting cell membrane and cytoskeletal damage. *Left panel is phase contrast optical microscopy images, right is AFM contact mode deflection image. Red arrows indicate holes in the membrane. Green arrows show where cytoskeleton is damaged, some cytoskeletal features around the periphery of the cell can be seen by phase contrast, but on the AFM image the cytoskeleton can be seen more clearly. These features are indicative of necrotic cell death mechanisms.*

A third population of cells was observed wherein cells appear dilapidated as mentioned in the previous section, these cells have morphological characteristics of apoptosis. The cell in Figure 6.11 below has a shriveled/dilapidated morphology, with numerous projections coming out of the cell body, with a very bright and large light halo artifact on the phase contrast image. The AFM height image reveals a cell that is an outlier in the Aβ treated group at 3.8 µm compared to the mean of 2.1 ± 0.6 µm, as illustrated on Figure 6.9 with an arrow. Most cells imaged by AFM with this type of morphology were far more loosely bound to the cell culture dish. During AFM imaging under forces from the probe tip (vertical and lateral), it was often observed that cells exhibiting this morphology would become detached from the dish and unable to be imaged. Large motion of the cell during AFM scanning was also observed that can best be seen by comparing the trace and retrace of the deflection image, where the cell moved 4.6 µm in the fast scan direction. Cytoskeletal features were only observable at the peripheral regions of the cell and not of the cell body, this is in part due to motion of the cell under AFM imaging and due to changes in cytoskeleton. These features indicate that the cells exhibiting this Aβ induced morphology were not as well-adhered to the plate, suggesting that Aβ toxicity involves interference with cellular adhesion. Cells of this type appear reminiscent of apoptotic cells, with a contracted cell body, and membrane blebbing and spherical cell bodies outside the periphery of

the cells (indicated by red arrows in Figure 6.11), and a reduction in cytoskeletal features. These cells could be in the later stage of apoptosis having progressed from the previous cell shown in Figure 6.10.

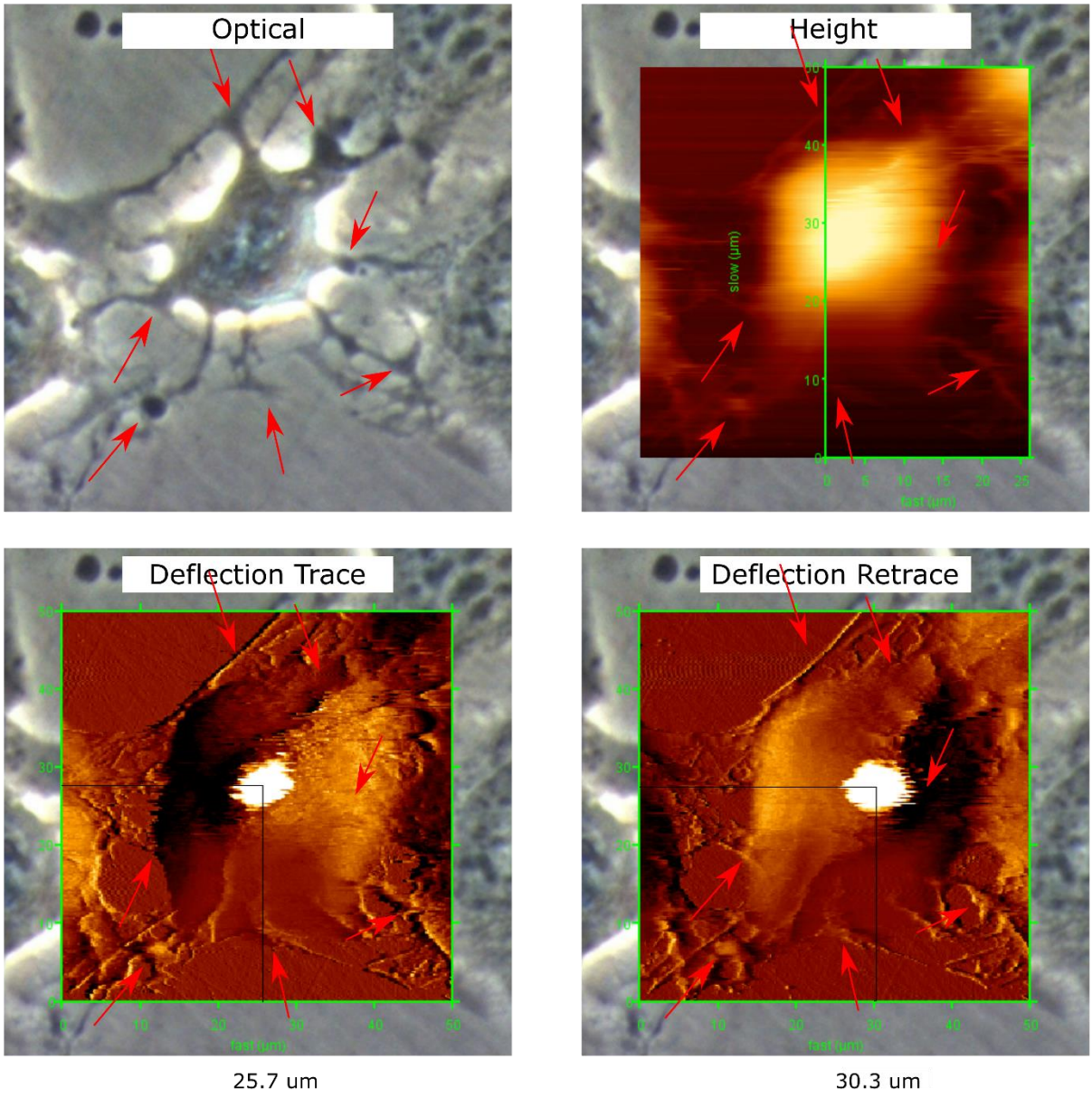

Figure 6.11. An HT22 cell treated with Aβ exhibiting dilapidated cell morphology. *Optical, Height and Trace/Retrace of HT22 cell treated with 5 µM Aβ (Cell 3 from Figure 6.8) exhibiting highly dilapidated morphology, observe apoptotic morphological features, including cell body shrinkage, membrane blebbing (indicated by red arrows) and low adhesion to the cell culture dish is apparent from comparing trace and retrace deflection images, where the cell is dragged by the probe tip by about 4.6 µm.*

6.4 Conclusion

Phase Contrast optical microscopy was used to evaluate morphological characterization of cellular populations of HT22 cells with depleted cholesterol compared to normal cholesterol

cells with or without treatment of 1 µM and 5 µM Aβ. A simple method to quantify changes in morphology of cellular populations using phase contrast microscopy using ImageJ are used to compute cell perimeter, area and sphericity is performed. It was observed that cells treated with 5µM oligomers exhibited dramatic changes in cellular morphology that indicate a disruption of cell adhesion, a tendency towards larger cell areas, perimeters, and a decrease in sphericity. These morphological changes were less pronounced in low cholesterol cells, suggesting that the mild protective mechanisms of cholesterol depletion detected in Chapter 4 involve maintenance of cell cytoskeleton and morphology. Unaggregated Aβ, assumed to be predominantly monomeric when cells were first treated, were far less likely to cause severe morphological changes in HT22 cells at 5 µM compared to oligomers, data not shown. This may indicate a difference in the toxic mechanisms of different Aβ species, whereas there are similar impacts on cellular metabolism (from MTT assay results), oligomers are more disruptive in the way of triggering apoptotic morphology.

On the single-cell level AFM analysis was used to assess the effect of Aβ aggregates on HT22 structure. There were several unique morphological changes induced by Aβ that suggest both necrotic and apoptotic cell death mechanisms. Some cells exhibited damage to the cell membrane through the appearance of large holes in cells alongside cytoskeletal disruption – indicative of necrosis. More readily detectable by optical microscopy were cells that appeared to have contracted cell bodies, disrupted cell adhesion, cell soma height was dramatically increased, membrane blebbing and spherical bodies and reduction in cytoskeletal features, which is indicative of apoptosis. These features were less prevalent on images of cells with depleted cholesterol, suggesting that cholesterol depletion may reduce apoptosis which could explain how cholesterol depletion can protect cells from Aβ toxicity.

Chapter 7: The Effects of Cholesterol and Amyloid-β on RTK Signaling in HT22 Cells

7.1 Introduction

The lipid bilayer anchors proteins that facilitate information exchange between environment and cells, therefore its structure and properties which are affected by lipid composition, are important for receptor signaling pathways and contribute to disease pathogenesis and progression[352,353]. Cholesterol is a key component of all mammalian plasma membranes and intracellular lipid membranes in the body. This is especially important in the central nervous system (CNS)[242], the most cholesterol rich system in the body due to the presence of oligodendrocytes which form the myelin around axons of neurons, and the extremely high number of synapses which require a high proportion of cholesterol to maintain[402]. Synaptic densities containing post-synaptic density-95, NMDA and AMPA receptors are found to highly colocalize with cholesterol-enriched detergent resistant membrane microdomains[402]. These cholesterol-enriched membrane microdomains physically support membrane receptors and their signaling partners, thus membrane microdomain composition changes or disruption from perturbed cholesterol homeostasis and Aβ can affect membrane receptor functionality.

Several receptor signaling pathways have been shown to be impaired by Aβ, including: vascular endothelial growth factor (VEGF) receptor [37,384,403]; insulin receptor[190,191]; NMDA receptors, both metabotropic and ionotropic receptors[39,196,197]; tyrosine receptor kinase B (TrkB) receptors, whose ligands are neurotrophin-3 (NT-3) and brain-derived neurotrophic factor (BDNF)[118,177,404]; and platelet-derived growth factor receptor-β (PDGFRβ)[38]. Many of these belong to the class of receptors called receptor tyrosine kinases (RTKs), which are an important class of growth factor receptors important during growth and development and for maintenance of healthy cells and tissues. With these RTKs the canonical signaling pathway involves heterodimerization of the receptors following ligand binding (though exceptions exist), and thus rely on being within close proximity with a high degree of probability for activation[112]. This would depend on RTK trafficking to and from the membrane and laterally within the membrane. Thus, it would be expected that these receptors would be sensitive to changes in membrane microdomain structure induced by alterations in cholesterol and lipid composition and Aβ-induced damage[112]. There are two types of PDGF receptors (α and β) that are activated by four

growth factors (PDGF-A, -B, -C and -D)[405]. PDGF forms homodimers, PDGF-AA, -BB and heterodimers, PDGF-AB. In general, PDGF-A activates PDGFRα, and PDGF-B activates PDGFRβ. PDGF-C and -D were identified more recently and are not as well understood.

In this chapter, a study of Aβ monomers and oligomers, cholesterol depletion and the interaction of these factors on baseline TrkB receptor signaling, as well as the effects on baseline, and phosphorylation of PDGFRα by acute PDGF-AA treatment is presented. The effects of these treatments were also evaluated on cell viability to study the effects PDGF-AA to rescue against Aβ toxicity. These RTKs and several important downstream secondary targets important in AD were evaluated including those in the mitogen-associated protein kinase pathway (MAPK), namely the extracellular receptor kinase 1 and 2 (ERK1/2)[406]; the activation of phospholipase C-γ1 (PLCγ1) which is a membrane-associated protein that directly associates with RTKs[407,408]; and lastly off-pathway, glycogen-synthase kinase-3β (GSK3β) which is involved in Aβ toxicity and tau phosphorylation, both of which are involved in AD pathology[217,409]. The results of these experiments demonstrate that the effects of cholesterol reduction have a far greater impact on RTK signaling pathways than Aβ at low and high toxicity levels. These results are discussed in relation to relevant literature and data from previous chapters on AFM (where membrane disruption by Aβ was assessed), cholesterol metabolism, toxicity and imaging studies presented in previous chapters. These data suggest that PDGFRα and TrkB signaling are not dominant pathways involved in the protective mechanisms of cholesterol depletion, and that other non-specific or receptor mediated pathways are involved.

7.2 Materials and Methods

7.2.1 Amyloid-β preparation

Recombinant Amyloid-β 1-42 (HFIP, rPeptide) was prepared in monomeric or oligomeric forms according to a modified version of protocols by Stine et al.,[385] as described in chapter 4.

7.2.2 Cell Culture

HT22 cells were cultured and treated as described in Chapter 5. However, PDGF-AA (Cedarlane) was applied acutely for 10 minutes to stimulate cells for Western Blot or was applied concurrently with Aβ during 24-hours for MTT assays. For Western Blot, to harvest cells

after treatment the 6-well plates were placed on ice, cells were washed with ice cold phosphate buffered saline (PBS). Next, 70µL of solubilization buffer (20 mM Tris-HCl at pH 7.5, 150 mM NaCl, 1 mM EDTA, 1 mM EGTA, 30 mM sodium pyrophosphate, 1 mM β-glycerophosphate, 1 mM sodium orthovanadate), containing Triton X-100 detergent (1%) and HALT protease and phosphatase inhibitor (Thermofisher) was added to each plate and cells were detached using a cell scraper. Cells were then transferred into chilled microcentrifuge tubes and lysed through a cold 22-gauge hypodermic needle at least 20 times. After lysing cells were spun in centrifuge at 15,000 × g for 20 minutes to separate the supernatant. Supernatant was transferred to a clean cold microcentrifuge tube and stored at -20 °C until ready for Western blot.

7.2.3 MTT Cell Viability Assay and Statistics

The effect of PDGF-AA and cholesterol depletion to rescue cells from 5 µM Aβ toxicity were measured using the MTT assay. In 96 well plates, cells were plated at a density of 10,000 cells/well than standard differentiation protocol used in Chapter 5 was performed: briefly, plated in complete media (DMEM/F12 +10% FBS + 1 % Pen/Strep) for 24 hours, media was exchanged for neurobasal + 10% N2 supplement + 2 mM L-Glutamine for 24 hours. Following differentiation cholesterol depletion was performed with 1-hour MβCD treatment, cells were then treated with either 5 µM Aβ monomers, 25 ng/ml PDGF-AA, or both. Each group was treated in triplicates all on one plate. After 24-hours, MTT cell viability assay was performed as in Chapter 5.

7.2.4 BCA Assay, SDS-PAGE and Western Blot

Total protein concentration was quantified for each sample by bicinchoninic acid (BCA) assay (ThermoFisher). Samples were mixed with 3x loading buffer (240 mM Tris-HCl at pH 6.8, 6% w/v sodium dodecyl sulfate (SDS), 30% v/v glycerol, 0.02% w/v bromophenol blue, 50 mM DTT, and 5% v/v β-mercaptoethanol) and boiled for 5 minutes before 15 µg of total protein was loaded into 8% or 4 – 16 % gradient polyacrylamide gels for electrophoresis (PAGE). SDS-PAGE was run on 15-well, 1.5 mm gels with Fisher EZ run pre-stained *Rec* protein ladder with 2 control lanes per gel at 70 V for 30 minutes and then at 120 V for 90 – 120 minutes. Running buffer composition was 25 mM Tris base, 190 mM glycine, 3.5 mM sodium dodecyl sulfate. After SDS-PAGE, protein was transferred to nitrocellulose membranes in chilled transfer buffer (25mM Tris-HCl, 190mM Glycine and 20% v/v methanol) for 90 min in constant voltage mode

at 100 V, or for 16 hours in constant current mode at 42 – 50 mA such that the resultant voltage was ~ 30 V. Membranes were than washed in Milli-Q water before being placed into blocking buffer (tris buffered saline 20mM Tris, 150 mM NaCl, pH 7.4 plus 0.1% Tween (TBST)) containing either 5% non-fat milk or 5% bovine serum albumin (BSA) for minimum 1 hour at room temperature or overnight at 4°C. Membranes were then incubated in primary antibody in matching blocking buffer for 1 - 2 hours at room temperature or between 12 and 18 hours at 4°C depending on the antibody. After incubation with primary antibody membranes were washed in TBST three times for ten minutes under gentle rocking. Secondary antibody was diluted at 1 to 5000 or 1 to 10000 in blocking buffer and was added to the membranes for 1 hour. Membranes were then washed three times for 10 minutes in TBST. Luminata crescendo Western HRP substrate (Millipore) for chemiluminescence detection was then added to membrane for 5 minutes. Membranes were then imaged using iBright FL1500 imaging station (ThermoFisher) using the auto-exposure setting, if pixel saturation was observed, reduction in exposure time was adjusted manually. The background corrected density was computed using the iBright Analysis Software (ThermoFisher) and used for analysis.

7.2.5 Antibodies

Anti-phospho-TrkB (Tyr816) Antibody, ABN1381 (Millipore); TrkB Antibody (H-181), sc-8316 (Santa Cruz Biotechnology); PDGFR-β Antibody (D-6) (Santa Cruz Biotechnology); Phospho-PDGFRB (Tyr1021) Rabbit anti-Human, Mouse, Invitrogen™ (ThermoFisher); PDGFRB Rabbit anti-Human, Polyclonal, Invitrogen™; PDGF Receptor α (D1E1E) XP® Rabbit mAb 3174 (Cell Signaling); Phospho-PDGF Receptor α (Tyr849)/PDGF Receptor β (Tyr857) (C43E9) Rabbit mAb 3170 (Cell Signaling); Phospho-PDGF Receptor α (Tyr754) (23B2) Rabbit mAb 2992; Phospho-PDGF Receptor α (Tyr1018) Antibody 4547; Phospho-p44/42 MAPK (Erk1/2) (Thr202/Tyr204) (D13.14.4E) XP® Rabbit mAb 4370 (Cell Signaling); p44/42 MAPK (Erk1/2) (137F5) Rabbit mAb (Cell Signaling); PLCγ1 (D9H10) XP® Rabbit mAb (Cell Signaling); Phospho-PLCγ1 (Tyr783) Antibody #2821S (Cell Signaling); PLCγ1 Antibody #2822S (Cell Signaling); GSK-3β (D5C5Z) XP® Rabbit mAb #12456 (Cell Signaling); phospho-GSK-3beta (Ser9) (D85E12) XP Rabbit mAb (Cell Signaling); β-Actin Antibody sc-81178 (ACTBD11B7) (Santa Cruz Biotechnology); Goat anti-Mouse IgG (H+L) Secondary Antibody, HRP (Thermo Fisher Scientific); Goat anti-Rabbit IgG (H+L) Secondary Antibody, HRP (Thermo Fisher Scientific).

7.2.6 Experimental Design of Western Blot

For TrkB signaling data baseline unstimulated HT22 cells were studied, it was not possible to quantify total full-length TrkB levels in the HT22 cells, therefore the phosphorylation data cannot be interpreted appropriately. Total truncated TrkB was still measured. To study PDGFRα signaling both baseline and PDGFAA-stimulated HT22 cells were studied. For baseline experiments, following 1-hour MβCD treatment (to deplete cells of cholesterol), cells were treated for 24-hours with Aβ, then were imaged and harvested. Stimulated datasets were collected in a similar fashion, however, following 24-hour Aβ treatment, cells were treated with 32 μM PDGFAA for 10 minutes before being harvested. Phosphorylated protein levels were measured as a means to quantify protein activation and were first normalized to β-actin and then expressed as a ratio to the normalized total protein signal and then to true untreated controls. Total protein levels were also normalized to β-actin.

7.2.7 Statistical Analysis

For MTT data Two-way ANOVA with Tukey's multiple comparison ($\alpha = 0.05$) was performed with the main effects being PDGFAA and Aβ treatment, which was run separately for low cholesterol and normal cholesterol groups. ANOVA also tested for interactions between PDGFAA and Aβ treatment groups and the control for n=5 independent experiments. The data were plotted separately on two charts for clarity. The statistical analysis for Western blotting data considered baseline and stimulated data separately, two factors were analyzed: cholesterol content and Aβ treatment. An ordinary two-way ANOVA, $\alpha=0.05$, with n=5 independent trials was performed to assess effects of each factor (cholesterol and Aβ) and their interaction. Multiple comparisons with Tukey's correction were performed in select datasets where more detailed comparisons were of interest.

7.3 Results and Discussion

7.3.1 The Interplay Between Cholesterol and Aβ on Baseline TrkB Activity

TrkB the receptor for BDNF, and to a lesser extent NT-3, is a critical receptor for neuronal cell growth, differentiation, and survival[410]. It is among the class of neurotrophic growth factor (NGF) receptors which as RTKs canonically have an extracellular ligand binding domain and an intracellular kinase domain that acts on downstream intracellular targets such as PLCγ, Akt, and mitogen associated protein kinases (MAPKs) namely, the extracellular receptor

kinases 1 and 2 (ERK1/2). However, TrkB receptors also have a more complex expression pattern with 3 major isoforms being expressed in humans[411]. These different isoforms include a full length (TrkB-FL) which contains the canonical ligand binding and kinase domains, a truncated TrkB (TrkB-T1) that only contains the ligand binding domain and a truncated isoform with the ligand- and shc- binding domains (TrkB-T-SHC), although there are other predicted isoforms these are less well characterized and less abundant in human neurophysiology. Shc is an adaptor protein that recruits different signaling molecules, effectively transducing extracellular signals into intracellular ones[412]. The role of truncated TrkB isoforms is not precisely known but may involve acting in competition to negatively regulate TrkB signaling by acting to sequester BDNF and neurotrophin-3 (NT-3) or by dimerizing with full length TrkB receptors. Activation of TrkB receptors by BDNF requires heterodimerization, so that two TrkB receptors must diffuse laterally within the plane of the lipid membrane and form a complex for signal cascade to be initiated making membrane microdomain structure and properties important.

It appears that total TrkB expression was limited in HT-22, with the total TrkB antibody only detecting one of the truncated TrkB isoforms (Figure 7.1 – top), this TrkB antibody was raised against the extracellular ligand binding domain. TrkB-T1 is expected to have a molecular weight around 95 KDa, with TrkB-SHC around 105 KDa. There was a statistically significant decrease in truncated TrkB expression following combined cholesterol reduction and Aβ (at both 1 and 5 μM), Figure 7.2 (two-way ANOVA, $\alpha=0.05$, $n=5$). When looking at the immunoblot for phospho-TrkB (Figure 7.1 – bottom), the primary antibody raised against the 13 amino acid peptides containing the tyrosine phosphorylation site, identified 3 different bands at 135, 120 and 105 KDa. Because the truncated forms of TrkB do not have the C-terminal kinase domain it is not possible for the two smaller bands at 120 and 105 KDa to correspond to phosphorylated TrkB at residue 816. Therefore, these bands are likely binding to similar recognition regions of another protein, this is not unexpected with phospho-proteins as they often contain similar recognition patterns for phosphorylation. The band at 135 KDa likely corresponds to TrkB-FL, which is predicted to be approximately 140 KDa.

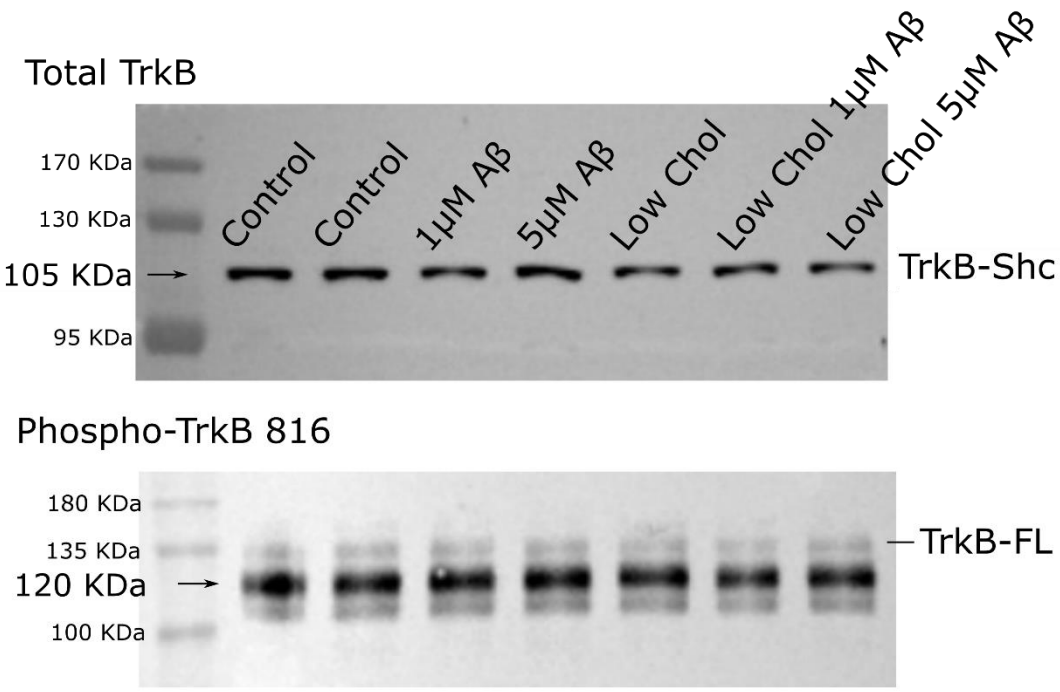

Figure 7.12. Western blot of total TrkB (top) and phospho-TrkB-tyr816 (bottom). *Predicted molecular weights for TrkB-FL, TrkB-Shc and TrkB-T1 are 140 KDa, 110 KDa and 95 KDa, respectively. Total TrkB antibody only detected TrkB-Shc, while phospho-TrkB816 detected a faint band near the expected molecular weight, however there was cross-specificity for an unknown highly abundant protein near 120 KDa and another unknown protein with a faint band around 105 KDa.*

There was no significant effect of Aβ at either concentration on TrkB-Shc expression levels in the HT22 cells. Sequestration of cholesterol from HT22 cells by methyl-β cyclodextrin (MBCD) in combination with Aβ resulted in some statistically significant changes in TrkB-Shc, though the effect sizes were small, and the confidence intervals were quite broad owing to the high variability and small number of independent replicates (Figure 7.2). Low cholesterol HT22 cells treated with 1 and 5 μM Aβ resulted in significant reductions of TrkB-Shc by 46.1 % (**$p<0.01$) and 39.6 % (*$p<0.05$), respectively by two-way ANOVA with Tukey's multiple comparison ($\alpha<0.05$). There was a trend towards reduction in low cholesterol no Aβ group, with a 33.7 % reduction, which was close to significance. This may imply that membrane disruption by MBCD alone was not significant to reduce TrkB-Shc at the membrane but with the combination of reduced cholesterol and Aβ-induced membrane disruption was enough to push these reductions into the range of statistical significance. TrkB receptors are membrane-associated and therefore lower cholesterol levels in neurons would be expected to have less membrane microdomains, and thus less regions in the membrane for these proteins to anchor[138,408]. The high expression levels of truncated TrkB over TrkB-FL may greatly influence

the lack of neuron-like characteristics of the HT-22 cells if the hypothesis that truncated TrkB negatively regulates BDNF activity is correct[411], as BDNF signaling is essential for neuronal differentiation[413].

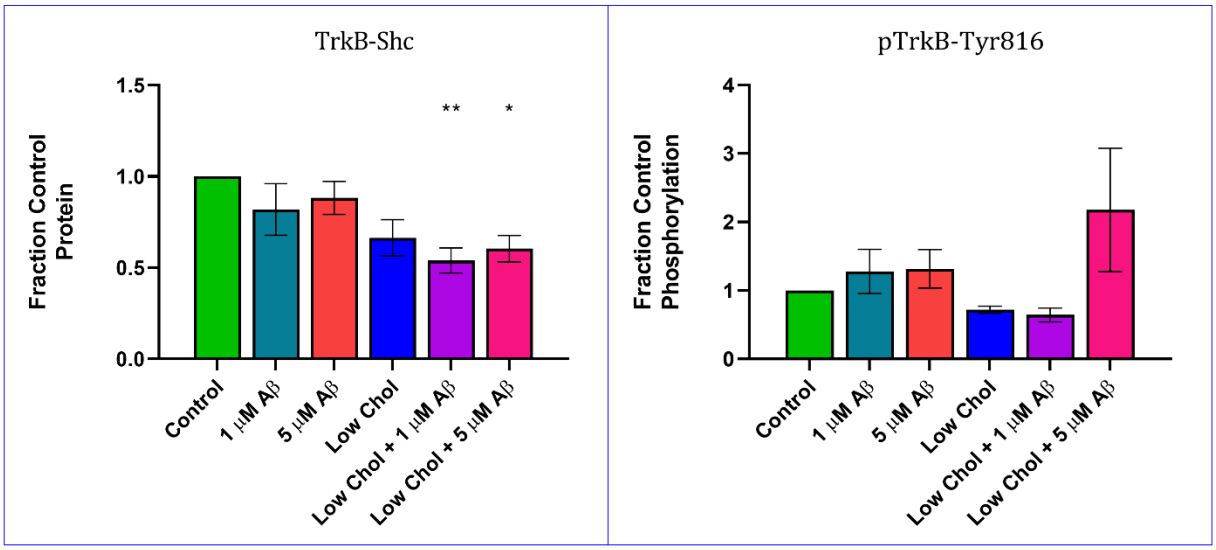

Figure 7.2. Expression of truncated TrkB-Shc and activation of phospho-TrkB tyrosine 816 levels*. Significant reductions in TrkB-Shc were detected for low cholesterol groups with multiple comparisons identifying 1 and 5 μM Aβ in particular, two-way ANOVA with Tukey's multiple comparison (*p<0.05, **p<0.01, n=5). No significant effect on absolute pTrkB levels were detected though interpretation of this result is null. Mean ± SEM reported.*

Due to the inability of total anti-TrkB antibody to detect full-length TrkB, there was no way to report the phosphorylated to total protein ratio, therefore it is not possible to interpret the results of the phospho-TrkB-tyrosine 816 western blot experiments properly. As is, there was no statistically significant effect of cholesterol reduction or Aβ on the absolute phospho-TrkB-tyrosine 816 levels. Relatively high variability in the phospho-TrkB levels was observed, especially for the low cholesterol 5 μM Aβ group, where in 2 out of 5 independent experiments a large increase in receptor phosphorylation was observed, whereas the other 3/5 experiments saw slight decreases. This may be further evidence of low baseline levels of TrkB-FL in the HT22 cells.

7.3.2 The Interplay Between Cholesterol and Aβ on PDGFRα Signaling

Platelet-derived growth factor receptor-α (PDGFRα) is an RTK and thus requires heterodimerization to activate the canonical signaling cascade (recall Figure 1.4). PDGF-AA binds to PDGFRα subunits triggering dimerization and initiating the transduction cascade to affect cell growth, differentiation, and survival. PDGFRα is most strongly associated with

oligodendrocyte differentiation during early development[414–416], however, PDGFRα has been detected in mature adult neurons while PDGFRβ has also been shown to have functional activity in hippocampal neurons[414,417]. Type-2 astrocytes and a subpopulation of glial fibrillary acidic protein (characteristic of astrocytes), expressing cells in subventricular zone also express PDGFRα[418]. Levels of PDGFRα may decrease in non-neuronal brain cells correlating with a decrease in oligodendrocyte progenitor cells during aging[414]. PDGFRα was chosen as a target for study in the HT22 cells as immunoblotting for PDGFRβ with three different antibodies yielded negative results, two phospho-PDGFRβ and one total PDGFRβ. Phospho-RTK proteomic assay was used to identify baseline levels of active RTKs in the HT22 cells (Figure 7.3). In HT22 cells, baseline phosphorylation is observed for ErbB2, the human ortholog is known as human epidermal growth factor receptor-2 (HER2) that is implicated in 15 to 30 % of breast cancers. This may be a result of the immortalization process the HT22 cells have gone through, which give them a cancerous phenotype[304,306]. The only other RTK with measurable baseline levels of phosphorylation in HT22 cells was the PDGFRα. This characteristic of HT22 cells makes it less physiologically relevant as a neuronal model for studying RTKs, since it does not express detectable basal levels of neuron-specific such as TrkA and TrkB receptors even when differentiated. Perhaps, the HT22 cells would be a more useful for studying glial or oligodendrocyte RTK signaling, however, the HT22 cells do not express GFAP which is a commonly used glial-specific protein, highlighting the limitations of using immortalized cell lines for research[306].

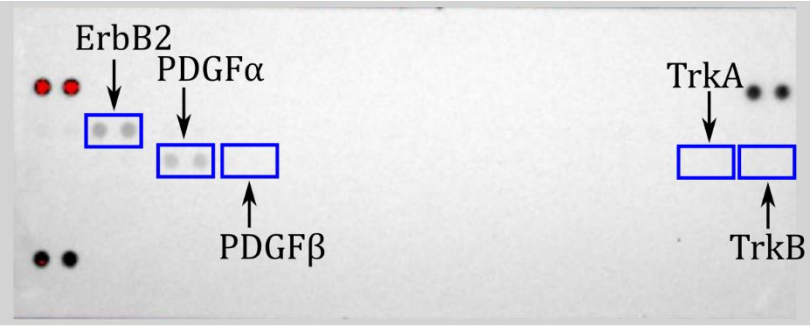

Figure 7.3. Phospho-RTK profiler assay kit. *Differentiated HT22 cells untreated, only PDGFRα and ErbB2 show appreciable baseline phosphorylation levels, no PDGFRβ, TrkA or Trk B receptors have measurable levels of baseline phosphorylation. Modified with permission from Sean Newbury who performed this experiment.*

Previous work in the Beazely lab identified that Aβ interfered with PDGFβR signaling in SH-SY5Y cells, and thus PDGFRα could be an interesting target to study in relation to AD in

HT22 cells[38]. After identifying PDGFRα as an active RTK in the HT22 cells the effects of Aβ and cholesterol depletion on baseline PDGFRα signaling followed by PDGF-AA induced phosphorylation of PDGFRα and downstream secondary messengers.

7.3.2.1 Effect of PDGF-AA treatment on MTT Assay

For MTT assays, HT22 cells were treated for 24 hours concurrently with PDGF-AA (32 μM) and Aβ (5 μM), with or without cholesterol depletion. PDGF-AA increased cell viability by 53% over control (Figure 7.4). This could be due to increase in cell count, as PDGF-AA is a mitogen and increases cellular proliferation of mesenchymal stem cells, osteoblasts and oligodendrocyte precursor cells[419]. PDGF-AA failed to rescue HT22 cells from 5μM Aβ toxicity, shown in Figure 7.5 there was no statistically significant difference between cells treated with 5μM Aβ alone (55 ± 2%) cell viability and combined PDGF-AA and 5μM Aβ (64 ± 10%). Cholesterol depleted cells were unresponsive to PDGF-AA treatment at the level of cell viability as tested with the MTT assay (118 ± 19% compared to 119 ± 10%), implying PDGF-AA was not able to stimulate proliferation of cholesterol depleted HT22 cells. Cholesterol depleted HT22 cells were sensitive to Aβ (66 ± 8%), and treatment with PDGAA had no effect on cell viability (59 ± 10%). This agrees with previous work in our lab, that indicated PDGF-BB induced proliferation of SH-SY5Y cells was impaired by 5μM Aβ[38].

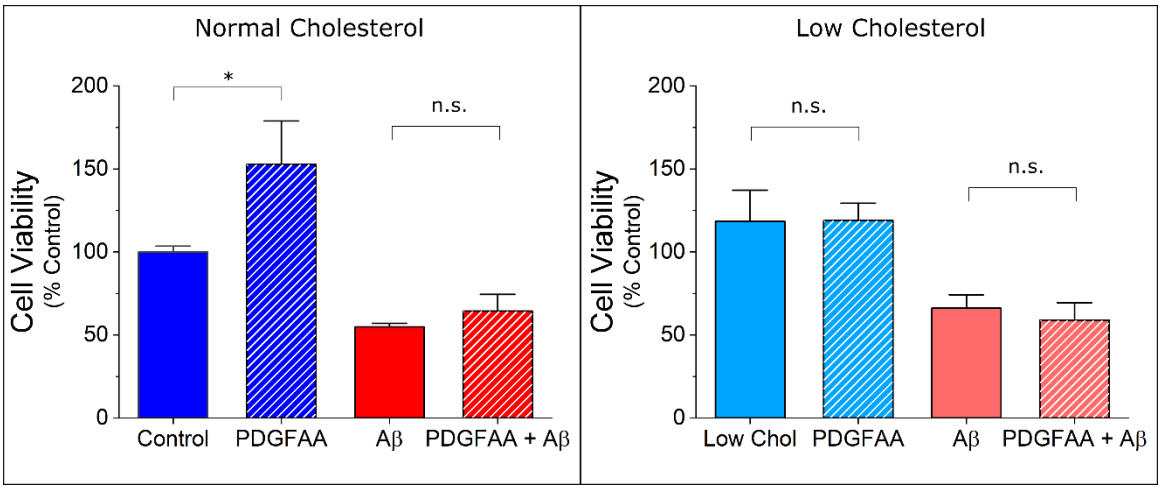

Figure 7.4. PDGF-AA rescue against 5μM Aβ following 24-hour treatment. *Left: PDGF-AA increased cell viability by 53% over control ($p<0.05$) but failed to rescue HT22 cells from Aβ toxicity. Right: cholesterol reduction had no statistically significant effect on cell viability and abolished the increase in cell viability caused by PDGFAA. Assessed by Two-way ANOVA with Tukey's multiple comparisons. Mean ± SEM reported (n=5).*

7.3.2.2 PDGFRα signaling by Western Blotting

We sought to characterize the effects of Aβ, cholesterol depletion and their interaction on PDGFRα signaling by Western blot, measuring total and phosphorylated (phosphor) protein levels of PDGFRα, ERK1/2, PLCγ1, and GSK3β. To do so, following differentiation protocol, cells were treated with 1 μM Aβ, 5 μM Aβ, or were depleted of cholesterol using MβCD and then treated with 1 μM Aβ and 5 μM Aβ before harvesting cells and measuring PDGFRα signaling to establish the effect on baseline activity. The same experimental conditions were then used but cells were stimulated with a 10 min PDGF-AA treatment prior to harvesting and Western blot. Representative blots are shown in the supplementary material in this chapter. Many factors may affect the relatively high variance across many different measures between each set of experiments including more or less effective cholesterol sequestration from MβCD during the oligomer data collection, or for small differences in PDGF-AA exposure times where ligand-induced internalization and degradation of PDGFRα may begin to occur[112]. Following activation, RTKs are known to have very large increases in the rate of internalization (namely ErbB2 and EGFR)[420], and subsequently there is up to a 50-fold increase in degradation[420,421]. With a treatment time of only 10 minutes this was not expected to be significant, however different cell types have different rates of receptor turnover, which can depend on the level of receptor expression, the concentration of ligand, and variety of other factors that affect receptor trafficking including lipid composition[420,422]. These internalization process may also involve cholesterol-dependent mechanisms and is influenced by a number of complex feedback loops over short and long time scales, involving downstream effectors such as MAPK, PLCγ, and PKA[112,420,422].

When looking at PDGFRα expression there was no statistically significant effect of Aβ at any concentration regardless of the baseline levels or levels in response to stimulation from PDGFAA. For both baseline and stimulated datasets there was a statistically significant effect following cholesterol depletion, where PDGFRα expression was reduced, approximately 40% for the baseline levels (Figure 7.5), with the stimulated data had a greater reduction of 61% **$p<0.01$ by two-way ANOVA. There was no interaction detected between Aβ treatment or cholesterol reduction in the total level of PDGFRα. The larger decrease in PDGFRα expression levels could be a result of ligand-dependent internalization of the receptor, mentioned above. Representative blot shown in supplementary material.

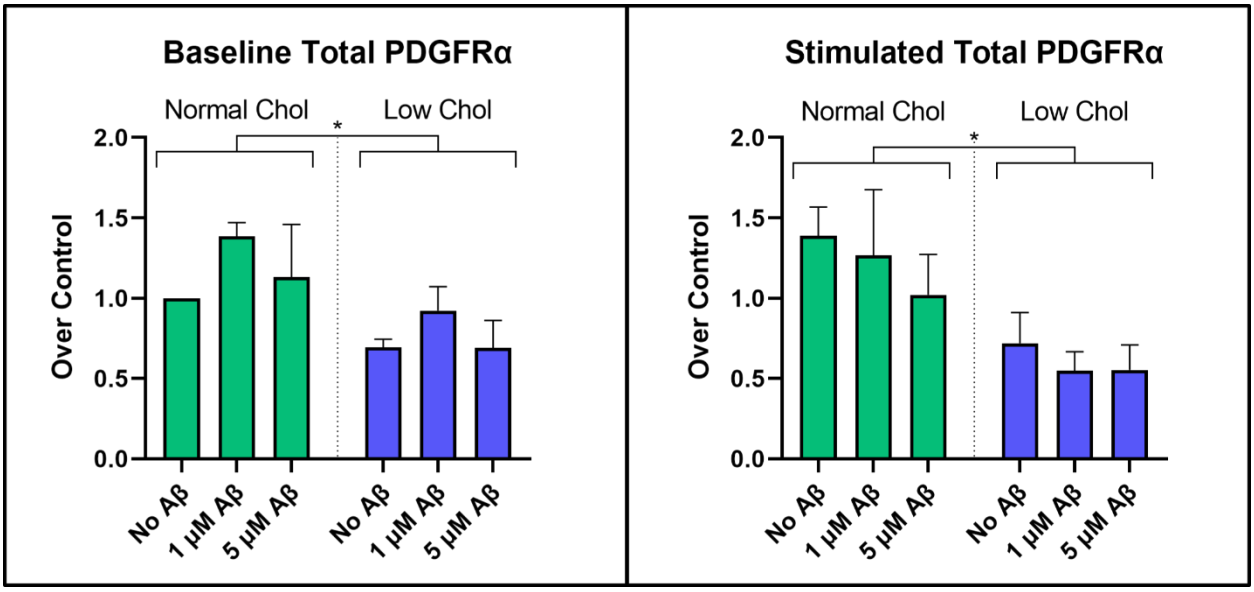

Figure 7.5. Total PDGFRα expression levels. *Left: Baseline levels following 24-hour treatment and Right: 24-hour treatment followed by stimulation with PDGFAA for 10 minutes. There was a significant reduction in receptor expression following cholesterol depletion by MβCD (two-way ANOVA, p<0.05*) in both cases. No statistically significant effect of Aβ was detected, for normal or low cholesterol HT22 cells on expression of PDGFRα nor was an interaction between the Aβ and cholesterol detected. Mean ± SEM reported (n=5).*

When looking at PDGFRα activation there was good phosphorylation signal at the tyrosine-857 residue, however neither the anti-phospho-PDGRFα Tyr754 nor Tyr1018 antibodies tested yielded signal. Representative blot shown in the supplementary material at the end of this chapter – Figure 7.13). There was no significant effect on baseline phosphorylation of HT22 cell PDGFRα in any of the low cholesterol, Aβ treatment, or combination treatment groups (Figure 7.6 left) – as assessed by two-way ANOVA, $\alpha < 0.05$.

Following PDGF-AA treatment (Figure 7.6 – right) stimulated HT22 cells exhibited an increase in PDFGRα activation over control baseline levels by a factor of 2.5 to 6.5 depending on cholesterol and Aβ treatment. This was expressed as the as the ratio of phospho-PDFGRα to total PDGFRα to account for changes in total receptor levels. In comparing the effects of Aβ pretreatment on PDGF-AA stimulation, there was a significant decrease in phosphorylation ratio in the normal cholesterol cells treated with 5μM Aβ oligomers by a factor of 2.4 (two-way ANOVA, *p<0.05 with Tukey's multiple comparison). This suggests Aβ is disruptive to PDGFRα activation, which correlates with the observation from the MTT data. For all three low cholesterol groups there was a significant decrease in phosphorylation compared to cells with normal cholesterol levels by a factor of 3.8 to 4 (***p<0.001, ANOVA with Tukey's multiple comparisons). No interaction between cholesterol depleted cells and Aβ treatment was detected,

as there was no difference in the effect between low cholesterol treated groups also treated with Aβ. Overall, cholesterol reduction by MβCD had a far greater impact on disrupting PDGFRα receptor levels and activation than Aβ, although the effects on cell metabolism from cholesterol depletion was not significant. PDGFAA is a mitotic growth factor and thus the increase in cell viability it caused was likely due to increased proliferation of HT22 cells. PDGFAA failed to rescue HT22 cells from Aβ toxicity and cholesterol reduction abolished the effect of proliferative PDGFAA on HT22 cells.

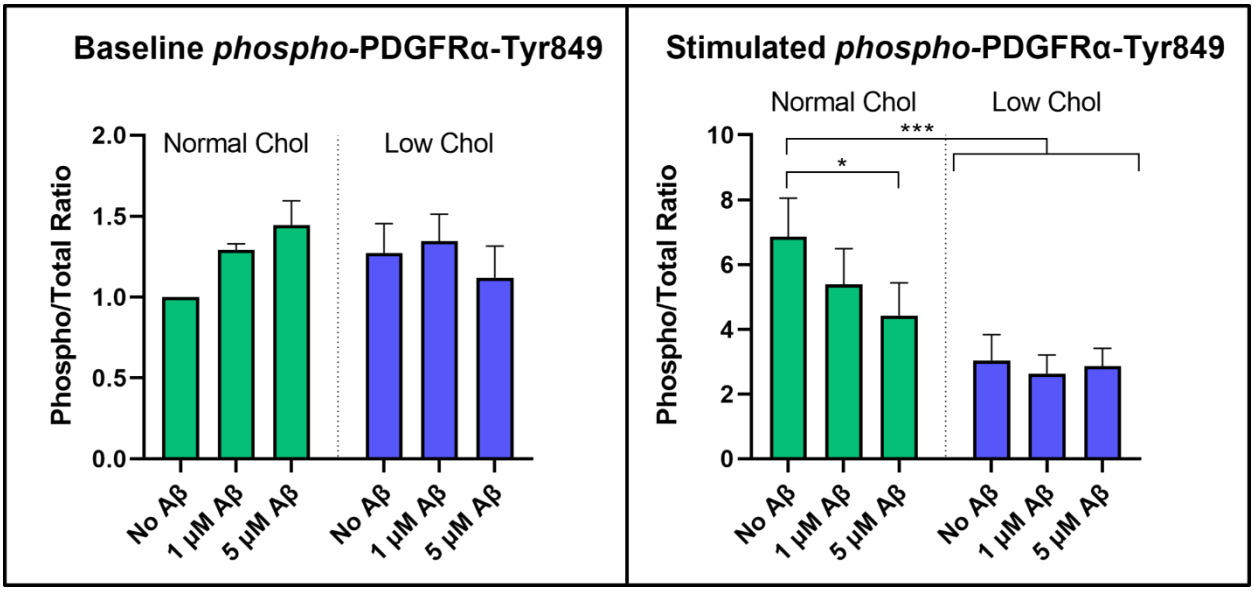

Figure 7.6. Phosphorylation of PDGFRα – Tyrosine-849*. Left: Baseline, where there was no difference between normal and low cholesterol, or with Aβ treatment. Right: Stimulation with PDGFAA caused a 7-fold increase in phospho-Tyr849 levels which was significantly reduced following 5μM Aβ treatment. Cholesterol depletion caused a dramatic reduction in phospho-Tyr849 levels. Two-way ANOVA did not demonstrate an interaction between cholesterol depletion and Aβ ($p<0.05$*, $p<0.001$***). Mean ± SEM reported ($n=5$).*

To further elucidate effects of cholesterol depletion, Aβ treatment and their interplay on PDGFRα signaling, downstream effector activation in this RTK signaling pathway were explored were quantified. The MAPK pathway is an important pathway that regulates all kinds of cellular functions, acting as an important signal transduction cascade between extracellular growth factor and hormone signals coming in from the environment at the cell membrane into changes gene expression for regulating cell and tissue homeostasis. After growth factor induced dimerization and RTK activation, Ras, a membrane associated secondary signal, dissociates from the kinase, binds to B-Raf, and activates MEK1/2 then ERK1/2[405]. ERK1/2 then phosphorylates transcription factors that bind activator protein-1 transcriptional DNA elements which trigger increases in cellular activity, promoting growth, proliferation, and survival. Thus ERK1/2

phosphorylation can be used as a measure of downstream RTK activation, though this is complicated by redundant pathways from other membrane receptors that influence MAPK signaling, and feedback from intracellular pathways.

In these experiments there was no effect of any of the treatments on the total ERK1/2 expression levels (Figure 7.7). In general, ERK 1 signal to noise levels were considerably lower than ERK 2 (representative blots shown in Figure 7.13 of the supplementary material). This is consistent with several Aβ toxicity studies where there was no change in total ERK1/2 levels in response to toxic levels of Aβ, across a wide range of concentrations even as high 10μM[218,423].

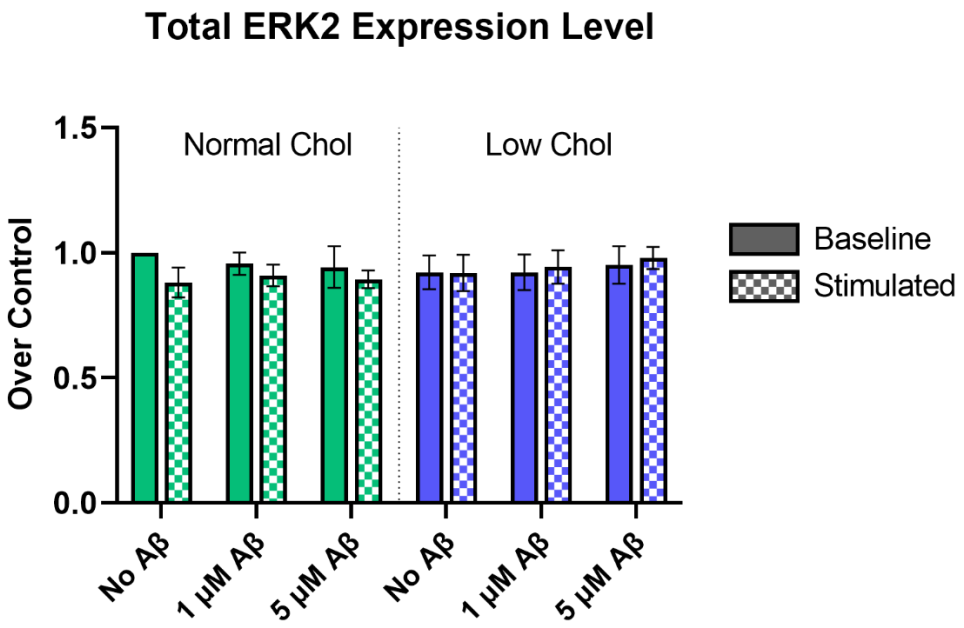

Figure 7.7. Total ERK2 expression levels. *No effect of Aβ, cholesterol depletion or PDGFAA stimulation was observed. Mean ± SEM reported (n=5).*

Activation of ERK 1/2 was measured by dividing the phospho-ERK Threonine 202/204 signal by the total ERK signal for both ERK 1 and ERK 2, separately. The trends for ERK1 and ERK2 were the same, the data for ERK2 is shown due to the better signal to noise (representative blots in Figure 7.13). In the baseline ERK activation there was an interaction detected between cholesterol and Aβ by two-way ANOVA ($p<0.05$*). There was an increase in baseline ERK2 phosphorylation levels in response to toxic levels of Aβ (5 μM) treatment (Figure 7.9 left), in agreement with previous reports of toxic levels of Aβ increasing ERK1/2 activation[216]. This result was significant in the two-way ANOVA with Tukey's multiple comparison ($p<0.05$*, n=5). Decreased ERK1/2 activation has been shown to correlate with a reduction in Aβ toxicity

from previous studies[216]. This aligns with what was observed here that low cholesterol HT22 cells treated with 5μM Aβ oligomers had normal levels of ERK1/2 activation not statistically different from control, this may be involved in the protective effects of low cholesterol observed in Chapter 4.

The effects of Aβ and cholesterol depletion after treatment with PDGF-AA stimulated cells on ERK1/2 activation are shown in Figure 7.8 right. The phospho/total ERK ratio was significantly increased for control HT22 cells by a factor of approximately 6.5 ± 2.5. There was trend towards decreased ERK activation with increasing Aβ concentration, but the result was not statistically significant (two-way ANOVA, n=5), this is in stark contrast to the baseline data where an increase was detected at higher Aβ concentration, suggesting an interaction that was confirmed by two-way ANOVA. Significant decreases in ERK1/2 phosphorylation were detected in all stimulated, low cholesterol HT22 cells, with a compounded effect for low cholesterol cells treated with 5μM – Figure 7.8 right (two-way ANOVA with Tukey's multiple comparison to control stimulated cells, p<0.05* and p<0.01**, n=5).

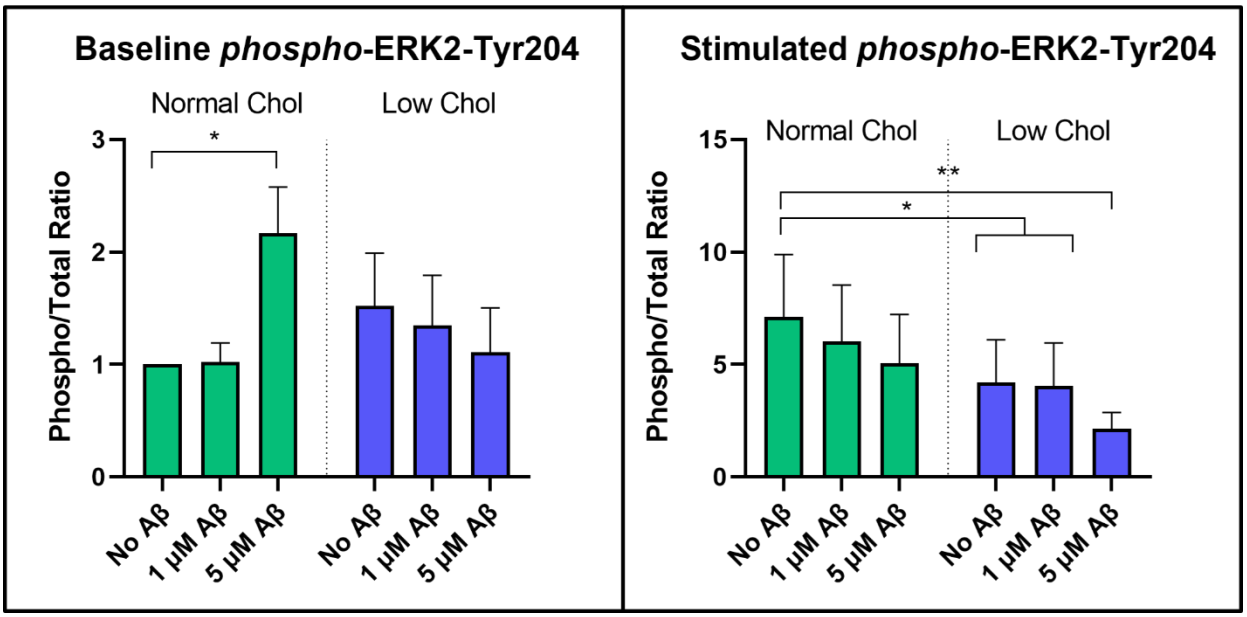

Figure 7.8. ERK1 and ERK2 phosphorylation on baseline (Left) and PDGFAA stimulated (Right) HT22. Left: *5μM Aβ oligomers caused an increase in baseline phosphorylation of ERK2, which was abolished in cells with low cholesterol, an interaction was detected (*p<0.05). This effect was not observed in cholesterol reduced cells and an interaction between cholesterol and Aβ was detected by two-way ANOVA p<0.05. There was a clear and consistent trend of PDGF-AA treatment activating downstream ERK2 causing phosphorylation. Unlike in baseline, there was no significant increase in ERK2 activation following PDGFAA treatment in the high concentration Aβ group two-way (n=5). ERK1/2 phosphorylation induced by PDGF-AA was significantly decreased in all low cholesterol groups (two-way ANOVA, Tukey's multiple comparison p<0.05*), an effect further compounded with high Aβ concentration (p<0.01**). Mean ± SEM reported (n=5).*

Activation of Ras-ERK signaling has been implicated in the pathophysiology of AD with neuronal exposure to Aβ42 oligomers enhancing Ras/ERK signaling cascade[216,217]. This may be a counter regulatory factor to increase the chances of cell survival in response to the toxic insult of Aβ but could contribute to toxicity if there is sustained overactivation, taxing cellular regulatory process involved in cell growth and proliferation that are impaired by the initial Aβ insult. In addition, neuroprotective properties of different compounds including agmatine, tanshinone II2 and several different neurosteroids and their metabolites, have been shown to involve reversal of ERK1/2 and GSK3β activation in neuronal cell lines, primary hippocampal cultures and in rodent models *in vivo*[216,218,423,424]. The reduction in ERK1/2 signaling from cholesterol reduction is correlated with reductions from PDGFRα, however membrane cholesterol reduction will undoubtedly affect a whole host of signaling pathways both at the cell membrane and intracellularly through membrane-associated proteins that have effects on MAPK signaling. These neuroprotective mechanisms may include other membrane receptors, as well as Ras and Rho superfamilies which include membrane-dependent GTPases that transduce signals from neuronal membrane receptors to downstream intracellular secondary messengers ultimately affecting gene expression[425]. All combined there appears to be a consistent effect of cholesterol depletion having a pronounced impact interfering with PDGF-AA signaling that may be exacerbated by high concentrations of Aβ oligomers.

PLCγ is a major downstream effector of many RTKs, with PLCγ1 being expressed in neuronal cell types. PLCγ has membrane lipid raft dependent activity in T-lymphocytes which is likely generalizable to other cell types and signaling pathways due to the non-specific actions of membrane lipid raft disruption[408]. The effects of cholesterol depletion and Aβ treatment on PDGF-AA induced activation of PLCγ1 correlating with activation of PDGFRα and ERK1/2 signaling, results shown in Figure 7.10. Like other experiments, there was no significant effect of any of the treatments on total protein levels in either the baseline or stimulated datasets (Figure 7.9); for representative blots see Figure 7.13. Activation of PLCγ1 was measured by the phosphorylation of tyrosine-783 expressed as a relative ratio over the total PLC γ1 protein level. Under baseline conditions there was no effect of any treatment, Aβ or cholesterol depletion on phosphoPLCγ1 levels (Figure 7.10 – left). Activation of PLCγ1 by PDGFAA resulted in a 4-fold increase in phosphorylation levels over untreated control. Under stimulation from PDGFAA no interaction between Aβ or cholesterol depletion was detected by two-way ANOVA. There was

no main effect for Aβ in any of the normal cholesterol groups, implying Aβ had no detectable effect on PLCγ1 activation. However, the main effect of cholesterol depletion significantly reduced the levels of phosphorylation in all low cholesterol groups and was the major source of variation across groups (two-way ANOVA, $p<0.05$*). For all low cholesterol groups there was a 2-fold reduction in PLCγ1 activation that had higher significance and greater reduction with increasing Aβ concentration, shown in Figure 7.10 – right ($p<0.05$* for low cholesterol, $p<0.01$** for low cholesterol + 1μM Aβ, and 5μM Aβ groups). No interaction was detected between Aβ and cholesterol depletion gain, it was observed that cholesterol has a pronounced influence on the disruption of PDGF-AA induced activation of RTK signaling pathways that may be compounded by high concentration Aβ, as with phospho-ERK data.

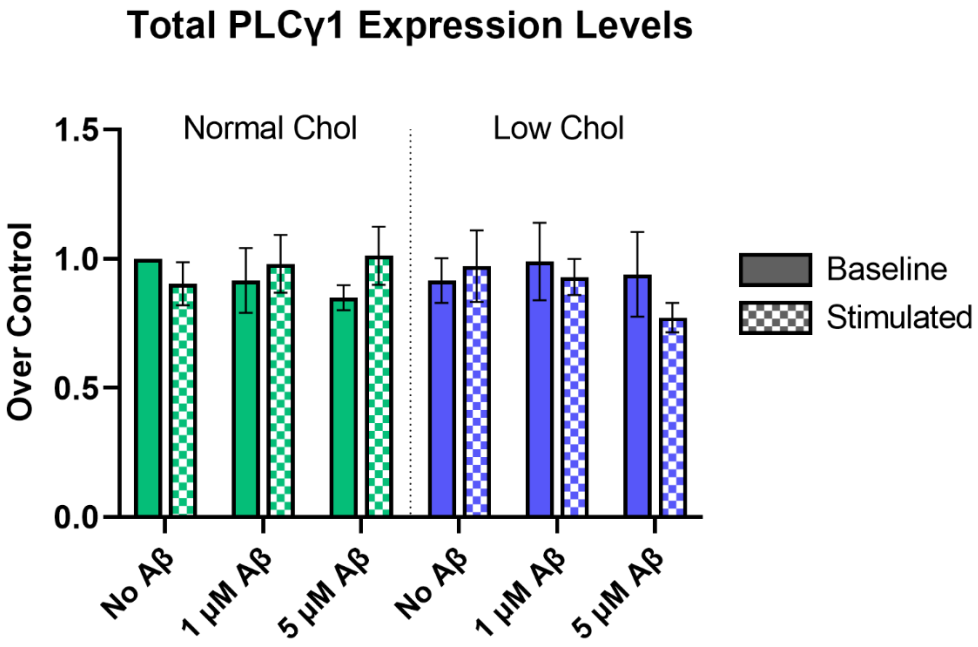

Figure 7.9. Total PLC γ1 expression levels *are unchanged for baseline and stimulated HT22 cells across all treatment conditions. Mean ± SEM reported (n=5).*

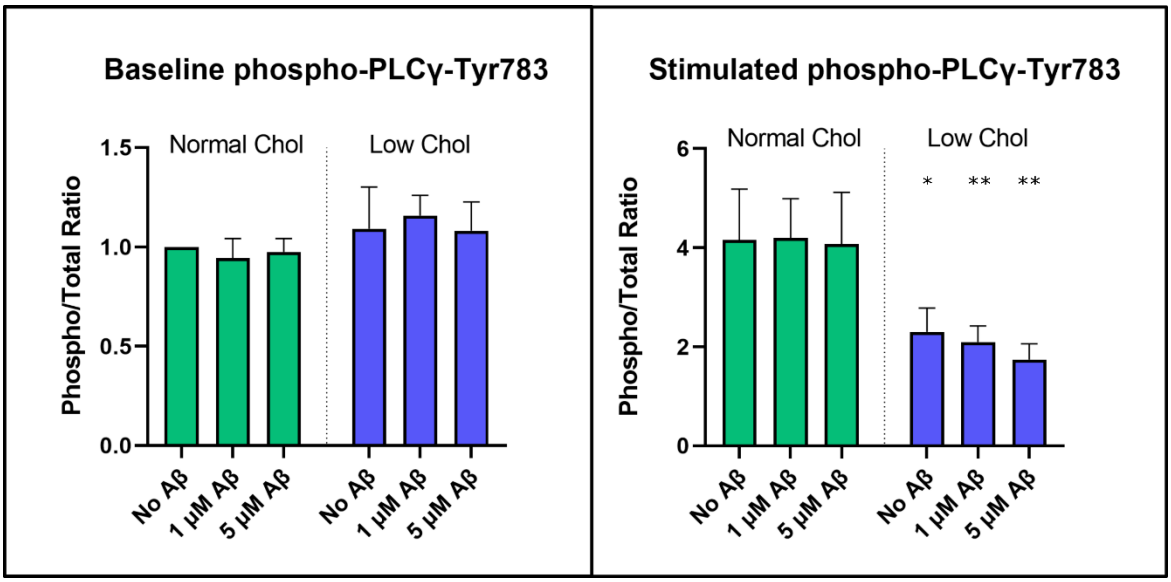

Figure 7.10. PLCγ1 activation in HT22 cells. *(Left) No effect on baseline PLCγ1 activation was detected for any group. (Right) Activation is reduced by cholesterol depletion (n=5, p<0.05)), but no statistically significant effect is observed for Aβ. Two-way ANOVA (α=0.05) with Tukey's multiple comparison, p<0.05*, p<0.01**. Mean ± SEM reported (n=5).*

GSK3β is an intracellular kinase that has activity on many different substrates including microtubule associated protein tau and it has been implicated in hyperphosphorylation of tau in AD[217,426–428]. GSK3β inhibition has been shown to reduce tau hyperphosphorylation and plaque deposition and may be protective against cognitive dysfunction in mice and fly models of AD[409,429]. In the present study there was no statistically significant effect of any treatment on total GSK3β protein levels in HT-22 cells (Figure 7.11), for baseline or stimulated data. The serine-9/21 phosphorylation site is inhibitory and was expected to be decreased in response to Aβ, as suggested by other studies in APP knockdown and AD patient brain analysis[217]. There were no effects observed here of cholesterol depletion or Aβ treatment on baseline GSK3β phosphorylation of serine-9 (Figure 7.12 left). A small increase in serine-9 phosphorylation occurred with PDGFAA stimulation by 40 to 70% for cells with normal cholesterol (Figure 7.12 right). The GSK3β activation identified in previous studies was detected in primary neuron cultures, and in AD patient brain samples which are more physiologically relevant than immortalized HT22 cells. This may represent a shortcoming of the HT22 cells which do not recapitulate important neuronal functions that are relevant in the effects of Aβ on the GSK3β pathway.

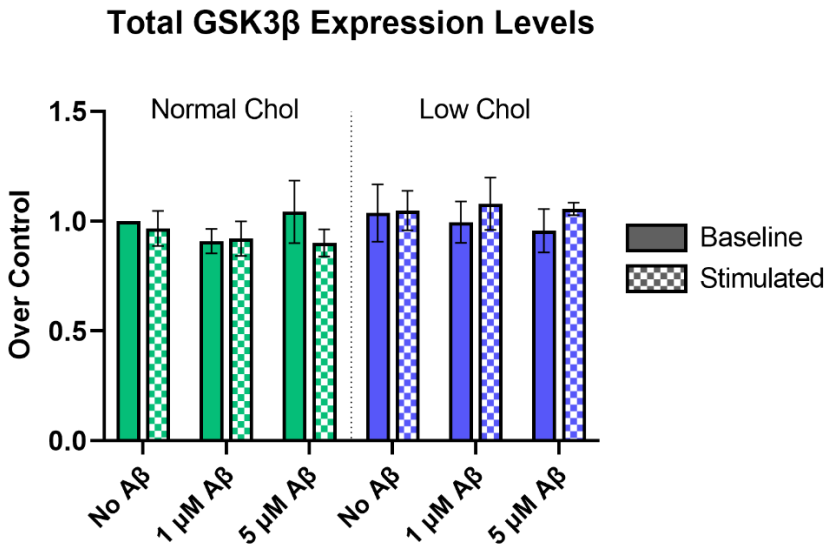

Figure 7.131. Total GSK3β expression levels *are unchanged for baseline and stimulated HT22 cells across all treatment conditions (two-way ANOVA, α=0.05). Mean ± SEM reported (n=5).*

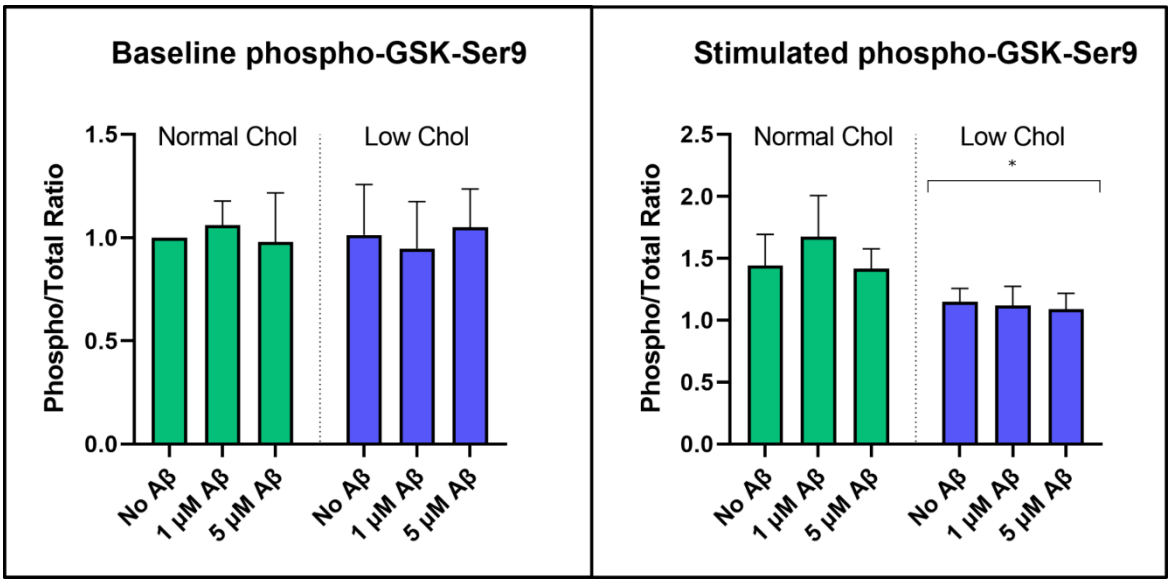

Figure 7.12. Effects on phospho-GSK3β-Ser9 levels. *Left: no effect on baseline cells. Right: In PDGFAA stimulated cells observed a significant decrease in GSK3β Ser-9 phosphorylation levels in low cholesterol groups compared to normal cholesterol. No effect of Aβ, or interactions between cholesterol levels and Aβ were detected, by two-way ANOVA, p<0.05*. Mean ± SEM reported (n=5).*

7.4 Conclusion

Cholesterol reduction reduces RTK expression levels, both in truncated TrkB and PDGFRα expression levels. Though in some instances this effect was not statistically significant it may likely be affected by the rebound in cholesterol levels and robust cholesterol biosynthesis in the HT22 cells that was reported in Chapter 4. This feature of active cholesterol biosynthesis

is necessary for cell proliferation of immortalized cell lines but is not a feature of mature neurons which rely on cholesterol produced and trafficked by glial cells in the brain. Furthermore, cholesterol depleted HT22 cells have reduced PDGFRα activation as evidenced by a reduction in PDGFRα phosphorylation followed by reduction on downstream ERK1/2 and PLCγ1 phosphorylation. Aβ alone did not have a statistically significant effect on PDGFRα signaling, though a trend towards slight decreases in phosphorylation levels were seen at high concentration. In addition, combined Aβ treatment and cholesterol reduction increased the probability of observing a statistically significant impairment in PDGFRα signaling and increased the effect size following cholesterol sequestration indicating that membrane disruption due to Aβ may compound with the effect of cholesterol depletion. Combined, this suggests that Aβ may have some small disruptive effects on PDGFRα signaling, but that cholesterol depletion does not restore this functionality and thus PDGFRα cannot be involved in the protective mechanisms of low cholesterol.

The protective mechanisms of cholesterol depletion correlate with reductions in truncated TrkB expression and with a reduction in PLCγ1, PDGFRα and ERK1/2 phosphorylation levels. However, cholesterol depletion results in a reduction in RTK signaling, which generally promotes cell survival and growth, and would be more likely to impair cell viability. Moreover, the impacts of Aβ on PDGF-AA induced activation of PDGFRα were minimal, though they compounded with cholesterol depletion. Overall, this implies that the protective effect of cholesterol sequestration is more likely due to different receptor signaling pathways, such as glutamatergic or cholinergic pathways, or non-specific binding and cell membrane damage and subsequent downstream oxidative stress.

7.5 Supplementary Material

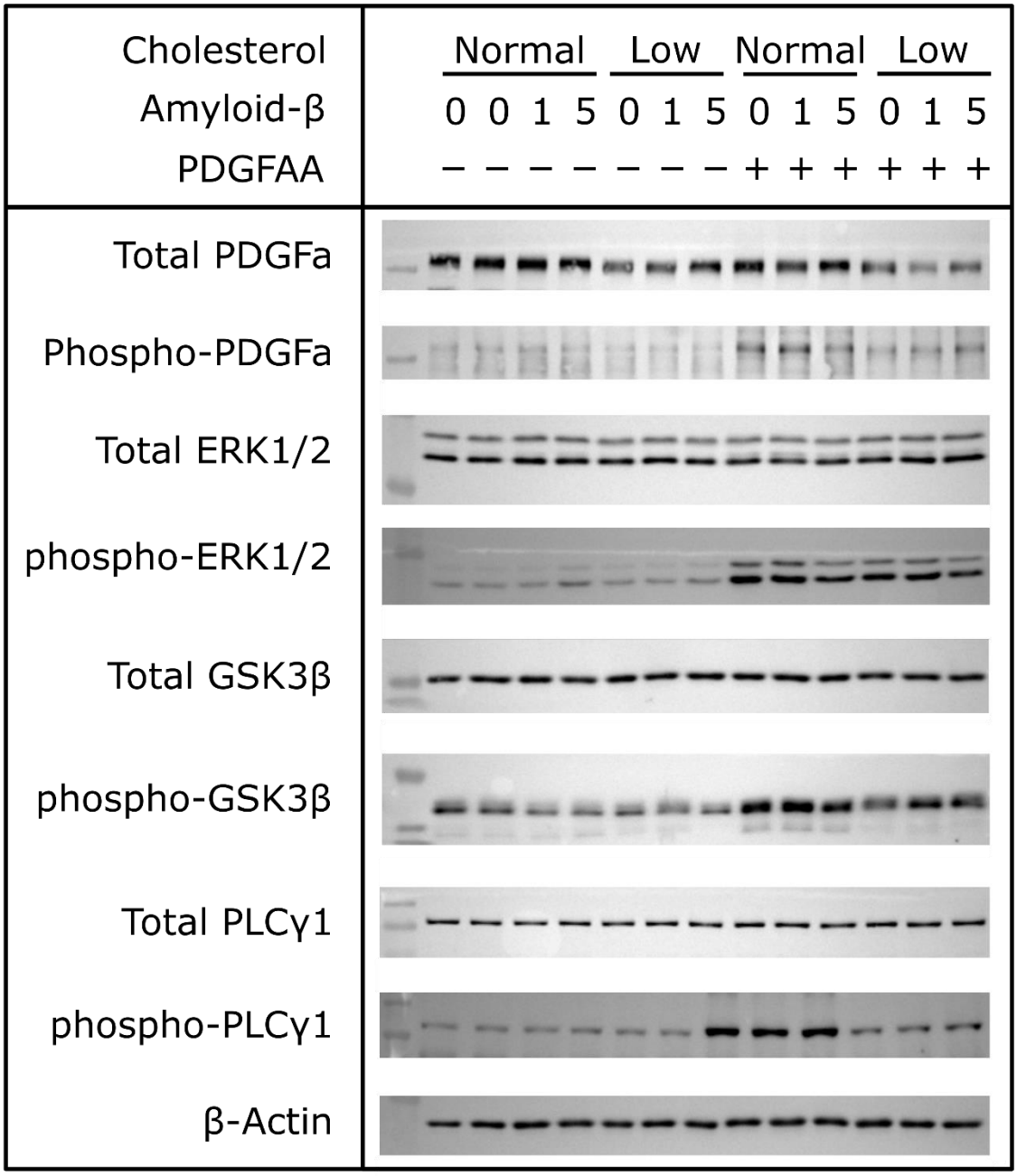

Figure 7.13. Representative Western blot images *for all the targets presented in this chapter.*

Chapter 8: Ca2+ Fluorescence Microscopy of HT22 cells

8.1 Introduction

The work presented in this chapter is preliminary.

Calcium signaling is crucial for neuronal function, including fundamental cell signaling processes and neuron specific functionality especially synaptic transmission and action potential propagation along nerve fibers. As such it is no surprise that Aβ has been shown to interfere with calcium signaling. Aβ binds to and interferes with NMDA receptors, which are an essential ligand gated calcium ion channel activated by glutamate, which along with AMPA receptors forms the basis of the majority of excitatory neurotransmission in the CNS. As well there is evidence to suggest that Aβ forms calcium selective membrane pores, that can be blocked by zinc ions. As such calcium signaling represents an important physiological process to experiment within the context of neuronal function.

Different ways to study calcium signaling include neurophysiological approaches, molecular biology methods to measure the downstream effects of Ca^{2+} ion channel activation, or to visualize changes in calcium using calcium-, or voltage-, sensitive fluorescent dyes. One common Ca^{2+} sensitive dye is Fluo-4 which is a Ca^{2+} chelator that fluoresces when it binds calcium. Fluo-4 can be modified with an ester to increase membrane permeability to study the intracellular levels of calcium change in response to drug treatments or different physiological states.

8.2 Methods

8.2.1 Loading Cells with Fluo-4 Ca^{2+} Sensitive Dye

Fluo-4 (as AM cell permeable ester) was reconstituted in DMSO with 0.1% Pluronic F-127 in HBSS to 3μM. Briefly, 44μl of DMSO was used to solubilize 50μg of Fluo-4 which was aliquoted to 11 μL and stored frozen at 4°C until day of use (~104μM). On the day of imaging, 2.25 μL Pluronic was added to 11 μL aliquot of Fluo-4 (AM) in DMSO to produce an 86 μM Fluo-4/Pluronic F-127 solution which is then diluted in 3.575mL HBSS to the final concentration. To load, cells were first washed with calcium and magnesium containing HBSS (Gibco) then treated with Fluo-4 solution and incubated at 37°C 5% CO_2 for 30 minutes. Cells

were then gently washed twice as long in HBSS supplemented with calcium and magnesium prior to imaging.

8.2.2 Fluorescence Microscopy

Cells were imaged at 10x magnification on an Olympus IX51 equipped with a FITC/GFP filter cube with excitation filter: 470nm, and emission filter: 535nm. The X-Cite 120W mercury vapor arc lamp excitation light source was set to 50% power. Images were captured on an Olympus DP26 camera, in a low illumination room. Once focused on the cells optical path was fixed. Baseline fluorescence signal was captured then HT22 cells were treated with 500 nM glutamate or epinephrine and imaged under the same conditions at intervals for 5-, 15-, 30-seconds, then 1-, 2-, 3-, 5-, 10-, and 15-minutes post-treatment. Between image acquisition the shutter was closed to reduce the effects of photobleaching from excitation of the Fluo-4 fluorophore.

8.3 Results

HT22 cells loaded with Fluo-4 Ca^{2+} sensitive dye can be used to study calcium signaling in response to different treatments. Before and after treatment can be compared by subtracting post-treatment images from the baseline image which can then be averaged over to get a change in Ca^{2+} signaling, this change was then expressed in arbitrary units (au) of intensity (0, 255) from the image acquisition software. Upon treatment with 500nM glutamate there is an increase in fluorescence signal that peaks around 2 minutes to 7.8 au. above the baseline signal, before decreasing slowly (Figure 8.1). Controls show a 10% decrease in fluorescence signal over a 15-minute imaging window which is typical of photobleaching, from 2.5 to 2.3 A.U. It is important to note that the change compared to baseline is most likely due to differences in camera noise between images, rather than any significant differences in Ca^{2+} levels within the first 5 seconds of image acquisition. The increase in fluorescence due to glutamate treatment is indicative of an increase in Ca^{2+} signaling induced by activation of cationic ion channels, NMDA and/or AMPA. HT22 cells are known to exhibit glutamate induced cytotoxicity, and express NR1 subunit of the NMDA receptor [308,430]. In contrast, epinephrine at 500 nM caused no significant net increase in fluorescence signal, Figure 8.2 (1.326 A.U. which was below the baseline of the control). This technique could be useful for studying the effects of Aβ and cholesterol depletion on glutamate

induced Ca^{2+} signaling because of the effect of Aβ on NMDA receptors and the ability of Aβ to form Ca^{2+} pores/ion channels.

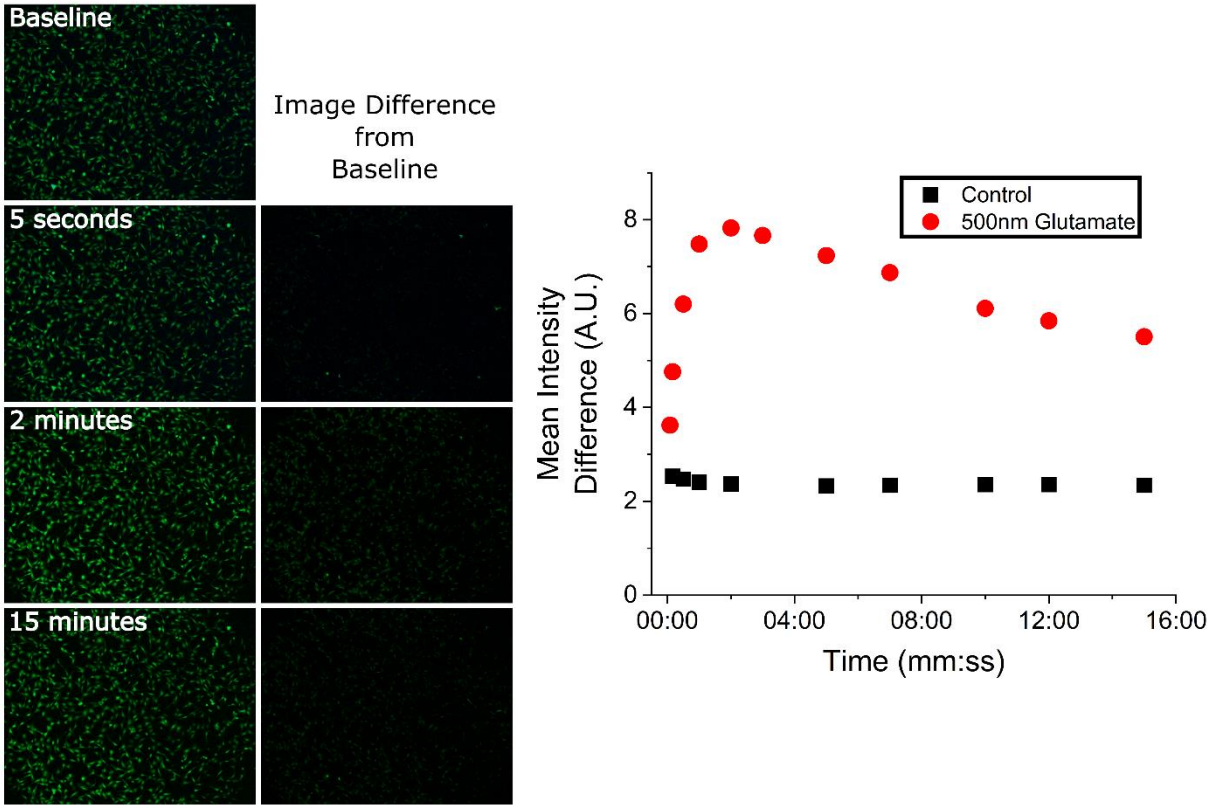

Figure 8.1. Ca2+ signaling within HT22 cells after 500nM glutamate, *reaches peak at approximately 2 minutes. Mean Intensity Difference is calculated by subtracting each time point from the baseline expressed in arbitrary units (A.U.). Control image sequence shows about 10% fluorescence photobleaching over 15:00 minute image sequence (right).*

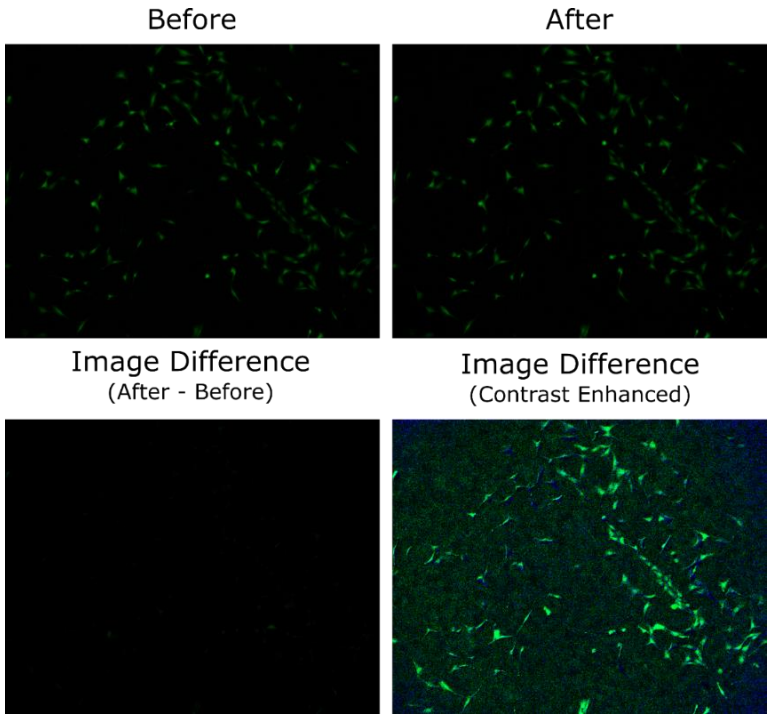

Figure 8.2. Ca2+ signaling within HT22 cells after 500nM epinephrine *before treatment (left) and 30 seconds post treatment (right). Small increase in signal within some HT22 cells, decrease in other cells.*

8.4 Conclusion

These preliminary experiments contribute to other aspects of HT22 cell biology and test the feasibility of using these methods to study the influence of cholesterol and Aβ on neurotransmitter and Ca^{2+} signaling in HT22 cells. Ca^{2+} signaling is extremely important in excitable cells such as neurons as it is a part of the principal pathway for activation of these cells. HT22 cells were not responsive to epinephrine, however they were mildly responsive to glutamate over a timescale of minutes, in line with previous characterization of HT22 cells as glutamate sensitive. That being said the response to glutamate was not fast/dramatic as in primary neurons, where peak glutamate activation and Ca^{2}+ signaling in primary neurons occurs on the order of seconds, not minutes. So even though HT22 cells may express functionally active NMDA receptors that increase Ca^{2+} upon exposure to glutamate, the dynamics of receptor activation is not representative of primary neuronal cultures or neurons *in vivo*.

Chapter 9: Conclusion and Future Directions

9.1 Conclusion

The role of the lipid membrane in Alzheimer's disease has long been recognized as the site of Aβ production and critical in pathogenesis but overlooked as a *modifiable* contributing factor in the main paradigm of AD and in Aβ toxicity. This is likely a consequence of the lipid membrane in general being viewed in biology as passive structure to support membrane proteins, rather than the dynamic structure that is actively involved in regulating membrane proteins. Therefore, strategies that emphasize the lipid membrane have not been the focus of therapeutic and diagnostic research efforts. The failures of targeting the amyloid cascade directly have highlighted that new directions in AD research are needed. One important direction is in looking at the membrane as a modifiable and important factor in Aβ toxicity. If the lipid membrane can be maintained in a healthy manner, with optimal composition, limiting influences of peroxidative and Aβ induced damage, it may be possible to forestall AD pathogenesis. This thesis has presented a novel series of studies spanning biomedical nanotechnology (AFM for membrane biophysics) and more traditional molecular biology (using cell-based assays, microscopy and protein analysis) to assess various aspects of this hypothesis and add to the body of literature that indicates the importance of the lipid membrane and its composition in Aβ toxicity.

In Chapter 3, the effects of melatonin on phase separated lipid bilayers were studied by AFM and AFS breakthrough forces for the first time. This study showed that the addition of melatonin from the aqueous phase visibly changed the topographical structure of a phase separated lipid bilayer, decreasing surface area of L_O domains due to melatonin incorporation into both phases along with an apparent displacement of cholesterol from the L_O phase, in a large subset of experiments. In terms of the biophysical properties of the lipid bilayer there was an increase in elastic modulus, decrease in indentation depth and bilayer thicknesses, corresponding to an increase of the extent of the L_D phase, this corresponds to an increase in membrane fluidity particularly of the disordered phase, but the overall membrane as well. Melatonin also reduced the work and force of adhesion of the probe to the membrane. The interaction of melatonin with cholesterol microdomains may be involved in the protective effects of melatonin against Aβ

toxicity, by reducing the extent of membrane microdomains that have been reported to act as seeds for Aβ oligomer binding and aggregation and by reducing adhesion to the lipid bilayer.

In Chapter 4, the use of contact mode HS-AFM for studying lipid bilayers and protein membrane interactions is presented for the first time. HS-AFM is effective and relatively non-destructive for imaging soft bilayers with detail that is comparable to standard contact AFM in liquid. The ability to image dynamic membrane processes on sub second timescales and over the course of few hours as well as collect several orders of magnitude more data in less time has exciting applications. These data show that imaging dynamic membrane processes involving membrane reorganization are possible with HS-AFM, but that during imaging addition of Aβ – a sticky aggregation prone peptide – results in destabilization of tip sample interactions which greatly affects imaging quality, but that after addition and rinsing of the sample, Aβ aggregates on the surface of the membrane are largely stable. In addition, this imaging data shows several different interaction mechanisms of Aβ with model lipid bilayers, including disruption of membrane domains, accumulation on ordered domains, and increase in surface roughness and hole formation that depend on aggregation state and lipid bilayer composition.

In Chapter 5, MTT cell viability and cholesterol oxidase assays were performed on HT22 cells treated with MβCD (to reduce membrane cholesterol) and Aβ prepared in two different ways, as unaggregated monomers and as preformed oligomers. It has been shown for the first time that Aβ does not affect cholesterol levels or cholesterol recovery following MβCD sequestration from HT22 cells. Also, a novel comparison between initially unaggregated Aβ and preformed Aβ oligomers yielded no significant difference in toxicity across a range of concentrations and in terms of the IC50 following 24-hour exposure to HT22 cells. This is likely due to substantial aggregation of the initially unaggregated monomer solution over the 24-hour treatment period and the high sensitivity of HT22 cells to Aβ. Cholesterol reduction was mildly protective against Aβ monomer toxicity but not oligomer toxicity, while 10μM melatonin was much more protective.

In Chapter 6, optical microscopy combined with AFM imaging reveals important information as to the mechanisms of Aβ toxicity based on the changes to HT22 cell morphology. A simple method to quantify changes in morphology of cellular populations using phase contrast microscopy using ImageJ was used to compute cell perimeter, area and sphericity. It was observed that cells treated with 5 μM Aβ oligomers dramatic changed cellular morphology in a

manner indicative of disrupted cell adhesion, a tendency towards larger cell areas, perimeters, and a decrease in sphericity. These morphological changes were less pronounced in low cholesterol cells, suggesting that the protective mechanisms of cholesterol depletion detected in Chapter 4 involve maintenance of cell cytoskeleton and morphology. Unaggregated Aβ, assumed to be predominantly monomeric when cells were first treated, were less likely to cause severe morphological changes in HT22 cells at 5 μM compared to oligomers, despite no significant difference in toxicity between preformed Aβ oligomers (shown in Chapter 4). This may indicate a difference in the toxic mechanisms of different Aβ species, whereas there are similar impacts on cellular metabolism (from MTT assay results), oligomers are more disruptive in the way of triggering changes in morphology. On the single-cell level AFM analysis was used to assess the effect of Aβ aggregates on individual HT22 cell morphology. There were several unique morphological changes induced by Aβ that are suggestive of both necrotic and apoptotic cell death mechanisms. Some cells exhibited damage to the cell membrane and cytoskeleton indicative of necrosis while other cells appeared to have contracted cell bodies, disrupted cell adhesion, membrane blebbing and spherical bodies which is indicative of apoptosis.

In Chapter 7, cell signaling data of HT22 cells with reduced cholesterol and/or treated with Aβ in two different aggregation states then with PDGF-AA growth factor are presented for the first time. Cholesterol reduction reduces RTK expression levels, both in truncated TrkB and PDGFRα expression levels. Furthermore, cholesterol depleted HT22 cells have reduced PDGFRα activation as measured by a reduction in PDGFRα phosphorylation corresponding to a decrease in downstream secondary messenger (ERK1/2 and PLCγ1) phosphorylation. Aβ alone did not cause a statistically significant effect on PDGFRα signaling, though a trend towards slight decreases in many of these protein phosphorylation levels were seen at high concentration with Aβ increasing the probability of observing a statistically significant impairment in PDGFRα signaling and increased the effect size following cholesterol sequestration suggesting that membrane disruption due to Aβ may compound with the effect of cholesterol depletion. Moreover, both Aβ and cholesterol reductions impaired the PDGF-AA induced increases in HT22 cell viability. Combined this suggests that Aβ may have some small disruptive effects on PDGFRα signaling and that cholesterol depletion does not restore this functionality.

When taken together with AFM, cell viability and microscopy data the protective mechanisms of cholesterol depletion are not likely to involve RTKs, but other receptor signaling

pathways, or in the prevention of non-specific cell membrane damage. Overall, this multidisciplinary series of scientific studies adds important knowledge to a variety of diverse scientific fields.

9.2 Future Directions

Merging the fields of membrane biophysics with cell and molecular biology in an interdisciplinary fashion is a necessary step in developing a more complete understanding physiological and disease processes that underlie cell signaling of membrane receptors. The state of the lipid bilayer is important in regulating cell membrane proteins, which in turn can affect cell signaling, adhesion, morphology, and metabolism. There are several experiments that were proposed that would add further insight and clarity into the mechanisms of Aβ toxicity in HT22 cells for instance to study the high cholesterol case, where cell membrane cholesterol would be increased by MβCD loaded with cholesterol. Repeating cell viability, signaling and microscopy data for the high cholesterol case would provide better understanding of the cholesterol dependence of Aβ toxicity.

Another set of experiments that would add a good deal of clarification as to the lipid membrane specific mechanisms of Aβ toxicity is cellular lipidomic and isolated lipid membrane structural analysis. It is unlikely that MβCD would only reduce cholesterol levels, so assessing the effects of this treatment on the cellular lipidome may identify other lipids removed by MβCD and the response of HT22 cells on lipid metabolism more generally. Performing lipidomic analysis on cell membrane microdomains fractions would also be an interesting experiment to examine how cholesterol depletion triggers changes in lipid trafficking between domains. These microdomain fractions could also be imaged by AFM to study their structure connecting Chapters 3 and 4 more directly to Chapters 5 – 7, allowing for direct correlations between neuronal function, lipid composition and membrane structure to be performed.

Although the HT22 cells are an appropriate model for high-throughput experiments, such as quick cell toxicity and drug screening for their ease and speed of growth, there are some major limitations that should acknowledged, and other approaches suggested for future directions. The high proliferation rate of HT22 cells due to their immortalized phenotype imply that they have non-neuronal lipid metabolism, with high rates of cholesterol biosynthesis that may confound some of the physiological relevance of these studies. In addition, HT22 cells lack expression and

activation of relevant neuron specific RTKs making them less useful for studying NGF and BDNF signaling. Although HT22 cells have been shown to express functional glutamate receptors (confirmed in Chapter 8), they do not have the levels of excitability of neuronal cells. Thus, further work in this area should be explored in more physiologically relevant, higher impact rodent primary cell culture, or human induced pluripotent stem cell model, both of which have more appropriate neuronal characteristics and overcome the limitations of immortalized cell lines.

References

(1) Feynman, R. The Value of Science, 1955. https://calteches.library.caltech.edu/1575/1/Science.pdf.

(2) Wong, S. L.; Gilmour, H.; Ramage-Morin, P. L. Alzheimer's Disease and Other Dementias in Canada. *Stat. Can.* **2016**, *27* (5), 11–16.

(3) Karran, E.; Mercken, M.; Strooper, B. D. The Amyloid Cascade Hypothesis for Alzheimer's Disease: An Appraisal for the Development of Therapeutics. *Nat. Rev. Drug Discov.* **2011**, *10* (9), 698–712. https://doi.org/10.1038/nrd3505.

(4) Hane, F. T.; Robinson, M.; Lee, B. Y.; Bai, O.; Leonenko, Z.; Albert, M. S. Recent Progress in Alzheimer's Disease Research, Part 3: Diagnosis and Treatment. *J. Alzheimers Dis.* **2017**, *57* (3), 645–665. https://doi.org/10.3233/JAD-160907.

(5) Dubois, B.; Feldman, H. H.; Jacova, C.; Cummings, J. L.; Dekosky, S. T.; Barberger-gateau, P.; Delacourte, A.; Frisoni, G.; Fox, N. C.; Galasko, D.; Gauthier, S.; Hampel, H.; Jicha, G. A.; Meguro, K.; Brien, J. O.; Pasquier, F.; Robert, P.; Rossor, M.; Salloway, S.; Sarazin, M.; Souza, L. C. D.; Stern, Y.; Visser, P. J.; Scheltens, P. Revising the Definition of Alzheimer's Disease: A New Lexicon. *Lancet Neurol.* **2010**, *9*, 1118–1127. https://doi.org/10.1016/S1474-4422(10)70223-4.

(6) Dubois, B.; Feldman, H. H.; Jacova, C.; Hampel, H.; Molinuevo, J. L.; Blennow, K.; Dekosky, S. T.; Gauthier, S.; Selkoe, D.; Bateman, R.; Cappa, S.; Crutch, S.; Engelborghs, S.; Frisoni, G. B.; Fox, N. C.; Galasko, D.; Habert, M.; Jicha, G. A.; Nordberg, A.; Pasquier, F.; Rabinovici, G.; Robert, P.; Rowe, C.; Salloway, S.; Sarazin, M.; Epelbaum, S.; Souza, L. C. D.; Vellas, B.; Visser, P. J.; Schneider, L.; Stern, Y.; Scheltens, P.; Cummings, J. L.; Curie-paris, P. M.; De, H. Advancing Research Diagnostic Criteria for Alzheimer's Disease : The IWG-2 Criteria. *Lancet Neurol.* **2014**, *13*, 614–629. https://doi.org/10.1016/S1474-4422(14)70090-0.

(7) Ballard, C.; Gauthier, S.; Corbett, A.; Brayne, C.; Aarsland, D.; Jones, E. Alzheimer's Disease. *The Lancet* **2011**, *377* (9770), 1019–1031. https://doi.org/10.1016/S0140-6736(10)61349-9.

(8) Walhovd, K. B.; Fjell, A. M.; Brewer, J.; McEvoy, L. K.; Fennema-Notestine, C.; Hagler, D. J.; Jennings, R. G.; Karow, D.; Dale, A. M.; Initiative, A. D. N. Combining MR Imaging, Positron-Emission Tomography, and CSF Biomarkers in the Diagnosis and Prognosis of Alzheimer Disease. *AJNR Am. J. Neuroradiol.* **2010**, *31* (2), 347–354. https://doi.org/10.3174/ajnr.A1809.

(9) Nelson, P. T.; Jicha, G. A.; Schmitt, F. A.; Liu, H.; Davis, D. G.; Mendiondo, M. S. Clinicopathologic Correlations in a Large Alzheimer Disease Center Autopsy Cohort: Neuritic Plaques and Neurofibrillary Tangles "Do Count" When Staging Disease Severity. *J. Neuropathol. Exp. Neurol.* **2007**, *661136–114*.

(10) Hyman, B. T.; Phelps, C. H.; Beach, T. G.; Bigio, E. H.; Cairns, N. J.; Carrillo, M. C.; Dickson, D. W.; Duyckaerts, C.; Frosch, M. P.; Masliah, E.; Mirra, S. S.; Nelson, P. T.; Schneider, J. A.; Thal, D. R.; Thies, B.; Trojanowski, J. Q.; Vinters, H. V.; Montine, T. J. National Institute on Aging-Alzheimer's Association Guidelines for the Neuropathologic Assessment of Alzheimer's Disease. *Alzheimers Dement. J. Alzheimers Assoc.* **2012**, *8* (1), 1–13. https://doi.org/10.1016/j.jalz.2011.10.007.

(11) Nagy, Z.; Esiri, M. M.; Jobst, K. A.; Morris, J. H.; King, E. M. F.; McDonald, B.; Litchfield, S.; Smith, A.; Barnetson, L.; Smith, A. D. Relative Roles of Plaques and Tangles in the Dementia of Alzheimer's Disease: Correlations Using Three Sets of Neuropathological Criteria. *Dement. Geriatr. Cogn. Disord.* **1995**, *6* (1), 21–31. https://doi.org/10.1159/000106918.

(12) Nelson, A. R.; Sweeney, M. D.; Sagare, A. P.; Zlokovic, B. V. Neurovascular Dysfunction and Neurodegeneration in Dementia and Alzheimer's Disease. *Biochim. Biophys. Acta - Mol. Basis Dis.* **2016**, *1862* (5), 887–900. https://doi.org/10.1016/j.bbadis.2015.12.016.

(13) Sperling, R. A.; Aisen, P. S.; Beckett, L. A.; Bennett, D. A.; Craft, S.; Fagan, A. M.; Iwatsubo, T.; Jack, C. R.; Kaye, J.; Montine, T. J.; Park, D. C.; Reiman, E. M.; Rowe, C. C.; Siemers, E.; Stern, Y.; Yaffe, K.; Carrillo, M. C.; Thies, B.; Morrison-Bogorad, M.; Wagster, M. V.; Phelps, C. H. Toward Defining the Preclinical Stages of Alzheimer's Disease: Recommendations from the National Institute on Aging and the Alzheimer's Association Workgroup. *Alzheimers Dement.* **2011**, *7* (3), 1–13. https://doi.org/10.1016/j.jalz.2011.03.005.

(14) McKhann, G. M.; Knopman, D. S.; Chertkow, H.; Hyman, B. T.; Jack, C. R.; Kawas, C. H.; Klunk, W. E.; Koroshetz, W. J.; Manly, J. J.; Mayeux, R.; Mohs, R. C.; Morris, J. C.; Rossor, M. N.; Scheltens, P.; Carrillo, M. C.; Thies, B.; Weintraub, S.; Phelps, C. H. The Diagnosis of Dementia Due to Alzheimer's Disease: Recommendations from the National Institute on Aging-Alzheimer's Association Workgroups on Diagnostic Guidelines for Alzheimer's Disease. *Alzheimers Dement.* **2011**, *7* (3), 263–269. https://doi.org/10.1016/j.jalz.2011.03.005.

(15) Albert, M. S.; Dekosky, S. T.; Dickson, D.; Dubois, B.; Feldman, H. H.; Fox, N. C.; Gamst, A.; Holtzman, D. M.; Jagust, W. J.; Petersen, R. C.; Snyder, P. J.; Carrillo, M. C.; Thies, B.; Phelps, C. H. The Diagnosis of Mild Cognitive Impairment Due to Alzheimer ' s Disease : Recommendations from the National Institute on Aging-Alzheimer ' s Association Workgroups on Diagnostic Guidelines for Alzheimer ' s Disease. *Alzheimers Dement.* **2011**, *7* (3), 270–279. https://doi.org/10.1016/j.jalz.2011.03.008.

(16) Vetrivel, K. S.; Thinakaran, G. Membrane Rafts in Alzheimer's Disease Beta-Amyloid Production. *Biochim. Biophys. Acta* **2010**, *1801* (8), 860–867. https://doi.org/10.1016/j.bbalip.2010.03.007.

(17) Rushworth, J. V.; Hooper, N. M. Lipid Rafts: Linking Alzheimer's Amyloid-β Production, Aggregation, and Toxicity at Neuronal Membranes. *Int. J. Alzheimers Dis.* **2010**, *2011* (1), 603052. https://doi.org/10.4061/2011/603052.

(18) Robinson, M.; Lee, B. Y.; Hane, F. T. Recent Progress in Alzheimer's Disease Research Part 2 - Genetics and Epidemiology. *J. Alzheimers Dis.* **2017**, *57* (2), 317–330. https://doi.org/10.3233/JAD-161149.

(19) Drolle, E.; Negoda, A.; Hammond, K.; Pavlov, E.; Leonenko, Z. Changes in Lipid Membranes May Trigger Amyloid Toxicity in Alzheimer's Disease. *PLoS ONE* **2017**, *12* (8), e0182194.

(20) Drolle, E.; Gaikwad, R. M.; Leonenko, Z. Nanoscale Electrostatic Domains in Cholesterol-Laden Lipid Membranes Create a Target for Amyloid Binding. *Biophys. J.* **2012**, *103* (4), 27–29. https://doi.org/10.1016/j.bpj.2012.06.053.

(21) Abramov, A. Y.; Ionov, M.; Pavlov, E.; Duchen, M. R. Membrane Cholesterol Content Plays a Key Role in the Neurotoxicity of β-Amyloid: Implications for Alzheimer's

Disease. *Aging Cell* **2011**, *10* (4), 595–603. https://doi.org/10.1111/j.1474-9726.2011.00685.x.

(22) Cecchi, C.; Nichino, D.; Zampagni, M.; Bernacchioni, C.; Evangelisti, E.; Pensalfini, A.; Liguri, G.; Gliozzi, A.; Stefani, M.; Relini, A. A Protective Role for Lipid Raft Cholesterol against Amyloid-Induced Membrane Damage in Human Neuroblastoma Cells. *Biochim. Biophys. Acta* **2009**, *1788* (10), 2204–2216. https://doi.org/10.1016/j.bbamem.2009.07.019.

(23) Barbash, S.; Garfinkel, B. P.; Maoz, R.; Simchovitz, A.; Nadorp, B.; Guffanti, A.; Bennett, E. R.; Nadeau, C.; Türk, A.; Paul, L.; Reda, T.; Li, Y.; Buchman, A. S.; Greenberg, D. S.; Seitz, A.; Bennett, D. A.; Giavalisco, P.; Soreq, H. Alzheimer's Brains Show Inter-Related Changes in RNA and Lipid Metabolism. *Neurobiol. Dis.* **2017**, *106*, 1–13. https://doi.org/10.1016/j.nbd.2017.06.008.

(24) Jones, L.; Harold, D.; Williams, J. Genetic Evidence for the Involvement of Lipid Metabolism in Alzheimer's Disease. *Biochim. Biophys. Acta* **2010**, *1801* (8), 754–761. https://doi.org/10.1016/j.bbalip.2010.04.005.

(25) Lambert, J. C.; Ibrahim-Verbaas, C. A.; Harold, D.; Naj, A. C.; Sims, R.; Bellenguez, C.; DeStafano, A. L.; Bis, J. C.; Beecham, G. W.; Grenier-Boley, B.; Russo, G.; Thorton-Wells, T. A.; Jones, N.; Smith, A. V.; Chouraki, V.; Thomas, C.; Ikram, M. A.; Zelenika, D.; Vardarajan, B. N.; Kamatani, Y.; Lin, C. F.; Gerrish, A.; Schmidt, H.; Kunkle, B.; Dunstan, M. L.; Ruiz, A.; Bihoreau, M. T.; Choi, S. H.; Reitz, C.; Pasquier, F.; Cruchaga, C.; Craig, D.; Amin, N.; Berr, C.; Lopez, O. L.; Jager, P. L. D.; Deramecourt, V.; Johnston, J. A.; Evans, D.; Lovestone, S.; Letenneur, L.; Morón, F. J.; Rubinsztein, D. C.; Eiriksdottir, G.; Sleegers, K.; Goate, A. M.; Fiévet, N.; Huentelman, M. W.; Gill, M.; Brown, K.; Kamboh, M. I.; Keller, L.; Barberger-Gateau, P.; McGuiness, B.; Larson, E. B.; Green, R.; Myers, A. J.; Dufouil, C.; Todd, S.; Wallon, D.; Love, S.; Rogaeva, E.; Gallacher, J.; George-Hyslop, P. S.; Clarimon, J.; Lleo, A.; Bayer, A.; Tsuang, D. W.; Yu, L.; Tsolaki, M.; Bossù, P.; Spalletta, G.; Proitsi, P.; Collinge, J.; Sorbi, S.; Sanchez-Garcia, F.; Fox, N. C.; Hardy, J.; Naranjo, M. C. D.; Bosco, P.; Clarke, R.; Brayne, C.; Galimberti, D.; Mancuso, M.; Matthews, F.; Moebus, S.; Mecocci, P.; Zompo, M. D.; Maier, W.; Hampel, H.; Pilotto, A.; Bullido, M.; Panza, F.; Caffarra, P.; Nacmias, B.; Gilbert, J. R.; Mayhaus, M.; Lannefelt, L.; Hakonarson, H.; Pichler, S.; Carrasquillo, M. M.; Ingelsson, M.; Beekly, D.; Alvarez, V.; Zou, F.; Valladares, O.; Younkin, S. G.; Coto, E.; Hamilton-Nelson, K. L.; Gu, W.; Razquin, C.; Pastor, P.; Mateo, I.; Owen, M. J.; Faber, K. M.; Jonsson, P. V.; Combarros, O.; O'Donovan, M. C.; Cantwell, L. B.; Soininen, H.; Blacker, D.; Mead, S.; Mosley, T. H.; Bennett, D. A.; Harris, T. B.; Fratiglioni, L.; Holmes, C.; Bruijn, R. F. de; Passmore, P.; Montine, T. J.; Bettens, K.; Rotter, J. I.; Brice, A.; Morgan, K.; Foroud, T. M.; Kukull, W. A.; Hannequin, D.; Powell, J. F.; Nalls, M. A.; Ritchie, K.; Lunetta, K. L.; Kauwe, J. S.; Boerwinkle, E.; Riemenschneider, M.; Boada, M.; Hiltuenen, M.; Martin, E. R.; Schmidt, R.; Rujescu, D.; Wang, L. S.; Dartigues, J. F.; Mayeux, R.; Tzourio, C.; Hofman, A.; Nöthen, M. M.; Graff, C.; Psaty, B. M.; Jones, L.; Haines, J. L.; Holmans, P. A.; Lathrop, M.; Pericak-Vance, M. A.; Launer, L. J.; Farrer, L. A.; Duijn, C. M. van; Broeckhoven, C. V.; Moskvina, V.; Seshadri, S.; Williams, J.; Schellenberg, G. D.; Amouyel, P. Meta-Analysis of 74,046 Individuals Identifies 11 New Susceptibility Loci for Alzheimer's Disease. *Nat. Genet.* **2013**, *45* (12), 1452–1458. https://doi.org/10.1038/ng.2802.

(26) Corder, E. H.; Saunders, a M.; Strittmatter, W. J.; Schmechel, D. E.; Gaskell, P. C.; Small, G. W.; Roses, a D.; Haines, J. L.; Pericak-Vance, M. a. Gene Dose of Apolipoprotein E Type 4 Allele and the Risk of Alzheimer's Disease in Late Onset Families. *Science* **1993**, *261* (5123), 921–923. https://doi.org/10.1126/science.8346443.

(27) Wightman, D. P.; Jansen, I. E.; Savage, J. E.; Shadrin, A. A.; Bahrami, S.; Holland, D.; Rongve, A.; Børte, S.; Winsvold, B. S.; Drange, O. K.; Martinsen, A. E.; Skogholt, A. H.; Willer, C.; Bråthen, G.; Bosnes, I.; Nielsen, J. B.; Fritsche, L. G.; Thomas, L. F.; Pedersen, L. M.; Gabrielsen, M. E.; Johnsen, M. B.; Meisingset, T. W.; Zhou, W.; Proitsi, P.; Hodges, A.; Dobson, R.; Velayudhan, L.; Heilbron, K.; Auton, A.; Sealock, J. M.; Davis, L. K.; Pedersen, N. L.; Reynolds, C. A.; Karlsson, I. K.; Magnusson, S.; Stefansson, H.; Thordardottir, S.; Jonsson, P. V.; Snaedal, J.; Zettergren, A.; Skoog, I.; Kern, S.; Waern, M.; Zetterberg, H.; Blennow, K.; Stordal, E.; Hveem, K.; Zwart, J.-A.; Athanasiu, L.; Selnes, P.; Saltvedt, I.; Sando, S. B.; Ulstein, I.; Djurovic, S.; Fladby, T.; Aarsland, D.; Selbæk, G.; Ripke, S.; Stefansson, K.; Andreassen, O. A.; Posthuma, D. A Genome-Wide Association Study with 1,126,563 Individuals Identifies New Risk Loci for Alzheimer's Disease. *Nat. Genet.* **2021**, *53* (9), 1276–1282. https://doi.org/10.1038/s41588-021-00921-z.

(28) Sperling, R. A.; Aisen, P. S.; Beckett, L. A.; Bennett, D. A.; Craft, S.; Fagan, A. M.; Iwatsubo, T.; Jack, C. R.; Kaye, J.; Montine, T. J.; Park, D. C.; Reiman, E. M.; Rowe, C. C.; Siemers, E.; Stern, Y.; Yaffe, K.; Carrillo, M. C.; Thies, B.; Morrison-bogorad, M.; Wagster, M. V.; Phelps, C. H. Toward Defining the Preclinical Stages of Alzheimer's Disease : Recommendations from the National Institute on Aging-Alzheimer ' s Association Workgroups on Diagnostic Guidelines for Alzheimer ' s Disease. *Alzheimers Dement.* **2011**, *7* (3), 280–292. https://doi.org/10.1016/j.jalz.2011.03.003.

(29) Glenner, G. G.; Wong, C. W. Alzheimer's Disease: Initial Report of the Purification and Characterization of a Novel Cerebrovascular Amyloid Protein. *Biochem. Biophys. Res. Commun.* **1984**, *120* (3), 885–890. https://doi.org/10.1016/s0006-291x(84)80190-4.

(30) Kang, J.; Lemaire, H. G.; Unterbeck, A.; Salbaum, J. M.; Masters, C. L.; Grzeschik, K. H.; Multhaup, G.; Beyreuther, K.; Müller-Hill, B. The Precursor of Alzheimer's Disease Amyloid A4 Protein Resembles a Cell-Surface Receptor. *Nature* **1987**, *325* (6106). https://doi.org/10.1038/325733a0.

(31) Hardy, J. A.; Higgins, G. A. Alzheimer's Disease: The Amyloid Cascade Hypothesis. *Science* **1992**, *256* (5054), 184–185. https://doi.org/10.1126/science.1566067.

(32) Haass, C.; Kaether, C.; Thinakaran, G.; Sisodia, S. Trafficking and Proteolytic Processing of APP. *Cold Spring Harb. Perspect. Med.* **2012**, *2* (5), a006270. https://doi.org/10.1101/cshperspect.a006270.

(33) Vetrivel, K. S.; Thinakaran, G. Amyloidogenic Processing of Beta-Amyloid Precursor Protein in Intracellular Compartments. *Neurology* **2006**, *66* (2 Suppl 1), S69-73. https://doi.org/10.1212/01.wnl.0000192107.17175.39.

(34) Kienlen-Campard, P. Intracellular Amyloid-Beta 1-42, but Not Extracellular Soluble Amyloid-Beta Peptides, Induces Neuronal Apoptosis. *J. Biol. Chem.* **2002**, *277* (18), 15666–15670. https://doi.org/10.1074/jbc.M200887200.

(35) Pensalfini, A.; Albay, R.; Rasool, S.; Wu, J. W.; Hatami, A.; Arai, H.; Margol, L.; Milton, S.; Poon, W. W.; Corrada, M. M.; Kawas, C. H.; Glabe, C. G. Intracellular Amyloid and the Neuronal Origin of Alzheimer Neuritic Plaques. *Neurobiol. Dis.* **2014**, *71*, 53–61. https://doi.org/10.1016/j.nbd.2014.07.011.

(36) Toh, W. H.; Gleeson, P. A. Dysregulation of Intracellular Trafficking and Endosomal Sorting in Alzheimer's Disease: Controversies and Unanswered Questions. *Biochem. J.* **2016**, *473* (14), 1977–1993. https://doi.org/10.1042/BCJ20160147.

(37) Angom, R. S.; Wang, Y.; Wang, E.; Pal, K.; Bhattacharya, S. VEGF Receptor-1 Modulates Amyloid b 1-42 Oligomer-Induced Senescence in Brain Endothelial Cells. **2019**, No. 9. https://doi.org/10.1096/fj.201802003R.

(38) Liu, H.; Saffi, G. T.; Vasefi, M. S.; Choi, Y.; Kruk, J. S.; Ahmed, N.; Gondora, N.; Mielke, J.; Leonenko, Z.; Beazely, M. A. Amyloid-β Inhibits PDGFβ Receptor Activation and Prevents PDGF-BB-Induced Neuroprotection. *Curr. Alzheimer Res.* **2018**, *15* (7), 618–627.

(39) Yamin, G. NMDA Receptor-Dependent Signaling Pathways That Underlie Amyloid β-Protein Disruption of LTP in the Hippocampus. *J. Neurosci. Res.* **2009**, *87* (8), 1729–1736. https://doi.org/10.1002/jnr.21998.

(40) Bieschke, J.; Herbst, M.; Wiglenda, T.; Friedrich, R. P.; Boeddrich, A.; Schiele, F.; Kleckers, D.; Amo, J. M. L. D.; Grüning, B. A.; Wang, Q.; Schmidt, M. R.; Lurz, R.; Anwyl, R.; Schnoegl, S.; Fändrich, M.; Frank, R. F.; Reif, B.; Günther, S.; Walsh, D. M.; Wanker, E. E. Small-Molecule Conversion of Toxic Oligomers to Nontoxic β-Sheetg-Rich Amyloid Fibrils. *Nat. Chem. Biol.* **2012**. https://doi.org/10.1038/nchembio.719.

(41) Ono, K.; Condron, M. M.; Teplow, D. B. Structure – Neurotoxicity Relationships of Amyloid Beta Protein Oligomers. *Proc. Natl. Acad. Sci. U. S. A.* **2009**, *106* (35), 14745. https://doi.org/10.1073/pnas.0905127106.

(42) Cecchi, C.; Stefani, M. The Amyloid-Cell Membrane System. The Interplay between the Biophysical Features of Oligomers/Fibrils and Cell Membrane Defines Amyloid Toxicity. *Biophys. Chem.* **2013**, *182*, 30–43. https://doi.org/10.1016/j.bpc.2013.06.003.

(43) Barrow, C. J.; Yasuda, A.; Kenny, P. T. M.; Zagorski, M. G. Solution Conformations and Aggregational Properties of Synthetic Amyloid β-Peptides of Alzheimer's Disease. Analysis of Circular Dichroism Spectra. *J. Mol. Biol.* **1992**, *225* (4), 1075–1093. https://doi.org/10.1016/0022-2836(92)90106-T.

(44) Tycko, R. Insights into the Amyloid Folding Problem from Solid-State NMR. *Biochemistry* **2003**, *42* (11), 3151–3159. https://doi.org/10.1021/bi027378p.

(45) Petkova, A. T.; Ishii, Y.; Balbach, J. J.; Antzutkin, O. N.; Leapman, R. D.; Delaglio, F.; Tycko, R. A Structural Model for Alzheimer's Beta β-Amyloid Fibrils Based on Experimental Constraints from Solid State NMR. *Proc. Natl. Acad. Sci. U. S. A.* **2002**, *99* (26), 16742–16747. https://doi.org/10.1073/pnas.262663499.

(46) Ahmed, M.; Davis, J.; Aucoin, D.; Sato, T.; Ahuja, S.; Aimoto, S.; Elliott, J. I.; Nostrand, W. E. V.; Smith, S. O. Structural Conversion of Neurotoxic Amyloid-B1–42 Oligomers to Fibrils. *Nat. Struct. Mol. Biol.* **2010**, *17* (5), 561–567. https://doi.org/10.1038/nsmb.1799.

(47) Cerf, E.; Sarroukh, R.; Tamamizu-Kato, S.; Breydo, L.; Derclaye, S.; Dufrêne, Y. F.; Narayanaswami, V.; Goormaghtigh, E.; Ruysschaert, J.-M.; Raussens, V. Antiparallel β-Sheet: A Signature Structure of the Oligomeric Amyloid β-Peptide. *Biochem. J.* **2009**, *421* (3), 415–423. https://doi.org/10.1042/BJ20090379.

(48) Bitan, G.; Vollers, S. S.; Teplow, D. B. Elucidation of Primary Structure Elements Controlling Early Amyloid β-Protein Oligomerization. *J. Biol. Chem.* **2003**, *278* (37), 34882–34889. https://doi.org/10.1074/jbc.M300825200.

(49) Liu-Seifert, H.; Siemers, E.; Holdridge, K. C.; Andersen, S. W.; Lipkovich, I.; Carlson, C.; Sethuraman, G.; Hoog, S.; Hayduk, R.; Doody, R.; Aisen, P. Delayed-Start Analysis: Mild Alzheimer's Disease Patients in Solanezumab Trials, 3.5 Years. *Alzheimers Dement. Transl. Res. Clin. Interv.* **2015**, *1* (2), 111–121. https://doi.org/10.1016/j.trci.2015.06.006.

(50) Sevigny, J.; Chiao, P.; Bussière, T.; Weinreb, P. H.; Williams, L.; Maier, M.; Dunstan, R.; Salloway, S.; Chen, T.; Ling, Y.; O'Gorman, J.; Qian, F.; Arastu, M.; Li, M.; Chollate, S.; Brennan, M. S.; Quintero-Monzon, O.; Scannevin, R. H.; Arnold, H. M.; Engber, T.; Rhodes, K.; Ferrero, J.; Hang, Y.; Mikulskis, A.; Grimm, J.; Hock, C.; Nitsch, R. M.; Sandrock, A. The Antibody Aducanumab Reduces Aβ Plaques in Alzheimer's Disease. *Nature* **2016**, *537* (7618), 50–56. https://doi.org/10.1038/nature19323.

(51) Panza, F.; Solfrizzi, V.; Imbimbo, B. P.; Tortelli, R.; Santamato, A.; Logroscino, G. Amyloid-Based Immunotherapy for Alzheimer's Disease in the Time of Prevention Trials: The Way Forward. *Expert Rev. Clin. Immunol.* **2014**, *10* (3), 405–419. https://doi.org/10.1586/1744666X.2014.883921.

(52) Knopman, D. S.; Jones, D. T.; Greicius, M. D. Failure to Demonstrate Efficacy of Aducanumab: An Analysis of the EMERGE and ENGAGE Trials as Reported by Biogen, December 2019. *Alzheimers Dement.* **2021**, *17* (4). https://doi.org/10.1002/alz.12213.

(53) Mahase, E. Aducanumab: 4 in 10 High Dose Trial Participants Experienced Brain Swelling or Bleeding. *BMJ* **2021**. https://doi.org/10.1136/bmj.n2975.

(54) Kuller, L. H.; Lopez, O. L. ENGAGE and EMERGE: Truth and Consequences? *Alzheimers Dement.* **2021**, *17* (4), 692–695. https://doi.org/10.1002/alz.12286.

(55) Wilcock, D. M.; Rojiani, A.; Rosenthal, A.; Subbarao, S.; Freeman, M. J.; Gordon, M. N.; Morgan, D. Passive Immunotherapy against Aβ in Aged APP-Transgenic Mice Reverses Cognitive Deficits and Depletes Parenchymal Amyloid Deposits in Spite of Increased Vascular Amyloid and Microhemorrhage. *J. Neuroinflammation* **2004**, *1* (1), 24. https://doi.org/10.1186/1742-2094-1-24.

(56) Tayeb, H. O.; Murray, E. D.; Price, B. H.; Tarazi, F. I. Bapineuzumab and Solanezumab for Alzheimer's Disease: Is the 'amyloid Cascade Hypothesis' Still Alive? *Expert Opin. Biol. Ther.* **2013**, *13* (7), 1075–1084. https://doi.org/10.1517/14712598.2013.789856.

(57) Salloway, S.; Sperling, R.; Fox, N. C.; Blennow, K.; Klunk, W.; Raskind, M.; Sabbagh, M.; Honig, L. S.; Porsteinsson, A. P.; Ferris, S.; Reichert, M.; Ketter, N.; Nejadnik, B.; Guenzler, V.; Miloslavsky, M.; Wang, D.; Lu, Y.; Lull, J.; Tudor, I. C.; Liu, E.; Grundman, M.; Yuen, E.; Black, R.; Brashear, H. R. Two Phase 3 Trials of Bapineuzumab in Mild-to-Moderate Alzheimer's Disease. *N. Engl. J. Med.* **2014**, *370* (4), 322–333. https://doi.org/10.1056/NEJMoa1304839.

(58) Light, D. W.; Lexchin, J.; Darrow, J. J. Institutional Corruption of Pharmaceuticals and the Myth of Safe and Effective Drugs. *J. Law Med. Ethics J. Am. Soc. Law Med. Ethics* **2013**, *41* (3), 590–600. https://doi.org/10.1111/jlme.12068.

(59) Lexchin, J. The Pharmaceutical Industry and the Canadian Government: Folie à Deux. *Healthc. Policy* **2017**, *13* (1), 10–16. https://doi.org/10.12927/hcpol.2017.25195.

(60) Rilfors, L.; Lindblom, G.; Wieslander, Å.; Christiansson, A. Lipid Bilayer Stability in Biological Membranes. In *Membrane Fluidity*; Kates, M., Manson, L. A., Eds.;

Biomembranes; Springer US: Boston, MA, 1984; pp 205–245. https://doi.org/10.1007/978-1-4684-4667-8_6.
(61) Hossain, M. M.; Suzuki, T.; Iimura, K. I.; Kato, T. Kinetic Appearance of First-Order Gas-Liquid Expanded and Liquid Expanded-Liquid Condensed Phase Transitions below the Triple Point. *Langmuir* **2006**, *22* (3), 1074–1078. https://doi.org/10.1021/la0522451.
(62) Frey, S. L.; Lee, K. Y. C. Number of Sialic Acid Residues in Ganglioside Headgroup Affects Interactions with Neighboring Lipids. *Biophys. J.* **2013**, *105* (6), 1421–1431. https://doi.org/10.1016/j.bpj.2013.07.051.
(63) Veatch, S. L.; Keller, S. L. Separation of Liquid Phases in Giant Vesicles of Ternary Mixtures of Phospholipids and Cholesterol. *Biophys. J.* **2003**, *85* (5), 3074–3083. https://doi.org/10.1016/S0006-3495(03)74726-2.
(64) Rinia, H. A.; Snel, M. M. E.; Eerden, J. P. J. M. V. D.; Kruijff, B. D. Visualizing Detergent Resistant Domains in Model Membranes with Atomic Force Microscopy. *FEBS Lett.* **2001**, *501* (1), 92–96. https://doi.org/10.1016/S0014-5793(01)02636-9.
(65) Almeida, R. F. M. de; Fedorov, A.; Prieto, M. Sphingomyelin/Phosphatidylcholine/Cholesterol Phase Diagram: Boundaries and Composition of Lipid Rafts. *Biophys. J.* **2003**, *85* (4), 2406–2416. https://doi.org/10.1016/S0006-3495(03)74664-5.
(66) Leonenko, Z. V.; Finot, E.; Ma, H.; Dahms, T. E. S.; Cramb, D. T. Investigation of Temperature-Induced Phase Transitions in DOPC and DPPC Phospholipid Bilayers Using Temperature-Controlled Scanning Force Microscopy. *Biophys. J.* **2004**, *86* (6), 3783–3793. https://doi.org/10.1529/biophysj.103.036681.
(67) Nickels, J. D.; Chatterjee, S.; Stanley, C. B.; Qian, S.; Cheng, X.; Myles, D. A. A.; Standaert, R. F.; Elkins, J. G.; Katsaras, J. The in Vivo Structure of Biological Membranes and Evidence for Lipid Domains. *PLoS Biol.* **2017**, *15* (5), 1–22. https://doi.org/10.1371/journal.pbio.2002214.
(68) Edidin, M. The State of Lipid Rafts: From Model Membranes to Cells. *Annu. Rev. Biophys. Biomol. Struct.* **2003**, *32*, 257–283. https://doi.org/10.1146/annurev.biophys.32.110601.142439.
(69) Marques-da-Silva, D.; Gutierrez-Merino, C. Caveolin-Rich Lipid Rafts of the Plasma Membrane of Mature Cerebellar Granule Neurons Are Microcompartments for Calcium/Reactive Oxygen and Nitrogen Species Cross-Talk Signaling. *Cell Calcium* **2014**, *56* (2), 108–123. https://doi.org/10.1016/j.ceca.2014.06.002.
(70) Pandit, S. A.; Vasudevan, S.; Chiu, S. W.; Mashl, R. J.; Jakobsson, E.; Scott, H. L. Sphingomyelin-Cholesterol Domains in Phospholipid Membranes: Atomistic Simulation. *Biophys. J.* **2004**, *87* (2), 1092–1100. https://doi.org/10.1529/biophysj.104.041939.
(71) Quinn, P. J. Structure of Sphingomyelin Bilayers and Complexes with Cholesterol Forming Membrane Rafts. *Langmuir* **2013**, *29* (30), 9447–9456. https://doi.org/10.1021/la4018129.
(72) Davis, J. H. The Description of Membrane Lipid Conformation, Order and Dynamics By2H-NMR. *BBA - Rev. Biomembr.* **1983**, *737* (1), 117–171. https://doi.org/10.1016/0304-4157(83)90015-1.
(73) Davis, J. H.; Clair, J. J.; Juhasz, J. Phase Equilibria in DOPC / DPPC-d 62 / Cholesterol Mixtures. *Biophysj* **2009**, *96* (2), 521–539. https://doi.org/10.1016/j.bpj.2008.09.042.
(74) Heberle, F. A.; Petruzielo, R. S.; Pan, J.; Drazba, P.; Kuc, N. Bilayer Thickness Mismatch Controls Domain Size in Model Membranes. **2013**.

(75) McMahon, H. T.; Boucrot, E. Membrane Curvature at a Glance. *J. Cell Sci.* **2015**, *128* (6), 1065–1070. https://doi.org/10.1242/jcs.114454.
(76) Cooke, I. R.; Deserno, M. Coupling between Lipid Shape and Membrane Curvature. *Biophys. J.* **2006**, *91* (2), 487–495. https://doi.org/10.1529/biophysj.105.078683.
(77) Pécheur, E. I.; Sainte-Marie, J.; Bienvenüe, A.; Hoekstra, D. Peptides and Membrane Fusion: Towards an Understanding of the Molecular Mechanism of Protein-Induced Fusion. *J. Membr. Biol.* **1999**, *167* (1), 1–17. https://doi.org/10.1007/s002329900466.
(78) Fessler, M. B.; Parks, J. S. Intracellular Lipid Flux and Membrane Microdomains as Organizing Principles in Inflammatory Cell Signaling. *J. Immunol. Baltim. Md 1950* **2011**, *187* (4), 1529–1535. https://doi.org/10.4049/jimmunol.1100253.
(79) Takei, K.; Slepnev, V. I.; Haucke, V.; Camilli, P. D. Functional Partnership between Amphiphysin and Dynamin in Clathrin-Mediated Endocytosis. *Nat. Cell Biol.* **1999**, *1* (1), 33–39. https://doi.org/10.1038/9004.
(80) Benfenati, F.; Greengard, P.; Brunner, J.; Bahler, M. Electrostatic and Hydrophobic Interactions of Synapsin I and Synapsin I Fragments with Phospholipid Bilayers. *J. Cell Biol.* **1989**, *108* (5), 1851–1862. https://doi.org/10.1083/jcb.108.5.1851.
(81) Calder, P. C. Fatty Acids and Inflammation: The Cutting Edge between Food and Pharma. *Eur. J. Pharmacol.* **2011**, *668* (SUPPL. 1), S50–S58. https://doi.org/10.1016/j.ejphar.2011.05.085.
(82) Kohli, P.; Levy, B. D. Resolvins and Protectins: Mediating Solutions to Inflammation. *Br. J. Pharmacol.* **2009**, *158* (4), 960–971. https://doi.org/10.1111/j.1476-5381.2009.00290.x.
(83) Morris, G.; Walder, K.; Puri, B. K.; Berk, M.; Maes, M. The Deleterious Effects of Oxidative and Nitrosative Stress on Palmitoylation, Membrane Lipid Rafts and Lipid-Based Cellular Signalling: New Drug Targets in Neuroimmune Disorders. *Mol. Neurobiol.* **2015**. https://doi.org/10.1007/s12035-015-9392-y.
(84) Williams, J. A.; Batten, S. E.; Harris, M.; Rockett, B. D.; Shaikh, S. R.; Stillwell, W.; Wassall, S. R. Docosahexaenoic and Eicosapentaenoic Acids Segregate Differently between Raft and Nonraft Domains. *Biophys. J.* **2012**, *103* (2), 228–237. https://doi.org/10.1016/j.bpj.2012.06.016.
(85) Martín, V.; Fabelo, N.; Santpere, G.; Puig, B.; Marín, R.; Ferrer, I.; Díaz, M. Lipid Alterations in Lipid Rafts from Alzheimer's Disease Human Brain Cortex. *J. Alzheimers Dis. JAD* **2010**, *19* (2), 489–502. https://doi.org/10.3233/JAD-2010-1242.
(86) Fabelo, N.; Martín, V.; Marín, R.; Moreno, D.; Ferrer, I.; Díaz, M. Altered Lipid Composition in Cortical Lipid Rafts Occurs at Early Stages of Sporadic Alzheimer's Disease and Facilitates APP/BACE1 Interactions. *Neurobiol. Aging* **2014**, *35* (8), 1801–1812. https://doi.org/10.1016/j.neurobiolaging.2014.02.005.
(87) Butterfield, D. A.; Castegna, A.; Lauderback, C. M.; Drake, J. Evidence That Amyloid Beta-Peptide-Induced Lipid Peroxidation and Its Sequelae in Alzheimer's Disease Brain Contribute to Neuronal Death. *Neurobiol. Aging* **2002**, *23* (5), 655–664. https://doi.org/10.1016/S0197-4580(01)00340-2.
(88) Butterfield, D. A.; Bader Lange, M. L.; Sultana, R. Involvements of the Lipid Peroxidation Product, HNE, in the Pathogenesis and Progression of Alzheimer's Disease. *Biochim. Biophys. Acta* **2010**, *1801* (8), 924–929. https://doi.org/10.1016/j.bbalip.2010.02.005.

(89) Peet, M.; Murphy, B.; Shay, J.; Horrobin, D. Depletion of Omega-3 Fatty Acid Levels in Red Blood Cell Membranes of Depressive Patients. *Biol. Psychiatry* **1998**, *43* (5), 315–319. https://doi.org/10.1016/S0006-3223(97)00206-0.

(90) Yajima, D.; Motani, H.; Hayakawa, M.; Sato, Y.; Sato, K.; Iwase, H. The Relationship between Cell Membrane Damage and Lipid Peroxidation under the Condition of Hypoxia-Reoxygenation: Analysis of the Mechanism Using Antioxidants and Electron Transport Inhibitors. *Cell Biochem. Funct.* **2009**, *27* (6), 338–343. https://doi.org/10.1002/cbf.1578.

(91) Rez, Â. R.; O, F. S. I. N.; Ari, C. S. A. N. T.-M.; Bioquõ, Â. A. D. D. Age-Related Changes in Membrane Lipid Composition , Fluidity and Respiratory Burst in Rat Peritoneal Neutrophils. **2001**.

(92) Wong-ekkabut, J.; Xu, Z.; Triampo, W.; Tang, I.-M.; Tieleman, D. P.; Monticelli, L. Effect of Lipid Peroxidation on the Properties of Lipid Bilayers: A Molecular Dynamics Study. *Biophys. J.* **2007**, *93* (12), 4225–4236. https://doi.org/10.1529/biophysj.107.112565.

(93) Porter, N. A.; Caldwell, S. E.; Mills, K. A. Mechanisms of Free Radical Oxidation of Unsaturated Lipids. *Lipids* **1995**, *30* (4), 277–290. https://doi.org/10.1007/BF02536034.

(94) Jacob, R. F.; Mason, R. P. Lipid Peroxidation Induces Cholesterol Domain Formation in Model Membranes. *J. Biol. Chem.* **2005**, *280* (47), 39380–39387. https://doi.org/10.1074/jbc.M507587200.

(95) Moghaddam, A. E.; Gartlan, K. H.; Kong, L.; Sattentau, Q. J. Reactive Carbonyls Are a Major Th2-Inducing Damage-Associated Molecular Pattern Generated by Oxidative Stress. *J. Immunol.* **2011**, *187* (4), 1626–1633. https://doi.org/10.4049/jimmunol.1003906.

(96) Cutler, R. G.; Kelly, J.; Storie, K.; Pedersen, W. A.; Tammara, A.; Hatanpaa, K.; Troncoso, J. C.; Mattson, M. P. Involvement of Oxidative Stress-Induced Abnormalities in Ceramide and Cholesterol Metabolism in Brain Aging and Alzheimer's Disease. *Proc. Natl. Acad. Sci. U. S. A.* **2004**, *101* (7), 2070–2075. https://doi.org/10.1073/pnas.0305799101.

(97) Nakamura, M.; Kondo, H.; Shimada, Y.; Waheed, A. A.; Ohno-Iwashita, Y. Cellular Aging-Dependent Decrease in Cholesterol in Membrane Microdomains of Human Diploid Fibroblasts. *Exp. Cell Res.* **2003**, *290* (2), 381–390. https://doi.org/10.1016/S0014-4827(03)00343-4.

(98) Orłowski, A.; Grzybek, M.; Bunker, A.; Pasenkiewicz-Gierula, M.; Vattulainen, I.; Männistö, P. T.; Rõg, T. Strong Preferences of Dopamine and l -Dopa towards Lipid Head Group: Importance of Lipid Composition and Implication for Neurotransmitter Metabolism. *J. Neurochem.* **2012**. https://doi.org/10.1111/j.1471-4159.2012.07813.x.

(99) Matam, Y.; Ray, B. D.; Petrache, H. I. Direct Affinity of Dopamine to Lipid Membranes Investigated by Nuclear Magnetic Resonance Spectroscopy. *Neurosci. Lett.* **2016**, *618*, 104–109. https://doi.org/10.1016/j.neulet.2016.02.052.

(100) Robinson, M.; Turnbull, S.; Lee, B. Y.; Leonenko, Z. The Effects of Melatonin, Serotonin, Tryptophan and NAS on the Biophysical Properties of DPPC Monolayers. *Biochim. Biophys. Acta - Biomembr.* **2020**, *1862* (9). https://doi.org/10.1016/j.bbamem.2020.183363.

(101) Wood, I.; Martini, M. F.; Pickholz, M. Similarities and Differences of Serotonin and Its Precursors in Their Interactions with Model Membranes Studied by Molecular Dynamics

Simulation. *J. Mol. Struct.* **2013**, *1045*, 124–130. https://doi.org/10.1016/j.molstruc.2013.04.011.
(102) Azouzi, S.; Santuz, H.; Morandat, S.; Pereira, C.; Côté, F.; Hermine, O.; Kirat, K. E.; Colin, Y.; Kim, C. L. V.; Etchebest, C.; Amireault, P. Antioxidant and Membrane Binding Properties of Serotonin Protect Lipids from Oxidation. *Biophys. J.* **2017**. https://doi.org/10.1016/j.bpj.2017.03.037.
(103) Engberg, O.; Bochicchio, A.; Brandner, A. F.; Gupta, A.; Dey, S.; Böckmann, R. A.; Maiti, S.; Huster, D. Serotonin Alters the Phase Equilibrium of a Ternary Mixture of Phospholipids and Cholesterol. *Front. Physiol.* **2020**, *11*.
(104) Akkas, S. B.; Inci, S.; Zorlu, F.; Severcan, F. Melatonin Affects the Order, Dynamics and Hydration of Brain Membrane Lipids. *J. Mol. Struct.* **2007**. https://doi.org/10.1016/j.molstruc.2006.12.018.
(105) Choi, Y.; Attwood, S. J.; Hoopes, M. I.; Drolle, E.; Karttunen, M.; Leonenko, Z. Melatonin Directly Interacts with Cholesterol and Alleviates Cholesterol Effects in Dipalmitoylphosphatidylcholine Monolayers. *Soft Matter* **2014**, *10* (1), 206–213. https://doi.org/10.1039/C3SM52064A.
(106) Yen, G.-C.; Hsieh, C.-L. Antioxidant Effects of Dopamine and Related Compounds. *Biosci. Biotechnol. Biochem.* **1997**, *61* (10), 1646–1649. https://doi.org/10.1271/bbb.61.1646.
(107) Antunes, F.; Barclay, L. R. C.; Ingold, K. U.; King, M.; Norris, J. Q.; Scaiano, J. C.; Xi, F. On the Antioxidant Activity of Melatonin. *Free Radic. Biol. Med.* **1999**. https://doi.org/10.1016/S0891-5849(98)00168-3.
(108) García, J. J.; López-Pingarrón, L.; Almeida-Souza, P.; Tres, A.; Escudero, P.; García-Gil, F. A.; Tan, D.-X.; Reiter, R. J.; Ramírez, J. M.; Bernal-Pérez, M. Protective Effects of Melatonin in Reducing Oxidative Stress and in Preserving the Fluidity of Biological Membranes: A Review. *J. Pineal Res.* **2014**, *56* (3), 225–237. https://doi.org/10.1111/jpi.12128.
(109) Rosenbaum, D. M.; Rasmussen, S. G. F.; Kobilka, B. K. The Structure and Function of G-Protein-Coupled Receptors. *Nature* **2009**, *459* (7245), 356–363. https://doi.org/10.1038/nature08144.
(110) Barnett-Norris, J.; Lynch, D.; Reggio, P. H. Lipids, Lipid Rafts and Caveolae: Their Importance for GPCR Signaling and Their Centrality to the Endocannabinoid System. In *Life Sciences*; 2005; Vol. 77, pp 1625–1639. https://doi.org/10.1016/j.lfs.2005.05.040.
(111) Millan, M. J.; Marin, P.; Bockaert, J.; Cour, C. M. la. Signaling at G-Protein-Coupled Serotonin Receptors: Recent Advances and Future Research Directions. *Trends Pharmacol. Sci.* **2008**, *29* (9), 454–464. https://doi.org/10.1016/j.tips.2008.06.007.
(112) Lemmon, M. A.; Schlessinger, J. Cell Signaling by Receptor Tyrosine Kinases. *Cell* **2010**, *141* (7), 1117–1134. https://doi.org/10.1016/j.cell.2010.06.011.
(113) Collingridge, G. L.; Olsen, R. W.; Peters, J.; Spedding, M. A Nomenclature for Ligand-Gated Ion Channels. *Neuropharmacology* **2009**, *56* (1), 2–5. https://doi.org/10.1016/j.neuropharm.2008.06.063.
(114) Baidya, M.; Dwivedi, H.; Shukla, A. K. Frozen in Action: Cryo-EM Structure of a GPCR-G-Protein Complex. *Nat. Struct. Mol. Biol.* **2017**, *24* (6), 500–502. https://doi.org/10.1038/nsmb.3418.

(115) Delcourt, N.; Bockaert, J.; Marin, P. GPCR-Jacking: From a New Route in RTK Signalling to a New Concept in GPCR Activation. *Trends Pharmacol. Sci.* **2007**, *28* (12), 602–607. https://doi.org/10.1016/j.tips.2007.09.007.

(116) Gupta, V. K.; You, Y.; Gupta, V. B.; Klistorner, A.; Graham, S. L. TrkB Receptor Signalling: Implications in Neurodegenerative, Psychiatric and Proliferative Disorders. *Int. J. Mol. Sci.* **2013**, *14* (5), 10122–10142. https://doi.org/10.3390/ijms140510122.

(117) Arancibia, S.; Silhol, M.; Moulière, F.; Meffre, J.; Höllinger, I.; Maurice, T.; Tapia-Arancibia, L. Protective Effect of BDNF against Beta-Amyloid Induced Neurotoxicity in Vitro and in Vivo in Rats. *Neurobiol. Dis.* **2008**, *31* (3), 316–326. https://doi.org/10.1016/j.nbd.2008.05.012.

(118) Jerónimo-Santos, A.; Vaz, S. H.; Parreira, S.; Rapaz-Lérias, S.; Caetano, A. P.; Scherrer, V. B.; Castrén, E.; Valente, C. A.; Blum, D.; Sebastião, A. M.; Diógenes, M. J. Dysregulation of TrkB Receptors and BDNF Function by Amyloid-β Peptide Is Mediated by Calpain. *Cereb. Cortex* **2015**, *25* (9), 3107–3121. https://doi.org/10.1093/cercor/bhu105.

(119) Numakawa, T.; Kumamaru, E.; Adachi, N.; Yagasaki, Y.; Izumi, A.; Kunugi, H. Glucocorticoid Receptor Interaction with TrkB Promotes BDNF-Triggered PLC-γ Signaling for Glutamate Release via a Glutamate Transporter. *Proc. Natl. Acad. Sci. U. S. A.* **2009**. https://doi.org/10.1073/pnas.0800888106.

(120) Yamada, K.; Nabeshima, T. Interaction of BDNF/TrkB Signaling with NMDA Receptor in Learning and Memory. *Drug News Perspect* **2004**, *17* (0214-0934 (Print)), 435–438. https://doi.org/10.1358/dnp.2004.17.7.863702.

(121) Samarajeewa, A.; Goldemann, L.; Vasefi, M. S.; Ahmed, N.; Gondora, N.; Khanderia, C.; Mielke, J. G.; Beazely, M. A. 5-HT7 Receptor Activation Promotes an Increase in TrkB Receptor Expression and Phosphorylation. *Front. Behav. Neurosci.* **2014**, *8*, 391. https://doi.org/10.3389/fnbeh.2014.00391.

(122) Vasefi, M. S.; Kruk, J. S.; Heikkila, J. J.; Beazely, M. A. 5-Hydroxytryptamine Type 7 Receptor Neuroprotection against NMDA-Induced Excitotoxicity Is PDGFβ Receptor Dependent. *J. Neurochem.* **2013**, *125* (1), 26–36. https://doi.org/10.1111/jnc.12157.

(123) Tall, A. R.; Yvan-charvet, L. Cholesterol, Inflammation and Innate Immunity. *Nat. Rev. Immunol.* **2015**, *15* (2), 104–116. https://doi.org/10.1038/nri3793.

(124) Zhu, X.; Owen, J. S.; Wilson, M. D.; Li, H.; Griffiths, G. L.; Thomas, M. J.; Hiltbold, E. M.; Fessler, M. B.; Parks, J. S. Macrophage ABCA1 Reduces MyD88-Dependent Toll-like Receptor Trafficking to Lipid Rafts by Reduction of Lipid Raft Cholesterol. *J. Lipid Res.* **2010**, *51* (11), 3196–3206. https://doi.org/10.1194/jlr.M006486.

(125) Karasinska, J. M.; Haan, W. de; Franciosi, S.; Ruddle, P.; Fan, J.; Kruit, J. K.; Stukas, S.; Lütjohann, D.; Gutmann, D. H.; Wellington, C. L.; Hayden, M. R. ABCA1 Influences Neuroinflammation and Neuronal Death. *Neurobiol. Dis.* **2013**, *54*, 445–455. https://doi.org/10.1016/j.nbd.2013.01.018.

(126) Navia-Pelaez, J. M.; Choi, S.-H.; dos Santos Aggum Capettini, L.; Xia, Y.; Gonen, A.; Agatisa-Boyle, C.; Delay, L.; Gonçalves dos Santos, G.; Catroli, G. F.; Kim, J.; Lu, J. W.; Saylor, B.; Winkels, H.; Durant, C. P.; Ghosheh, Y.; Beaton, G.; Ley, K.; Kufareva, I.; Corr, M.; Yaksh, T. L.; Miller, Y. I. Normalization of Cholesterol Metabolism in Spinal Microglia Alleviates Neuropathic Pain. *J. Exp. Med.* **2021**, *218* (7), e20202059. https://doi.org/10.1084/jem.20202059.

(127) Minagawa, H.; Gong, J. S.; Jung, C. G.; Watanabe, A.; Lund-Katz, S.; Phillips, M. C.; Saito, H.; Michikawa, M. Mechanism Underlying Apolipoprotein E (ApoE) Isoform-Dependent Lipid Efflux from Neural Cells in Culture. *J. Neurosci. Res.* **2009**, *87* (11), 2498–2508. https://doi.org/10.1002/jnr.22073.

(128) Perry, V. H. The Influence of Systemic Inflammation on Inflammation in the Brain: Implications for Chronic Neurodegenerative Disease. *Brain. Behav. Immun.* **2004**, *18* (5), 407–413. https://doi.org/10.1016/j.bbi.2004.01.004.

(129) Miklossy, J.; McGeer, P. L. Common Mechanisms Involved in Alzheimer's Disease and Type 2 Diabetes: A Key Role of Chronic Bacterial Infection and Inflammation. *Aging* **2016**, *8* (3), 1–14. https://doi.org/10.18632/aging.100921.

(130) Gutierrez, M. G.; Mansfield, K. S.; Malmstadt, N. The Functional Activity of the Human Serotonin 5-HT1A Receptor Is Controlled by Lipid Bilayer Composition. *Biophys. J.* **2016**. https://doi.org/10.1016/j.bpj.2016.04.042.

(131) Pucadyil, T. J.; Chattopadhyay, A. Cholesterol Modulates Ligand Binding and G-Protein Coupling to Serotonin1A Receptors from Bovine Hippocampus. *Biochim. Biophys. Acta - Biomembr.* **2004**. https://doi.org/10.1016/j.bbamem.2004.03.010.

(132) Björk, K.; Sjögren, B.; Svenningsson, P. Regulation of Serotonin Receptor Function in the Nervous System by Lipid Rafts and Adaptor Proteins. *Exp. Cell Res.* **2010**, *316* (8), 1351–1356. https://doi.org/10.1016/j.yexcr.2010.02.034.

(133) Ramírez-Anguita, J. M.; Rodríguez-Espigares, I.; Guixà-González, R.; Bruno, A.; Torrens-Fontanals, M.; Varela-Rial, A.; Selent, J. Membrane Cholesterol Effect on the 5-HT $_{2A}$ Receptor: Insights into the Lipid-Induced Modulation of an Antipsychotic Drug Target. *Biotechnol. Appl. Biochem.* **2017**, No. October, 29–37. https://doi.org/10.1002/bab.1608.

(134) Goddard, A. D.; Watts, A. Regulation of G Protein-Coupled Receptors by Palmitoylation and Cholesterol. *BMC Biol.* **2012**, *10* (1), 27. https://doi.org/10.1186/1741-7007-10-27.

(135) Besshoh, S.; Bawa, D.; Teves, L.; Wallace, M. C.; Gurd, J. W. Increased Phosphorylation and Redistribution of NMDA Receptors between Synaptic Lipid Rafts and Post-Synaptic Densities Following Transient Global Ischemia in the Rat Brain. *J. Neurochem.* **2005**, *93* (1), 186–194. https://doi.org/10.1111/j.1471-4159.2004.03009.x.

(136) Hou, Q.; Huang, Y.; Amato, S.; Snyder, S. H.; Huganir, R. L.; Man, H.-Y. Regulation of AMPA Receptor Localization in Lipid Rafts. *Mol. Cell. Neurosci.* **2008**, *38* (2), 213–223. https://doi.org/10.1016/j.mcn.2008.02.010.

(137) Korinek, M.; Vyklicky, V.; Borovska, J.; Lichnerova, K.; Kaniakova, M.; Krausova, B.; Krusek, J.; Balik, A.; Smejkalova, T.; Horak, M.; Vyklicky, L. Cholesterol Modulates Open Probability and Desensitization of NMDA Receptors. *J. Physiol.* **2015**, *593* (10), 2279–2293. https://doi.org/10.1113/jphysiol.2014.288209.

(138) Suzuki, S.; Numakawa, T.; Shimazu, K.; Koshimizu, H.; Hara, T.; Hatanaka, H.; Mei, L.; Lu, B.; Kojima, M. BDNF-Induced Recruitment of TrkB Receptor into Neuronal Lipid Rafts: Roles in Synaptic Modulation. *J. Cell Biol.* **2004**, *167* (6), 1205–1215. https://doi.org/10.1083/jcb.200404106.

(139) Abulrob, A.; Tauskela, J. S.; Mealing, G.; Brunette, E.; Faid, K.; Stanimirovic, D. Protection by Cholesterol-Extracting Cyclodextrins: A Role for N-Methyl-D-Aspartate Receptor Redistribution. *J. Neurochem.* **2005**, *92* (6), 1477–1486. https://doi.org/10.1111/j.1471-4159.2005.03001.x.

(140) Evangelisti, E.; Wright, D.; Zampagni, M.; Cascella, R.; Fiorillo, C.; Bagnoli, S.; Relini, A.; Nichino, D.; Scartabelli, T.; Nacmias, B.; Sorbi, S.; Cecchi, C. Lipid Rafts Mediate Amyloid-Induced Calcium Dyshomeostasis and Oxidative Stress in Alzheimer's Disease. *Curr. Alzheimer Res.* **2013**, *10* (2), 143–153. https://doi.org/10.2174/1567205011310020004.

(141) Zampagni, M.; Evangelisti, E.; Cascella, R.; Liguri, G.; Becatti, M.; Pensalfini, A.; Uberti, D.; Cenini, G.; Memo, M.; Bagnoli, S.; Nacmias, B.; Sorbi, S.; Cecchi, C. Lipid Rafts Are Primary Mediators of Amyloid Oxidative Attack on Plasma Membrane. *J. Mol. Med.* **2010**, *88* (6), 597–608. https://doi.org/10.1007/s00109-010-0603-8.

(142) Thinakaran, G.; Koo, E. H. Amyloid Precursor Protein Trafficking, Processing, and Function. *J. Biol. Chem.* **2008**, *283* (44), 29615–29619. https://doi.org/10.1074/jbc.R800019200.

(143) Guardia-Laguarta, C.; Coma, M.; Pera, M.; Clarimón, J.; Sereno, L.; Agulló, J. M.; Molina-Porcel, L.; Gallardo, E.; Deng, A.; Berezovska, O.; Hyman, B. T.; Blesa, R.; Gómez-Isla, T.; Lleó, A. Mild Cholesterol Depletion Reduces Amyloid-β Production by Impairing APP Trafficking to the Cell Surface. *J. Neurochem.* **2009**, *110* (1), 220–230. https://doi.org/10.1111/j.1471-4159.2009.06126.x.

(144) Abad-Rodriguez, J.; Ledesma, M. D.; Craessaerts, K.; Perga, S.; Medina, M.; Delacourte, A.; Dingwall, C.; Strooper, B. D.; Dotti, C. G. Neuronal Membrane Cholesterol Loss Enhances Amyloid Peptide Generation. *J. Cell Biol.* **2004**, *167* (5), 953–960. https://doi.org/10.1083/jcb.200404149.

(145) Riddell, D. R.; Christie, G.; Hussain, I.; Dingwall, C. Compartmentalization of β-Secretase (Asp2) into Low-Buoyant Density, Noncaveolar Lipid Rafts. *Curr. Biol.* **2001**, *11* (16), 1288–1293. https://doi.org/10.1016/S0960-9822(01)00394-3.

(146) Wahrle, S.; Das, P.; Nyborg, A. C.; McLendon, C.; Shoji, M.; Kawarabayashi, T.; Younkin, L. H.; Younkin, S. G.; Golde, T. E. Cholesterol-Dependent γ-Secretase Activity in Buoyant Cholesterol-Rich Membrane Microdomains. *Neurobiol. Dis.* **2002**, *9* (1), 11–23. https://doi.org/10.1006/nbdi.2001.0470.

(147) Markesbery, W. R.; Kryscio, R. J.; Lovell, M. A.; Morrow, J. D. Lipid Peroxidation Is an Early Event in the Brain in Amnestic Mild Cognitive Impairment. *Ann. Neurol.* **2005**, *58* (5), 730–735. https://doi.org/10.1002/ana.20629.

(148) Grimm, M. O. W.; Grimm, H. S.; Pätzold, A. J.; Zinser, E. G.; Halonen, R.; Duering, M.; Tschäpe, J. A.; Strooper, B. D.; Müller, U.; Shen, J.; Hartmann, T. Regulation of Cholesterol and Sphingomyelin Metabolism by Amyloid-Beta and Presenilin. *Nat. Cell Biol.* **2005**, *7* (11), 1118–1123. https://doi.org/10.1038/ncb1313.

(149) Zinser, E. G.; Hartmann, T.; Grimm, M. O. W. Amyloid Beta-Protein and Lipid Metabolism. *Biochim. Biophys. Acta* **2007**, *1768*, 1991–2001. https://doi.org/10.1016/j.bbamem.2007.02.014.

(150) Behl, C.; Davis, J. B.; Klier, F. G.; Schubert, D. Amyloid Beta Peptide Induces Necrosis Rather than Apoptosis. *Brain Res.* **1994**, *645* (0006-8993 (Print)), 253–264.

(151) Loo, D. T.; Copani, A.; Pike, C. J.; Whittemore, E. R.; Walencewicz, A. J.; Cotman, C. W. Apoptosis Is Induced by Beta-Amyloid in Cultured Central Nervous System Neurons. *Proc. Natl. Acad. Sci. U. S. A.* **1993**, *90* (17), 7951–7955. https://doi.org/10.1073/pnas.90.17.7951.

(152) Nicholson, A. M.; Ferreira, A. Increased Membrane Cholesterol Might Render Mature Hippocampal Neurons More Susceptible to Beta-Amyloid-Induced Calpain Activation

and Tau Toxicity. *J. Neurosci. Off. J. Soc. Neurosci.* **2009**, *29* (14), 4640–4651. https://doi.org/10.1523/JNEUROSCI.0862-09.2009.

(153) Nicholson, A. M.; Methner, D. N. R.; Ferreira, A. Membrane Cholesterol Modulates β-Amyloid-Dependent Tau Cleavage by Inducing Changes in the Membrane Content and Localization of N-Methyl-D-Aspartic Acid Receptors. *J. Biol. Chem.* **2011**, *286* (2), 976–986. https://doi.org/10.1074/jbc.M110.154138.

(154) Wang, S. S. S.; Rymer, D. L.; Good, T. A. Reduction in Cholesterol and Sialic Acid Content Protects Cells from the Toxic Effects of β-Amyloid Peptides. *J. Biol. Chem.* **2001**, *276* (45), 42027–42034. https://doi.org/10.1074/jbc.M102834200.

(155) Arispe, N.; Doh, M. Plasma Membrane Cholesterol Controls the Cytotoxicity of Alzheimer's Disease AbetaP (1-40) and (1-42) Peptides. *FASEB J.* **2002**, *16* (12), 1526–1536. https://doi.org/10.1096/fj.02-0829com.

(156) Yip, C. M.; Elton, E. A.; Darabie, A. A.; Morrison, M. R.; McLaurin, J. Cholesterol, a Modulator of Membrane-Associated Abeta-Fibrillogenesis and Neurotoxicity. *J. Mol. Biol.* **2001**, *311* (4), 723–734. https://doi.org/10.1006/jmbi.2001.4881.

(157) Herzer, S.; Meldner, S.; Rehder, K.; Gröne, H.-J.; Nordström, V. Lipid Microdomain Modification Sustains Neuronal Viability in Models of Alzheimer's Disease. *Acta Neuropathol. Commun.* **2016**, *4* (1), 103. https://doi.org/10.1186/s40478-016-0354-z.

(158) Hane, F.; Drolle, E.; Gaikwad, R.; Faught, E.; Leonenko, Z. Amyloid-β Aggregation on Model Lipid Membranes: An Atomic Force Microscopy Study. *J. Alzheimers Dis.* **2011**, *26* (3), 485–494. https://doi.org/10.3233/JAD-2011-102112.

(159) Kakio, A.; Nishimoto, S. I.; Yanagisawa, K.; Kozutsumi, Y.; Matsuzaki, K. Cholesterol-Dependent Formation of GM1 Ganglioside-Bound Amyloid β-Protein, an Endogenous Seed for Alzheimer Amyloid. *J. Biol. Chem.* **2001**, *276* (27), 24985–24990. https://doi.org/10.1074/jbc.M100252200.

(160) Williams, T. L.; Johnson, B. R. G.; Urbanc, B.; Jenkins, A. T. A.; Connell, S. D. A.; Serpell, L. C. Aβ42 Oligomers, but Not Fibrils, Simultaneously Bind to and Cause Damage to Ganglioside-Containing Lipid Membranes. *Biochem. J.* **2011**, *439* (1), 67–77. https://doi.org/10.1042/BJ20110750.

(161) Choucair, A.; Chakrapani, M.; Chakravarthy, B.; Katsaras, J.; Johnston, L. J. Preferential Accumulation of Aβ(1-42) on Gel Phase Domains of Lipid Bilayers: An AFM and Fluorescence Study. *Biochim. Biophys. Acta - Biomembr.* **2007**, *1768* (1), 146–154. https://doi.org/10.1016/j.bbamem.2006.09.005.

(162) Sciacca, M. F. M.; Kotler, S. A.; Brender, J. R.; Chen, J.; Lee, D. K.; Ramamoorthy, A. Two-Step Mechanism of Membrane Disruption by Aβ through Membrane Fragmentation and Pore Formation. *Biophys. J.* **2012**, *103* (4), 702–710. https://doi.org/10.1016/j.bpj.2012.06.045.

(163) Demuro, A.; Mina, E.; Kayed, R.; Milton, S. C.; Parker, I.; Glabe, C. G. Calcium Dysregulation and Membrane Disruption as a Ubiquitous Neurotoxic Mechanism of Soluble Amyloid Oligomers. *J. Biol. Chem.* **2005**, *280* (17), 17294–17300. https://doi.org/10.1074/jbc.M500997200.

(164) Lin, H. A. I.; Bhatia, R.; Lal, R. Amyloid β Protein Forms Ion Channels: Implications for Alzheimer's Disease Pathophysiology. *FASEB J* **2001**, *15* (13), 2433–2444. https://doi.org/10.1096/fj.01-0377com.

(165) Hane, F.; Drolle, E.; Leonenko, Z. Effect of Cholesterol and Amyloid-β Peptide on Structure and Function of Mixed-Lipid Films and Pulmonary Surfactant BLES: An

Atomic Force Microscopy Study. *Nanomedicine Nanotechnol. Biol. Med.* **2010**, *6* (6), 808–814. https://doi.org/10.1016/j.nano.2010.05.001.

(166) Hayashi, T.; Shishido, N.; Nakayama, K.; Nunomura, A.; Smith, M. A.; Perry, G.; Nakamura, M. Lipid Peroxidation and 4-Hydroxy-2-Nonenal Formation by Copper Ion Bound to Amyloid-β Peptide. *Free Radic. Biol. Med.* **2007**, *43* (11), 1552–1559. https://doi.org/10.1016/j.freeradbiomed.2007.08.013.

(167) Bucciantini, M.; Nosi, D.; Forzan, M.; Russo, E.; Calamai, M.; Pieri, L.; Formigli, L.; Quercioli, F.; Soria, S.; Pavone, F.; Savistchenko, J.; Melki, R.; Stefani, M. Toxic Effects of Amyloid Fibrils on Cell Membranes: The Importance of Ganglioside GM1. *FASEB J.* **2012**, *26* (2), 818–831. https://doi.org/10.1096/fj.11-189381.

(168) Bode, D. C.; Freeley, M.; Nield, J.; Palma, M.; Viles, J. H. Amyloid-β Oligomers Have a Profound Detergent-like Effect on Lipid Membrane Bilayers, Imaged by Atomic Force and Electron Microscopy. *J. Biol. Chem.* **2019**, *294* (19), 7566–7572. https://doi.org/10.1074/jbc.AC118.007195.

(169) Feuillie, C.; Lambert, E.; Ewald, M.; Azouz, M.; Henry, S.; Marsaudon, S.; Cullin, C.; Lecomte, S.; Molinari, M. High Speed AFM and NanoInfrared Spectroscopy Investigation of Aβ1–42 Peptide Variants and Their Interaction With POPC/SM/Chol/GM1 Model Membranes. *Front. Mol. Biosci.* **2020**, *7*.

(170) Abramov, A. Y.; Canevari, L.; Duchen, M. R. SS-Amyloid Peptides Induce Mitochondrial Dysfunction and Oxidative Stress in Astrocytes and Death of Neurons through Activation of NADPH Oxidase. *J. Neurosci.* **2004**, *24* (2), 565–575. https://doi.org/10.1523/JNEUROSCI.4042-03.2004.

(171) Camilleri, A.; Zarb, C.; Caruana, M.; Ostermeier, U.; Ghio, S.; Högen, T.; Schmidt, F.; Giese, A.; Vassallo, N. Mitochondrial Membrane Permeabilisation by Amyloid Aggregates and Protection by Polyphenols. *Biochim. Biophys. Acta - Biomembr.* **2013**, *1828* (11), 2532–2543. https://doi.org/10.1016/j.bbamem.2013.06.026.

(172) Rodrigues, C. M.; Solá, S.; Brito, M. a; Brondino, C. D.; Brites, D.; Moura, J. J. Amyloid Beta-Peptide Disrupts Mitochondrial Membrane Lipid and Protein Structure: Protective Role of Tauroursodeoxycholate. *Biochem. Biophys. Res. Commun.* **2001**, *281* (2), 468–474. https://doi.org/10.1006/bbrc.2001.4370.

(173) Rosales-Corral, S. A.; Lopez-Armas, G.; Cruz-Ramos, J.; Melnikov, V. G.; Tan, D. X.; Manchester, L. C.; Munoz, R.; Reiter, R. J. Alterations in Lipid Levels of Mitochondrial Membranes Induced by Amyloid-β: A Protective Role of Melatonin. *Int. J. Alzheimers Dis.* **2012**. https://doi.org/10.1155/2012/459806.

(174) Raffa, D. F.; Rauk, A. Molecular Dynamics Study of the Beta Amyloid Peptide of Alzheimer's Disease and Its Divalent Copper Complexes. *J. Phys. Chem. B* **2007**, *111* (14), 3789–3799. https://doi.org/10.1021/jp0689621.

(175) Tang, Y.; Nyengaard, J. R.; De Groot, D. M. G.; Gundersen, H. J. G. Total Regional and Global Number of Synapses in the Human Brain Neocortex. *Synapse* **2001**, *41* (3), 258–273. https://doi.org/10.1002/syn.1083.

(176) Scheff, S. W.; Price, D. A.; Schmitt, F. A.; Mufson, E. J. Hippocampal Synaptic Loss in Early Alzheimer's Disease and Mild Cognitive Impairment. *Neurobiol. Aging* **2006**, *27* (10), 1372–1384. https://doi.org/10.1016/j.neurobiolaging.2005.09.012.

(177) Wong, J.; Higgins, M.; Halliday, G.; Garner, B. Amyloid Beta Selectively Modulates Neuronal TrkB Alternative Transcript Expression with Implications for Alzheimer's

Disease. *Neuroscience* **2012**, *210*, 363–374. https://doi.org/10.1016/j.neuroscience.2012.02.037.

(178) Kemppainen, S.; Rantamäki, T.; Jerónimo-Santos, A.; Lavasseur, G.; Autio, H.; Karpova, N.; Kärkkäinen, E.; Stavén, S.; Miranda, H. V.; Outeiro, T. F.; Diógenes, M. J.; Laroche, S.; Davis, S.; Sebastião, A. M.; Castrén, E.; Tanila, H. Impaired TrkB Receptor Signaling Contributes to Memory Impairment in APP/PS1 Mice. *Neurobiol. Aging* **2012**, *33* (6). https://doi.org/10.1016/j.neurobiolaging.2011.11.006.

(179) Liu, S. J.; Gasperini, R.; Foa, L.; Small, D. H. Amyloid-β Decreases Cell-Surface AMPA Receptors by Increasing Intracellular Calcium and Phosphorylation of GluR2. *J. Alzheimers Dis.* **2010**, *21* (2), 655–666. https://doi.org/10.3233/JAD-2010-091654.

(180) Miñano-Molina, A. J.; España, J.; Martín, E.; Barneda-Zahonero, B.; Fadó, R.; Solé, M.; Trullás, R.; Saura, C. A.; Rodríguez-Alvarez, J. Soluble Oligomers of Amyloid-β Peptide Disrupt Membrane Trafficking of β-Amino-3-Hydroxy-5-Methylisoxazole-4-Propionic Acid Receptor Contributing to Early Synapse Dysfunction. *J. Biol. Chem.* **2011**, *286* (31), 27311–27321. https://doi.org/10.1074/jbc.M111.227504.

(181) Lanctôt, K. L.; Herrmann, N.; Yau, K. K.; Khan, L. R.; Liu, B. A.; LouLou, M. M.; Einarson, T. R. Efficacy and Safety of Cholinesterase Inhibitors in Alzheimer's Disease: A Meta-Analysis. *CMAJ Can. Med. Assoc. J. J. Assoc. Medicale Can.* **2003**, *169* (6), 557–564. https://doi.org/za2963e q8za9 q8zb8 q8zc9 q8zd4 q8zeb q8zf5 q8zg5.

(182) Craig, L. A.; Hong, N. S.; McDonald, R. J. Revisiting the Cholinergic Hypothesis in the Development of Alzheimer's Disease. *Neurosci. Biobehav. Rev.* **2011**, *35* (6), 1397–1409. https://doi.org/10.1016/j.neubiorev.2011.03.001.

(183) Raina, P.; Santaguida, P.; Ismaila, A.; Patterson, C.; Cowan, D.; Levine, M.; Booker, L.; Oremus, M. Effectiveness of Cholinesterase Inhibitors and Memantine for Treating Dementia: Evidence Review for a Clinical Practice Guideline (Structured Abstract). *Ann. Intern. Med.* **2008**, *148* (5), 379–397. https://doi.org/148/5/379 [pii].

(184) Seeman, P.; Caruso, C.; Lasaga, M. Memantine Agonist Action at Dopamine D2High Receptors. *Synapse* **2008**, *62* (2), 149–153. https://doi.org/10.1002/syn.20472.

(185) Rammes, G.; Rupprecht, R.; Ferrari, U.; Zieglgänsberger, W.; Parsons, C. G. The N-Methyl-D-Aspartate Receptor Channel Blockers Memantine, MRZ 2/579 and Other Amino-Alkyl-Cyclohexanes Antagonise 5-HT3 Receptor Currents in Cultured HEK-293 and N1E-115 Cell Systems in a Non-Competitive Manner. *Neurosci. Lett.* **2001**, *306* (1–2), 81–84. https://doi.org/10.1016/S0304-3940(01)01872-9.

(186) Hashemi-Firouzi, N.; Komaki, A.; Asl, A. S.; Shahidi, S. The Effects of the 5-HT7 Receptor on Hippocampal Long-Term Potentiation and Apoptosis in a Rat Model of Alzheimer's Disease. *Brain Res. Bull.* **2017**, *135*, 85–91. https://doi.org/10.1016/j.brainresbull.2017.10.004.

(187) Yaar, M.; Zhai, S.; Pilch, P. F.; Doyle, S. M.; Eisenhauer, P. B.; Fine, R. E.; Gilchrest, B. A. Binding of Beta-Amyloid to the P75 Neurotrophin Receptor Induces Apoptosis. A Possible Mechanism for Alzheimer's Disease. *J. Clin. Invest.* **1997**, *100* (9), 2333–2340. https://doi.org/10.1172/JCI119772.

(188) Knowles, J. K.; Rajadas, J.; Nguyen, T.-V. V.; Yang, T.; LeMieux, M. C.; Griend, L. V.; Ishikawa, C.; Massa, S. M.; Wyss-Coray, T.; Longo, F. M. The P75 Neurotrophin Receptor Promotes Amyloid- (1-42)-Induced Neuritic Dystrophy In Vitro and In Vivo. *J. Neurosci.* **2009**, *29* (34), 10627–10637. https://doi.org/10.1523/JNEUROSCI.0620-09.2009.

(189) McDermott, J. R.; Gibson, A. M. Degradation of Alzheimer's Beta-Amyloid Protein by Human and Rat Brain Peptidases: Involvement of Insulin-Degrading Enzyme. *Neurochem. Res.* **1997**, *22* (1), 49–56.
(190) Xie, L.; Helmerhorst, E.; Taddei, K.; Plewright, B.; Bronswijk, W. V.; Martins, R. Alzheimer's Beta-Amyloid Peptides Compete for Insulin Binding to the Insulin Receptor. *J. Neurosci. Off. J. Soc. Neurosci.* **2002**, *22* (10), RC221. https://doi.org/20026383.
(191) Zhao, W.-Q.; Felice, F. G. D.; Fernandez, S.; Chen, H.; Lambert, M. P.; Quon, M. J.; Krafft, G. A.; Klein, W. L. Amyloid Beta Oligomers Induce Impairment of Neuronal Insulin Receptors. *FASEB J.* **2007**, *22* (1), 246–260. https://doi.org/10.1096/fj.06-7703com.
(192) Sdat, A. D.; Gottfries, C.; Adolfsson, R.; Aquilonius, S.; Carlsson, A.; Eckernas, S.; Nordberg, A.; Oreland, L.; Svennerholm, L. Biochemical Changes in Dementia Disorders of Alzheimer Type. **1983**, *4*, 261–271.
(193) Whitehouse, P. J.; Price, D. L.; Clark, a W.; Coyle, J. T.; DeLong, M. R. Alzheimer Disease: Evidence for Selective Loss of Cholinergic Neurons in the Nucleus Basalis. *Ann. Neurol.* **1981**, *10* (2), 122–126. https://doi.org/10.1002/ana.410100203.
(194) Ong, W.-Y.; Tanaka, K.; Dawe, G. S.; Ittner, L. M.; Farooqui, A. A. Slow Excitotoxicity in Alzheimer's Disease. *J. Alzheimers Dis. JAD* **2013**, *35* (4), 643–668. https://doi.org/10.3233/JAD-121990.
(195) Howard, R.; McShane, R.; Lindesay, J.; Ritchie, C.; Baldwin, A.; Barber, R.; Burns, A.; Dening, T.; Findlay, D.; Holmes, C.; Hughes, A.; Jacoby, R.; Jones, R.; Jones, R.; McKeith, I.; Macharouthu, A.; O'Brien, J.; Passmore, P.; Sheehan, B.; Juszczak, E.; Katona, C.; Hills, R.; Knapp, M.; Ballard, C.; Brown, R.; Banerjee, S.; Onions, C.; Griffin, M.; Adams, J.; Gray, R.; Johnson, T.; Bentham, P.; Phillips, P. Donepezil and Memantine for Moderate-to-Severe Alzheimer's Disease. *N. Engl. J. Med.* **2012**, *366* (10), 893–903. https://doi.org/10.1056/NEJMoa1106668.
(196) Peters, C.; Sepúlveda, F. J.; Fernández-Pérez, E. J.; Peoples, R. W.; Aguayo, L. G. The Level of NMDA Receptor in the Membrane Modulates Amyloid-β Association and Perforation. *J. Alzheimers Dis.* **2016**, *53* (1), 197–207. https://doi.org/10.3233/JAD-160170.
(197) Snyder, E. M.; Nong, Y.; Almeida, C. G.; Paul, S.; Moran, T.; Choi, E. Y.; Nairn, A. C.; Salter, M. W.; Lombroso, P. J.; Gouras, G. K.; Greengard, P. Regulation of NMDA Receptor Trafficking by Amyloid-Beta. *Nat. Neurosci.* **2005**, *8* (8), 1051–1058. https://doi.org/10.1038/nn1503.
(198) Renner, M.; Lacor, P. N.; Velasco, P. T.; Xu, J.; Contractor, A.; Klein, W. L.; Triller, A. Deleterious Effects of Amyloid β Oligomers Acting as an Extracellular Scaffold for MGluR5. *Neuron* **2010**, *66* (5), 739–754. https://doi.org/10.1016/j.neuron.2010.04.029.
(199) Rodríguez, J. J.; Noristani, H. N.; Verkhratsky, A. The Serotonergic System in Ageing and Alzheimer's Disease. *Prog. Neurobiol.* **2012**, *99* (1), 15–41. https://doi.org/10.1016/j.pneurobio.2012.06.010.
(200) Cassel, J. C.; Jeltsch, H. Serotonergic Modulation of Cholinergic Function in the Central Nervous System: Cognitive Implications. *Neuroscience* **1995**, *69* (1), 1–41. https://doi.org/10.1016/0306-4522(95)00241-A.
(201) Cai, X.; Gu, Z.; Zhong, P.; Ren, Y.; Yan, Z. Serotonin 5-HT1A Receptors Regulate AMPA Receptor Channels through Inhibiting Ca2+/Calmodulin-Dependent Kinase II in

Prefrontal Cortical Pyramidal Neurons. *J. Biol. Chem.* **2002**, *277* (39), 36553–36562. https://doi.org/10.1074/jbc.M203752200.

(202) Vasefi, M. S.; Yang, K.; Li, J.; Kruk, J. S.; Heikkila, J. J.; Jackson, M. F.; MacDonald, J. F.; Beazely, M. A. Acute 5-HT7 Receptor Activation Increases NMDA-Evoked Currents and Differentially Alters NMDA Receptor Subunit Phosphorylation and Trafficking in Hippocampal Neurons. *Mol. Brain* **2013**, *6*, 24. https://doi.org/10.1186/1756-6606-6-24.

(203) Yuen, E. Y. Serotonin 5-HT1A Receptors Regulate NMDA Receptor Channels through a Microtubule-Dependent Mechanism. *J. Neurosci.* **2005**, *25* (23), 5488–5501. https://doi.org/10.1523/JNEUROSCI.1187-05.2005.

(204) Kruk, J. S.; Vasefi, M. S.; Heikkila, J. J.; Beazely, M. A. Reactive Oxygen Species Are Required for 5-HT-Induced Transactivation of Neuronal Platelet-Derived Growth Factor and TrkB Receptors, but Not for ERK1/2 Activation. *PLoS ONE* **2013**, *8* (9). https://doi.org/10.1371/journal.pone.0077027.

(205) Kruk, J. S.; Vase, M. S.; Liu, H.; Heikkila, J. J.; Beazely, M. A. 5-HT 1A Receptors Transactivate the Platelet-Derived Growth Factor Receptor Type Beta in Neuronal Cells. **2013**, *25*, 133–143. https://doi.org/10.1016/j.cellsig.2012.09.021.

(206) Kruk, J. S.; Vasefi, M. S.; Gondora, N.; Ahmed, N.; Heikkila, J. J.; Beazely, M. A. Fluoxetine-Induced Transactivation of the Platelet-Derived Growth Factor Type β Receptor Reveals a Novel Heterologous Desensitization Process. *Mol. Cell. Neurosci.* **2015**, *65*, 45–51. https://doi.org/10.1016/j.mcn.2015.02.013.

(207) Jaffar, S.; Counts, S. E.; Ma, S. Y.; Dadko, E.; Gordon, M. N.; Morgan, D.; Mufson, E. J. Neuropathology of Mice Carrying Mutant APP(Swe) and/or PS1(M146L) Transgenes: Alterations in the P75(NTR) Cholinergic Basal Forebrain Septohippocampal Pathway. *Exp. Neurol.* **2001**, *170* (2), 227–243. https://doi.org/10.1006/exnr.2001.7710.

(208) Chakravarthy, B.; Ménard, M.; Ito, S.; Gaudet, C.; Prà, I. D.; Armato, U.; Whitfield, J. Hippocampal Membrane-Associated P75NTR Levels Are Increased in Alzheimer's Disease. *J. Alzheimers Dis. JAD* **2012**, *30*, 675–684. https://doi.org/10.3233/JAD-2012-120115.

(209) Devi, L.; Ohno, M. TrkB Reduction Exacerbates Alzheimer's Disease-like Signaling Aberrations and Memory Deficits without Affecting β-Amyloidosis in 5XFAD Mice. *Transl. Psychiatry* **2015**, *5* (5), e562. https://doi.org/10.1038/tp.2015.55.

(210) Sandhya, V. K.; Raju, R.; Verma, R.; Advani, J.; Sharma, R.; Radhakrishnan, A.; Nanjappa, V.; Narayana, J.; Somani, B. L.; Mukherjee, K. K.; Pandey, A.; Christopher, R.; Prasad, T. S. K. A Network Map of BDNF/TRKB and BDNF/P75NTR Signaling System. *J. Cell Commun. Signal.* **2013**, *7* (4), 301–307. https://doi.org/10.1007/s12079-013-0200-z.

(211) Steen, E.; Terry, B. M.; Rivera, E. J.; Cannon, J. L.; Neely, T. R.; Tavares, R.; Xu, X. J.; Wands, J. R.; Monte, S. M. D. L. Impaired Insulin and Insulin-like Growth Factor Expression and Signaling Mechanisms in Alzheimer's Disease - Is This Type 3 Diabetes? *J. Alzheimers Dis.* **2005**, *7* (1), 63–80. https://doi.org/10.3233/JAD-2005-7107.

(212) Qiu, W. Q.; Walsh, D. M.; Ye, Z.; Vekrellis, K.; Zhang, J.; Podlisny, M. B.; Rosner, M. R.; Safavi, A.; Hersh, L. B.; Selkoe, D. J. Insulin-Degrading Enzyme Regulates Extracellular Levels of Amyloid Beta-Protein by Degradation. *J. Biol. Chem.* **1998**, *273* (49), 32730–32738. https://doi.org/10.1074/jbc.273.49.32730.

(213) Glass, C. K.; Olefsky, J. M. Inflammation and Lipid Signaling in the Etiology of Insulin Resistance. *Cell Metab.* **2012**, *15* (5), 635–645. https://doi.org/10.1016/j.cmet.2012.04.001.

(214) Posey, K. A.; Clegg, D. J.; Printz, R. L.; Byun, J.; Morton, G. J.; Vivekanandan-Giri, A.; Pennathur, S.; Baskin, D. G.; Heinecke, J. W.; Woods, S. C.; Schwartz, M. W.; Niswender, K. D. Hypothalamic Proinflammatory Lipid Accumulation, Inflammation, and Insulin Resistance in Rats Fed a High-Fat Diet. *Am. J. Physiol. Endocrinol. Metab.* **2009**, *296* (5), E1003-12. https://doi.org/10.1152/ajpendo.90377.2008.

(215) Noh, H. S.; Hah, Y.-S.; Zada, S.; Ha, J. H.; Sim, G.; Hwang, J. S.; Lai, T. H.; Nguyen, H. Q.; Park, J.-Y.; Kim, H. J.; Byun, J.-H.; Hahm, J. R.; Kang, K. R.; Kim, D. R. PEBP1, a RAF Kinase Inhibitory Protein, Negatively Regulates Starvation-Induced Autophagy by Direct Interaction with LC3. *Autophagy* **2016**, *12* (11), 2183–2196. https://doi.org/10.1080/15548627.2016.1219013.

(216) Mendell, A. L.; Creighton, C. E.; Kalisch, B. E.; MacLusky, N. J. 5α-Androstane-3α,17β-Diol Inhibits Neurotoxicity in SH-SY5Y Human Neuroblastoma Cells and Mouse Primary Cortical Neurons. *Endocrinology* **2016**, *157* (12), 4570–4578. https://doi.org/10.1210/en.2016-1508.

(217) Kirouac, L.; Rajic, A. J.; Cribbs, D. H.; Padmanabhan, J. Activation of Ras-ERK Signaling and GSK-3 by Amyloid Precursor Protein and Amyloid Beta Facilitates Neurodegeneration in Alzheimer's Disease. *Eneuro* **2017**, *4* (2), ENEURO.0149-16.2017. https://doi.org/10.1523/ENEURO.0149-16.2017.

(218) Mendell, A. L.; Chung, B. Y. T.; Creighton, C. E.; Kalisch, B. E.; Bailey, C. D. C.; MacLusky, N. J. Neurosteroid Metabolites of Testosterone and Progesterone Differentially Inhibit ERK Phosphorylation Induced by Amyloid β in SH-SY5Y Cells and Primary Cortical Neurons. *Brain Res.* **2018**, *1686*, 83–93. https://doi.org/10.1016/j.brainres.2018.02.023.

(219) George, A. J.; Holsinger, R. M. D.; McLean, C. A.; Tan, S.-S.; Scott, H. S.; Cardamone, T.; Cappai, R.; Masters, C. L.; Li, Q.-X. Decreased Phosphatidylethanolamine Binding Protein Expression Correlates with Aβ Accumulation in the Tg2576 Mouse Model of Alzheimer's Disease. *Neurobiol. Aging* **2006**, *27* (4), 614–623. https://doi.org/10.1016/j.neurobiolaging.2005.03.014.

(220) Moore, C.; Perry, A. C. F.; Love, S.; Hall, L. Sequence Analysis and Immunolocalisation of Phosphatidylethanolamine Binding Protein (PBP) in Human Brain Tissue. *Mol. Brain Res.* **1996**, *37* (1), 74–78. https://doi.org/10.1016/0169-328X(95)00285-Z.

(221) Sato, T.; Ohi, Y.; Kato, D.; Mizuno, M.; Takase, H.; Kanamori, T.; Borlongan, C. V.; Haji, A.; Matsukawa, N. Hippocampal Cholinergic Neurostimulating Peptide as a Possible Modulating Factor against Glutamatergic Neuronal Disability by Amyloid Oligomers. *Cell Transplant.* **2017**, *26* (9), 1542–1550. https://doi.org/10.1177/0963689717721232.

(222) Cordy, J. M.; Hooper, N. M.; Turner, A. J. The Involvement of Lipid Rafts in Alzheimer's Disease. *Mol. Membr. Biol.* **2006**, *23* (1), 111–122. https://doi.org/10.1080/09687860500496417.

(223) Naudí, A.; Cabré, R.; Jové, M.; Ayala, V.; Gonzalo, H.; Portero-Otín, M.; Ferrer, I.; Pamplona, R. Chapter Five - Lipidomics of Human Brain Aging and Alzheimer's Disease Pathology. In *International Review of Neurobiology*; Hurley, M. J., Ed.; Omic

Studies of Neurodegenerative Disease: Part B; Academic Press, 2015; Vol. 122, pp 133–189. https://doi.org/10.1016/bs.irn.2015.05.008.

(224) Chan, R. B.; Oliveira, T. G.; Cortes, E. P.; Honig, L. S.; Duff, K. E.; Small, S. A.; Wenk, M. R.; Shui, G.; Paolo, G. D. Comparative Lipidomic Analysis of Mouse and Human Brain with Alzheimer Disease. *J. Biol. Chem.* **2012**, *287* (4), 2678–2688. https://doi.org/10.1074/jbc.M111.274142.

(225) Heppner, F. L.; Ransohoff, R. M.; Becher, B. Immune Attack: The Role of Inflammation in Alzheimer Disease. *Nat Rev Neurosci* **2015**, *16* (6), 358–372. https://doi.org/10.1038/nrn3880.

(226) Lee, Y. J.; Han, S. B.; Nam, S. Y.; Oh, K. W.; Hong, J. T. Inflammation and Alzheimer's Disease. *Arch. Pharm. Res.* **2010**, *33* (10), 1539–1556. https://doi.org/10.1007/s12272-010-1006-7.

(227) Qiu, C.; Kivipelto, M.; Strauss, E. von. Epidemiology of Alzheimer's Disease: Occurrence, Determinants, and Strategies toward Intervention. *Dialogues Clin. Neurosci.* **2009**, *11* (2), 111–128.

(228) Roher, A. E.; Weiss, N.; Kokjohn, T. A.; Kuo, Y. M.; Kalback, W.; Anthony, J.; Watson, D.; Luehrs, D. C.; Sue, L.; Walker, D.; Emmerling, M.; Goux, W.; Beach, T. Increased Aβ Peptides and Reduced Cholesterol and Myelin Proteins Characterize White Matter Degeneration in Alzheimer's Disease. *Biochemistry* **2002**, *41* (37), 11080–11090. https://doi.org/10.1021/bi026173d.

(229) Leskovjan, A. C.; Kretlow, A.; Miller, L. M. Reduced Unsaturated Lipid Content in the Hippocampus of a Mouse Model of Alzheimer ' s Disease. **2010**, *82* (7), 2711–2716.

(230) Pettegrew, J. W.; Panchalingam, K.; Hamilton, R. L.; Mcclure, R. J. Brain Membrane Phospholipid Alterations in Alzheimer's Disease. *Neurochem. Res.* **2001**, *26* (7), 771–782. https://doi.org/10.1023/A:1011603916962.

(231) He, X.; Huang, Y.; Li, B.; Gong, C. X.; Schuchman, E. H. Deregulation of Sphingolipid Metabolism in Alzheimer's Disease. *Neurobiol. Aging* **2010**, *31* (3), 398–408. https://doi.org/10.1016/j.neurobiolaging.2008.05.010.

(232) Ariga, T.; McDonald, M. P.; Yu, R. K. Role of Ganglioside Metabolism in the Pathogenesis of Alzheimer's Disease–a Review. *J. Lipid Res.* **2008**, *49* (6), 1157–1175. https://doi.org/10.1194/jlr.R800007-JLR200.

(233) Wong, M. L.; Xie, B.; Beatini, N.; Phu, P.; Marathe, S.; Johns, A.; Gold, P. W.; Hirsch, E.; Williams, K. J.; Licinio, J.; Tabas, I. Acute Systemic Inflammation Up-Regulates Secretory Sphingomyelinase in Vivo: A Possible Link between Inflammatory Cytokines and Atherogenesis. *Proc Natl Acad Sci U A* **2000**, *97* (15), 8681–8686. https://doi.org/10.1073/pnas.150098097.

(234) Zhang, J.; Liu, Q. Cholesterol Metabolism and Homeostasis in the Brain. *Protein Cell* **2015**, *6* (4), 254–264. https://doi.org/10.1007/s13238-014-0131-3.

(235) Campion, D.; Martinez, M.; Hannequin, D.; Brice, A.; Thomas-Anterion, C.; Michon, A.; Babron, M. C.; Dubois, B.; Goas, Y.; Jaillard-Serradt, A.; Ledoze, F.; Pasquier, F.; Puel, M.; Zimmerman, M. A.; Bellis, M.; Mallet, J.; Agid, Y.; Clerget-Darpoux, F. Characteristics of Familial Aggregation in Early-Onset Alzheimer's Disease: Evidence of Subgroups. *Am. J. Med. Genet.* **1995**, *60* (3), 221–227. https://doi.org/10.1002/ajmg.1320600310.

(236) St George-Hyslop, P. H.; Tanzi, R. E.; Polinsky, R. J.; Haines, J. L.; Nee, L.; Watkins, P. C.; Myers, R. H.; Feldman, R. G.; Pollen, D.; Drachman, D.; Growdon, J.; Bruni, A.;

Foncin, J.-F.; Salmon, D.; Frommelt, P.; Amaducci, L.; Sorbi, S.; Piacentini, S.; Stewart, G. D.; Hobbs, W. J.; Conneally, P. M.; Gusella, J. F. The Genetic Defect Causing Familial Alzheimer's Disease Maps on Chromosome 21. *Science* **1987**, *235* (4791), 885–890. https://doi.org/10.1126/science.2880399.

(237) Bertram, L.; Tanzi, R. E. Thirty Years of Alzheimer's Disease Genetics: The Implications of Systematic Meta-Analyses. *Nat. Rev. Neurosci.* **2008**, *9* (10), 768–778. https://doi.org/10.1038/nrn2494.

(238) Woodruff-pak, D. S. Animal Models of Alzheimer ' s Disease : Therapeutic Implications. **2008**, *15*, 507–521.

(239) Ho, L.; Qin, W.; Pompl, P. N.; Xiang, Z.; Wang, J.; Zhao, Z.; Peng, Y.; Cambareri, G.; Rocher, A.; Mobbs, C. V.; Hof, P. R.; Pasinetti, G. M. Diet-Induced Insulin Resistance Promotes Amyloidosis in a Transgenic Mouse Model of Alzheimer's Disease. *FASEB J.* **2004**, *18* (7), 902–904. https://doi.org/10.1096/fj.03-0978fje.

(240) Matsubara, E.; Bryant-Thomas, T.; Quinto, J. P.; Henry, T. L.; Poeggeler, B.; Herbert, D.; Cruz-Sanchez, F.; Chyan, Y. J.; Smith, M. A.; Perry, G.; Shoji, M.; Abe, K.; Leone, A.; Grundke-Ikbal, I.; Wilson, G. L.; Ghiso, J.; Williams, C.; Refolo, L. M.; Pappolla, M. A. Melatonin Increases Survival and Inhibits Oxidative and Amyloid Pathology in a Transgenic Model of Alzheimer's Disease. *J. Neurochem.* **2003**, *85* (5), 1101–1108. https://doi.org/10.1046/j.1471-4159.2003.01654.x.

(241) Tanzi, R. E.; Bertram, L. Twenty Years of the Alzheimer's Disease Amyloid Hypothesis: A Genetic Perspective. *Cell* **2005**, *120* (4), 545–555. https://doi.org/10.1016/j.cell.2005.02.008.

(242) Orth, M.; Bellosta, S. Cholesterol: Its Regulation and Role in Central Nervous System Disorders. *Cholesterol* **2012**, *2012*, 292598. https://doi.org/10.1155/2012/292598.

(243) Björkhem, I.; Meaney, S.; Fogelman, A. M. Brain Cholesterol: Long Secret Life behind a Barrier. *Arterioscler. Thromb. Vasc. Biol.* **2004**, *24* (5), 806–815. https://doi.org/10.1161/01.ATV.0000120374.59826.1b.

(244) Lambert, J. C.; Grenier-Boley, B.; Chouraki, V.; Heath, S.; Zelenika, D.; Fievet, N.; Hannequin, D.; Pasquier, F.; Hanon, O.; Brice, A.; Epelbaum, J.; Berr, C.; Dartigues, J. F.; Tzourio, C.; Campion, D.; Lathrop, M.; Amouyel, P. Implication of the Immune System in Alzheimer's Disease: Evidence from Genome-Wide Pathway Analysis. *J. Alzheimers Dis.* **2010**, *20* (4), 1107–1118. https://doi.org/10.3233/JAD-2010-100018.

(245) Harold, D.; Abraham, R.; Hollingworth, P.; Sims, R.; Gerrish, A.; Hamshere, M. L.; Pahwa, J. S.; Moskvina, V.; Dowzell, K.; Williams, A.; Jones, N.; Thomas, C.; Stretton, A.; Morgan, A. R.; Lovestone, S.; Powell, J.; Proitsi, P.; Lupton, M. K.; Brayne, C.; Rubinsztein, D. C.; Gill, M.; Lawlor, B.; Lynch, A.; Morgan, K.; Brown, K. S.; Passmore, P. A.; Craig, D.; McGuinness, B.; Todd, S.; Holmes, C.; Mann, D.; Smith, A. D.; Love, S.; Kehoe, P. G.; Hardy, J.; Mead, S.; Fox, N.; Rossor, M.; Collinge, J.; Maier, W.; Jessen, F.; Schürmann, B.; Heun, R.; Bussche, H. van den; Heuser, I.; Kornhuber, J.; Wiltfang, J.; Dichgans, M.; Frölich, L.; Hampel, H.; Hüll, M.; Rujescu, D.; Goate, A. M.; Kauwe, J. S. K.; Cruchaga, C.; Nowotny, P.; Morris, J. C.; Mayo, K.; Sleegers, K.; Bettens, K.; Engelborghs, S.; Deyn, P. P. D.; Broeckhoven, C. V.; Livingston, G.; Bass, N. J.; Gurling, H.; McQuillin, A.; Gwilliam, R.; Deloukas, P.; Al-Chalabi, A.; Shaw, C. E.; Tsolaki, M.; Singleton, A. B.; Guerreiro, R.; Mühleisen, T. W.; Nöthen, M. M.; Moebus, S.; Jöckel, K.-H.; Klopp, N.; Wichmann, H.-E.; Carrasquillo, M. M.; Pankratz, V. S.; Younkin, S. G.; Holmans, P. A.; O'Donovan, M.; Owen, M. J.; Williams, J.

Genome-Wide Association Study Identifies Variants at CLU and PICALM Associated with Alzheimer's Disease. *Nat. Genet.* **2009**, *41* (10), 1088–1093. https://doi.org/10.1038/ng.440.

(246) Nemetz, P. N.; Leibson, C.; Naessens, J. M.; Beard, M.; Kokmen, E.; Annegers, J. F.; Kurland, L. T. Traumatic Brain Injury and Time to Onset of Alzheimer's Disease: A Population-Based Study. *Am. J. Epidemiol.* **1999**, *149* (1), 32–40. https://doi.org/10.1093/oxfordjournals.aje.a009724.

(247) Ownby, R. L.; Crocco, E.; Acevedo, A.; John, V.; Loewenstein, D. Depression and Risk for Alzheimer Disease. *Arch. Gen. Psychiatry* **2006**, *63* (5), 530. https://doi.org/10.1001/archpsyc.63.5.530.

(248) Caraci, F.; Copani, A.; Nicoletti, F.; Drago, F. Depression and Alzheimer's Disease: Neurobiological Links and Common Pharmacological Targets. *Eur. J. Pharmacol.* **2010**, *626* (1), 64–71. https://doi.org/10.1016/j.ejphar.2009.10.022.

(249) Rao, J. S.; Keleshian, V. L.; Klein, S.; Rapoport, S. I. Epigenetic Modifications in Frontal Cortex from Alzheimer's Disease and Bipolar Disorder Patients. *Transl. Psychiatry* **2012**, *2* (7), e132. https://doi.org/10.1038/tp.2012.55.

(250) Xu, W. L.; Strauss, E. von; Qiu, C. X.; Winblad, B.; Fratiglioni, L. Uncontrolled Diabetes Increases the Risk of Alzheimer's Disease: A Population-Based Cohort Study. *Diabetologia* **2009**, *52* (6), 1031–1039. https://doi.org/10.1007/s00125-009-1323-x.

(251) Graham, L. C.; Harder, J. M.; Soto, I.; Vries, W. N. D.; John, S. W. M.; Howell, G. R. Chronic Consumption of a Western Diet Induces Robust Glial Activation in Aging Mice and in a Mouse Model of Alzheimer's Disease. *Sci. Rep.* **2016**, *6*. https://doi.org/10.1038/srep21568.

(252) Kanoski, S. E.; Davidson, T. L. Western Diet Consumption and Cognitive Impairment: Links to Hippocampal Dysfunction and Obesity. *Physiol. Behav.* **2011**, *103* (1), 59–68. https://doi.org/10.1016/j.physbeh.2010.12.003.

(253) Seneff, S.; Wainwright, G.; Mascitelli, L. European Journal of Internal Medicine Nutrition and Alzheimer ' s Disease : The Detrimental Role of a High Carbohydrate Diet. *Eur. J. Intern. Med.* **2011**, *22* (2), 134–140. https://doi.org/10.1016/j.ejim.2010.12.017.

(254) Scarmeas, N.; Stern, Y.; Tang, M.-X.; Mayeux, R.; Luchsinger, J. A. Mediterranean Diet and Risk for Alzheimer's Disease. *Ann. Neurol.* **2006**, *59* (6), 912–921. https://doi.org/10.1002/ana.20854.

(255) Yusufov, M.; Weyandt, L. L.; Piryatinsky, I. Alzheimer's Disease and Diet: A Systematic Review. *Int. J. Neurosci.* **2017**, *127* (2), 161–175. https://doi.org/10.3109/00207454.2016.1155572.

(256) Singh, B.; Parsaik, A. K.; Mielke, M. M.; Erwin, P. J.; Knopman, D. S.; Petersen, R. C.; Roberts, R. O. Association of Mediterranean Diet with Mild Cognitive Impairment and Alzheimer's Disease: A Systematic Review and Meta-Analysis. *J. Alzheimers Dis. JAD* **2014**, *39* (2), 271–282. https://doi.org/10.3233/JAD-130830.

(257) Navarro, V.; Sanchez-Mejias, E.; Jimenez, S.; Muñoz-Castro, C.; Sanchez-Varo, R.; Davila, J. C.; Vizuete, M.; Gutierrez, A.; Vitorica, J. Microglia in Alzheimer's Disease: Activated, Dysfunctional or Degenerative. *Front. Aging Neurosci.* **2018**, *10*.

(258) Griciuc, A.; Serrano-Pozo, A.; Parrado, A. R.; Lesinski, A. N.; Asselin, C. N.; Mullin, K.; Hooli, B.; Choi, S.; Hyman, B. T.; Tanzi, R. E. Alzheimer's Disease Risk Gene Cd33 Inhibits Microglial Uptake of Amyloid Beta. *Neuron* **2013**, *78* (4), 631–643. https://doi.org/10.1016/j.neuron.2013.04.014.

(259) Koenigsknecht-Talboo, J. Microglial Phagocytosis Induced by Fibrillar β-Amyloid and IgGs Are Differentially Regulated by Proinflammatory Cytokines. *J. Neurosci.* **2005**, *25* (36), 8240–8249. https://doi.org/10.1523/JNEUROSCI.1808-05.2005.

(260) Hickman, S. E.; Allison, E. K.; Khoury, J. E. Microglial Dysfunction and Defective Beta-Amyloid Clearance Pathways in Aging Alzheimer's Disease Mice. *J. Neurosci. Off. J. Soc. Neurosci.* **2008**, *28* (33), 8354–8360. https://doi.org/10.1523/JNEUROSCI.0616-08.2008.

(261) Lee, C. Y. D.; Landreth, G. E. The Role of Microglia in Amyloid Clearance from the AD Brain. *J. Neural Transm.* **2010**, *117* (8), 949–960. https://doi.org/10.1007/s00702-010-0433-4.

(262) Craft, S. Insulin Resistance Syndrome and Alzheimer's Disease : Age- and Obesity-Related Effects on Memory , Amyloid , and Inflammation. **2005**, 65–69. https://doi.org/10.1016/j.neurobiolaging.2005.08.021.

(263) Newsholme P. Verdile G., F. P. E., Keane K. N. ,. Cruzat V. F. ,. Medic S. ,. Sabale M. ,. Rowles J. ,. Wijesekara N. ,. Martins R. N. Inflammation and Oxidative Stress: The Molecular Connectivity between Insulin Resistance, Obesity, and Alzheimer's Disease. *Mediators Inflamm.* **2015**, *105828*, 1–17. https://doi.org/10.1155/2015/105828.

(264) Dantzer, R.; O'Connor, J. C.; Freund, G. G.; Johnson, R. W.; Kelley, K. W. From Inflammation to Sickness and Depression: When the Immune System Subjugates the Brain. *Nat. Rev. Neurosci.* **2008**, *9* (1), 46–56. https://doi.org/10.1038/nrn2297.

(265) Kubera, M.; Obuchowicz, E.; Goehler, L.; Brzeszcz, J.; Maes, M. In Animal Models, Psychosocial Stress-Induced (Neuro)Inflammation, Apoptosis and Reduced Neurogenesis Are Associated to the Onset of Depression. *Prog. Neuropsychopharmacol. Biol. Psychiatry* **2011**, *35* (3), 744–759. https://doi.org/10.1016/j.pnpbp.2010.08.026.

(266) Stefanou, M.-I.; Palaiodimou, L.; Bakola, E.; Smyrnis, N.; Papadopoulou, M.; Paraskevas, G. P.; Rizos, E.; Boutati, E.; Grigoriadis, N.; Krogias, C.; Giannopoulos, S.; Tsiodras, S.; Gaga, M.; Tsivgoulis, G. Neurological Manifestations of Long-COVID Syndrome: A Narrative Review. *Ther. Adv. Chronic Dis.* **2022**, *13*, 20406223221076890. https://doi.org/10.1177/20406223221076890.

(267) Reiken, S.; Sittenfeld, L.; Dridi, H.; Liu, Y.; Liu, X.; Marks, A. R. Alzheimer's-like Signaling in Brains of COVID-19 Patients. *Alzheimers Dement.* **2022**, *18* (5), 955–965. https://doi.org/10.1002/alz.12558.

(268) Fernando P. Polack; Stephen J. Thomas; Nicholas Kitchin; Judith Absalon; Alejandra Gurtman; Stephen Lockhart; John L. Perez; Gonzalo Pérez Marc; Edson D. Moreira; Cristiano Zerbini; Ruth Bailey; Kena A. Swanson; Satrajit Roychoudhury; Kenneth Koury; Ping Li; Warren V. Kalina; David Cooper; Robert W. Frenck; Laura L. Hammitt; Özlem Türeci; Haylene Nell; Axel Schaefer; Serhat Ünal; Dina B. Tresnan; Susan Mather; Philip R. Dormitzer; Uğur Şahin; Kathrin U. Jansen; William C. Gruber. Safety and Efficacy of the BNT162b2 MRNA Covid-19 Vaccine. *N. Engl. J. Med.* **2020**, *383* (27), 2603–2615. https://doi.org/10.1056/NEJMoa2034577.

(269) Heath, P. T.; Galiza, E. P.; Baxter, D. N.; Boffito, M.; Browne, D.; Burns, F.; Chadwick, D. R.; Clark, R.; Cosgrove, C.; Galloway, J.; Goodman, A. L.; Heer, A.; Higham, A.; Iyengar, S.; Jamal, A.; Jeanes, C.; Kalra, P. A.; Kyriakidou, C.; McAuley, D. F.; Meyrick, A.; Minassian, A. M.; Minton, J.; Moore, P.; Munsoor, I.; Nicholls, H.; Osanlou, O.; Packham, J.; Pretswell, C. H.; San Francisco Ramos, A.; Saralaya, D.; Sheridan, R. P.; Smith, R.; Soiza, R. L.; Swift, P. A.; Thomson, E. C.; Turner, J.; Viljoen,

M. E.; Albert, G.; Cho, I.; Dubovsky, F.; Glenn, G.; Rivers, J.; Robertson, A.; Smith, K.; Toback, S. Safety and Efficacy of NVX-CoV2373 Covid-19 Vaccine. *N. Engl. J. Med.* **2021**, *385* (13), 1172–1183. https://doi.org/10.1056/NEJMoa2107659.

(270) Margolis, K. L.; Poland, G. A.; Nichol, K. L.; MacPherson, D. S.; Meyer, J. D.; Korn, J. E.; Lofgren, R. P. Frequency of Adverse Reactions after Influenza Vaccination. *Am. J. Med.* **1990**, *88* (1), 27–30. https://doi.org/10.1016/0002-9343(90)90123-u.

(271) Wu, Y.; Dissing-Olesen, L.; MacVicar, B. A.; Stevens, B. Microglia: Dynamic Mediators of Synapse Development and Plasticity. *Trends Immunol.* **2015**, *36* (10), 605–613. https://doi.org/10.1016/j.it.2015.08.008.

(272) Deane, R.; Wu, Z.; Zlokovic, B. V. RAGE (Yin) versus LRP (Yang) Balance Regulates Alzheimer Amyloid β-Peptide Clearance through Transport across the Blood-Brain Barrier. *Stroke* **2004**, *35* (11 SUPPL. 1), 2628–2631. https://doi.org/10.1161/01.STR.0000143452.85382.d1.

(273) Origlia, N.; Bonadonna, C.; Rosellini, A.; Leznik, E.; Arancio, O.; Yan, S. S.; Domenici, L. Microglial Receptor for Advanced Glycation End Product-Dependent Signal Pathway Drives Beta-Amyloid-Induced Synaptic Depression and Long-Term Depression Impairment in Entorhinal Cortex. *J. Neurosci. Off. J. Soc. Neurosci.* **2010**, *30* (34), 11414–11425. https://doi.org/10.1523/JNEUROSCI.2127-10.2010.

(274) Calcia, M. A.; Bonsall, D. R.; Bloomfield, P. S.; Selvaraj, S.; Barichello, T.; Howes, O. D. Stress and Neuroinflammation: A Systematic Review of the Effects of Stress on Microglia and the Implications for Mental Illness. *Psychopharmacology (Berl.)* **2016**, *233* (9), 1637–1650. https://doi.org/10.1007/s00213-016-4218-9.

(275) Holmes, C. Systemic Infection, Interleukin 1beta, and Cognitive Decline in Alzheimer's Disease. *J. Neurol. Neurosurg. Psychiatry* **2003**, *74* (6), 788–789. https://doi.org/10.1136/jnnp.74.6.788.

(276) Maheshwari, P.; Eslick, G. D. Bacterial Infection and Alzheimer's Disease: A Meta-Analysis. *J. Alzheimers Dis. JAD* **2015**, *43* (3), 957–966. https://doi.org/10.3233/JAD-140621.

(277) Suzuki, R.; Lee, K.; Jing, E.; Biddinger, S. B.; McDonald, J. G.; Montine, T. J.; Craft, S.; Kahn, C. R. Diabetes and Insulin in Regulation of Brain Cholesterol Metabolism. *Cell Metab.* **2010**, *12* (6), 567–579. https://doi.org/10.1016/j.cmet.2010.11.006.

(278) Kleinridders, A.; Ferris, H. A.; Cai, W.; Kahn, C. R. Insulin Action in Brain Regulates Systemic Metabolism and Brain Function. *Diabetes* **2014**, *63* (7), 2232–2243. https://doi.org/10.2337/db14-0568.

(279) Streicher, R.; Kotzka, J.; Muller-Wieland, D.; Siemeister, G.; Munck, M.; Avci, H.; Krone, W. SREBP-1 Mediates Activation of the Low Density Lipoprotein Receptor Promoter by Insulin and Insulin-like Growth Factor-I. *J. Biol. Chem.* **1996**, *271* (12), 7128–7133. https://doi.org/10.1074/jbc.271.12.7128.

(280) Eberlé, D.; Hegarty, B.; Bossard, P.; Ferré, P.; Foufelle, F. SREBP Transcription Factors: Master Regulators of Lipid Homeostasis. *Biochimie* **2004**, *86* (11), 839–848. https://doi.org/10.1016/j.biochi.2004.09.018.

(281) Pfrieger, F. W. Outsourcing in the Brain: Do Neurons Depend on Cholesterol Delivery by Astrocytes? *BioEssays* **2003**, *25* (1), 72–78. https://doi.org/10.1002/bies.10195.

(282) Reid, P. C.; Urano, Y.; Kodama, T.; Hamakubo, T. Alzheimer's Disease: Cholesterol, Membrane Rafts, Isoprenoids and Statins. *J. Cell. Mol. Med.* **2007**, *11* (3), 383–392. https://doi.org/10.1111/j.1582-4934.2007.00054.x.

(283) Weber, C.; Noels, H. Atherosclerosis: Current Pathogenesis and Therapeutic Options. *Nat. Med.* **2011**, *17* (11), 1410–1422. https://doi.org/10.1038/nm.2538.
(284) Jain, M. K.; Ridker, P. M. Anti-Inflammatory Effects of Statins: Clinical Evidence and Basic Mechanisms. *Nat. Rev. Drug Discov.* **2005**, *4* (12), 977–987. https://doi.org/10.1038/nrd1901.
(285) S. Antonopoulos, A.; Margaritis, M.; Lee, R.; Channon, K.; Antoniades, C. Statins as Anti-Inflammatory Agents in Atherogenesis: Molecular Mechanisms and Lessons from the Recent Clinical Trials. *Curr. Pharm. Des.* **2012**, *18* (11), 1519–1530. https://doi.org/10.2174/138161212799504803.
(286) Muldoon, M. F.; Barger, S. D.; Ryan, C. M.; Flory, J. D.; Lehoczky, J. P.; Matthews, K. A.; Manuck, S. B. Effects of Lovastatin on Cognitive Function and Psychological Well-Being∗∗Access the "Journal Club" Discussion of This Paper at Http://Www.Elsevier.Com/Locate/Ajmselect/. *Am. J. Med.* **2000**, *108* (7), 538–546. https://doi.org/10.1016/S0002-9343(00)00353-3.
(287) Muldoon, M. F.; Ryan, C. M.; Sereika, S. M.; Flory, J. D.; Manuck, S. B. Randomized Trial of the Effects of Simvastatin on Cognitive Functioning in Hypercholesterolemic Adults. *Am. J. Med.* **2004**, *117* (11), 823–829. https://doi.org/10.1016/j.amjmed.2004.07.041.
(288) Ott, B. R.; Daiello, L. A.; Dahabreh, I. J.; Springate, B. A.; Bixby, K.; Murali, M.; Trikalinos, T. A. Do Statins Impair Cognition? A Systematic Review and Meta-Analysis of Randomized Controlled Trials. *J. Gen. Intern. Med.* **2015**, *30* (3), 348–358. https://doi.org/10.1007/s11606-014-3115-3.
(289) Wolozin, B.; Kellman, W.; Ruosseau, P.; Celesia, G. G.; Siegel, G. Decreased Prevalence of Alzheimer Disease Associated With 3-Hydroxy-3-Methyglutaryl Coenzyme A Reductase Inhibitors. *Arch. Neurol.* **2000**, *57* (10), 1439–1443. https://doi.org/10.1001/archneur.57.10.1439.
(290) Wong, W. B.; Lin, V. W.; Boudreau, D.; Devine, E. B. Statins in the Prevention of Dementia and Alzheimer's Disease: A Meta-Analysis of Observational Studies and an Assessment of Confounding. *Pharmacoepidemiol. Drug Saf.* **2013**, *22* (4), 345–358. https://doi.org/10.1002/pds.3381.
(291) Benito-León, J.; Louis, E. D.; Vega, S.; Bermejo-Pareja, F. Statins and Cognitive Functioning in the Elderly: A Population-Based Study. *J. Alzheimers Dis.* **2010**, *21* (1), 95–102. https://doi.org/10.3233/JAD-2010-100180.
(292) Sano, M.; Bell, K. L.; Galasko, D.; Galvin, J. E.; Thomas, R. G.; Dyck, C. H. van; Aisen, P. S. A Randomized, Double-Blind, Placebo-Controlled Trial of Simvastatin to Treat Alzheimer Disease. *Neurology* **2011**, *77* (6), 556–563. https://doi.org/10.1212/WNL.0b013e318228bf11.
(293) Sinyavskaya, L.; Gauthier, S.; Renoux, C.; Dell'Aniello, S.; Suissa, S.; Brassard, P. Comparative Effect of Statins on the Risk of Incident Alzheimer Disease. *Neurology* **2018**, *90* (3), e179–e187. https://doi.org/10.1212/WNL.0000000000004818.
(294) Sahebzamani, F. M.; Munro, C.; Marroquin, O.; Diamond, D.; Keller, E.; Kip, K. Examination of the FDA Warning for Statins and Cognitive Dysfunction. **2014**. https://doi.org/10.4172/2329-6887.1000141.
(295) Szoka, F.; Papahadjopoulos, D. Comparative Properties and Methods of Preparation of Lipid Vesicles (Liposomes). *Annu. Rev. Biophys. Bioeng.* **1980**, *9*, 467–508. https://doi.org/10.1146/annurev.bb.09.060180.002343.

(296) Lapinski, M. M.; Castro-Forero, A.; Greiner, A. J.; Ofoli, R. Y.; Blanchard, G. J. Comparison of Liposomes Formed by Sonication and Extrusion: Rotational and Translational Diffusion of an Embedded Chromophore. *Langmuir* **2007**, *23* (23), 11677–11683. https://doi.org/10.1021/la7020963.

(297) Cho, N.-J.; Hwang, L. Y.; Solandt, J. J. R.; Frank, C. W. Comparison of Extruded and Sonicated Vesicles for Planar Bilayer Self-Assembly. *Materials* **2013**, *6* (8), 3294–3308. https://doi.org/10.3390/ma6083294.

(298) Maulucci, G.; De Spirito, M.; Arcovito, G.; Boffi, F.; Castellano, A. C.; Briganti, G. Particle Size Distribution in DMPC Vesicles Solutions Undergoing Different Sonication Times. *Biophys. J.* **2005**, *88* (5), 3545–3550. https://doi.org/10.1529/biophysj.104.048876.

(299) Binnig, G.; Quate, C. F. Atomic Force Microscope. *Phys. Rev. Lett.* **1986**, *56* (9), 930–933. https://doi.org/10.1103/PhysRevLett.56.930.

(300) Drolle, E.; Hane, F.; Lee, B.; Leonenko, Z. Atomic Force Microscopy to Study Molecular Mechanisms of Amyloid Fibril Formation and Toxicity in Alzheimer's Disease. *Drug Metab. Rev.* **2014**, *46* (2), 207–223. https://doi.org/10.3109/03602532.2014.882354.

(301) Hoh, J. H.; Hansma, P. K. Atomic Force Microscopy for High-Resolution Imaging in Cell Biology. *Trends Cell Biol.* **1992**, *2* (7), 208–213. https://doi.org/10.1016/0962-8924(92)90248-L.

(302) Mehrazma, B.; Robinson, M.; Opare, S. K. A.; Petoyan, A.; Lou, J.; Hane, F. T.; Rauk, A.; Leonenko, Z. Pseudo-Peptide Amyloid-β Blocking Inhibitors: Molecular Dynamics and Single Molecule Force Spectroscopy Study. *Biochim. Biophys. Acta - Proteins Proteomics* **2017**, *1865* (11). https://doi.org/10.1016/j.bbapap.2017.07.022.

(303) Binnig, G.; Quate, C. F.; Gerber, C. Atomic Force Microscope. *Phys Rev Lett* **1986**, *56* (9), 930. https://doi.org/10.1103/PhysRevLett.56.930.

(304) Davis, J. B.; Maher, P. Protein Kinase C Activation Inhibits Glutamate-Induced Cytotoxicity in a Neuronal Cell Line. *Brain Res.* **1994**, *652* (1), 169–173. https://doi.org/10.1016/0006-8993(94)90334-4.

(305) Whittemore, S. R.; Holets, V. R.; Keane, R. W.; Levy, D. J.; McKay, R. D. G. Transplantation of a Temperature-Sensitive, Nerve Growth Factor-Secreting, Neuroblastoma Cell Line into Adult Rats with Fimbria–Fornix Lesions Rescues Cholinergic Septal Neurons. *J. Neurosci. Res.* **1991**, *28* (2), 156–170. https://doi.org/10.1002/jnr.490280203.

(306) Morimoto, B. H.; Koshland, D. E. Induction and Expression of Long- and Short-Term Neurosecretory Potentiation in a Neural Cell Line. *Neuron* **1990**, *5* (6), 875–880. https://doi.org/10.1016/0896-6273(90)90347-I.

(307) Morimoto, B. H.; Koshland, D. E. Excitatory Amino Acid Uptake and N-Methyl-D-Aspartate-Mediated Secretion in a Neural Cell Line. *Proc. Natl. Acad. Sci.* **1990**, *87* (9), 3518–3521. https://doi.org/10.1073/pnas.87.9.3518.

(308) Zhao, Z.; Lu, R.; Zhang, B.; Shen, J.; Yang, L.; Xiao, S.; Liu, J.; Suo, W. Z. Differentiation of HT22 Neurons Induces Expression of NMDA Receptor That Mediates Homocysteine Cytotoxicity. *Neurol. Res.* **2012**, *34* (1), 38–43. https://doi.org/10.1179/1743132811Y.0000000057.

(309) Liu, J.; Li, L.; Suo, W. Z. HT22 Hippocampal Neuronal Cell Line Possesses Functional Cholinergic Properties. *Life Sci.* **2009**, *84* (9–10), 267–271. https://doi.org/10.1016/j.lfs.2008.12.008.
(310) Wu, M.; Jia, J.; Lei, C.; Ji, L.; Chen, X.; Sang, H.; Xiong, L. Cannabinoid Receptor CB1 Is Involved in Nicotine-Induced Protection Against Aβ 1-42 Neurotoxicity in HT22 Cells. *J. Mol. Neurosci.* **2014**, *55* (3), 778–787. https://doi.org/10.1007/s12031-014-0422-4.
(311) Robinson, M.; Lou, J.; Mehrazma, B.; Rauk, A.; Beazely, M.; Leonenko, Z. Pseudopeptide Amyloid Aggregation Inhibitors: In Silico, Single Molecule and Cell Viability Studies. *Int. J. Mol. Sci.* **2021**, *22* (3). https://doi.org/10.3390/ijms22031051.
(312) Davidson, M. W.; Abramowitz, M. Optical Microscopy. In *Encyclopedia of Imaging Science and Technology*; John Wiley & Sons, Ltd, 2002. https://doi.org/10.1002/0471443395.img074.
(313) Park, Y.; Depeursinge, C.; Popescu, G. Quantitative Phase Imaging in Biomedicine. *Nat. Photonics* **2018**, *12* (10), 578–589. https://doi.org/10.1038/s41566-018-0253-x.
(314) Zicha, D.; Dunn, G. A. An Image Processing System for Cell Behaviour Studies in Subconfluent Cultures. *J. Microsc.* **1995**, *179* (1), 11–21. https://doi.org/10.1111/j.1365-2818.1995.tb03609.x.
(315) Park, Y.; Best, C. A.; Auth, T.; Gov, N. S.; Safran, S. A.; Popescu, G.; Suresh, S.; Feld, M. S. Metabolic Remodeling of the Human Red Blood Cell Membrane. *Proc. Natl. Acad. Sci.* **2010**, *107* (4), 1289–1294. https://doi.org/10.1073/pnas.0910785107.
(316) Brzezinski, A. Melatonin in Humans. *N. Engl. J. Med.* **1997**, *336* (3), 186–195.
(317) Falcón, J.; Besseau, L.; Fuentès, M.; Sauzet, S.; Magnanou, E.; Boeuf, G. Structural and Functional Evolution of the Pineal Melatonin System in Vertebrates. *Ann. N. Y. Acad. Sci.* **2009**, *1163* (ii), 101–111. https://doi.org/10.1111/j.1749-6632.2009.04435.x.
(318) Cardinali, D. P.; Furio, A. M.; Brusco, L. I. Clinical Aspects of Melatonin Intervention in Alzheimer's Disease Progression. *Curr. Neuropharmacol.* **2010**, *8*, 218–227. https://doi.org/10.2174/157015910792246209.
(319) Rosales-Corral, S. A.; Acuña-Castroviejo, D.; Coto-Montes, A.; Boga, J. A.; Manchester, L. C.; Fuentes-Broto, L.; Korkmaz, A.; Ma, S.; Tan, D. X.; Reiter, R. J. Alzheimer's Disease: Pathological Mechanisms and the Beneficial Role of Melatonin. *J. Pineal Res.* **2012**, *52* (2), 167–202. https://doi.org/10.1111/j.1600-079X.2011.00937.x.
(320) Hane, F. T.; Robinson, M.; Lee, B. Y.; Bai, O.; Leonenko, Z.; Albert, M. S. Recent Progress in Alzheimer's Disease Research, Part 3: Diagnosis and Treatment. *J. Alzheimers Dis.* **2017**, *57* (3). https://doi.org/10.3233/JAD-160907.
(321) Hane, F. T.; Lee, B. Y.; Leonenko, Z. Recent Progress in Alzheimer's Disease Research Part 1 – Pathology. *J. Alzheimers Dis.* **2017**, *57* (Preprint), 1–27.
(322) Friedman, R.; Pellarin, R.; Caflisch, A. Amyloid Aggregation on Lipid Bilayers and Its Impact on Membrane Permeability. *J. Mol. Biol.* **2009**, *387* (2), 407–415. https://doi.org/10.1016/j.jmb.2008.12.036.
(323) Ali, T.; Kim, M. O. Melatonin Ameliorates Amyloid Beta-Induced Memory Deficits, Tau Hyperphosphorylation and Neurodegeneration via PI3/Akt/GSk3β Pathway in the Mouse Hippocampus. *J. Pineal Res.* **2015**, *59* (1), 47–59. https://doi.org/10.1111/jpi.12238.
(324) Pappolla, M. A.; Sos, M.; Omar, R. A.; Bick, R. J.; Hickson-Bick, D. L.; Reiter, R. J.; Efthimiopoulos, S.; Robakis, N. K. Melatonin Prevents Death of Neuroblastoma Cells

Exposed to the Alzheimer Amyloid Peptide. *J. Neurosci. Off. J. Soc. Neurosci.* **1997**, *17* (5), 1683–1690. https://doi.org/10.1523/JNEUROSCI.17-05-01683.1997.

(325) Pappolla, M.; Simovich, M.; Bryant-Thomas, T.; Chyan, Y.; Poeggeler, B.; Dubocovich, M.; Bick, R.; Perry, G.; Cruz-Sanchez, F.; Smith, M. The Neuroprotective Activities of Melatonin against the Alzheimer Beta-Protein Are Not Mediated by Melatonin Membrane Receptors. *J. Pineal Res.* **2002**, *32* (3), 135–142. https://doi.org/10.1034/j.1600-079x.2002.1o838.x.

(326) Dragicevic, N.; Copes, N.; O'Neal-Moffitt, G.; Jin, J.; Buzzeo, R.; Mamcarz, M.; Tan, J.; Cao, C.; Olcese, J. M.; Arendash, G. W.; Bradshaw, P. C. Melatonin Treatment Restores Mitochondrial Function in Alzheimer's Mice: A Mitochondrial Protective Role of Melatonin Membrane Receptor Signaling. *J. Pineal Res.* **2011**, *51* (1), 75–86. https://doi.org/10.1111/j.1600-079X.2011.00864.x.

(327) Chyan, Y. J.; Poeggeler, B.; Omar, R. A.; Chain, D. G.; Frangione, B.; Ghiso, J.; Pappolla, M. A. Potent Neuroprotective Properties against the Alzheimer β-Amyloid by an Endogenous Melatonin-Related Indole Structure, Indole-3-Propionic Acid. *J. Biol. Chem.* **1999**, *274* (31), 21937–21942. https://doi.org/10.1074/jbc.274.31.21937.

(328) Pappolla, M. a; Chyan, Y. J.; Poeggeler, B.; Frangione, B.; Wilson, G.; Ghiso, J.; Reiter, R. J. An Assessment of the Antioxidant and the Antiamyloidogenic Properties of Melatonin: Implications for Alzheimer's Disease. *J. Neural Transm. Vienna Austria 1996* **2000**, *107* (2), 203–231. https://doi.org/10.1007/s007020050018.

(329) Garcia, J. J.; Reiter, R. J.; Guerrero, J. M.; Escames, G.; Yu, B. P.; Oh, C. S.; Muñoz-hoyos, A.; Health, T.; Drive, F. C.; Antonio, S. Melatonin Prevents Changes in Microsomal Membrane Fluidity during Induced Lipid Peroxidation. **1997**, *408*, 297–300. https://doi.org/10.1016/S0014-5793(97)00447-X.

(330) Bongiorno, D.; Ceraulo, L.; Ferrugia, M.; Filizzola, F.; Ruggirello, A.; Liveri, V. T. Localization and Interactions of Melatonin in Dry Cholesterol/Lecithin Mixed Reversed Micelles Used as Cell Membrane Models. *J. Pineal Res.* **2005**. https://doi.org/10.1111/j.1600-079X.2005.00211.x.

(331) Bolmatov, D.; McClintic, W. T.; Taylor, G.; Stanley, C. B.; Do, C.; Collier, C. P.; Leonenko, Z.; Lavrentovich, M. O.; Katsaras, J. Deciphering Melatonin-Stabilized Phase Separation in Phospholipid Bilayers. *Langmuir* **2019**. https://doi.org/10.1021/acs.langmuir.9b01534.

(332) Ceraulo, L.; Fanara, S.; Liveri, V. T.; Ruggirello, A.; Panzeri, W.; Mele, A. Orientation and Molecular Contacts of Melatonin Confined into AOT and Lecithin Reversed Micellar Systems. *Colloids Surf. Physicochem. Eng. Asp.* **2008**. https://doi.org/10.1016/j.colsurfa.2007.09.022.

(333) Drolle, E.; Kučerka, N.; Hoopes, M. I.; Choi, Y.; Katsaras, J.; Karttunen, M.; Leonenko, Z. Effect of Melatonin and Cholesterol on the Structure of DOPC and DPPC Membranes. *Biochim. Biophys. Acta - Biomembr.* **2013**, *1828* (9), 2247–2254. https://doi.org/10.1016/j.bbamem.2013.05.015.

(334) Dies, H.; Cheung, B.; Tang, J.; Rheinst??dter, M. C. The Organization of Melatonin in Lipid Membranes. *Biochim. Biophys. Acta - Biomembr.* **2015**, *1848* (4), 1032–1040. https://doi.org/10.1016/j.bbamem.2015.01.006.

(335) Mei, N.; Robinson, M.; Davis, J. H.; Leonenko, Z. Melatonin Alters Fluid Phase Coexistence in POPC/DPPC/Cholesterol Membranes. *Biophys. J.* **2020**, *119* (12). https://doi.org/10.1016/j.bpj.2020.10.030.

(336) Choi, Y.; Attwood, S. J.; Hoopes, M. I.; Drolle, E.; Karttunen, M.; Leonenko, Z. Melatonin Directly Interacts with Cholesterol and Alleviates Cholesterol Effects in Dipalmitoylphosphatidylcholine Monolayers. *Soft Matter* **2014**, *10* (1), 206–213. https://doi.org/10.1039/c3sm52064a.

(337) Lévy, R.; Maaloum, M. Measuring the Spring Constant of Atomic Force Microscope Cantilevers: Thermal Fluctuations and Other Methods. *Nanotechnology* **2001**, *13* (1), 33–37. https://doi.org/10.1088/0957-4484/13/1/307.

(338) Nickels, J. D.; Cheng, X.; Mostofian, B.; Stanley, C.; Lindner, B.; Heberle, F. A.; Perticaroli, S.; Feygenson, M.; Egami, T.; Standaert, R. F.; Smith, J. C.; Myles, D. A. A.; Ohl, M.; Katsaras, J. Mechanical Properties of Nanoscopic Lipid Domains. *J. Am. Chem. Soc.* **2015**, *137* (50), 15772–15780. https://doi.org/10.1021/jacs.5b08894.

(339) Sullan, R. M. A.; Li, J. K.; Hao, C.; Walker, G. C.; Zou, S. Cholesterol-Dependent Nanomechanical Stability of Phase-Segregated Multicomponent Lipid Bilayers. *Biophys. J.* **2010**, *99* (2), 507–516. https://doi.org/10.1016/j.bpj.2010.04.044.

(340) Lu, H.; Martí, J. Binding and Dynamics of Melatonin at the Interface of Phosphatidylcholine-Cholesterol Membranes. *PLOS ONE* **2019**, *14* (11), e0224624. https://doi.org/10.1371/journal.pone.0224624.

(341) Hane, F. T.; Attwood, S. J.; Leonenko, Z. Comparison of Three Competing Dynamic Force Spectroscopy Models to Study Binding Forces of Amyloid-β (1-42). *Soft Matter* **2014**, *10* (12), 1924–1930. https://doi.org/10.1039/c3sm52257a.

(342) Moreno-Cencerrado, A.; Iturri, J.; Pecorari, I.; D.M. Vivanco, M.; Sbaizero, O.; Toca-Herrera, J. L. Investigating Cell-Substrate and Cell–Cell Interactions by Means of Single-Cell-Probe Force Spectroscopy. *Microsc. Res. Tech.* **2017**, *80* (1), 124–130. https://doi.org/10.1002/jemt.22706.

(343) Viji Babu, P. K.; Rianna, C.; Mirastschijski, U.; Radmacher, M. Nano-Mechanical Mapping of Interdependent Cell and ECM Mechanics by AFM Force Spectroscopy. *Sci. Rep.* **2019**, *9* (1), 12317. https://doi.org/10.1038/s41598-019-48566-7.

(344) Goksu, E. I.; Vanegas, J. M.; Blanchette, C. D.; Lin, W.-C.; Longo, M. L. AFM for Structure and Dynamics of Biomembranes. *Biochim. Biophys. Acta BBA - Biomembr.* **2009**, *1788* (1), 254–266. https://doi.org/10.1016/j.bbamem.2008.08.021.

(345) Chyasnavichyus, M.; Young, S. L.; Geryak, R.; Tsukruk, V. V. Probing Elastic Properties of Soft Materials with AFM: Data Analysis for Different Tip Geometries. *Polymer* **2016**, *102*, 317–325. https://doi.org/10.1016/j.polymer.2016.02.020.

(346) Mathai, J. C.; Tristram-Nagle, S.; Nagle, J. F.; Zeidel, M. L. Structural Determinants of Water Permeability through the Lipid Membrane. *J. Gen. Physiol.* **2008**, *131* (1), 69–76. https://doi.org/10.1085/jgp.200709848.

(347) Leonenko, Z.; Finot, E.; Cramb, D. AFM Study of Interaction Forces in Supported Planar DPPC Bilayers in the Presence of General Anesthetic Halothane. *Biochim. Biophys. Acta - Biomembr.* **2006**, *1758* (4), 487–492. https://doi.org/10.1016/j.bbamem.2006.02.033.

(348) Leonenko, Z. V.; Carnini, A.; Cramb, D. T. Supported Planar Bilayer Formation by Vesicle Fusion: The Interaction of Phospholipid Vesicles with Surfaces and the Effect of Gramicidin on Bilayer Properties Using Atomic Force Microscopy. *Biochim. Biophys. Acta - Biomembr.* **2000**, *1509* (1–2), 131–147. https://doi.org/10.1016/S0005-2736(00)00288-1.

(349) Marquês, J. T.; Viana, A. S.; De Almeida, R. F. M. Ethanol Effects on Binary and Ternary Supported Lipid Bilayers with Gel/Fluid Domains and Lipid Rafts. *Biochim.*

Biophys. Acta BBA - Biomembr. **2011**, *1808* (1), 405–414. https://doi.org/10.1016/j.bbamem.2010.10.006.

(350) Dey, S.; Surendran, D.; Engberg, O.; Gupta, A.; Fanibunda, S. E.; Das, A.; Maity, B. K.; Dey, A.; Visvakarma, V.; Kallianpur, M.; Scheidt, H. A.; Walker, G.; Vaidya, V. A.; Huster, D.; Maiti, S. Altered Membrane Mechanics Provides a Receptor-Independent Pathway for Serotonin Action. *Chem. – Eur. J.* **2021**, *27* (27), 7533–7541. https://doi.org/10.1002/chem.202100328.

(351) Benloucif, S.; Burgess, H. J.; Klerman, E. B.; Lewy, A. J.; Middleton, B.; Murphy, P. J.; Parry, B. L.; Revell, V. L. Measuring Melatonin in Humans. *J. Clin. Sleep Med.* **2008**, *4* (1), 66–69.

(352) Tsui-Pierchala, B. A.; Encinas, M.; Milbrandt, J.; Johnson, E. M. Lipid Rafts in Neuronal Signaling and Function. *Trends Neurosci.* **2002**, *25* (8), 412–417. https://doi.org/10.1016/S0166-2236(02)02215-4.

(353) Hicks, D. A.; Nalivaeva, N. N.; Turner, A. J. Lipid Rafts and Alzheimer's Disease: Protein-Lipid Interactions and Perturbation of Signaling. *Front. Physiol.* **2012**, *3 JUN*. https://doi.org/10.3389/fphys.2012.00189.

(354) Hane, F.; Drolle, E.; Gaikwad, R.; Faught, E.; Leonenko, Z. Amyloid-?? Aggregation on Model Lipid Membranes: An Atomic Force Microscopy Study. *J. Alzheimers Dis.* **2011**, *26* (3), 485–494. https://doi.org/10.3233/JAD-2011-102112.

(355) Pécheur, E. I.; Sainte-Marie, J.; Bienvenüe, A.; Hoekstra, D. Peptides and Membrane Fusion: Towards an Understanding of the Molecular Mechanism of Protein-Induced Fusion. *Journal of Membrane Biology*. 1999, pp 1–17. https://doi.org/10.1007/s002329900466.

(356) Drolle, E.; Ku??erka, N.; Hoopes, M. I.; Choi, Y.; Katsaras, J.; Karttunen, M.; Leonenko, Z. Effect of Melatonin and Cholesterol on the Structure of DOPC and DPPC Membranes. *Biochim. Biophys. Acta - Biomembr.* **2013**, *1828* (9), 2247–2254. https://doi.org/10.1016/j.bbamem.2013.05.015.

(357) Drolle, E.; Gaikwad, R. M.; Leonenko, Z. Nanoscale Electrostatic Domains in Cholesterol-Laden Lipid Membranes Create a Target for Amyloid Binding. *Biophys. J.* **2012**, *103* (4). https://doi.org/10.1016/j.bpj.2012.06.053.

(358) Caillon, L.; Killian, J. A.; Lequin, O.; Khemtémourian, L. Biophysical Investigation of the Membrane-Disrupting Mechanism of the Antimicrobial and Amyloid-Like Peptide Dermaseptin S9. *PLoS ONE* **2013**, *8* (10). https://doi.org/10.1371/journal.pone.0075528.

(359) Matsuzaki, K. Peptide-Membrane Interactions in Biological Sciences: Antimicrobial Peptides and Alzheimer's Beta-Amyloid Peptides as Paradigms. *Pept. Sci.* **2005**, *41st*, 87–88.

(360) Butterfield, S. M.; Lashuel, H. A. Amyloidogenic Protein-Membrane Interactions: Mechanistic Insight from Model Systems. *Angewandte Chemie - International Edition*. 2010, pp 5628–5654. https://doi.org/10.1002/anie.200906670.

(361) Lad, M. D.; Birembaut, F.; Clifton, L. a; Frazier, R. a; Webster, J. R. P.; Green, R. J. Antimicrobial Peptide-Lipid Binding Interactions and Binding Selectivity. *Biophys. J.* **2007**, *92* (10), 3575–3586. https://doi.org/10.1529/biophysj.106.097774.

(362) Zampagni, M.; Evangelisti, E.; Cascella, R.; Liguri, G.; Becatti, M.; Pensalfini, A.; Uberti, D.; Cenini, G.; Memo, M.; Bagnoli, S.; Nacmias, B.; Sorbi, S.; Cecchi, C. Lipid Rafts Are Primary Mediators of Amyloid Oxidative Attack on Plasma Membrane. *J. Mol. Med.* **2010**, *88* (6), 597–608. https://doi.org/10.1007/s00109-010-0603-8.

(363) Nicholson, A. M.; Ferreira, A. Increased Membrane Cholesterol Might Render Mature Hippocampal Neurons More Susceptible to Beta-Amyloid-Induced Calpain Activation and Tau Toxicity. *J. Neurosci. Off. J. Soc. Neurosci.* **2009**, *29* (14), 4640–4651. https://doi.org/10.1523/JNEUROSCI.0862-09.2009.

(364) ARISPE, N. Plasma Membrane Cholesterol Controls the Cytotoxicity of Alzheimer's Disease AbetaP (1-40) and (1-42) Peptides. *FASEB J.* **2002**, *16* (12), 1526–1536. https://doi.org/10.1096/fj.02-0829com.

(365) Cecchi, C.; Stefani, M. The Amyloid-Cell Membrane System. The Interplay between the Biophysical Features of Oligomers/Fibrils and Cell Membrane Defines Amyloid Toxicity. *Biophys. Chem.* **2013**, *182*, 30–43. https://doi.org/10.1016/j.bpc.2013.06.003.

(366) Soscia, S. J.; Kirby, J. E.; Washicosky, K. J.; Tucker, S. M.; Ingelsson, M.; Hyman, B.; Burton, M. A.; Goldstein, L. E.; Duong, S.; Tanzi, R. E.; Moir, R. D. The Alzheimer's Disease-Associated Amyloid ??-Protein Is an Antimicrobial Peptide. *PLoS ONE* **2010**, *5* (3). https://doi.org/10.1371/journal.pone.0009505.

(367) Kumar, D. K. V.; Choi, S. H.; Washicosky, K. J.; Eimer, W. A.; Tucker, S.; Ghofrani, J.; Lefkowitz, A.; McColl, G.; Goldstein, L. E.; Tanzi, R. E.; Moir, R. D. Amyloid- Peptide Protects against Microbial Infection in Mouse and Worm Models of Alzheimers Disease. *Sci. Transl. Med.* **2016**, *8* (340), 340ra72-340ra72. https://doi.org/10.1126/scitranslmed.aaf1059.

(368) Kummer, C.; Wehner, S.; Quast, T.; Werner, S.; Herzog, V. Expression and Potential Function of β-Amyloid Precursor Proteins during Cutaneous Wound Repair. *Exp. Cell Res.* **2002**, *280* (2), 222–232. https://doi.org/10.1006/excr.2002.5631.

(369) Drolle, E.; Hane, F.; Lee, B.; Leonenko, Z. Atomic Force Microscopy to Study Molecular Mechanisms of Amyloid Fibril Formation and Toxicity in Alzheimer's Disease. *Drug Metab. Rev.* **2014**, *46* (2), 207–223. https://doi.org/10.3109/03602532.2014.882354.

(370) Humphris, A. D. L.; Miles, M. J.; Hobbs, J. K. A Mechanical Microscope: High-Speed Atomic Force Microscopy. *Appl. Phys. Lett.* **2005**, *86* (3), 1–3. https://doi.org/10.1063/1.1855407.

(371) Payton, O. D.; Picco, L.; Miles, M. J.; Homer, M. E.; Champneys, A. R. Improving the Signal-to-Noise Ratio of High-Speed Contact Mode Atomic Force Microscopy. *Review of Scientific Instruments*. 2012. https://doi.org/10.1063/1.4747455.

(372) Picco, L. M.; Bozec, L.; Ulcinas, A.; Engledew, D. J.; Antognozzi, M.; Horton, M. A.; Miles, M. J. Breaking the Speed Limit with Atomic Force Microscopy. *Nanotechnology* **2007**, *18* (4), 44030. https://doi.org/10.1088/0957-4484/18/4/044030.

(373) Picco, L. M.; Dunton, P. G.; Ulcinas, A.; Engledew, D. J.; Hoshi, O.; Ushiki, T.; Miles, M. J. High-Speed AFM of Human Chromosomes in Liquid. *Nanotechnology* **2008**, *19* (38), 384018. https://doi.org/10.1088/0957-4484/19/38/384018.

(374) Pyne, A.; Marks, W.; M Picco, L.; G Dunton, P.; Ulcinas, A.; E Barbour, M.; B Jones, S.; Gimzewski, J.; J Miles, M. High-Speed Atomic Force Microscopy of Dental Enamel Dissolution in Citric Acid. *Arch. Histol. Cytol.* **2009**, *72* (4–5), 209–215. https://doi.org/JST.JSTAGE/aohc/72.209 [pii].

(375) Stine, W. B.; Jungbauer, L.; Yu, C.; LaDu, M. J. Preparing Synthetic Aβ in Different Aggregation States. *Methods Mol. Biol.* **2011**, *670*, 13–32. https://doi.org/10.1007/978-1-60761-744-0-2.

(376) Quinn, P. J. Structure of Sphingomyelin Bilayers and Complexes with Cholesterol Forming Membrane Rafts. *Langmuir* **2013**, *29* (30), 9447–9456. https://doi.org/10.1021/la4018129.
(377) Kan, C. C.; Ruan, Z. S.; Bittman, R. Interaction of Cholesterol with Sphingomyelin in Bilayer Membranes: Evidence That the Hydroxy Group of Sphingomyelin Does Not Modulate the Rate of Cholesterol Exchange between Vesicles. *Biochemistry* **1991**, *30* (31), 7759–7766. https://doi.org/10.1021/bi00245a013.
(378) Lin, H.; Bhatia, R.; Lal, R. Amyloid β Protein Forms Ion Channels: Implications for Alzheimer's Disease Pathophysiology. *FASEB J.* **2001**, *15* (13), 2433–2444. https://doi.org/10.1096/fj.01-0377com.
(379) Hardy, J. Alzheimer's Disease: The Amyloid Cascade Hypothesis: An Update and Reappraisal. *J. Alzheimers Dis. JAD* **2006**, *9* (3 Suppl), 151–153.
(380) Raffy, S.; Teissié, J. Control of Lipid Membrane Stability by Cholesterol Content. *Biophys. J.* **1999**, *76* (4), 2072–2080. https://doi.org/10.1016/S0006-3495(99)77363-7.
(381) Martin, M. G.; Perga, S.; Trovo, L.; Rasola, A.; Holm, P.; Rantama, T.; Harkany, T.; Castren, E.; Chiara, F.; Dotti, C. G. Cholesterol Loss Enhances TrkB Signaling in Hippocampal Neurons Aging in Vitro. *Mol. Biol. Cell* **2008**, *19* (1), 2101–2112. https://doi.org/10.1091/mbc.E07.
(382) Alonso, M. A.; Millán, J. The Role of Lipid Rafts in Signalling and Membrane Trafficking in T Lymphocytes. **2001**.
(383) Egawa, J.; Pearn, M. L.; Lemkuil, B. P.; Patel, P. M.; Head, B. P. Membrane Lipid Rafts and Neurobiology: Age-Related Changes in Membrane Lipids and Loss of Neuronal Function. *J. Physiol.* **2016**, *594* (16), 4565–4579. https://doi.org/10.1113/JP270590.
(384) Patel, N. S.; Mathura, V. S.; Bachmeier, C.; Beaulieu-Abdelahad, D.; Laporte, V.; Weeks, O.; Mullan, M.; Paris, D. Alzheimer's β-Amyloid Peptide Blocks Vascular Endothelial Growth Factor Mediated Signaling via Direct Interaction with VEGFR-2. *J. Neurochem.* **2010**. https://doi.org/10.1111/j.1471-4159.2009.06426.x.
(385) Stine, W. B.; Jungbauer, L.; Yu, C.; LaDu, M. J. Preparing Synthetic Aβ in Different Aggregation States. *Methods Mol. Biol.* **2011**, *670*, 13–32. https://doi.org/10.1007/978-1-60761-744-0-2.
(386) Zidovetzki, R.; Levitan, I. Use of Cyclodextrins to Manipulate Plasma Membrane Cholesterol Content: Evidence, Misconceptions and Control Strategies. *Biochim. Biophys. Acta - Biomembr.* **2007**, *1768* (6), 1311–1324. https://doi.org/10.1016/j.bbamem.2007.03.026.
(387) Edlund, C.; Söderberg, M.; Kristensson, K. Isoprenoids in Aging and Neurodegeneration. *Neurochem. Int.* **1994**, *25* (1), 35–38. https://doi.org/10.1016/0197-0186(94)90050-7.
(388) Jeong, A.; Suazo, K. F.; Wood, W. G.; Distefano, M. D.; Li, L. Isoprenoids and Protein Prenylation: Implications in the Pathogenesis and Therapeutic Intervention of Alzheimer's Disease. *Crit. Rev. Biochem. Mol. Biol.* **2018**, *53* (3), 279–310. https://doi.org/10.1080/10409238.2018.1458070.
(389) Penke, B.; Szűcs, M.; Bogár, F. Oligomerization and Conformational Change Turn Monomeric β-Amyloid and Tau Proteins Toxic: Their Role in Alzheimer's Pathogenesis. *Molecules* **2020**, *25* (7), 1659. https://doi.org/10.3390/molecules25071659.
(390) Stroud, J. C.; Liu, C.; Teng, P. K.; Eisenberg, D. Toxic Fibrillar Oligomers of Amyloid-β Have Cross-β Structure. *Proc. Natl. Acad. Sci.* **2012**, *109* (20), 7717–7722. https://doi.org/10.1073/pnas.1203193109.

(391) Livadiotis, G.; Assas, L.; Dayeh, M. A.; Elaydi, S.; Phea, C.; Roberts, J. L.; Samman, Y.; Tchen, R. Experimental Analysis of Interacting HT22 Plasma Membrane Cholesterol and β-Amyloid. *Adv. Alzheimers Dis.* **2017**, *06* (04), 75–96. https://doi.org/10.4236/aad.2017.64006.

(392) Feng, Z.; Zhang, J.-T. Protective Effect of Melatonin on Beta-Amyloid-Induced Apoptosis in Rat Astroglioma C6 Cells and Its Mechanism. *Free Radic. Biol. Med.* **2004**, *37* (11), 1790–1801. https://doi.org/10.1016/j.freeradbiomed.2004.08.023.

(393) Robinson, M.; Turnbull, S.; Lee, B. Y.; Leonenko, Z. The Effects of Melatonin, Serotonin, Tryptophan and NAS on the Biophysical Properties of DPPC Monolayers. *Biochim. Biophys. Acta - Biomembr.* **2020**. https://doi.org/10.1016/j.bbamem.2020.183363.

(394) Sepulveda, F. J.; Parodi, J.; Peoples, R. W.; Opazo, C.; Aguayo, L. G. Synaptotoxicity of Alzheimer Beta Amyloid Can Be Explained by Its Membrane Perforating Property. *PLoS ONE* **2010**, *5* (7), 1–9. https://doi.org/10.1371/journal.pone.0011820.

(395) Shankar, G. M.; Bloodgood, B. L.; Townsend, M.; Walsh, D. M.; Selkoe, D. J.; Sabatini, B. L. Natural Oligomers of the Alzheimer Amyloid- Protein Induce Reversible Synapse Loss by Modulating an NMDA-Type Glutamate Receptor-Dependent Signaling Pathway. *J. Neurosci.* **2007**, *27* (11), 2866–2875. https://doi.org/10.1523/JNEUROSCI.4970-06.2007.

(396) Knobloch, M.; Mansuy, I. M. Dendritic Spine Loss and Synaptic Alterations in Alzheimer's Disease. *Mol. Neurobiol.* **2008**, *37* (1), 73–82. https://doi.org/10.1007/s12035-008-8018-z.

(397) Parpura, V.; Haydon, P. G.; Henderson, E. Three-Dimensional Imaging of Living Neurons and Glia with the Atomic Force Microscope. *J. Cell Sci.* **1993**, *104 (Pt 2*, 427–432.

(398) Xiong, Y.; Aih, C. L.; Suter, D. M.; Lee, G. U. Topography and Nanomechanics of Live Neuronal Growth Cones Analyzed by Atomic Force Microscopy. *Biophys. J.* **2009**, *96* (12), 5060–5072. https://doi.org/10.1016/j.bpj.2009.03.032.

(399) Bhatia, R.; Lin, H.; Lal, R. Fresh and Globular Amyloid β Protein (1–42) Induces Rapid Cellular Degeneration: Evidence for AβP Channel-mediated Cellular Toxicity. *FASEB J.* **2000**, *14* (9), 1233–1243. https://doi.org/10.1096/fasebj.14.9.1233.

(400) Lulevich, V.; Zimmer, C. C.; Hong, H. -s; Jin, L. -w; Liu, G. -y. Single-Cell Mechanics Provides a Sensitive and Quantitative Means for Probing Amyloid- Peptide and Neuronal Cell Interactions. *Proc. Natl. Acad. Sci.* **2010**, *107* (31), 13872–13877. https://doi.org/10.1073/pnas.1008341107.

(401) Ungureanu, A. A.; Benilova, I.; Krylychkina, O.; Braeken, D.; Strooper, B. D.; Haesendonck, C. V.; Dotti, C. G.; Bartic, C. Amyloid Beta Oligomers Induce Neuronal Elasticity Changes in Age-Dependent Manner: A Force Spectroscopy Study on Living Hippocampal Neurons. *Sci. Rep.* **2016**, *6* (May), 1–13. https://doi.org/10.1038/srep25841.

(402) Westra, M.; Gutierrez, Y.; MacGillavry, H. D. Contribution of Membrane Lipids to Postsynaptic Protein Organization. *Front. Synaptic Neurosci.* **2021**, *13*.

(403) Yang, S. P.; Kwon, B. O.; Gho, Y. S.; Chae, C. B. Specific Interaction of VEGF with Beta-Amyloid, and Its Protective Effect on Beta-Amyloid-Induced Neurotoxicity. *J.Neurochem.* **2005**, *93* (1), 118–127.

(404) Kemppainen, S.; Rantamäki, T.; Jerónimo-Santos, A.; Lavasseur, G.; Autio, H.; Karpova, N.; Kärkkäinen, E.; Stavén, S.; Miranda, H. V.; Outeiro, T. F.; Diógenes, M. J.; Laroche, S.; Davis, S.; Sebastião, A. M.; Castrén, E.; Tanila, H. Impaired TrkB Receptor Signaling Contributes to Memory Impairment in APP/PS1 Mice. *Neurobiol. Aging* **2012**, *33* (6), 1122.e23-1122.e39. https://doi.org/10.1016/j.neurobiolaging.2011.11.006.

(405) Chen, P.-H.; Chen, X.; He, X. Platelet-Derived Growth Factors and Their Receptors: Structural and Functional Perspectives. *Biochim. Biophys. Acta* **2013**, *1834* (10), 2176–2186. https://doi.org/10.1016/j.bbapap.2012.10.015.

(406) Palavicini, J. P.; Wang, C.; Chen, L.; Hosang, K.; Wang, J.; Tomiyama, T.; Mori, H.; Han, X. Oligomeric Amyloid-Beta Induces MAPK-Mediated Activation of Brain Cytosolic and Calcium-Independent Phospholipase A2 in a Spatial-Specific Manner. *Acta Neuropathol. Commun.* **2017**, *5* (1), 56. https://doi.org/10.1186/s40478-017-0460-6.

(407) Morrison, D. K.; Kaplan, D. R.; Rhee, S. G.; Williams, L. T. Platelet-Derived Growth Factor (PDGF)-Dependent Association of Phospholipase C-g with the PDGF Receptor Signaling Complex. *Mol. Cell. Biol.* **1990**, *10* (5), 2359–2366.

(408) Verí, M.-C.; DeBell, K. E.; Seminario, M.-C.; DiBaldassarre, A.; Reischl, I.; Rawat, R.; Graham, L.; Noviello, C.; Rellahan, B. L.; Miscia, S.; Wange, R. L.; Bonvini, E. Membrane Raft-Dependent Regulation of Phospholipase Cγ-1 Activation in T Lymphocytes. *Mol. Cell. Biol.* **2001**, *21* (20), 6939–6950. https://doi.org/10.1128/MCB.21.20.6939-6950.2001.

(409) Hurtado, D. E.; Molina-Porcel, L.; Carroll, J. C.; Macdonald, C.; Aboagye, A. K.; Trojanowski, J. Q.; Lee, V. M.-Y. Selectively Silencing GSK-3 Isoforms Reduces Plaques and Tangles in Mouse Models of Alzheimer's Disease. *J. Neurosci. Off. J. Soc. Neurosci.* **2012**, *32* (21), 7392–7402. https://doi.org/10.1523/JNEUROSCI.0889-12.2012.

(410) Webster, M. J.; Herman, M. M.; Kleinman, J. E.; Weickert, C. S. BDNF and TrkB MRNA Expression in the Hippocampus and Temporal Cortex during the Human Lifespan. **2006**, *6*, 941–951. https://doi.org/10.1016/j.modgep.2006.03.009.

(411) Wong, J.; Garner, B. Evidence That Truncated TrkB Isoform, TrkB-Shc Can Regulate Phosphorylated TrkB Protein Levels. *Biochem. Biophys. Res. Commun.* **2012**, *420* (2), 331–335. https://doi.org/10.1016/j.bbrc.2012.02.159.

(412) Ahmed, S. B. M.; Prigent, S. A. Insights into the Shc Family of Adaptor Proteins. *J. Mol. Signal. 12*, 2. https://doi.org/10.5334/1750-2187-12-2.

(413) Lim, J. Y.; Park, S. I.; Oh, J. H.; Kim, S. M.; Jeong, C. H.; Jun, J. A.; Lee, K.-S.; Oh, W.; Lee, J.-K.; Jeun, S.-S. Brain-Derived Neurotrophic Factor Stimulates the Neural Differentiation of Human Umbilical Cord Blood-Derived Mesenchymal Stem Cells and Survival of Differentiated Cells through MAPK/ERK and PI3K/Akt-Dependent Signaling Pathways. *J. Neurosci. Res.* **2008**, *86* (10), 2168–2178. https://doi.org/10.1002/jnr.21669.

(414) Oumesmar, B. N.; Vignais, L.; Evercooren, A. B.-V. Developmental Expression of Platelet-Derived Growth Factor α-Receptor in Neurons and Glial Cells of the Mouse CNS. *J. Neurosci.* **1997**, *17* (1), 125–139. https://doi.org/10.1523/JNEUROSCI.17-01-00125.1997.

(415) Sil, S.; Periyasamy, P.; Thangaraj, A.; Chivero, E. T.; Buch, S. PDGF/PDGFR Axis in the Neural Systems. *Mol. Aspects Med.* **2018**, *62*, 63–74. https://doi.org/10.1016/j.mam.2018.01.006.

(416) Yeh, H. J.; Silos-Santiago, I.; Wang, Y. X.; George, R. J.; Snider, W. D.; Deuel, T. F. Developmental Expression of the Platelet-Derived Growth Factor Alpha-Receptor Gene in Mammalian Central Nervous System. *Proc. Natl. Acad. Sci.* **1993**, *90* (5), 1952–1956. https://doi.org/10.1073/pnas.90.5.1952.

(417) Beazely, M. a; Lim, A.; Li, H.; Trepanier, C.; Chen, X.; Sidhu, B.; MacDonald, J. F. Platelet-Derived Growth Factor Selectively Inhibits NR2B-Containing N-Methyl-D-Aspartate Receptors in CA1 Hippocampal Neurons. *J. Biol. Chem.* **2009**, *284* (12), 8054–8063. https://doi.org/10.1074/jbc.M805384200.

(418) Jackson, E. L.; Garcia-Verdugo, J. M.; Gil-Perotin, S.; Roy, M.; Quinones-Hinojosa, A.; VandenBerg, S.; Alvarez-Buylla, A. PDGFRα-Positive B Cells Are Neural Stem Cells in the Adult SVZ That Form Glioma-like Growths in Response to Increased PDGF Signaling. *Neuron* **2006**, *51* (2), 187–199. https://doi.org/10.1016/j.neuron.2006.06.012.

(419) Baron, W.; Shattil, S. J.; ffrench-Constant, C. The Oligodendrocyte Precursor Mitogen PDGF Stimulates Proliferation by Activation of Avβ3 Integrins. *EMBO J.* **2002**, *21* (8), 1957–1966. https://doi.org/10.1093/emboj/21.8.1957.

(420) Sorkin, A.; Goh, L. K. Endocytosis and Intracellular Trafficking of ErbBs. *Exp. Cell Res.* **2009**, *315* (4), 683–696. https://doi.org/10.1016/j.yexcr.2008.07.029.

(421) Lund, K. A.; Opresko, L. K.; Starbuck, C.; Walsh, B. J.; Wiley, H. S. Quantitative Analysis of the Endocytic System Involved in Hormone-Induced Receptor Internalization. *J. Biol. Chem.* **1990**, *265* (26), 15713–15723. https://doi.org/10.1016/S0021-9258(18)55456-9.

(422) Pike, L. J.; Casey, L. Cholesterol Levels Modulate EGF Receptor-Mediated Signaling by Altering Receptor Function and Trafficking. *Biochemistry* **2002**, *41* (32), 10315–10322. https://doi.org/10.1021/bi025943i.

(423) Hooshmandi, E.; Ghasemi, R.; Iloun, P.; Moosavi, M. The Neuroprotective Effect of Agmatine against Amyloid β-Induced Apoptosis in Primary Cultured Hippocampal Cells Involving ERK, Akt/GSK-3β, and TNF-α. *Mol. Biol. Rep.* **2019**, *46* (1), 489–496. https://doi.org/10.1007/s11033-018-4501-4.

(424) Lin, L.; Jadoon, S. S.; Liu, S.-Z.; Zhang, R.-Y.; Li, F.; Zhang, M.-Y.; Ai-Hua, T.; You, Q.-Y.; Wang, P. Tanshinone IIA Ameliorates Spatial Learning and Memory Deficits by Inhibiting the Activity of ERK and GSK-3β. *J. Geriatr. Psychiatry Neurol.* **2019**, *32* (3), 152–163. https://doi.org/10.1177/0891988719837373.

(425) Arrazola Sastre, A.; Luque Montoro, M.; Gálvez-Martín, P.; Lacerda, H. M.; Lucia, A.; Llavero, F.; Zugaza, J. L. Small GTPases of the Ras and Rho Families Switch on/off Signaling Pathways in Neurodegenerative Diseases. *Int. J. Mol. Sci.* **2020**, *21* (17), 6312. https://doi.org/10.3390/ijms21176312.

(426) Ochalek, A.; Mihalik, B.; Avci, H. X.; Chandrasekaran, A.; Téglási, A.; Bock, I.; Giudice, M. L.; Táncos, Z.; Molnár, K.; László, L.; Nielsen, J. E.; Holst, B.; Freude, K.; Hyttel, P.; Kobolák, J.; Dinnyés, A. Neurons Derived from Sporadic Alzheimer's Disease IPSCs Reveal Elevated TAU Hyperphosphorylation, Increased Amyloid Levels, and GSK3B Activation. *Alzheimers Res. Ther.* **2017**, *9* (1), 1–19. https://doi.org/10.1186/s13195-017-0317-z.

(427) Tu, S.; Okamoto, S.; Lipton, S. A.; Xu, H. Oligomeric A β -Induced Synaptic Dysfunction in Alzheimer ' s Disease. *Mol. Neurodegener.* **2014**, *48* (9), 1–12. https://doi.org/10.1186/1750-1326-9-48.

(428) Zhang, F.; Gannon, M.; Chen, Y.; Yan, S.; Zhang, S.; Feng, W.; Tao, J.; Sha, B.; Liu, Z.; Saito, T.; Saido, T.; Keene, C. D.; Jiao, K.; Roberson, E. D.; Xu, H.; Wang, Q. β-Amyloid Redirects Norepinephrine Signaling to Activate the Pathogenic GSK3β/Tau Cascade. *Sci. Transl. Med.* **2020**, *12* (526), eaay6931. https://doi.org/10.1126/scitranslmed.aay6931.

(429) Sofola, O.; Kerr, F.; Rogers, I.; Killick, R.; Augustin, H.; Gandy, C.; Allen, M. J.; Hardy, J.; Lovestone, S.; Partridge, L. Inhibition of GSK-3 Ameliorates Aβ Pathology in an Adult-Onset Drosophila Model of Alzheimer's Disease. *PLOS Genet.* **2010**, *6* (9), e1001087. https://doi.org/10.1371/journal.pgen.1001087.

(430) Kulawiak, B.; Szewczyk, A. Glutamate-Induced Cell Death in HT22 Mouse Hippocampal Cells Is Attenuated by Paxilline, a BK Channel Inhibitor. *Mitochondrion* **2012**, *12* (1), 169–172. https://doi.org/10.1016/j.mito.2011.12.001.